

TOPOLOGICAL INSULATORS / SUPERCONDUCTORS

PROSEMINAR IN THEORETICAL PHYSICS
INSTITUT FÜR THEORETISCHE PHYSIK
ETH ZÜRICH

Prof. Dr. Johann W. Blatter

FS14

typeset, compilation & editing by O. Zilberberg
© 2014, ETH Zürich

TABLE OF CONTENTS

1	INTEGER QUANTUM HALL EFFECT — CONTINUUM [PATRICK HAUGHIAN]	1
1.1	Introduction	1
1.2	Electrons in two dimensions	4
1.3	Quantization of Hall resistivity	6
1.4	Disorder	7
1.5	Berry phase	8
1.6	Linear response	10
1.7	Chern number	13
1.8	Summary	15
2	2D QUANTUM HALL EFFECT ON A LATTICE [LUDOVIC SCYBOZ]	19
2.1	Introduction	19
2.2	Magnetic Translation Group	20
2.3	Středa Formula	28
2.4	Diophantine Equation	30
2.5	Bulk-Edge Correspondence	31
2.6	Concluding remarks	31
3	GRAPHENE [MARLON AZINOVIC AND TOBIAS WOLF]	37
3.1	Introduction	37
3.2	Tight-binding model	38
3.3	Topology of a 2×2 Hamiltonian	44
3.4	Graphene ribbons and nearest neighbour hopping	48
3.5	Chern Insulator	54
3.6	Graphene ribbons in Haldane model	58
3.7	Kane Mele Model	63

TABLE OF CONTENTS

4 TI IN 2D AND 3D: THE QUANTUM SPIN HALL EFFECT IN HGTE QUANTUM WELLS AND A SHORT INTRO. TO 3D TI [ERIK CHEAH]	71
4.1 Introduction	72
4.2 Role of spin-orbit coupling in topological insulators	73
4.3 Semiconductor band structures around the Γ -point and the concept of double groups	73
4.4 Band Structure of HgTe	78
4.5 HgTe Quantum Wells and the Bernevig-Hughes-Zhang model	79
4.6 Experiments	85
4.7 Inverted type II semiconductor	94
4.8 3D Topological Insulators - A brief Introduction	94
4.9 Summary	98
5 TOPOLOGICAL INSULATORS [JOHAN ANDBERGER]	103
5.1 Introduction	103
5.2 \mathbb{Z}_2 index for systems with time-reversal symmetry	105
5.3 \mathbb{Z}_2 index for systems with time-reversal symmetry and inversion symmetry	108
5.4 Graphene	110
5.5 Concluding remarks	112
6 TOPOLOGICAL FIELD THEORY FOR INSULATORS [FLORIAN JOHNE]	117
6.1 Introduction	117
6.2 Topological Field Theory in (2+1)-D	118
6.3 Topological Field Theory in (4+1)-D	124
6.4 Topological Field Theories in Higher Dimensions	129
6.5 Conclusion	130
6.6 Appendix	130
7 BCS THEORY OF SUPERCONDUCTIVITY [PAOLO MOLIGNINI]	141
7.1 Outline	141
7.2 Introduction	142
7.3 Standard BCS Theory	147
7.4 Generalized BCS theory	162
7.5 Summary and Conclusion	166
8 TOPOLOGICAL SUPERCONDUCTORS [PAOLO MOLIGNINI]	173
8.1 Outline	173
8.2 Introduction	174
8.3 Topological invariants in superconductors	179

TABLE OF CONTENTS

8.4	Green's function formalism	187
8.5	Summary and Conclusion	196
9	TOPOLOGICAL SUPERCONDUCTORS [LENNART SCHMIDT]	209
9.1	Introduction	209
9.2	Symmetry classifications of gap functions	210
9.3	Topological aspects and numerical simulations	223
9.4	Summary and Conclusions	238
9.5	Appendix A - The Projection Formula	238
9.6	Appendix B - # cc = # irreps	240
10	POLARIZATION AND TOPOLOGICAL INSULATORS [THOMAS GUMBSCH]	245
10.1	Introduction	245
10.2	Polarization on a lattice	246
10.3	Time reversal symmetry	247
10.4	$U(2N)$ gauge invariance of the chern number	248
10.5	Concluding remarks	251
10.6	Appendix: General behaviour under $U(2N)$ transformation	252
11	CLASSIFICATION OF TOPOLOGICAL INSULATORS AND SUPERCONDUCTORS [STEFAN HUBER]	257
11.1	Introduction	258
11.2	Symmetry Classification of non-interacting Hamiltonians	260
11.3	Gapped bulk Hamiltonians	272
11.4	Mathematical concepts from topology	273
11.5	Nonlinear sigma models	278
11.6	Topological Invariants	279
11.7	Examples	281
11.8	Conclusion	285

TABLE OF CONTENTS

CHAPTER 1

INTEGER QUANTUM HALL EFFECT — CONTINUUM

PATRICK HAUGHIAN

SUPERVISOR: ODED ZILBERBERG

A two-dimensional electron gas subjected to a perpendicular magnetic field displays resistivity quantization known as the quantum Hall effect. We discuss the continuum model of the integer quantum Hall effect with the goal of arriving at the quantization of resistivity on two different paths: First, we motivate the existence of current-carrying edge states and discuss how quantization of off-diagonal resistivity ρ_{xy} arises in this picture. Second, we give an outline of how the Hall conductivity can be derived from linear response in the bulk. In doing so, we obtain a topological characterization of the Hall conductivity as an integral over a Berry curvature.

1.1 INTRODUCTION

The Hall effect is observed when a current $\mathbf{j} = j_y \mathbf{e}_y$ of electrons with velocity $\mathbf{v} = v_y \mathbf{e}_y$ is led through a quasi-two-dimensional rectangular bar subjected to a perpendicular magnetic field $\mathbf{B} = B_z \mathbf{e}_z$ (see fig. 1.1). The resulting Lorentz force causes a drift of electrons toward one of the edges of the bar, which gives rise to an electrical field $\mathbf{E} = E_x \mathbf{e}_x$ between the edges, perpendicular to both \mathbf{B} and \mathbf{j} , which in equilibrium takes the form $E_x = -v_y B_z$. Since the current density is given by $j_y = -nev_y$, with the electron density n , we see that the field can be written as $E_x = \sigma_{xy} j_y$, where the coefficient $\sigma_{xy} = ne/B$ is the

1.1 Introduction

Hall conductivity. In particular, this implies that the transverse resistivity $\rho_{xy} = (\sigma^{-1})_{xy}$ is proportional to B_z .

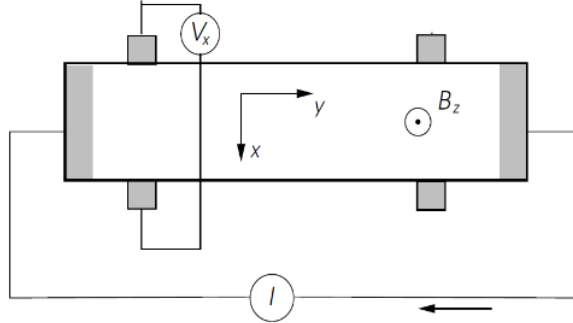


Figure 1.1: A Hall bar [1]. A magnetic field B_z is applied perpendicular to the bar and a current j_y is led through it. The Hall effect can then be observed in the form of a voltage between the edges.

In the so-called quantum Hall effect, a quantization of the transverse conductivity, σ_{xy} , occurs at strong magnetic fields and if the movement of the electrons is strictly confined to two dimensions. The latter can be achieved, for example, in a sample consisting of a two-layer system of semiconductors, one of which has its conduction band at higher energies than the other, as seen in fig. 1.2. The Fermi energy of the material with the higher conduction band is now pinned by n-dopants to lie between the two conduction bands. The donated electrons diffuse across the interface and the resulting polarization bends the conduction bands in such a way that electrons are trapped in a triangular potential well close to the interface in the conduction band of the second material. For sufficiently low temperatures the excited levels of these confined electrons are frozen out, and their only remaining freedom is to move along the two-dimensional interface, thus behaving as a two-dimensional electron gas (2DEG).

A Hall measurement performed on such a 2DEG system, at temperatures of $T \lesssim 4$ K, and in a strong magnetic field $B \gtrsim 1$ T, led von Klitzing *et al.* [3] to discover the breakdown of the proportionality $\rho_{xy} \propto B$. Instead, a quantization of the resistivity curve as a function of magnetic field into plateaus at values

$$\rho_{xy} = \frac{h}{\nu e^2}; \quad \nu \in \mathbb{N}, \quad (1.1)$$

is observed (see fig. 1.3).

This seminal result opened up a wide area of research in condensed matter physics. In this chapter, we shall detail the theoretical analysis of this phenomenon. In the following section 1.2, we shall give a description of the quantum

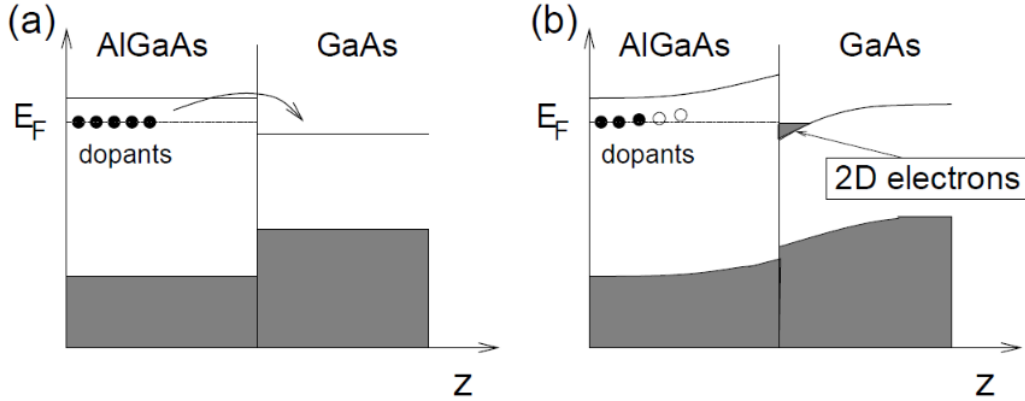


Figure 1.2: 2DEG realization: (a) donor ions in an AlGaAs layer pin the Fermi energy E_F above conduction band in an GaAs layer, (b) donated e^- populate conduction band in GaAs layer, resulting in a polarization that bends the bands. Thus, a potential well forms near the interface between the two materials [2].

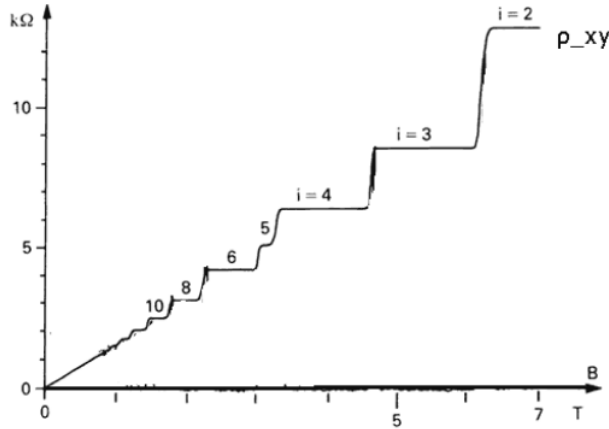


Figure 1.3: Quantization of Hall resistivity [4].

hall effect in terms of edge states, which was first given in [5]; we shall present the arguments as laid out in [6]. A topological characterization of Hall conductivity quantization as a winding number was first given in [7]. This result was formulated using the language of a Berry phase, conceived in [8], in [9]. The introduction of Berry phase in section 1.5 of the present chapter follows [8] and [10], the latter of which also provides us with a detailed write-up of the linear-response calculation required to obtain the result of the Hall conductivity σ_{xy} as a winding number, of which an outline shall be given in section 1.6.

1.2 Electrons in two dimensions

1.2 ELECTRONS IN TWO DIMENSIONS

Our first task in understanding the mechanics of the quantum Hall effects is to model the dynamics of the underlying two-dimensional electron gas. This will be done in several steps (cf. [6]).

1.2.1 CLASSICAL DYNAMICS

Initially, we consider the electrons as classical particles and write their classical equations of motion in an electromagnetic field as $\dot{\mathbf{p}} = -e(\mathbf{E} + \mathbf{v} \times \mathbf{B})$, where $\dot{\mathbf{p}}$ is the time derivative of the particle momentum, $-e$ is the electron charge, \mathbf{v} its velocity, and \mathbf{B} is the magnetic field. This picture gives rise to two observations: first, in the quasistatic case $\dot{\mathbf{p}} = 0$, the electric field \mathbf{E} is related to the electron current $\mathbf{j} = -ne\mathbf{v}$ via

$$\begin{pmatrix} E_x \\ E_y \end{pmatrix} = -\frac{e}{B} \begin{pmatrix} v_y \\ v_x \end{pmatrix} \implies \mathbf{j} = ne\mathbf{v} \equiv \frac{ne}{B} \begin{pmatrix} 0 & -1 \\ 1 & 0 \end{pmatrix} \mathbf{E}, \quad (1.2)$$

which confirms the expression for the Hall conductivity given in section 1.1. Second, if we examine the case of $\mathbf{E} = 0$, we find that the electrons are localized on circular orbits

$$\mathbf{x} = R(\cos(\omega_c t); \sin(\omega_c t)), \quad \omega_c = \frac{eB}{m}, \quad (1.3)$$

where ω_c is the cyclotron frequency, and m is the electron mass. This classical calculation fails to give any insight into the observed quantization of resistivity; in the regime of strong magnetic fields where this observation is made, the quantum structure of the electrons becomes apparent, which we shall now exhibit.

1.2.2 LANDAU LEVELS

The influence of a magnetic field on a two-dimensional system of free particles is described by the minimal-coupling Hamiltonian

$$\mathcal{H} = \frac{1}{2m} \left(\mathbf{p} - \frac{e}{c} \mathbf{A} \right)^2, \quad (1.4)$$

where \mathbf{A} is a vector potential that generates the magnetic field $\mathbf{B} = Be_z$. A convenient gauge for \mathbf{A} is the *Landau gauge* $\mathbf{A} = xBe_y$, which results in the Hamiltonian

$$\mathcal{H} = \frac{1}{2m} \left(p_x^2 + \left(p_y + \frac{eB}{c}x \right)^2 \right). \quad (1.5)$$

As a result of this choice of gauge, \mathcal{H} does not depend on y , reflecting translational invariance. This enables us to write the electron wave function as a product of a plane wave propagating in y -direction and a function f_k that is indexed by the y -momentum number k , but does not depend on y itself, $\psi_k(x, y) = e^{iky} f_k(x)$. The one-dimensional Schrödinger equation for f_k then reads, after completing the square, $h_k f_k \equiv \left(\frac{1}{2m} p_x^2 + \frac{1}{2} m \omega_c^2 (x + k\ell^2)^2 \right) f_k = \epsilon_k f_k$, where we defined the magnetic length¹ $\ell = \sqrt{\frac{\hbar c}{eB}}$. This Hamiltonian describes a one-dimensional harmonic oscillator of frequency equal to the cyclotron frequency, centered at $x_k \equiv -k\hbar c/eB$. It is to be pointed out that the energy levels of this oscillator, the *Landau levels*, $\epsilon_{kn} = (n + \frac{1}{2})\hbar\omega_c$, are degenerate in the y -momentum number k , whereas the x -coordinate of the oscillator centers x_k is proportional to k . Furthermore, the separation between the Landau levels is proportional to the magnetic field, which leads us to conjecture that this quantization is noticeable in the strong-field quantum Hall regime.

The Landau levels are exponentially localized in x and hence do not by themselves give rise to a current in y -direction, as can be seen by evaluating (for $n = 0$) the expectation value

$$\langle J_y \rangle = -e \frac{1}{m} \left\langle \psi_k \left| \left(p_y + \frac{e}{c} A_y \right) \right| \psi_k \right\rangle \propto \int dx e^{-x^2} x = 0. \quad (1.6)$$

In order to obtain a non-vanishing current in this picture, an additional ingredient is needed, namely a potential $V(x)$. A natural candidate for this is provided by the confinement of particles due to the finite width L_x of the bar. Hence we include a potential $V(x)$ similar to the one seen in fig. 1.4 into the Hamiltonian h_k .

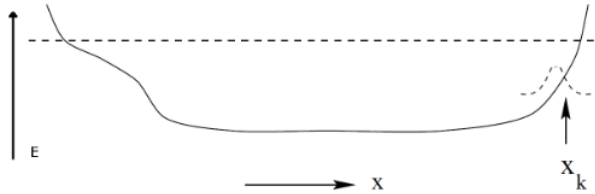


Figure 1.4: confining potential $V(x)$ arising from the finite width of the sample for the electron gas, [6]

Making use of the localization of the oscillator states in x -direction, we expand V in x around x_k and insert this expansion into the Hamiltonian. In doing so,

¹The name of this quantity is due to the fact that an area of $2\pi\ell^2$ contains one flux quantum $\Phi_0 = \frac{\hbar c}{e}$.

1.3 Quantization of Hall resistivity

we find that the oscillator centers are displaced by a term $\propto V'(x_k)$ and that the k -degeneracy of the Landau levels is lifted by a term $\propto x_k$. The first observation now has important consequences for the transport properties near the edges of the sample, where V' is large, i.e. we find a group velocity

$$\langle v_G \rangle = \frac{1}{\hbar} \frac{\partial \epsilon_k}{\partial k} = \frac{1}{\hbar} \frac{\partial \epsilon_k}{\partial x_k} \frac{\partial x_k}{\partial k}. \quad (1.7)$$

Hence, the slopes of the potential $V(x)$ give rise to currents in $\pm y$ -directions, running along the edges. This is the quantum analog to the correspondence between E_x and j_y in the classical Hall effect.

1.3 QUANTIZATION OF HALL RESISTIVITY

These edge states now enable us to give an explanation to the quantization of Hall resistivity. First note that, in general, there is no reason to expect a *net* current in y -direction, since the edge states run in opposite directions. Applying a voltage bias ΔV between the edges changes this, however. Let us consider a single Landau level. We can write the net current I_y as the sum over all group velocities of the states comprising the level:

$$I_y = -\frac{e}{L_y} \int_{-\infty}^{\infty} dk \frac{L_y}{2\pi} \frac{\partial \epsilon_k}{\partial k} n_k, \quad (1.8)$$

where n_k is the Fermi distribution. We have seen that $\partial \epsilon_k / \partial k$ is non-vanishing only on the edges; hence this integral essentially counts the edge states, with signs according to their velocities. In the case of zero temperature, n_k is a step function with value 1 below the Fermi level and value 0 above it. The voltage bias between the edges now results in a difference in the Fermi energies and thus ensures that the current contributions do not cancel, but instead a net current $\propto \Delta V$ survives. Using the chain rule we write

$$I_y = -\frac{e}{h} \int_{\mu_R}^{\mu_L} d\epsilon = -\frac{e}{h} \Delta \mu = -\frac{e^2}{h} \Delta V. \quad (1.9)$$

This result lets us easily obtain the desired quantization: if the magnetic field is lowered so that $\nu \in \mathbb{N}$ Landau levels are below the Fermi energies at the edges, a current

$$I_y = -\nu \frac{e^2}{h} \Delta V \quad (1.10)$$

is observed, which reproduces the expression for the quantized resistivity stated in the introduction.

1.4 DISORDER

Until now, we have been dealing with an ideal sample. Naturally, the question arises whether the quantization result is stable with respect to unavoidable disorder in the sample. A semi-classical picture can be used to motivate that the result obtained previously is unaffected by disorder: Consider a sample with a disorder potential $V(x, y)$ in the bulk. First note that the Landau levels are broadened by the disorder, since different localization sites for electrons in the bulk correspond to shifted energies as a result of the inhomogeneous variation of $V(x, y)$ in x . Now imagine the situation that by decreasing the magnetic field a Landau level is pulled below the Fermi energy, as seen in fig. 1.5.

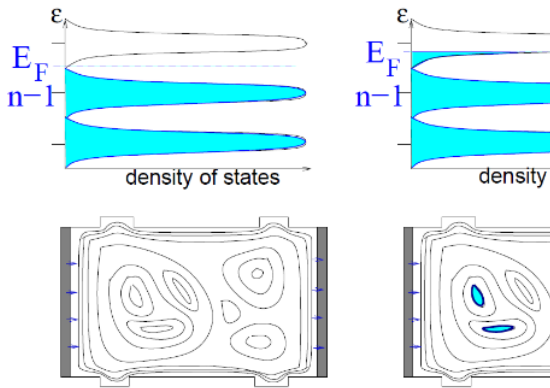


Figure 1.5: filling of potential landscape in bulk as the magnetic field is lowered: as the energy distribution of the n th Landau level crosses reaches the Fermi energy E_F , the states in this level are gradually filled. Both tails of the distribution are populated by states that are localized in the “valleys” and “summits” of the potential landscape given by $V(x, y)$, respectively. These do not contribute to the edge currents; only when the middle of the distribution crosses E_F , extended states are populated that change the resistivity. [2]

During this process, the broadened level is slowly filled with electronic states. These states, however, are localized in the “valleys” of the potential landscape in the bulk and hence do not carry any current, so the resistivity remains constant. As B is decreased further, the filling of the potential landscape with electrons increases, until finally the equipotential lines at the boundaries of “electron lakes” have become long enough to connect opposite edges of the sample. At this point, the resistivity falls from one integer plateau to the next. After the next-lowest plateau has been reached, the resistivity again stops falling even though the Landau level has not been completely filled, because only the localized “summits”

1.5 Berry phase

of the potential remain unpopulated, which again has no bearing on the current. In particular, this picture provides an argument why the quantum Hall effect is independent of the details of the disorder $V(x, y)$.

At this point, we have succeeded in explaining the most striking feature of the quantum Hall effect – the quantization of transverse resistivity – using Landau level quantization and edge states. In the next sections, we want to employ bulk consideration of topological nature to arrive at the same result.

1.5 BERRY PHASE

The purpose of this section is to introduce the concepts of Berry phase and Berry curvature in a general setting, following [10], which will be used later to give a topological argument for the Hall quantization.

Consider an arbitrary system described by a Hamiltonian $\mathcal{H}(\mathbf{R})$ that depends smoothly on some set of parameters \mathbf{R} , making the assumption that for each \mathbf{R} there exists an orthonormal basis of eigenstates $|n(\mathbf{R})\rangle$ with non-degenerate eigenvalues $E_n(\mathbf{R})$. We want to investigate how an eigenstate evolves as \mathbf{R} is slowly varied. The central feature of the eigenstates in this discussion is that their phase is a gauge freedom, meaning that they are defined up to a gauge transformation $|n(\mathbf{R})\rangle \mapsto e^{i\zeta(\mathbf{R})} |n(\mathbf{R})\rangle$. If the system is prepared in an initial eigenstate $|n(\mathbf{R}(0))\rangle$ and if \mathbf{R} is then varied along some path $\mathcal{C}: t \mapsto \mathbf{R}(t)$, the adiabatic theorem asserts that for each time t , the system will be in a state proportional to $|n(\mathbf{R}(t))\rangle$. The phase factor $\theta(t)$ however, is yet to be determined. To this end we denote the evolved state at time t by $|\psi(t)\rangle = e^{i\theta(t)} |n(\mathbf{R}(t))\rangle$. At each point on the path, the Schrödinger equation $H(\mathbf{R}) |\psi\rangle = i\hbar \frac{d}{dt} |\psi\rangle$ holds for this ansatz, which after applying $\langle n(\mathbf{R})|$ leaves us with

$$E_n(\mathbf{R}) - i\hbar \langle n(\mathbf{R}) | \frac{d}{dt} n(\mathbf{R}) \rangle = \hbar \frac{d}{dt} \theta, \quad (1.11)$$

and by integration we obtain

$$\theta(t) = \underbrace{\frac{1}{\hbar} \int_0^t dt' E_n(\mathbf{R}(t'))}_{\text{dynamical phase}} - \underbrace{i \int_0^t dt' \langle n(\mathbf{R}(t')) | \frac{d}{dt'} n(\mathbf{R}(t')) \rangle}_{\text{Berry phase } \gamma_n \in \mathbb{R}}. \quad (1.12)$$

The first term is reminiscent of the phase acquired by a state that is evolved with a time-independent Hamiltonian and is hence referred to as dynamical phase. The object of interest here is the second term, γ_n , called *Berry phase*.

We shall now show that, for a closed path \mathcal{C} , the Berry phase is gauge-independent. To see this, first note that the time integration in γ_n can be replaced by a line

integral

$$\gamma_n = i \int_C d\mathbf{R} \langle n(\mathbf{R}) | \nabla_{\mathbf{R}} | n(\mathbf{R}) \rangle \equiv \int_C d\mathbf{R} \cdot \mathbf{A}_n(\mathbf{R}), \quad (1.13)$$

where we define the *Berry potential* $\mathbf{A}_n(\mathbf{R}) = i \langle n(\mathbf{R}) | \nabla_{\mathbf{R}} | n(\mathbf{R}) \rangle$. By Stokes's theorem, the above can be written as a surface integral,

$$\gamma_n = -\text{Im} \int_{\text{int } C} d\mathbf{S} \cdot \nabla \times \langle n(\mathbf{R}) | \nabla | n(\mathbf{R}) \rangle, \quad (1.14)$$

where for the sake of simplicity we take the parameter space to be three-dimensional. The integrand in the last expression is gauge-invariant: under the transformation $|n(\mathbf{R})\rangle \mapsto e^{i\zeta(\mathbf{R})} |n(\mathbf{R})\rangle$, the matrix element $\langle n(\mathbf{R}) | \nabla | n(\mathbf{R}) \rangle$ only picks up the summand $\nabla \zeta(\mathbf{R})$, which has no curl and hence does not contribute. From the integrand we define the *Berry curvature* $F_{jk} = \langle \partial_j n(\mathbf{R}) | \partial_k n(\mathbf{R}) \rangle - (j \longleftrightarrow k)$, which is the object that will appear during the investigation of the Hall conductance. This section has so far provided us with the remarkable result that a gauge-dependent phase factor can be used to construct a gauge-independent quantity. We now wish to give a geometric description of the Berry phase factor. For this, it will be calculationally expedient to rewrite the expression found above as follows: First insert a factor of $\mathbb{1} = \sum_m |m\rangle \langle m|$ into the Berry curvature,

$$\begin{aligned} \epsilon_{ijk} \langle \partial_j n(\mathbf{R}) | \partial_k n(\mathbf{R}) \rangle &= \underbrace{\epsilon_{ijk} \langle \partial_j n(\mathbf{R}) | n \rangle \langle n | \partial_k n(\mathbf{R}) \rangle}_{\in \mathbb{R}, \text{ so drop this}} + \\ &\quad + \sum_{m \neq n} \epsilon_{ijk} \langle \partial_j n(\mathbf{R}) | m \rangle \langle m | \partial_k n(\mathbf{R}) \rangle, \end{aligned} \quad (1.15)$$

where we can drop the first term because only the imaginary part contributes. Next, we note that since the eigenstates form an orthonormal basis, applying $\langle m | \neq \langle n |$ to $\mathcal{H}(\mathbf{R}) |n(\mathbf{R})\rangle = E_n(\mathbf{R})$ followed by differentiating with respect to \mathbf{R} yields

$$\langle m(\mathbf{R}) | \nabla | n(\mathbf{R}) \rangle = \frac{\langle m(\mathbf{R}) | \nabla \mathcal{H}(\mathbf{R}) | n(\mathbf{R}) \rangle}{E_n(\mathbf{R}) - E_m(\mathbf{R})}. \quad (1.16)$$

After these manipulations, the Berry phase appears as

$$\gamma_n = -\text{Im} \int_{\text{int } C} d\mathbf{S} \cdot \sum_{m \neq n} \frac{\langle n(\mathbf{R}) | \nabla \mathcal{H} | m(\mathbf{R}) \rangle \times \langle m(\mathbf{R}) | \nabla \mathcal{H} | n(\mathbf{R}) \rangle}{(E_m(\mathbf{R}) - E_n(\mathbf{R}))^2}. \quad (1.17)$$

Consider now the case of a system with two energy levels, denoted $|+\rangle$ and $|-\rangle$. In general, a Hamiltonian for such a system is written $\mathcal{H}(\mathbf{R}) = \epsilon(\mathbf{R}) \mathbb{1}_2 + \mathbf{d}(\mathbf{R}) \boldsymbol{\sigma}$,

1.6 Linear response

where $\sigma_{x,y,z}$ are the Pauli matrices. We shift the energies such that the first term vanishes and also rotate $\mathbf{d}(\mathbf{R})$ onto \mathbf{R} , as well as \mathbf{R} onto the z -axis. Note that there is an energy degeneracy at the point $R = 0$. We now consider a closed path \mathcal{C} that avoids $R = 0$, as seen in fig. 1.6. In order to calculate the Berry phase for this path, we use expression (1.17), noting that in the present case $\nabla\mathcal{H} = \boldsymbol{\sigma}$. The problem of computing the Berry curvature is thus reduced to applying Pauli matrices to the states $|\pm\rangle$, which results in only one nonzero term in the integrand:

$$\text{Im} \frac{\langle +|+\rangle \langle -|i|-\rangle - \langle +|-i|+\rangle \langle -|- \rangle}{4R^2} = \frac{1}{2R^2}, \quad (1.18)$$

or, undoing the alignment of \mathbf{R} with the z -axis, $\mathbf{R}/2R^3$.

The Berry phase for \mathcal{C} is hence found to be

$$\gamma_+(\mathcal{C}) = - \int_{\text{int } \mathcal{C}} d\mathbf{S} \cdot \frac{\mathbf{R}}{R^3} = -\frac{1}{2}\Omega(\mathcal{C}), \quad (1.19)$$

where $\Omega_{\mathcal{C}}$ is the solid angle subtended by \mathcal{C} as seen from the degeneracy point 0. The last statement can be seen by taking $\text{int } \mathcal{C}$ to lie on a sphere. In particular, if we restrict to two dimensions, this implies that we obtain no Berry phase if the degeneracy point does not lie within $\text{int } \mathcal{C}$, and $-\pi$ if it does.

1.6 LINEAR RESPONSE

Having introduced the Berry curvature, the task at hand is to exhibit this object in the context of the quantum Hall system. The method to achieve this is by calculating the transverse conductivity as a linear response in the two-dimensional bulk. We shall give a detailed account of the setup of this calculation, as presented in [10], since it is of rather general nature and then outline the remaining steps. The object of study in this section is a two-dimensional translationally invariant system in momentum space, governed by the Hamiltonian

$$\mathcal{H} = \sum_k c_{k\alpha}^\dagger h_k^{\alpha\beta} c_{k\beta}, \quad (1.20)$$

where c_k and c_k^\dagger are fermionic destruction and creation operators with (pseudo-)momentum label k , respectively, and α and β denote orbital degrees of freedom. However, it is instructive to first work with a Hamiltonian for an arbitrary system of particles in a weak field $A(x, t)$,

$$\mathcal{H} = \sum_i \frac{1}{2}(p_i - eA(x_i, t))^2 + \sum_{i < j} V_{ij}. \quad (1.21)$$

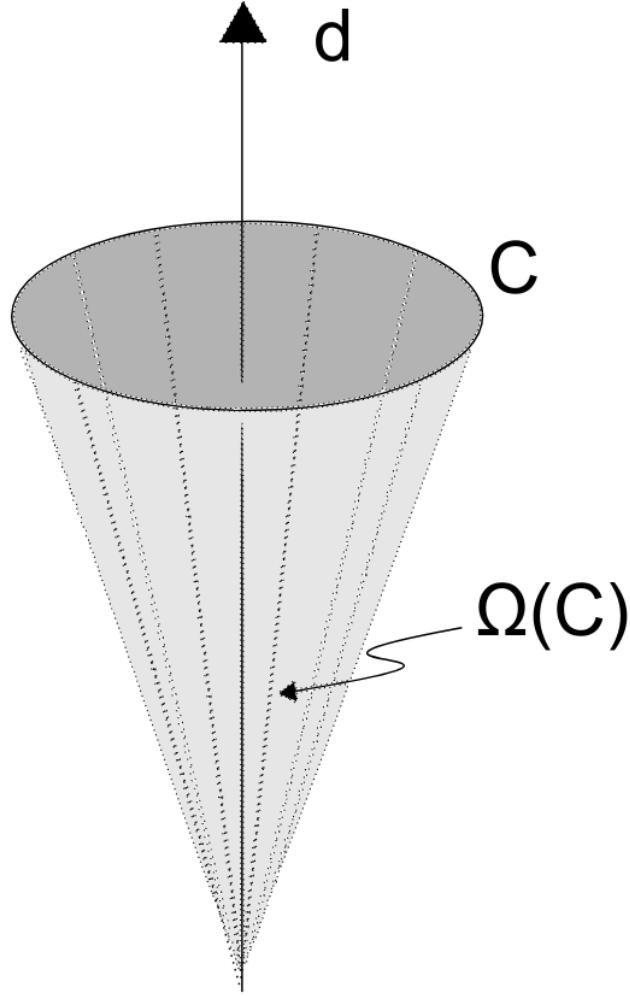


Figure 1.6: Evolution of a two-level Hamiltonian defined by a vector \mathbf{d} along a closed path \mathcal{C} . The corresponding Berry phase is found to be proportional to the solid angle subtended by that path

Defining the current as a functional derivative of the Hamiltonian with respect to the field,

$$J_i(x, t) = \frac{1}{2} ((p_i - eA)\delta(x - x_i) + \delta(x - x_i)(p_i - eA)) , \quad (1.22)$$

we can rewrite \mathcal{H} to first order in $A(x, t)$,

$$\mathcal{H} = \mathcal{H}_0 - e \int d^3x \sum_i A(x, t) j_i(x) \equiv \mathcal{H}_0 + \mathcal{H}_{\text{ext}}. \quad (1.23)$$

1.6 Linear response

Here \mathcal{H}_0 does no longer depend on $A(x, t)$, and $j_i = J_i - e\delta(x - x_i)A$ is the current without the diamagnetic component, which we drop since it ultimately will not contribute to the off-diagonal Hall conductivity.

The evolution of a state $|n\rangle$ with the full Hamiltonian \mathcal{H} can now be systematically approximated by the evolution with \mathcal{H}_0 and correction terms. We use the interaction picture to set apart the evolutions with \mathcal{H}_0 and \mathcal{H}_{ext} :

$$|n(t)\rangle = e^{-i\mathcal{H}_0 t} U_{\text{ext}}(t) |n\rangle, \quad (1.24)$$

where an expression for the propagator $U_{\text{ext}}(t)$ can be derived from the Schrödinger equation $i\partial_t |n(t)\rangle = \mathcal{H} |n(t)\rangle$ which implies $i\partial_t U_{\text{ext}} |n\rangle = \mathcal{H}_{\text{ext}}(t) U_{\text{ext}} |n\rangle$; the field-dependent Hamiltonian is evolved with the static one: $\mathcal{H}_{\text{ext}}(t) = e^{i\mathcal{H}_0 t} \mathcal{H}_{\text{ext}} e^{-i\mathcal{H}_0 t}$. Integrating this result leaves us with

$$U_{\text{ext}}(t) = 1 - i \int_0^t dt' \mathcal{H}_{\text{ext}}(t') U_{\text{ext}}(t'), \quad (1.25)$$

the solution of which to first order in \mathcal{H}_{ext} is given by

$$U_{\text{ext}}(t) = 1 - i \int_0^t dt' \mathcal{H}_{\text{ext}}(t'). \quad (1.26)$$

Having found an expression for the evolution of states with \mathcal{H} , we can now also evolve operator expectation values: for the current we obtain

$$\langle N(t) | J_i | N(t) \rangle = \langle N | j_i | N \rangle + i \int_0^t dt' \langle N | [\mathcal{H}_{\text{ext}}, j_i] | N \rangle \quad (1.27)$$

$$= \langle N | j_i | N \rangle + \int_{-\infty}^{\infty} dt' \int d^3x \sum_j R_{ij}(x - x', t - t') A_j(x', t'), \quad (1.28)$$

if we assume the field to be switched on like a Heaviside function, $\theta(t)$. The integration kernel R is then given by

$$R_{ij}(x - x', t - t') = -i\theta(t - t') \langle N | [j_i(x, t), j_j(x', t')] | N \rangle - ne\delta_{ij}\delta(x - x')\delta(t - t'). \quad (1.29)$$

Once again, we disregard the second term in the following since it is diagonal. The remaining term is referred to as a *retarded Green's function* G^R . So far, we have learned that to find the linear response of the current to a field is given by the integral of an expectation value of current-current commutators. Moreover, the relation between this result and the Hall conductivity is now easy to see: if we translate the above result into Fourier space, the convolution theorem implies

that the evolved current expectation value is equal to a product of the Fourier-transformed R and the vector potential A , i.e.

$$\langle j_i(\mathbf{q}, \omega) \rangle = R_{ij}(\mathbf{q}, \omega) A_j(\mathbf{q}, \omega) = \frac{i}{\omega} R_{ij}(\mathbf{q}, \omega) E_j(\mathbf{q}, \omega), \quad (1.30)$$

where we used the definition of the electric field, $E = \partial_t A$. Since this statement is in the form of Ohm's law, we conclude $\sigma_{ij}(\mathbf{q}, \omega) = \frac{i}{\omega} R_{ij}(\mathbf{q}, \omega)$, and hence the calculation of $R_{ij}(\mathbf{q}, \omega)$ will indeed produce the conductivity σ_{ij} .

The path that leads to the final result for $R_{ij}(\mathbf{q}, \omega)$ is both rather arduous and well-documented, cf. chap. 3 of [10], so we shall content ourselves with conveying the main steps. Returning to the two-dimensional Hamiltonian 1.20, we first need to find an expression for the current j . This is done by invoking the continuity equation $\dot{\rho} + \nabla \cdot \mathbf{J} = 0$, Fourier transforming it and using the equation of motion to arrive at

$$\mathbf{j}_q = \sum_k c_{k+q/2}^\dagger \frac{\partial h(k)}{\partial k_i} c_{k-q/2}. \quad (1.31)$$

The task at hand is thus to compute expectation values of quartic expressions in the fermion operators. One way to attack this problem is to first consider the imaginary-time-ordered Green's function G^T , for which the quartic term can be split into quadratic terms by means of Wick's theorem. These can then easily be computed. To return from this intermediary result to the retarded Green's function, one can observe that G^T is periodic in time and that its Fourier coefficients can be analytically continued to yield G^R . After taking care of orbital degrees of freedom, we can write the result for the Hall conductivity in the long-wavelength, zero-temperature, and zero-frequency limits in terms of Bloch states $|m k\rangle$ as

$$\sigma_{ij} = \int_{\text{BZ}} \frac{d^2 k}{4\pi^2} \sum_m (\langle \partial_j(m k) | \partial_i(m k) \rangle - (i \leftrightarrow j)), \quad (1.32)$$

where m and k denote the Bank index and momentum, respectively. Finally, we recognize the integrand as the Berry curvature, here being integrated not over the interior of a path, but over the entire Brillouin zone.

1.7 CHERN NUMBER

The central feature of the Hall conductivity – its quantization – has not yet been exhibited, but can be made apparent in the result (1.32). This shall be the

1.7 Chern number

last goal of the present article. We shall continue to follow [10]. Restoring all prefactors and adopting the notation from section 1.5, we have

$$\sigma_{xy} = \frac{e^2}{h} \frac{1}{2\pi i} \int_{\text{BZ}} d\mathbf{k} \cdot \nabla \times \mathbf{A}(k). \quad (1.33)$$

Note that the Brillouin zone is a torus and in particular has no boundary; a naive application of Stokes's theorem would therefore always yield zero conductivity. This is not a valid conclusion, however, since there is no reason to expect the Berry potential $\mathbf{A}(k)$ to be defined on the entirety of the Brillouin zone. To illustrate the issue, we want to work in a gauge that makes a component of the Bloch states real: $|n k\rangle \mapsto e^{if(k)} |n k\rangle$ with the gauge factor $\psi_1(k) \equiv e^{if(k)} = |\langle k | e^{-i\theta} m : k_1 | / |\langle m | k \rangle_1|$. Now observe that f cannot be continuously defined on neighborhoods of zeros² k_0 of $|n k\rangle$.

The solution to this problem is to cut out small neighborhoods of these points,

$$R_\epsilon = \{k \in \text{BZ}: |k - k_0| < \epsilon, |\langle m | k_0 \rangle_1 = 0\} \quad (1.34)$$

and use a different gauge $\psi_2 \equiv e^{ig}$ there (see fig. 1.7).

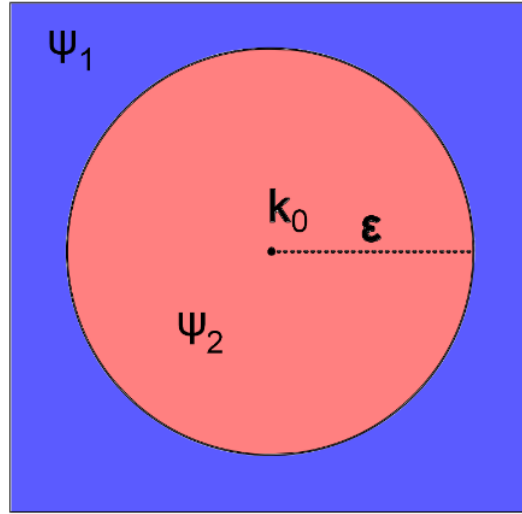


Figure 1.7: Illustration of our gauge convention near points k_0 where the gauge ψ_1 is ill-defined. We choose a different gauge on a small disk R_ϵ around such a point, which enables the use of Stokes' theorem on the entire Brillouin zone.

²An argument for the existence of such points is given in [9].

On the boundary ∂R_ϵ the different gauges are then related by the transformation $\psi_2 = e^{i\chi}\psi_1$, and the Berry potentials differ by a gradient: $\mathbf{A}_2 = \mathbf{A}_1 + \nabla\chi$. Thus we obtain

$$\sigma_{xy} = \frac{e^2}{h} \frac{1}{2\pi i} \left(\int_{\text{BZ}-R_\epsilon^s} d\mathbf{k} \cdot \nabla \times \mathbf{A}_1(k) + \int_{R_\epsilon^s} d\mathbf{k} \cdot \nabla \times \mathbf{A}_2(k) \right) \quad (1.35)$$

$$\stackrel{\text{Stokes}}{=} \frac{e^2}{h} \frac{1}{2\pi i} \int_{\partial R_\epsilon} d\mathbf{k} \cdot (\mathbf{A}_2(k) - \mathbf{A}_1(k)) = \quad (1.36)$$

$$= \frac{e^2}{h} \frac{1}{2\pi i} \int_{\partial R_\epsilon} d\mathbf{k} \cdot i\nabla\chi(k) \equiv \frac{e^2}{h} \nu, \quad (1.37)$$

where the integral

$$n \equiv \frac{1}{2\pi i} \int_{\partial R_\epsilon^s} d\mathbf{k} \cdot i\nabla\chi(k) \quad (1.38)$$

is indeed an integer since $e^{i\chi}$ is single-valued at each point of ∂R_ϵ and hence going around this boundary can only result in accumulation of phase for χ that is an integer multiple of $2\pi i$. This integer is referred to as a *Chern number*.

1.8 SUMMARY

We have given an account of two fundamentally different ways of deriving the integer quantization of Hall conductivity: On the one hand, we started from the description of electrons in a magnetic field to arrive the existence of edge currents and saw how these can give rise to a quantized Hall conductivity; on the other hand we used linear response theory in the bulk to produce a result that we identified as being connected to topological features of the band structure.

1.8 Summary

BIBLIOGRAPHY

- [1] M. Sigrist, *Solid state physics* (2013), <http://www.itp.phys.ethz.ch/education/fs13/sst/Lecture-Notes.pdf>.
- [2] M. O. Goerbig, *Quantum hall effects* (1999), <http://arxiv.org/abs/0909.1998v2>.
- [3] K. v. Klitzing, G. Dorda, and M. Pepper, *New method for high-accuracy determination of the fine-structure constant based on quantized hall resistance*, Phys. Rev. Lett. **45**, 494 (1980).
- [4] T. R. S. A. of Sciences, *Press release: The nobel prize in physics 1998* (1998), http://www.nobelprize.org/nobel_prizes/physics/laureates/1998/press.html.
- [5] R. B. Laughlin, *Quantized hall conductivity in two dimensions*, Phys. Rev. B **23**, 5632 (1981).
- [6] S. Girvin, *The quantum hall effect: Novel excitations and broken symmetries* (1998), <http://arxiv.org/abs/cond-mat/9907002v1>.
- [7] D. J. Thouless, M. Kohmoto, M. P. Nightingale, and M. den Nijs, *Quantized hall conductance in a two-dimensional periodic potential*, Phys. Rev. Lett. **49**, 405 (1982).
- [8] M. V. Berry, *Quantal phase factors accompanying adiabatic changes*, Proceedings of the Royal Society of London. Series A, Mathematical and Physical Sciences **392**, pp. 45 (1984), ISSN 00804630.
- [9] M. Kohmoto, *Topological invariant and the quantization of the Hall conductance*, Annals of Physics **160**, 343 (1985).
- [10] B. A. Bernevig and T. L. Hughes, *Topological Insulators and Topological Superconductors* (Princeton University Press, 2013).

BIBLIOGRAPHY

CHAPTER 2

2D QUANTUM HALL EFFECT ON A LATTICE

LUDOVIC SCYBOZ

SUPERVISOR: ODED ZILBERBERG

Characterizing the properties of a Quantum Hall Effect Hamiltonian on the square lattice, the magnetic translation group is derived for a rational magnetic flux. The same formalism is applied to a tight-binding, nearest-neighbour hopping Hamiltonian, leading to the statement and solution of the Hofstadter problem. Band structure as well as topological order for the Hofstadter butterfly are apprehended both from the TKNN argument and the Diophantine equation. Finally, the topological nature of the Hall conductance is shown numerically to be related to the Chern number of localized edge states.

2.1 INTRODUCTION

Historically, the Quantum Hall Effect has always been synonym of an unimaginably deep thought pool for theoretical physicists. Next to the two-dimensional Integer Quantum Hall Effect in the continuum, whose existence was demonstrated by von Klitzing *et al.* [1] in 1980, one can consider 2D lattice electrons hopping from site to site in the presence of a strong magnetic field perpendicular to the lattice plane. We propose to address the problem of the two-dimensional Integer Quantum Hall Effect on the square lattice, which represents a simple and easily generalizable version of possibly more complicated systems displaying the same fundamental phenomena.

2.2 Magnetic Translation Group

While the 2D QHE is characterized in the continuum by the emergence of quantized Landau levels, the requirement of a periodic lattice potential discloses its own occurrences, along a wide range of distinct spectral structures. The crucial ingredient at play in the continuum view of the QHE, i.e. the cyclotron motion of electrons, will be challenged by a new length scale introduced through the interplay between lattice and magnetic flux. This will in turn lead to the splitting of Landau levels into a number of subbands, each of which will variably contribute to the Hall conductivity: in general, the spectrum will be revealed to be topologically non-trivial. While the lattice spacing is usually too small for typical lattice effects to be observed (in this limit, the system behaves like in the continuum case), recent experiments [2] have shown that 2D crystals engineered specifically to increase the effective lattice constant behave as was theoretically predicted.

In this chapter, we propose to review the advancements accomplished in the domain of the 2D QHE on a lattice, largely following the thread woven by Bernevig in the Chapters 5-6 of his book, *Topological Insulators and Topological Superconductors*. More specifically, Ch. 2.2 will derive a new translation symmetry for the lattice unit cell once the magnetic field is introduced. This formalism will then be applied to the Hofstadter problem, and will help to uncover the spectral and topological properties of the Hofstadter butterfly. As a more general overview, Ch. 2.3 and 2.4 will give an outlook on two natural tools, namely the Středa formula and the Diophantine equation, which will help consolidate our understanding of lattice-applied problems and obtain an intuition for the quantization of the Hall conductivity. Finally, a brief epilogue constituting Ch. 2.5 will give the reader, supposing he is acquainted with the analogous phenomenon in the continuum framework, a recalling of the articulation between non-zero Hall conductivity and edge states.

2.2 MAGNETIC TRANSLATION GROUP

2.2.1 PEIERLS SUBSTITUTION

First, from a want to accomodate the mechanics from the continuum problem to a lattice model where electrons move in the presence of atoms, we may use the tight-binding approximation: the physical description of the problem as well as its numerical computation then greatly simplify. Starting from a generic tight-binding Hamiltonian $\mathcal{H} = \sum_{mna\beta} c_{ma}^\dagger h_{mn}^{\alpha\beta} c_{n\beta}$, the description of electron motions on the lattice is particularly straightforward: the electron positions are discretized and their wavefunctions are localized around lattice sites. Yet they are able to

hop from lattice position m to n and degree of freedom (atom type in the unit cell, orbital, spin) α to β with an energy cost $h_{mn}^{\alpha\beta}$. This hopping constant can be interpreted as a complex amplitude for the probability of hopping, and encodes the whole effect of the restraining atom potential. The electrons will be assumed to be spinless throughout this chapter: furthermore, the lattice and hopping constants will be set to 1 for simplicity's sake.

Keeping in mind that this second-quantized, tight-binding formulation of the Hamiltonian comes in handy, we would like to consider adapting it to the peculiar context of the Quantum Hall Effect. By introducing a magnetic field perpendicular to the lattice plane, the Hamiltonian is modified by the gauge-dependent magnetic potential \mathbf{A} according to the minimal coupling principle, $\mathbf{p} \rightarrow \mathbf{p} - \frac{e}{c}\mathbf{A}$. Instead of deriving a new tight-binding Hamiltonian, Peierls proposed [3] to incorporate the Aharonov-Bohm phase collected by an electron moving in the presence of an \mathbf{A} potential around a closed path into the hopping constant: moving along a path from m to n , the electron's wavefunction picks up a phase proportional to the path integral of the magnetic potential, where the magnetic flux is given in units of flux quanta $\phi_0 = h/e$:

$$h_{mn}^{\alpha\beta} \rightarrow h_{mn}^{\alpha\beta} e^{i\frac{1}{\phi_0} \int_m^n \mathbf{A} \cdot d\mathbf{l}} \quad (2.1)$$

2.2.2 MAGNETIC UNIT CELL

Now, one can see that even if the magnetic field \mathbf{B} is homogeneous, the magnetic potential \mathbf{A} breaks the translation symmetry of the lattice: the translation operators by one lattice constant in x - or y -direction do not commute with the Hamiltonian anymore, and a new set of good quantum numbers has to be found. Formally, re-writing the Hamiltonian as a sum of translation operators $\mathcal{H} = T_x + T_y + h.c.$,

$$\begin{aligned} T_x &= \sum_{mn} c_{m+1,n}^\dagger c_{mn} e^{i\vartheta_{mn}^x}, & \vartheta_{mn}^x &= \int_m^{m+1} \mathbf{A} \cdot d\mathbf{l} \\ T_y &= \sum_{mn} c_{m,n+1}^\dagger c_{mn} e^{i\vartheta_{mn}^y}, & \vartheta_{mn}^y &= \int_n^{n+1} \mathbf{A} \cdot d\mathbf{l} \end{aligned} \quad (2.2)$$

one can apply these translation operators T_x , T_y to the one-site state $|\psi_{mn}\rangle = c_{mn}^\dagger |0\rangle$ and compute $T_x T_y \psi_{mn}$ as well as $T_y T_x \psi_{mn}$. For a general gauge, we have $[T_x, T_y] \neq 0$: the translation operators do not commute. To help simplify some formulae, let us introduce *lattice derivatives* as discretized differences $\Delta_x f_{mn} = f_{m+1,n} - f_{mn}$ and $\Delta_y f_{mn} = f_{m,n+1} - f_{mn}$ for any function on the lattice. Moreover, the lattice curl of the phase factors introduced above relates to the magnetic flux by:

2.2 Magnetic Translation Group

$$\begin{aligned}\text{rot} \vartheta &= \Delta_x \vartheta_{mn}^y - \Delta_y \vartheta_{mn}^x = \vartheta_{m+1,n}^y - \vartheta_{mn}^y - \vartheta_{m,n+1}^x + \vartheta_{mn}^x \\ &= \frac{e}{\hbar} \int_C \mathbf{A} \cdot d\mathbf{l} = 2\pi \frac{e}{\hbar} \int B \cdot dS = 2\pi \phi_{mn}\end{aligned}\quad (2.3)$$

Note that the magnetic flux is expressed in units of ϕ_0 . With these preliminaries, the usual canonical commutation relations can be applied to the translation operators T_x and T_y , and one might easily compute $T_x T_y |\psi_{mn}\rangle = T_x c_{m,n+1}^\dagger e^{i\vartheta_{mn}^y} |0\rangle = e^{i(\vartheta_{m,n+1}^x + \vartheta_{mn}^y)} c_{m+1,n+1}^\dagger |0\rangle$ and $T_y T_x |\psi_{mn}\rangle = T_y c_{m+1,n}^\dagger e^{i\vartheta_{mn}^x} |0\rangle = e^{i(\vartheta_{m+1,n}^y + \vartheta_{mn}^x)} c_{m+1,n+1}^\dagger |0\rangle$.

On a physical standpoint, the successive application of the translation operators gives different phase factors, depending on whether the electron moves along the path $(m, n) \rightarrow (m+1, n) \rightarrow (m+1, n+1)$ or $(m, n) \rightarrow (m, n+1) \rightarrow (m+1, n+1)$ (see Fig. 2.1). For a given magnetic flux, the translation operators generally don't commute: using Eq. 2.3, one obtains $T_y T_x |\psi_{mn}\rangle = e^{i2\pi\phi_{mn}} T_x T_y |\psi_{mn}\rangle$. This means that the translation operators generally do not commute with the Hamiltonian (which is a sum of both T_x and T_y). How can we modify the translation operators to overcome this violation of the original translation symmetry?

Since the only degree of freedom left is the gauge choice for the magnetic potential A , one might consider the following reasonable ansatz for new commuting operators:

$$\begin{aligned}\widehat{T}_x &= \sum_{mn} c_{m+1,n}^\dagger c_{mn} e^{i\chi_{mn}^x} \\ \widehat{T}_y &= \sum_{mn} c_{m,n+1}^\dagger c_{mn} e^{i\chi_{mn}^y}\end{aligned}\quad (2.4)$$

where χ_{mn}^x, χ_{mn}^y are requested to fulfill the commutation relations $[\widehat{T}_x, T_x] = [\widehat{T}_x, T_y] = 0$, and analogously for \widehat{T}_y . These operators are named *magnetic translation operators*. The commutation requirements yield four equations for the new phase factor χ_{mn} ,

$$\begin{aligned}\Delta_x \chi_{mn}^x &= \Delta_x \vartheta_{mn}^x, \quad \Delta_y \chi_{mn}^x = \Delta_x \vartheta_{mn}^y = \Delta_y \vartheta_{mn}^x + 2\pi \phi_{mn} \\ \Delta_y \chi_{mn}^y &= \Delta_y \vartheta_{mn}^y, \quad \Delta_x \chi_{mn}^y = \Delta_y \vartheta_{mn}^x = \Delta_x \vartheta_{mn}^y - 2\pi \phi_{mn}.\end{aligned}\quad (2.5)$$

Solutions to these requirements are given by $\chi_{mn}^x = \vartheta_{mn}^x + 2\pi n \phi_{mn}$ and $\chi_{mn}^y = \vartheta_{mn}^y - 2\pi m \phi_{mn}$. Note that both ϑ_{mn} and χ_{mn} describe the same magnetic flux through each plaquette, being related to the same magnetic potential up to a gauge phase. The original symmetry has now been partially restored: the magnetic translation operators commute with the Hamiltonian. Trying to express the latter in terms of the formers, one might still be concerned that the magnetic translation operators do not commute with each other. Applying them once more to the (m, n) -state $|\psi_{mn}\rangle = c_{mn}^\dagger |0\rangle$, the commutation indeed yields $\widehat{T}_x \widehat{T}_y |\psi_{mn}\rangle = e^{i(\chi_{m,n+1}^x + \chi_{mn}^y)} c_{m+1,n+1}^\dagger |0\rangle$, whereas $\widehat{T}_y \widehat{T}_x |\psi_{mn}\rangle = e^{i(\chi_{mn}^x + \chi_{m+1,n}^y)} c_{m+1,n+1}^\dagger |0\rangle$.

Let us choose a Landau gauge $A_y = B \cdot x = 2\pi\phi m$. Computing $\widehat{T}_x \widehat{T}_y = e^{i(\Delta_y \chi_{mn}^x - \Delta_x \chi_{mn}^y)} \widehat{T}_y \widehat{T}_x = e^{i(\Delta_x \vartheta_{mn}^y - \Delta_y \vartheta_{mn}^x)} \widehat{T}_y \widehat{T}_x = e^{i2\pi\phi} \widehat{T}_y \widehat{T}_x$, both operators still do not commute for a general flux. Yet, considering the additional requirement that the flux be rational, $\phi = p/q$ for p and q coprime, and applying the translation operator in x -direction q times yields:

$$\widehat{T}_x^q \widehat{T}_y = e^{i2\pi\phi q} \widehat{T}_y \widehat{T}_x^q = e^{i2\pi p} \widehat{T}_y \widehat{T}_x^q = \widehat{T}_y \widehat{T}_x^q \quad (2.6)$$

We conclude that the translation operators \widehat{T}_x^q and \widehat{T}_y define a new set of good quantum numbers, and describe a modified translation symmetry. Indeed, still with respect to the Landau gauge, these can be expressed as $\widehat{T}_x = \sum_{mn} c_{m+1,n}^\dagger c_{mn} e^{i2\pi n\phi}$ and $\widehat{T}_y = \sum_{mn} c_{m,n+1}^\dagger c_{mn}$; the commuting operators \widehat{T}_x^q , respectively \widehat{T}_y , translate a bound electron state by q lattice constants in x -direction, respectively one lattice constant in y -direction: $\widehat{T}_x^q c_{mn}^\dagger |0\rangle = c_{m+q,n}^\dagger |0\rangle$, as well as $\widehat{T}_y c_{mn}^\dagger |0\rangle = c_{m,n+1}^\dagger |0\rangle$.

In summary, the original translation symmetry of the square lattice is broken by the introduction of the magnetic potential in the Hamiltonian. Still, if the magnetic flux per plaquette is considered to be rational, $\phi = p/q$, the spatial square unit cell may be replaced with a q -times greater *magnetic unit cell*: especially, in the Landau gauge, the new unit cell has a width of q -times the lattice constant in x -direction, and one lattice constant in y -direction.

Finally, now that a translation symmetry has been restored, we may label the states by their new good quantum number, namely momentum. The boost operators in Fourier space simply have to be replaced by their magnetic counterparts:

$$\begin{aligned} \mathcal{H}|\mathbf{k}\rangle &= E(\mathbf{k})|\mathbf{k}\rangle \\ \widehat{T}_x^q |\mathbf{k}\rangle &= e^{iqk_x} |\mathbf{k}\rangle \\ \widehat{T}_y |\mathbf{k}\rangle &= e^{ik_y} |\mathbf{k}\rangle \end{aligned} \quad (2.7)$$

2.2.3 ENERGY DEGENERACY

Remark that the energy degeneracy of such a Quantum Hall system can be read off in a straightforward fashion by considering the magnetic translation group formalism. Assuming $|k_x, k_y\rangle$ to be an eigenstate of the Hamiltonian \mathcal{H} and using the fact that the latter commutes with \widehat{T}_x , \widehat{T}_y , the state $\widehat{T}_x |k_x, k_y\rangle$ has to be an eigenstate of \mathcal{H} , albeit at another momentum wavevector. Noticing that $\widehat{T}_y \widehat{T}_x |k_x, k_y\rangle = e^{-i2\pi\phi} \widehat{T}_x \widehat{T}_y |k_x, k_y\rangle = e^{i(k_y - 2\pi\phi)} \widehat{T}_x |k_x, k_y\rangle$ and by comparison with Eq. 2.7, it can be ascertained that $\widehat{T}_x |k_x, k_y\rangle = |k_x, k_y - 2\pi\phi\rangle$ has the same energy as $|k_x, k_y\rangle$. Since $\phi = p/q$, the magnetic translation operator \widehat{T}_x may be applied

2.2 Magnetic Translation Group

$q - 1$ times to yield q different wavevectors with equal energy eigenvalue: the spectrum is q -fold degenerate.

2.2.4 HARPER'S EQUATION

Let's consider one more time the original tight-binding Hamiltonian in the presence of a magnetic flux per plaquette $\phi = p/q$ in the Landau gauge,

$$\mathcal{H} = \sum_{mn} -t_a c_{m+1,n}^\dagger c_{mn} - t_b c_{m,n+1}^\dagger c_{mn} + h.c. \quad (2.8)$$

where we have set the hopping constant in x -direction to be $-t_a$, in y -direction $-t_b$. To diagonalize this Hamiltonian and infer its more interesting properties (namely topological order), let us Fourier-transform it to momentum space. First transform the fermionic creation and annihilation operators:

$$c_{mn} = \frac{1}{2\pi^2} \int_{-\pi}^{\pi} dk_x \int_{-\pi}^{\pi} dk_y e^{i(k_x m + k_y n)} c_{k_x, k_y} \quad (2.9)$$

By explicitly computing the transformation of the Hamiltonian, a (somewhat expected) surprise presents itself. For $-\pi \leq k_x, k_y \leq \pi$, the Peierls phase accompanying the Hamiltonian mixes different k_x areas, making it undiagonalizable in k_y . Indeed, we obtain a mixed expression in k_y along the nearest-neighbour hopping term in k_x :

$$\begin{aligned} \mathcal{H} = & \frac{1}{(2\pi)^2} \int_{-\pi}^{\pi} dk_x \int_{-\pi}^{\pi} dk_y \left[-2t_a \cos(k_x) c_{k_x, k_y}^\dagger c_{k_x, k_y} \right. \\ & \left. - t_b \left(e^{-ik_y} c_{k_x+2\pi\phi, k_y}^\dagger c_{k_x, k_y} + e^{ik_y} c_{k_x-2\pi\phi, k_y}^\dagger c_{k_x, k_y} \right) \right] \end{aligned} \quad (2.10)$$

Of course, this undesired effect should have been prevented: knowing that the magnetic unit cell is q -times larger than the original spatial unit cell, we surmise that the magnetic Brillouin zone area has been reduced by a factor q . Re-dimensionalizing the magnetic Brillouin zone with $-\pi/q \leq k_{x,0} \leq \pi/q$, $-\pi \leq k_y \leq \pi$, the Hamiltonian is transformed into

$$\mathcal{H} = \frac{1}{2\pi^2} \int_{-\pi/q}^{\pi/q} dk_{x,0} \int_{-\pi}^{\pi} dk_y \hat{\mathcal{H}}(k_{x,0}, k_y) \quad (2.11)$$

with the substitution $k_x = k_{x,0} + 2\pi\phi n$, and the integrand given as:

$$\hat{\mathcal{H}} = \sum_{n=0}^{q-1} \left[-2t_a \cos(k_{x,0} + 2\pi\phi n) c_{k_{x,0}+2\pi\phi n, k_y}^\dagger c_{k_{x,0}+2\pi\phi n, k_y} \right. \\ \left. - t_b \left(e^{-ik_y} c_{k_x+2\pi\phi(n+1), k_y}^\dagger c_{k_x+2\pi\phi n, k_y} \right. \right. \\ \left. \left. + e^{ik_y} c_{k_x+2\pi\phi(n-1), k_y}^\dagger c_{k_x+2\pi\phi n, k_y} \right) \right] \quad (2.12)$$

As of now, the Hamiltonian does not mix different k_x areas anymore, but is rather composed as a sum of q states at different momenta. The form of the Schrödinger equation $\hat{\mathcal{H}}(k_{x,0}, k_y)|\psi\rangle = E(k_{x,0}, k_y)|\psi\rangle$ suggests that since $\hat{\mathcal{H}}$ is expressed as a q -site operator at different momenta, a plausible eigenstate would be represented by the same expansion, $|\psi\rangle = \sum_{n=0}^{q-1} a_n c_{k_{x,0}+2\pi\phi n, k_y}^\dagger |0\rangle$. The Schrödinger equation for the eigenstate then becomes an equation for the expansion coefficients a_n , namely $-2t_a \cos(k_{x,0} + 2\pi\phi n) a_n - t_b (e^{-ik_y} a_{n-1} + e^{ik_y} a_{n+1}) a_n = E \cdot a_n$. Finally, in prevision to the computation of the eigenvalues in a linear framework, the substitution $a_n = b_n e^{-ik_y n}$ yields the final form of the Harper equation:

$$-2t_a \cos(k_{x,0} + 2\pi\phi n) b_n - t_b b_{n-1} - t_b b_{n+1} = E(k_{x,0}, k_y) b_n \quad (2.13)$$

Although the explicit dependency on k_y seems to disappear, in reality it is only embedded in the boundary condition on b_n : the periodicity of a_n leads to $b_{n+q} = e^{ik_y q} b_n$. Note that under this form, the q -fold energy degeneracy can be written unequivocally as $E(k_{x,0}, k_y) = E(k_{x,0}, k_y + \frac{2\pi n}{q})$. In matrix notation, the corresponding eigenvalue problem is solvable, for $v_i = -2t_a \cos(k_{x,0} + 2\pi\phi i)$,

$$\begin{vmatrix} v_1 - E & -t_b & 0 & \dots & 0 & -t_b e^{-iqk_y} \\ -t_b & v_2 - E & -t_b & \dots & 0 & 0 \\ 0 & -t_b & v_3 - E & \ddots & \vdots & \vdots \\ \vdots & \vdots & \ddots & \ddots & -t_b & 0 \\ 0 & 0 & \dots & -t_b & v_{q-1} - E & -t_b \\ -t_b e^{iqk_y} & 0 & \dots & 0 & -t_b & v_q - E \end{vmatrix} = 0 \quad (2.14)$$

In general, for this $q \times q$ matrix, the eigenvalue problem has q solutions for the energy. In the next subsection, we will ascertain that not only are there q energy eigenvalues, but there is also invariably a gap opening between the different bands, each of which contributes to the Hall current according to their Chern number.

2.2.5 THE HOFSTADTER BUTTERFLY

By solving the Harper equation (Eq. 2.14) for different values of the magnetic flux per plaquette $\phi = p/q$ and plotting their respective energy eigenvalues, we obtain in Fig. 2.3 the so-called *Hofstadter butterfly* (originally [4]). It depicts

2.2 Magnetic Translation Group

the energy spectrum as a function of the magnetic flux $\phi = p/q$, and exhibits a fractal, self-similar configuration. As ϕ varies, the fundamental gap structure, but also its topological properties, vary. Thouless, Kohmoto, Nightingale and de Nijs (TKNN) proposed an argument [5] to support the existence of a gapped energy band spectrum. Their idea is the following: first, assume the hopping in y -direction is disabled, *i.e.* $t_b = 0$. The two-dimensional system is then composed of parallel, uncoupled one-dimensional wires. The energy eigenvalue solutions may be directly read off the Harper equation, $E_m(k_{x,0}, k_y) = -2t_a \cos(k_{x,0} + 2\pi\phi m)$, as can be read in Fig. 2.2 on the left. As such, the dispersion in k_y is nonexistent, and bands cross at $k_{x,0} = 0, \pm \frac{\pi}{q}$ in the magnetic Brillouin zone. If the hopping in y -direction is turned on, $t_b \neq 0$, the degeneracy at the crossing points is lifted, and a gap opens. Since the bands cross at $q - 1$ different energy values, a total of $q - 1$ gaps open in general (discounting the bottom and top bands).

To determine topological order for the Hofstadter problem, one might numerically compute the Chern number of all filled bands to find the Hall conductivity. Formally, if the Fermi level stands in the r -th gap, its Hall conductivity consists of the integral over the Brillouin zone of the Berry curvature $\mathcal{F}_{xy}(\mathbf{k}) = \nabla_{\mathbf{k}} \times \mathbf{A}(\mathbf{k})$:

$$\sigma_{xy} = \frac{e^2}{h} \frac{1}{2\pi} \iint dk_x dk_y \mathcal{F}_{xy}(\mathbf{k}) = \frac{e^2}{h} t_r \quad (2.15)$$

where $\mathbf{A}(\mathbf{k}) = -i \sum \langle n(\mathbf{k}) | \nabla_{\mathbf{k}} | n(\mathbf{k}) \rangle$ is the Berry potential. Note that in the computation of the Berry potential, the sum runs over all filled bands, $1 \leq n \leq r - 1$. Naturally enough, we find that the Chern number t_r is an integer and comes from the contribution of all filled bands, which contrary to the 2D Quantum Hall Effect can take any integer value¹. By assigning a color code to the Chern number value of each gap, so arises the so-called *colored Hofstadter butterfly* [6]. The figure obtained in this fashion exhibits the topological nature of the problem (see Fig. 2.3).

Along their proof of a gap opening in the energy band spectrum, TKNN also argued that the gaps are generally associated with a non-vanishing Chern number. Returning to the perspective where gaps emerge from the splitting of perturbed degenerate crossings, topological order stems from the coupling between the various energy bands $E_m = -2t_a \cos(k_{x,0} + 2\pi\phi m)$. Indeed, for two energy bands m_1 and m_2 crossing in the magnetic Brillouin zone, the coupling is given as $\Delta \cdot e^{-ik_y t_r}$, where $\Delta \sim t_b^{t_r}$ and $t_r \in \mathbb{Z}$ is the order of the coupling. Recalling that the term $-t_b (e^{-ik_y} b_{n-1} + e^{ik_y} b_{n+1})$ in Harper's equation only couples adjacent

¹Typically, in the integer QHE, the filled Landau levels contribute one integer multiple of $\frac{e^2}{h}$ to the Hall conductivity (Chern number 1).

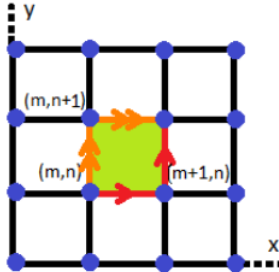


Figure 2.1: General square lattice for the tight-binding approximation: electrons' positions are required to be multiple of the lattice constant, and a perpendicular magnetic field per plaquette frustrates the nearest-neighbour hopping Hamiltonian. The translation operators clearly do not commute: the Peierls phase is different whether the electron follows the single- or the double-arrowed path.

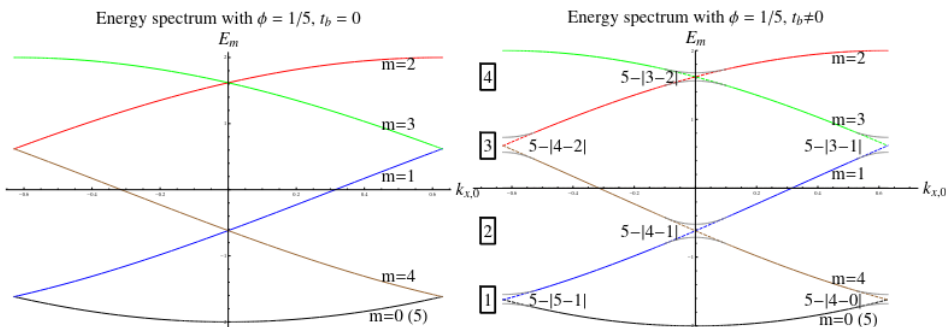


Figure 2.2: On the left is the energy spectrum in the case of a turned off coupling in y -direction. The energy eigenvalues are cosine functions of $k_{x,0}$. On the right, the same dependence is depicted with a non-vanishing coupling term $t_b \neq 0$. The gap number is indicated on the left (framed number) and is shown to correspond to $q - |m_1 - m_2|$ for two crossing bands m_1, m_2 .

2.3 Středa Formula

sites, we need to apply perturbation theory several times to couple wavefunctions localized at distant sites (the reader is invited to work this out with the help of Fig. 2.2). By carefully labelling the energy bands, one might control that $t_r = \min\{|m_1 - m_2|, q - |m_1 - m_2|\}$. Solving for the perturbed energy eigenvalues

$$\begin{pmatrix} \epsilon & \Delta \cdot e^{-ik_y t_r} \\ \Delta \cdot e^{ik_y t_r} & -\epsilon \end{pmatrix} \begin{pmatrix} \psi_{m_1} \\ \psi_{m_2} \end{pmatrix} = E \begin{pmatrix} \psi_{m_1} \\ \psi_{m_2} \end{pmatrix} \quad (2.16)$$

the Hall conductivity arising from the mixing of both bands m_1, m_2 can be computed through $\sigma_{xy} = \frac{e^2}{h} \frac{1}{2\pi i} \int d^2k [\nabla_k \times (\psi^* \nabla_k \psi)] = \frac{e^2}{h} (t_r - t_{r-1})$. Note that $t_r - t_{r-1}$ is the Chern number of the band standing between the $(r-1)$ -th and r -th gap. In summary, the Chern number t_r of the r -th gap is strictly given as the order to which the different bands couple to form this gap when degeneracy is lifted (for a direct proof, see [7]).

As a final remark, the structure of the energy spectrum can be outlined as a function of q from the direct analysis of the characteristic polynomial in the matrix form of the Harper equation, see Eq. 2.14. It can be shown very straightforwardly that energy bands never touch if q is odd, therefore that gaps are strictly open in that case. The situation is different if q is even: then, the two bands found symmetrically around $E = 0$ touch in q different points, and form Dirac nodes at the following momenta:

$$\begin{cases} k_{x,0} = 0, & k_y = \frac{2\pi m}{q} & \text{if } q = 4n \\ k_{x,0} = \pm \frac{\pi}{q}, & k_y = \frac{(2m+1)\pi}{q} & \text{if } q = 4n + 2 \end{cases} \quad (2.17)$$

2.3 STŘEDA FORMULA

The achieved solution to the Harper equation presented above gives rise to a specific question: how can the physics accomodate such a discontinuous problem? As we already emphasized, the structure of the energy spectrum does not depend on the absolute value of the magnetic flux per plaquette $\phi = p/q$, but rather solely on the denominator q of its fractional representation. This means that even an infinitesimal change in the amplitude of the magnetic field breeds tremendous changes in the spectrum. As a matter of fact, Wannier, who was Hofstadter's thesis advisor, was bothered by this very unphysical spectral discontinuity: he came up with a smoother interpretation of the butterfly, tracking the density of states rather than the gap labelling itself.

To highlight the more continuous form of the Hofstadter problem, consider the definition of the transversal Hall conductivity $j_i = \sigma_H \epsilon_{ij} E_j$. The conservation of

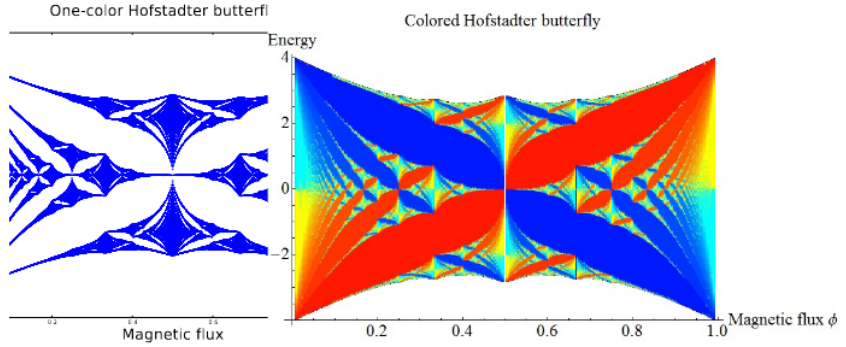


Figure 2.3: Energy spectrum depending on the magnetic flux ϕ . The spectrum is obviously discrete and self-similar. On the right, the gaps are colored according to their Chern number: red hues are for positive, blue hues for negative Chern numbers. The greater the Chern number, the more luminous the color.

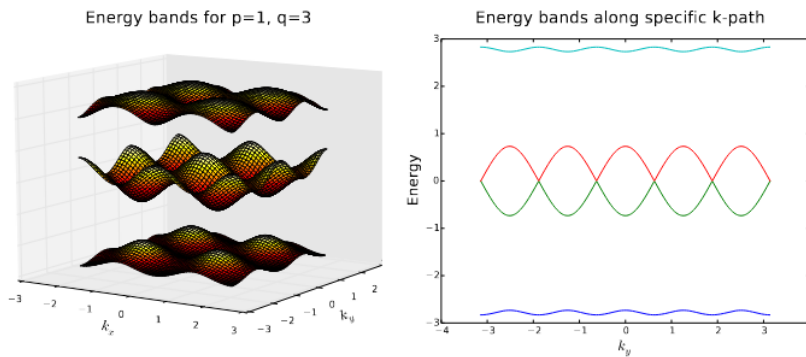


Figure 2.4: On the left, the energy bands $E(k_{x,0}, k_y)$ are shown for $\phi = 1/3$: the gaps between the three bands are all open. On the right, the situation is depicted for $\phi = 1/4$: as expected, the spectrum is composed of four bands, but the two bands around $E = 0$ touch. Here, energy values are swept along a path in $(k_{x,0}, k_y)$ -space through the Dirac points.

2.4 Diophantine Equation

the four-current can be written as $\frac{\partial \rho_{el}}{\partial t} = -\nabla \cdot \mathbf{j} = -\sigma_{xy} \left(\frac{\partial E_y}{\partial x} - \frac{\partial E_x}{\partial y} \right) = \sigma_{xy} \frac{\partial B}{\partial t}$, where we used the Faraday law in the third equality. Finally, linking the electric density ρ_{el} to the density of states ρ_{states} results in the *Středa formula*:

$$\sigma_{xy} = \frac{\partial \rho_{el}}{\partial B} = \frac{e^2}{\hbar} \frac{1}{V} \frac{\partial \rho_{states}}{\partial B} \quad (2.18)$$

where $B \cdot V$ is the magnetic flux per unit cell, and V the unit cell area. Hence, the Hall conductivity is proportional to the derivative of the density of states with respect to the magnetic field. This behaviour is also rendered more understandable by *Wannier plots*: both the lines of constant chemical potential and the density of states evolve continuously with the magnetic flux, as shown in Fig. 2.5.

2.4 DIOPHANTINE EQUATION

More than just demonstrating the background continuity in the seemingly discontinuous Hofstadter butterfly, the Středa formula is a decisive step in the derivation of the Diophantine equation. The coming subsection reveals a very simple formulation of the Hall conductivity for the square lattice. Let us rephrase the original Quantum Hall Effect on the lattice in parametric terms: for a bulk insulating system with Fermi level in the r -th gap, where $0 \leq r \leq q$ (this time labelling the bottom and top gaps as well) and a rational magnetic flux $\phi = p/q$ perpendicular to the lattice plane, the system is described by the three integer parameters $r \in [0, q], p, q \in \mathbb{N}$, where p and q are coprime. The Darboux theorem states that for three given integers r, p, q :

$$\exists t_r, s_r \in \mathbb{N}, |t_r| \leq \frac{q}{2} : \quad r = pt_r + qs_r \quad (2.19)$$

where the window on t_r guarantees the uniqueness of the solution (note that the Diophantine equation itself determines t_r only up to a modulo q ambiguity). Using the same symbol t_r for the solution of the Diophantine equation as in the TKNN perturbation argument, see Eq. 2.16, is no accident. Indeed, the integer t_r is precisely the Chern number of the r -th gap: if the Fermi level stands in the r -th gap, the density of states is easy to compute. Since there are r filled bands below the r -th gap, and the total number of bands is q , the density of states is given as $\rho_{states} = \frac{r}{q} = \frac{p}{q} t_r + s_r = \frac{BV}{2\pi} t_r + s_r$, where we used $BV = 2\pi\phi = 2\pi\frac{p}{q}$. Finally, inserting this expression for the density of states in the Středa formula yields

$$\sigma_{xy} = \frac{e^2}{\hbar} \frac{1}{V} \frac{\partial \rho_{\text{states}}}{\partial B} = \frac{e^2}{h} t_r \quad (2.20)$$

As a brief summary: for the square lattice, instead of computing the Chern number for a gap from the standard Berry formalism as in Eq. 2.15, one may directly deduce the Chern number by solving the Diophantine equation (Eq. 2.19). For a magnetic flux $\phi = p/q$, the Chern number of the r -th gap is the unique solution of Eq. 2.19 for t_r .

2.5 BULK-EDGE CORRESPONDENCE

Finally, although a real system has open gaps and is in practice a bulk insulator, the Hall conductivity is still found to be non-zero. Analogously to the case of the continuum QHE, there is a strong relation between the topological nature of the Hall current and the existence of localized edge states. By choosing periodic boundary conditions in one lattice direction and a finite sample size in the other direction (thereby artificially adding two edges to the system), one can again solve the Harper equation: in this case, since we got rid of spatial periodicity in one direction, the original Harper equation, see Eq. 2.13, will be Fourier-transformed in one momentum dimension only. The numerical solution of this problem (see Fig. 2.6) exhibits two kinds of states: q bulk bands, but also edge states existing in the various gaps. Note that the number of edge modes (therefore the Chern number) of such states can be inferred from their linking number. Using a constant Fermi level in the gap, the number of times the edge state "winds" around it (with a sign convention chosen beforehand) yields the Chern number of the gap times the number of edges. For example, in Fig. 2.6, the Chern number of the second gap is $t_2 = +4/2 = +2$ while that of the third is $t_3 = -4/2 = -2$ with a sign convention fixed arbitrarily at first.

2.6 CONCLUDING REMARKS

In summary, the following achievements were needed in order to build the theoretical construct befitting the 2D Quantum Hall Effect on a (square) lattice: first, acknowledging the violation of translational symmetry by the presence of a magnetic field, we tried to force its restoring, leading to the discovery of the magnetic translation group for a rational flux. This diagnosis then helped to unveil the discrete, fractal spectrum arising from a tight-binding, nearest-neighbour hopping Hamiltonian, namely the Hofstadter butterfly. The topological order

2.6 Concluding remarks

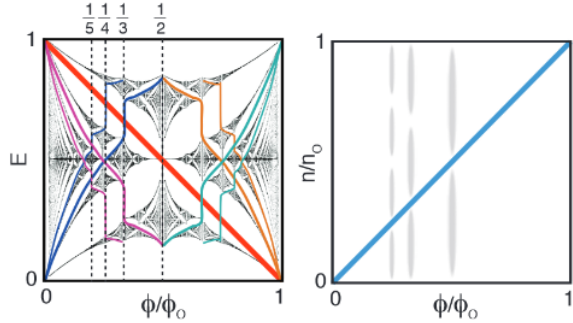


Figure 2.5: (C. Dean et al., *Hofstadter's butterfly in moiré superlattices*, 2012 [2]) Wannier plots emphasize variables depending continuously on the magnetic flux rather than the gap structure itself, which varies discontinuously with infinitesimal changes in the magnetic flux ϕ . On the left are depicted lines of constant chemical potential; on the right, the density of states n shows a linear dependence on the magnetic flux.

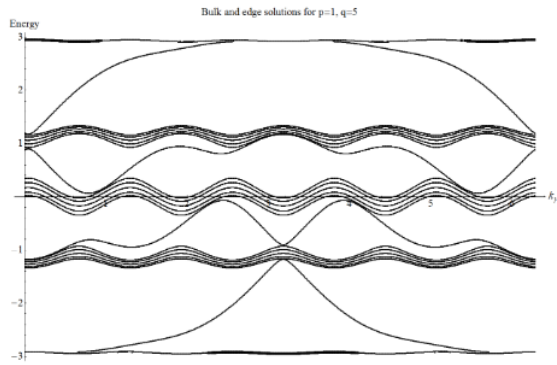


Figure 2.6: Edge modes connecting the bulk bands. Energy $E(k_y)$ is only depicted as a function of momentum k_y , assuming a finite sample size in the spatial x -direction. In each gap, one can compute the edge state's linking number around the gap and, recalling there are two edges for a two-dimensional plane with only one periodic boundary condition, deduce the gap's Chern number.

predicted by TKNN's argument was put numerically in evidence, showing a generally non-disappearing Chern number for each band on the Brillouin zone. Then, trying to bypass the Berry formalism for the computation of the quantized Hall conductivity, the Středa formula and the Diophantine equation were introduced. Specifically, the Diophantine equation represents a very powerful tool: although it takes the particular form presented above only for the square lattice, it can be generalized and used for other lattice geometries as well. Finally, in parallel to the formal approach, the topological phase can also be resolved by counting the edge states' contribution to the Hall current (linking number around the gap): more than that, the existence of localized edge states is essential to the comprehension of the quantization of the Hall conductance itself.

2.6 Concluding remarks

BIBLIOGRAPHY

- [1] K. von Klitzing, G. Dorda, and M. Pepper, *New Method for High-Accuracy Determination of the Fine-Structure Constant Based on Quantized Hall Resistance*, Phys. Rev. Lett. **45**, 494 (1980).
- [2] C. R. Dean, L. Wang, P. Maher, C. Forsythe, F. Ghahari, Y. Gao, J. Katoch, M. Ishigami, P. Moon, M. Koshino, et al., *Hofstadter's butterfly in moiré superlattices: A fractal quantum Hall effect*, Nature **497**, 598 (2012).
- [3] R. Peierls, *Zur Theorie des Diamagnetismus von Leitungselektronen*, Z. Phys. **80**, 763 (1933).
- [4] D. R. Hofstadter, *Energy levels and wave functions of Bloch electrons in rational and irrational magnetic field*, Phys. Rev. B **14**, 2239 (1976).
- [5] D. J. Thouless, M. Kohmoto, M. P. Nightingale, and M. den Nijs, *Quantized Hall Conductance in a Two-Dimensional Periodic Potential*, Phys. Rev. Lett. **49**, 405 (1982).
- [6] J. E. Avron, *Colored hofstadter butterflies* (2003), (arXiv:math-ph/0308030).
- [7] B. A. Bernevig and T. L. Hughes, *Topological Insulators and Topological Superconductors* (Princeton University Press, Princeton, 2013).

BIBLIOGRAPHY

CHAPTER 3

FIRST EXAMPLE FOR A NON-TRIVIAL INSULATOR

MARLON AZINOVIC AND TOBIAS WOLF
SUPERVISOR: LEI WANG

We analyse the band structure of the two-dimensional honeycomb lattice in the context of Topological Insulators by introducing the appropriate Tight-binding model with respective hoppings and analysing the symmetries of these terms trying to find criteria for gap openings. We employ topological tools to find the Chern number and consider phase transitions. A numerical analysis supports discussions on how the results can be extended to finite lattices.

3.1 INTRODUCTION

Analyzing electronic properties of solid state matter is a branch of physics research that has great significance for development of information technologies. Finding "exotic" electronic phases usually comes with a great potential for exciting new applications, as it has been, *e.g.*, for semiconductors and superconductors. Another in comparison rather young discovery was the "*Topological Insulator*", a phase that had been predicted in Graphene by theorists even before it had been experimentally observed - but in other materials since the effect is too weak in Graphene due to weak spin-orbit coupling [1]. In the following this new phase in Graphene shall be subject of closer theoretical examination, following a similar course as Bernevig [2] which will also illuminate the historical development.

3.2 Tight-binding model

We will introduce the honeycomb lattice, calculate the band structure - which for intrinsic Graphene is a gapless two-band *semi-metal* - and analyze *gap-opening interaction terms* in the hamiltonian by means of symmetries. This will lead us to obtain "*topologically distinct*" insulating phases with *non-zero Hall conductance*. In each case the model is transferred to the case where boundaries between Graphene and the vacuum are present, thus reducing the lattice to an infinite *strip*. This allows interesting phenomena to emerge on the interface between these two phases, similar to the Quantum Hall effect [3] but with important differences. What gave this topic great relevance was the discovery of a method to isolate single layers of Graphene from prepared samples of Graphite using the *Scotch Tape Method* by André Geim and Konstantin Novoselov in 2005 which was rewarded with a Nobel Prize only 5 years later. This allowed to measure many interesting material properties and to compare them to theoretical predictions [4].

3.2 TIGHT-BINDING MODEL

Graphene is a two-dimensional honeycomb lattice formed by carbon atoms by $2s2p_x2p_y$ hybridization in the xy -plane and one valence electron per site in the $2p_z$ orbital configuration. Thus the overlap of their wave functions can be assumed to be small which means they are localized at the atoms forming the lattice. This justifies a *tight-binding* ansatz [5], here in second-quantization formulation.

3.2.1 LATTICE HAMILTONIAN

In order to achieve translational invariance the smallest unit cell of the hexagonal lattice must contain two sites, "A" and "B", which form two interlocking triangular lattices. The lattice vectors

$$\vec{a}_1 = \frac{a}{2} \begin{pmatrix} 3 \\ \sqrt{3} \end{pmatrix}, \quad \vec{a}_2 = \frac{a}{2} \begin{pmatrix} 3 \\ -\sqrt{3} \end{pmatrix} \quad (3.1)$$

generate the lattice as illustrated in Fig. 3.1, where a is distance between atoms ($a = 1$ in computations).

The reciprocal lattice vectors

$$\vec{b}_1 = \frac{2\pi}{3a} \begin{pmatrix} 1 \\ \sqrt{3} \end{pmatrix}, \quad \vec{b}_2 = \frac{2\pi}{3a} \begin{pmatrix} 1 \\ -\sqrt{3} \end{pmatrix} \quad (3.2)$$

defined by $\vec{a}_i \cdot \vec{b}_j = 2\pi\delta_{ij}$ are needed to calculate the band structure in reciprocal space. The Brillouin zone is constructed as seen in Fig. 3.1 by using the Wigner-Seitz method. The points K, K' are images of one another under time reversal,

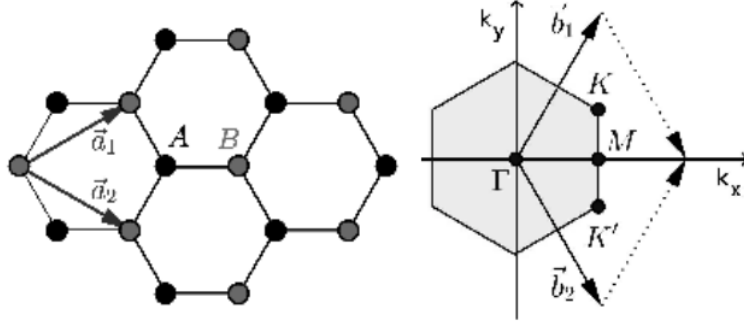


Figure 3.1: Lattice and Brillouin zone of the hexagonal lattice

since $-\vec{K} \equiv \vec{K}'$ modulo \vec{b}_1, \vec{b}_2 which will give them a special role in the band structure later on.

The Hamiltonian for N sites in this lattice can be described using a generic tight-binding ansatz in second-quantization formulation

$$H = \sum_{\vec{i}, \vec{j}} \sum_{\alpha, \beta} c_{i\alpha}^\dagger t_{i,j}^{\alpha\beta} c_{j\beta} \quad (3.3)$$

where \vec{i}, \vec{j} labels the unit cells by their position, α, β labels internal degrees of freedom, e.g. sublattice, orbital or spin. The operators $c_{i\alpha}^{(\dagger)}$ are the annihilation and creation operators for an electron at cell i in degree of freedom α . This effectively describes an electron transition from unit cell \vec{i} to \vec{j} and DOF α to β as destroying and recreating it in the respective states which is called "hopping" for obvious reasons.

The physics of this problem is now contained in the *hopping matrix elements* $t_{i,j}^{\alpha\beta}$ which have to be specified to analyze a system - and in general this can and will be very complicated unless higher order hopping is neglected. Diagonal elements $t_{i,i}^{\alpha\alpha}$ stem not from kinetic energy terms but are from on-site potentials which can be overall shifted by adding a constant term $\mu \mathbb{1}$ called chemical potential.

Performing the Fourier-transform

$$c_{i\alpha} = \frac{1}{\sqrt{N}} \sum_{\vec{k}} c_{\vec{k}\alpha} e^{-i\vec{k}\cdot\vec{i}} \quad (3.4)$$

on the \mathbb{R} -space operators significantly simplifies the problem by exploiting the discrete translational invariance $t_{i,j}^{\alpha\beta} = t_{\pm(\vec{i}-\vec{j})}^{\alpha\beta} \equiv t_{\vec{\delta}}^{\alpha\beta}$. The result is a block diagonal form with respect to \vec{k} :

$$\hat{H} = \sum_{\vec{k}} \sum_{\alpha, \beta} c_{\vec{k}\alpha}^\dagger h_{\vec{k}}^{\alpha\beta} c_{\vec{k}\beta} \quad (3.5)$$

3.2 Tight-binding model

with the so-called *Bloch* Hamiltonian

$$h_{\vec{k}}^{\alpha\beta} = \sum_{\vec{\delta}} t_{\vec{\delta}}^{\alpha\beta} e^{i\vec{k}\cdot\vec{\delta}} \quad (3.6)$$

where $\vec{\delta}$ are displacement vectors to all neighboring unit cells starting from a fixed one.

3.2.2 NEAREST-NEIGHBOR HOPPING

To start with a simple model all spin interactions are neglected so that the two only degrees of freedom are from the sublattice: *A* and *B*. Furthermore, only homogeneous *nearest neighbor* hopping between *A* and *B* is considered:

$$t_{\vec{\delta}}^{AB} = -t, \quad \vec{\delta} \in \left\{ \vec{0}, \vec{a}_1, \vec{a}_2 \right\} \quad (3.7)$$

$$t_{\vec{\delta}}^{BA} = -t, \quad \vec{\delta} \in \left\{ \vec{0}, -\vec{a}_1, -\vec{a}_2 \right\} \quad (3.8)$$

Another matrix term that shall be included stems from staggered potential terms

$$t_{\vec{0}}^{AA} = M, \quad t_{\vec{0}}^{BB} = -M \quad (3.9)$$

accounting for possibly different on-site energies between *A* and *B* sublattice which would correspond to a case where the lattice, in contrast to Graphene, has two different atoms as considered by Semenoff [6]. This would be the case of Boron Nitride.

Using Eq. 3.6 the Bloch operator can be written explicitly as a 2×2 matrix

$$h(\vec{k}) = \begin{bmatrix} M & -t(1 + e^{i\vec{k}\cdot\vec{a}_1} + e^{i\vec{k}\cdot\vec{a}_2}) \\ -t(1 + e^{-i\vec{k}\cdot\vec{a}_1} + e^{-i\vec{k}\cdot\vec{a}_2}) & -M \end{bmatrix} \quad (3.10)$$

where t and M are now the only parameters of this model. It can be decomposed into

$$\begin{aligned} h(\vec{k}) &= d_i(\vec{k}) \sigma_i \\ &= d_0(\vec{k}) \mathbb{1} + \vec{d}_{(\vec{k})} \cdot \vec{\sigma} \end{aligned} \quad (3.11)$$

where σ_i , $i = 0, 1, 2, 3$ are the Pauli matrices and $d_i(\vec{k})$, $i = 1, 2, 3$ are real.

For the specific case in Eq. 3.10 this leads to

$$d_0(\vec{k}) = 0 \quad (3.12a)$$

$$d_1(\vec{k}) = -t \left[1 + \cos(\vec{k} \cdot \vec{a}_1) + \cos(\vec{k} \cdot \vec{a}_2) \right] \quad (3.12b)$$

$$d_2(\vec{k}) = t \left[\sin(\vec{k} \cdot \vec{a}_1) + \sin(\vec{k} \cdot \vec{a}_2) \right] \quad (3.12c)$$

$$d_3(\vec{k}) = M \quad (3.12d)$$

3.2.3 BAND STRUCTURE AND LOW-ENERGY EXPANSION

The band structure is the solution to the time-independent Schrödinger equation

$$h(\vec{k}) |\vec{k}\rangle_n = E_n(\vec{k}) |\vec{k}\rangle_n \quad (3.13)$$

where $E_n(\vec{k})$ is called *dispersion relation* for the quantum number \vec{k} with corresponding eigenstate $|\vec{k}\rangle$ and n labels the band of which there are as many as degrees of freedom.

The general solution for $h(\vec{k})$ as in Eq. 3.11 is

$$E(\vec{k}) = |d_0| \pm \sqrt{\vec{d}^2} \quad (3.14)$$

which applied to Eq. 3.12 yields the result

$$E(\vec{k}) = \pm \sqrt{M^2 + t^2 \left(3 + 2 \sum_{\vec{a} \in \{ \vec{a}_1, \vec{a}_2, \vec{a}_1 - \vec{a}_2 \}} \cos(\vec{k} \cdot \vec{a}) \right)} \quad (3.15)$$

for which examples can be seen in Fig. 3.2 and 3.3 which show that without on-site potentials Graphene is a semi-metal [5] - whereas when they are present it is a gapped insulator.

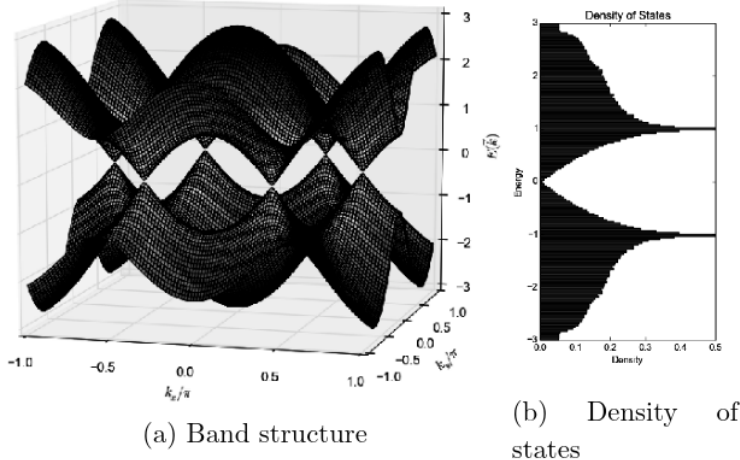


Figure 3.2: Example with model parameters $t = 1$ and $M = 0$.

By analysing Eq. 3.15 one can find that the gap is smallest at the K and K' points. Another interesting aspect to this band structure is that for $M = 0$ the dispersion around K and K' is linear which can be seen well in Fig. 3.4.

The Fermi level is between the lower and the upper band which can be deduced by observing that for $2N$ electrons we find a spectrum with $2N$ available energy

3.2 Tight-binding model

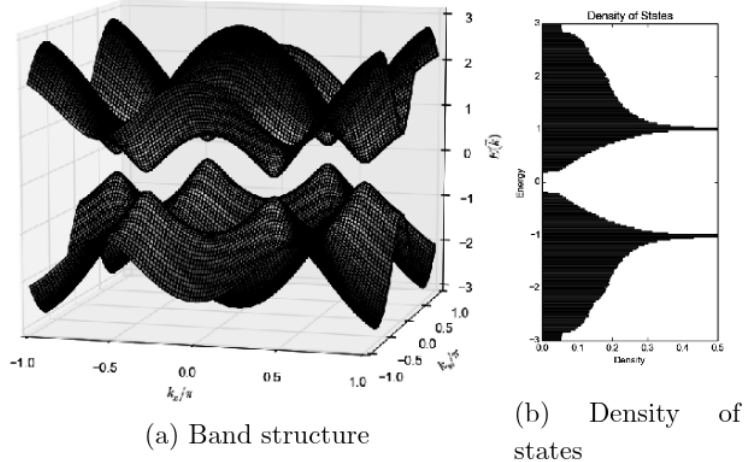


Figure 3.3: Example with model parameters $t = 1$ and $M = 0.2$.

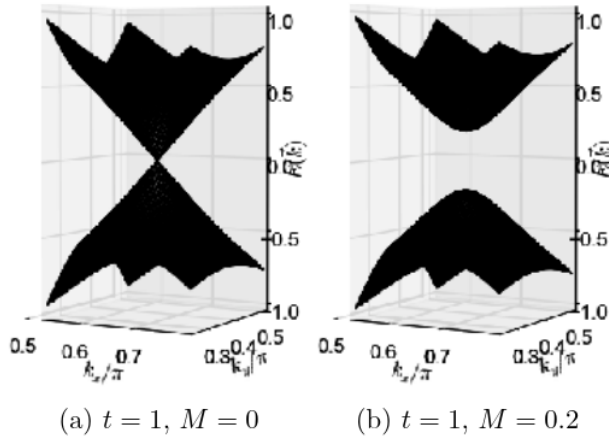


Figure 3.4: Band structure zoomed in on K point.

levels - so with spin degeneracy $2N$ for each band: the lower band is completely filled at $T = 0$ and the upper band completely empty.

Low energy excitations, *e.g.* thermal, will cause energies above the Fermi niveau to be occupied. Thus the physics of the system is primarily determined by the dispersion relation around K and K' [7] which means that the Hamiltonian in Eq. 3.10 can be expanded for the limit $|\vec{\kappa} \cdot \vec{a}_i| \ll 1$:

$$h(\vec{K} + \vec{\kappa}) \approx +\kappa_x \sigma_x + \kappa_y \sigma_y + M \sigma_z \quad (3.16a)$$

$$h(\vec{K}' + \vec{\kappa}) \approx -\kappa_x \sigma_x + \kappa_y \sigma_y + M \sigma_z \quad (3.16b)$$

These expressions are called *Dirac Hamiltonians* because of their formal similarity

to the $(2 + 1)$ -dimensional Dirac equation

$$\begin{pmatrix} mc & \hbar k_x + i\hbar k_y \\ \hbar k_x - i\hbar k_y & -mc \end{pmatrix} \psi = \frac{E}{c} \psi \quad (3.17)$$

from relativistic quantum physics.

3.2.4 SYMMETRIES

Analyzing the consequences of symmetries is an important method to get deeper insight into general traits of the band structure of a system. The most general approach for this analysis would start from group theory, *e.g.* in our case of the point group C_{6v} , and find all irreducible representations [8]. Together with symmetry conditions only few terms would remain and would thus specify a general Graphene Hamiltonian as in Kane's and Mele's considerations [9].

For the purposes of this review, however, a slightly less abstract analysis analogously to Bernevig's course of action [2] will suffice. This is because we are mainly interested in specific symmetries and their restrictions on the Hamilton operator.

The time-reversal operator T acts on a state by flipping signs of momentum and spin. This means that T is different for the spin-less case and for the case where spin needs to be flipped by T as well. By considering the transformation of expectancy values one finds

- $T = \mathcal{K}$ without spin and
- $T = -i\sigma_y \mathcal{K}$ for spin-1/2 systems.

In *both* cases can be shown

$$\tilde{h}(\vec{k}) = Th(-\vec{k})T^{-1} \quad (3.18)$$

for a general Bloch Hamiltonian $h(\vec{k})$ and its image under time reversal $\tilde{h}(\vec{k})$. This result can be found by considering how the operators $c_{\vec{k}}^s$ in \vec{k} -space transform given that $T c_{\vec{j}}^s T^{-1} = c_{-\vec{j}}^{-s}$ in real space where s is a possible spin degree of freedom.

Another relevant symmetry operation is the spatial inversion I . We can show that it acts on the Bloch Hamiltonian of Graphene, which is 2×2 and swaps the two sub-lattices for A and B , as

$$Ih(\vec{k})I^{-1} = \sigma_x h(-\vec{k})\sigma_x \quad (3.19)$$

3.3 Topology of a 2×2 Hamiltonian

which again can be seen by starting from equation $I c_{\vec{j}}^A I^{-1} = c_{-\vec{j}}^B$ and in the same fashion for $c_{\vec{j}}^B$.

Using Eq. 3.18 and 3.19 we immediately obtain the condition for *time-reversal invariance*

$$Th(-\vec{k})T^{-1} \stackrel{!}{=} h(\vec{k}) \quad (3.20)$$

and for *inversion symmetry*

$$\sigma_x h(-\vec{k})\sigma_x \stackrel{!}{=} h(\vec{k}) \quad (3.21)$$

and immediately obtain that the nearest neighbor model $h(\vec{k})$ in Eq. 3.10 is in any case symmetric with respect to time reversal symmetry but only invariant upon inversion if $M = 0$.

We could also go to the low-energy limit as in Eq. 3.16 and relate the two expansions since $K \equiv -K'$ and both Eq. 3.20 and 3.19 relate these points to find that the two Dirac cones are not independent from each other.

One more important consideration is the consequence of both time reversal *and* inversion symmetry

$$(IT) h(\vec{k})(IT)^{-1} \stackrel{!}{=} h(\vec{k}) \quad (3.22)$$

at the same time which using Eq. 3.20 and 3.21 *without spin* becomes equivalent to

$$\sigma_x h(\vec{k})\sigma_x = h(\vec{k}) \quad (3.23)$$

and imposes

$$d_3(\vec{k}) = -d_3(\vec{k}) = 0 \quad (3.24)$$

in Eq. 3.11 which forbids σ_z . Thus a gap can only occur when time reversal symmetry *and/or* inversion symmetry is *broken* [7]. Since we want to consider insulators we either have to break symmetry or we need to introduce spin.

3.3 TOPOLOGY OF A 2×2 HAMILTONIAN

Studying the Quantum Hall Effect revealed a lot of useful tools [NOTE FOR FINAL COMPILATION: Reference to Patrick's and Ludovic's part] which allowed to see whether transverse conductance occurs when applying an external electric field by analyzing the band structure and eigen-states. In order to find non-trivial insulators it seems sensible to transfer these concepts.

Diagonalizing a 2×2 Hamiltonian as in Eq. 3.11 yields the solution

$$E_{\pm}(\vec{k}) = |d_0| \pm \sqrt{\vec{d}^2} = |d_0| \pm d, \quad (3.25)$$

$$\psi_{\pm} = \frac{1}{\sqrt{2d(d \pm d_3)}} \begin{pmatrix} d_3 \pm d \\ d_1 + id_2 \end{pmatrix} \quad (3.26)$$

where E_{\pm} is eigenvalue with eigenvector ψ_{\pm} .

Since the lower band is filled, we want to calculate the *Berry connection* which results in

$$\begin{aligned} A_i(\vec{k}) &:= i \langle \psi_- | \partial_{k_i} | \psi_- \rangle \\ &= \frac{1}{2d(d-d_3)} (d_2 \partial_i d_1 - d_1 \partial_i d_2) \end{aligned} \quad (3.27)$$

for $i = x, y$ where we used Eq. 3.26 and simplified. Now we could compute the Berry phase but we are more interested in the *Berry curvature* since we can relate it to the transverse Hall conductance:

$$\begin{aligned} F_{ij} &:= \partial_i A_j - \partial_j A_i \\ &= \frac{1}{2d^3} \varepsilon_{abc} d_a \partial_i d_b \partial_j d_c \\ &= \frac{1}{2} \varepsilon_{abc} \hat{d}_a \partial_i \hat{d}_b \partial_j \hat{d}_c \end{aligned} \quad (3.28)$$

where we defined $\hat{d}_a := d_a/d$, inserted Eq. 3.27 and did a lot of algebraic simplification on the way to find

$$F_{ij} = \frac{1}{2d^3} (\partial_i \vec{d} \times \partial_j \vec{d}) \cdot \vec{d} = \frac{1}{2} (\partial_i \hat{d} \times \partial_j \hat{d}) \cdot \hat{d} \quad (3.29)$$

for the general *Berry curvature* of a 2×2 system. This is the "Jacobian" of the map $\vec{k} \mapsto \vec{d}/d$ which maps between the two manifolds BZ and S^2 :

$$\int_{S^2 = \hat{d}(\text{BZ})} \hat{d} \cdot d\vec{\sigma} = \int_{\text{BZ}} \hat{d} \cdot (\partial_{k_x} \hat{d} \times \partial_{k_y} \hat{d}) dk_x dk_y \quad (3.30)$$

The left site of Eq. 3.30 is a flux integral of \hat{d} through the unit sphere and thus a winding number for this mapping which is why it *must* be an integer multiple of 4π .

3.3.1 BERRY VORTICITY AND CHERN NUMBER

The Berry phase is

$$\oint_{E(\vec{k})=E_F} \vec{A}_{(\vec{k})} \cdot d\vec{k} \quad (3.31)$$

where the path is the intersection between band structure and Fermi level (which yields a \vec{k} -path around the cone). It can be used as a way to characterize the vorticity within the gauging choice of our wave functions.

It could be treated analytically for a Dirac Hamiltonian but since we can compute the Hall conductance more easily using Stokes' theorem (yielding Eq. 3.32), it

3.3 Topology of a 2×2 Hamiltonian

might at the point be more instructive to just look at the Berry curvature in Fig. 3.5 to see the vorticity of $\vec{A}(\vec{k})$.

The Chern number is defined as integral of the Berry curvature over the Brillouin zone:

$$\begin{aligned}\nu &= \frac{1}{2\pi} \iint_{\text{BZ}} dk_x dk_y F_{xy} \\ &= \frac{1}{4\pi} \iint_{\text{BZ}} dk_x dk_y (\partial_{k_x} \hat{d} \times \partial_{k_y} \hat{d}) \cdot \hat{d}\end{aligned}\quad (3.32)$$

By the argument made from Eq. 3.30 it is immediately apparent that the Chern number is an integer. But apart from this insight it is in general hard to evaluate analytically by considering Eq. 3.32 alone - which is why we will later examine the topology of a Dirac Hamiltonian. We could in principle also try to evaluate the integral numerically but that as well is generally rather difficult because of high singularities in the integrand as can be seen in Fig. 3.5.

In the case of time-reversal invariance the Chern number can easily be evaluated by considering how the Berry curvature $F(\vec{k})$ transforms on time reversal:

$$TF(\vec{k})T^{-1} = -F(-\vec{k}) \quad (3.33)$$

which can be proven by applying $T = \mathcal{K}$, explicitly for systems without spin, to Eq. 3.28 and 3.27. We immediately find

$$\begin{aligned}\nu &= \frac{1}{4\pi} \iint_{\text{BZ}} dk_x dk_y TF(\vec{k})T^{-1} \\ &= \frac{1}{4\pi} \iint_{\text{BZ}} dk_x dk_y (-1)F(-\vec{k}) \\ &= -\nu\end{aligned}\quad (3.34)$$

and get the result that a time-reversal invariant system *without spin* must have zero transverse hall conductance.

3.3.2 DIRAC HAMILTONIAN

As already seen in section 3.2.3 our low-energy behavior is given by a Dirac Hamiltonian. This gives hope that maybe some information about the full systems' Chern number might still be contained in this expansion.

For this reason we will now consider the 2×2 Hamiltonian

$$h(\vec{k}) = k_i \mathcal{A}_{ij} \sigma_j + m \sigma_3, \quad i, j \in 1, 2 \quad (3.35)$$

which we will call *continuum Dirac Hamiltonian*. It has no periodicity in \vec{k} -space since it essentially describes a free particle which of course does not obey

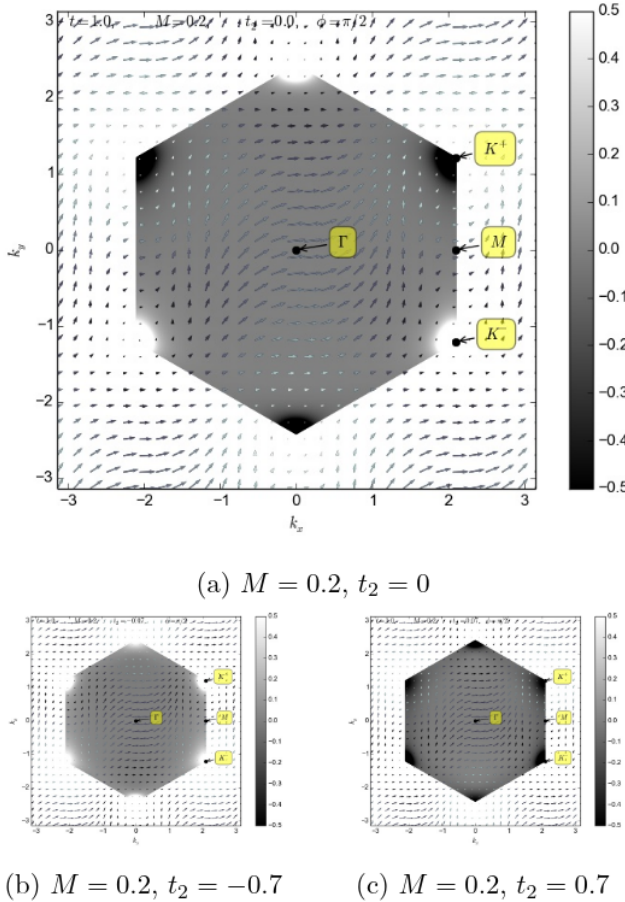


Figure 3.5: Chern integrand (*Berry curvature*) from Eq. 3.32 on BZ $t = 1, \phi = \frac{\pi}{2}$ but different M/t_2 . The vector field is the projection of $\hat{d}(k_x, k_y)$ onto the $x - y$ -plane. The "hotspots" are the vorticity of the Berry potential and provide the only relevant contribution to the Integral (and thus the chern number) in Eq. 3.32.

any discrete translational invariance. This means that our Brillouin zone is the *non-compact* manifold \mathbb{R}^2 .

To transfer the results from before we rewrite 3.35:

$$h(\vec{k}) = \vec{d} \cdot \vec{\sigma} = \begin{pmatrix} k_x \mathcal{A}_{11} + k_y \mathcal{A}_{21} \\ k_x \mathcal{A}_{12} + k_y \mathcal{A}_{22} \\ m \end{pmatrix} \cdot \vec{\sigma} \quad (3.36)$$

3.3 Topology of a 2×2 Hamiltonian

Using this specific \vec{d} and Eq. 3.29 we find the Berry curvature

$$F_{xy}(\vec{k}) = \frac{1}{2} \frac{1}{(d_{(k_x, k_y)})^3} m \det \mathcal{A} \quad (3.37)$$

where

$$\begin{aligned} d_{(k_x, k_y)} = & (k_x^2 (\mathcal{A}_{11}^2 + \mathcal{A}_{12}^2) + k_y^2 (\mathcal{A}_{21}^2 + \mathcal{A}_{22}^2) \\ & + 2k_x k_y (\mathcal{A}_{11}\mathcal{A}_{21} + \mathcal{A}_{12}\mathcal{A}_{22}) + m^2)^{1/2} \end{aligned}$$

At this point the Chern number can be computed analytically from Eq. 3.32 by transforming to polar coordinates:

$$\begin{aligned} \nu &= \frac{m \det \mathcal{A}}{4\pi} \iint_{\mathbb{R}^2} dk_x dk_y \frac{1}{(d(k_x, k_y))^3} \\ &= \frac{m \det \mathcal{A}}{4\pi} \int_0^{2\pi} d\theta \int_0^\infty dk k \frac{1}{(d(k \sin \theta, k \cos \theta))^3} \\ &\stackrel{(...)}{=} \frac{m \det \mathcal{A}}{4\pi} \frac{2\pi}{|m| |\det \mathcal{A}|} \\ &= \frac{1}{2} \text{sgn}(m) \text{sgn}(\det \mathcal{A}) \end{aligned} \quad (3.38)$$

The Chern number in this case is *not* an integer which at first glimpse seems to violate an earlier result - *however* this is to be expected since one very important aspect has changed: the Brillouin zone is not a compact manifold any more and thus 3.30 does not work since S^2 is a compact manifold.

This immediately shows that the low-energy approximation cannot directly give us the Chern number for the lattice system. But there is in fact a theorem that states that *changes* in our lattice Chern number are given by *changes* in the Chern number of the Dirac Hamiltonians at gap-opening and closing transition points [10].

An intuitive argument is that in order to take the step from low-energy description back to the full system the energy bands which extend infinitely in \vec{k} -space actually have to bend down and join with their neighboring cones so that the periodic structure is restored. The bending however would be another Fermion if we could actually excite to this energy without destroying the system and there we get another half-integer contribution to the Chern number. Since this contribution does not change at low energy gap-opening transitions the only change comes from the Dirac Hamiltonian.

3.4 GRAPHENE RIBBONS AND NEAREST NEIGHBOUR HOPPING

So far only infinite systems were considered. Now we want to consider a Graphene ribbon to investigate if the presence of edges influences the properties of Graphene. If one imagines a topological insulator with some Chern-number $\nu \neq 0$ in vacuum, the Chern-number changes uncontinuously on the edge of the insulator, which indicates that interesting physics might be happening on the edge. There are several ways to cut a Graphene ribbon. The two most popular ways are called *zigzag* edge and *armchair* edge. See Fig.3.6 We choose the y-axis along the direction in

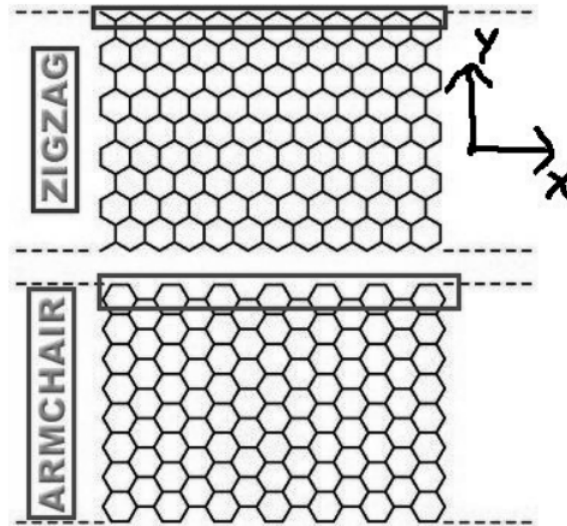


Figure 3.6: [11] We see two ribbons of Graphene. The upper with zigzag, the lower with armchair edge. The ribbon is chosen to be finite along y-direction

which the ribbon is finite and the x-axis along the infinite direction.

We label each position in the lattice using x and y. The y label ranges from 0 to $N_y < \infty$ while $x \in \mathbb{Z}_0$. One can imagine chains along the y-axis which have the same x label. y is then labeling the position within each chain. The tight binding Hamiltonian is given by

$$H = -t \sum_{x,y,x',y'} c_{x',y'}^\dagger c_{x,y} + \sum_{x,y} c_{x,y}^\dagger c_{x,y} V_{x,y}. \quad (3.39)$$

Now we only consider nearest neighbour (NN) hopping which leads to a Hamil-

3.4 Graphene ribbons and nearest neighbour hopping

tonian given by

$$\begin{aligned}
H = & -t \sum_x \sum_{y=0}^{N_y-1} \underbrace{c_{x,y+1}^\dagger c_{x,y}}_{\text{intra-chain-hopping}} \\
& - t \sum_x \sum_{y=0}^{N_y-1} \underbrace{\delta_{y \bmod 4, 0} c_{x+1,y+1}^\dagger c_{x,y} + \delta_{y \bmod 4, 3} c_{x+1,y-1}^\dagger c_{x,y}}_{\text{inter-chain-hopping}} \\
& + \underbrace{\text{h.c.}}_{\text{accounts for hoppings in the oposite direction}} \\
& - \sum_x \sum_{y=0}^{N_y-1} \underbrace{c_{x,y}^\dagger c_{x,y} (-1)^y M}_{\text{on-site-energies}}
\end{aligned}$$

where intra-chain-hopping is referring to the hoppings within each of the chains in y direction (which all have the same x -label) and inter-chain-hopping is referring to hoppings between these chains.

Performing a Fourier transform on the x label yields

$$c_{x,y}^\dagger = \frac{1}{\sqrt{N_x}} \sum_{k_x} e^{ik_x x} c_{k_x,y} \quad (3.40)$$

and hence

$$H = \sum_{k_x} H_{k_x}$$

where

$$\begin{aligned}
H_{k_x} = & -t \sum_{y=0}^{N_y-1} \underbrace{c_{k_x,y+1}^\dagger c_{k_x,y}}_{\text{intra-chain-hopping}} \\
& - t \sum_{y=0}^{N_y-1} \underbrace{\delta_{y \bmod 4, 0} c_{k_x,y+1}^\dagger c_{k_x,y} e^{ik_x} + \delta_{y \bmod 4, 3} c_{k_x,y-1}^\dagger c_{k_x,y} e^{ik_x}}_{\text{inter-chain-hopping}} \\
& + \underbrace{\text{h.c.}}_{\text{accounts for hoppings in the oposite direction}} \\
& - \sum_{y=0}^{N_y-1} \underbrace{c_{k_x,y}^\dagger c_{k_x,y} (-1)^y M}_{\text{on-site-energies}}
\end{aligned}$$

And in matrix form, choosing a mesh for k_x :

$$H = \begin{pmatrix} H_{k_x=0} & & & \\ & H_{k_x=\dots} & & \\ & & \ddots & \\ & & & H_{k_x=2\pi} \end{pmatrix}$$

where each H_{k_x} is a $N_y \times N_y$ matrix. Since H is block-diagonal we can diagonalize each H_{k_x} separately. Numerical methods are used to look at the energy spectrum. One obtains the plots shown in Fig.3.7. The first thing to notice is that a on-site

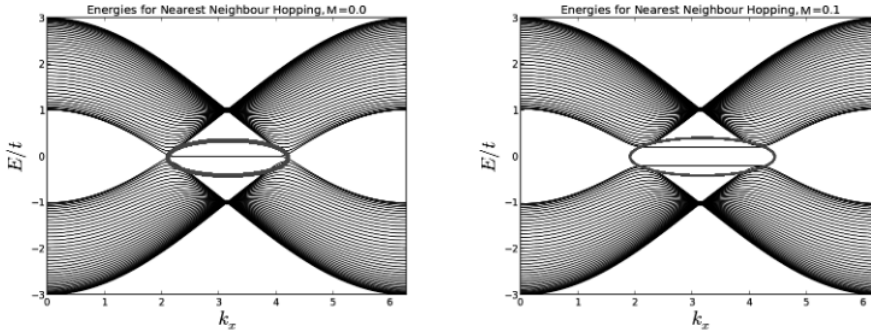


Figure 3.7: NN hopping energies for a zigzag ribbon of Graphene

potential will still gap out the energy bands. Also, TR symmetry is still present which (for spin-less systems as we have right now) implies the insulator is not topological. One notices the two lines which are out of the bulk around $k_x = \pi$ (they are encircled red in Fig.3.7). In the infinite case there weren't any energies out of the bulk so one could suspect the appearance of them might be connected to the presence of edges. One quick check on this can be performed by connecting the edges of the graphene ribbon to another yielding a nanotube. We then look at the energy spectrum. See Fig.3.8. For a nanotube there are no energies out of the bulk which indicates, that the presence of these energies is indeed depending on the presence of edges.

To further investigate these out-of-the-bulk energies one can look at the corresponding wavefunctions. Plotting the absolute value squared of the corresponding wavefunction dependant on the y position one obtains Fig.3.9. One notices that the wavefunctions corresponding to the out-of-the-bulk energies are strongly localized on the edges, in the k_x region where the energies are out of the bulk and expected to be in the middle of the ribbon where the energies are behaving like the bulk. This is why the states belonging to the out-of-the-bulk energies are *edgestates*. One also notices that the edgestates with lower energy is localized a

3.4 Graphene ribbons and nearest neighbour hopping

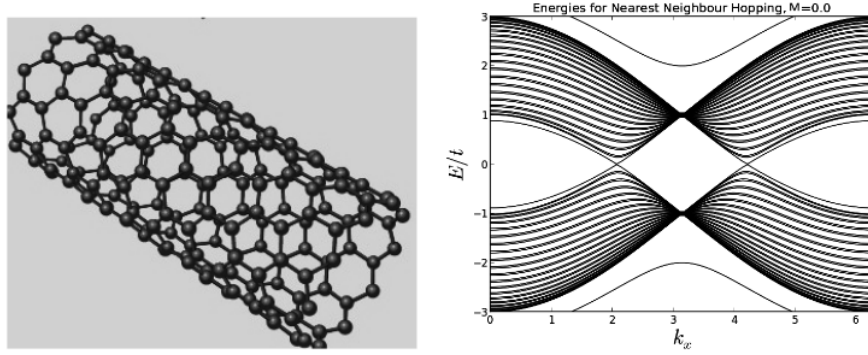


Figure 3.8: NN hopping energies for a nanotube

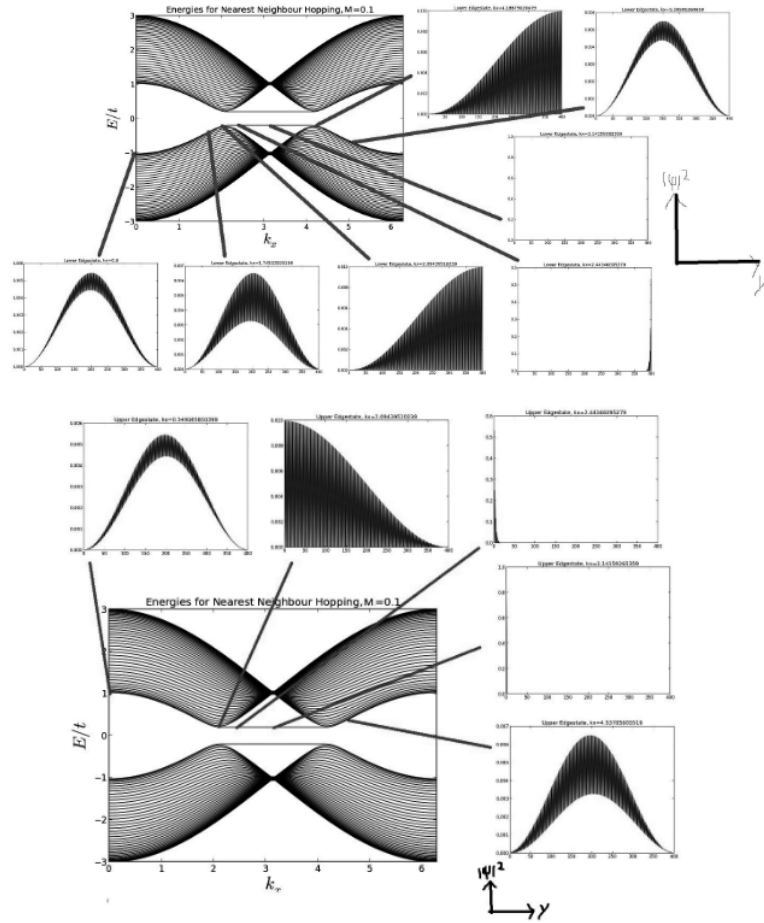


Figure 3.9: Absolute value squared of the wavefunctions corresponding to the out-of-the-bulk energies as a function of y

the edge of the ribbon for which the on-site potential is given by $-M$ (which is the bottom edge ($y = N_y$) in Fig.3.9). Another way to confirm this result is to directly look at the expectation value of the y-coordinate for these energies. One obtains Fig. 3.10. One again confirms that the electrons corresponding to this

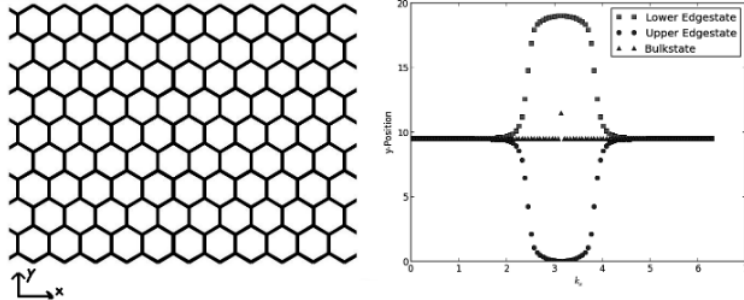


Figure 3.10: Mean transverse localization $\langle y \rangle_{\psi_{\text{edgestate}}}$ as a function of k_x .

out-of-the bulk energies are indeed localized on the two edges of the Graphene ribbon. The whole time one should keep in mind that since we have TR symmetry as well as a spin-less system the Chern-number is still zero. This means the presence of edgestates alone is not sufficient for a material to be called topological.

One also notices in Fig. 3.7 that around $k_x = \pi$ the energybands of the edgestates are flat and hence the group velocity of the corresponding wavefunctions is zero. Which means the particles can not travel along an edge. A hand-waving argument for this can be given by remembering the overall probability to hop between $y = 0$ and $y = 1$ as well as between $y = N_y - 1$ and $y = N_y$ is given by $t(1 + e^{\pm ik_x})$ (where the \pm is accounting for the direction of the hop) which (for $k_x = \pi$) is vanishing. This means a particle localised at $y = 0$ or at $y = N_y$ (as it is the case for an edgestate) can not hop to a position with different y-label. If only NN hopping is considered, the particle hence can not hop at all, which means the group velocity should also vanish. If one would allow for next nearest neighbour (NNN) hopping, we would expect that hopping along the edge should be possible. And indeed, when we consider NNN hopping in Haldane's model we will confirm a non-vanishing group velocity for the edgestates. The insulating properties of an armchair edge are not as well defined as for the zigzag edge. If a ribbon of Graphene is a bulk insulator or not, in the case of an armchair edge, is depending on the value of $N_y \bmod 3$ which indicates an instability [12]. Hence we do not want to further consider armchair edged ribbons.

3.5 CHERN INSULATOR

A central result of section 3.3.1 was that if the system does not have a spin degree of freedom, the Chern number - and thus the Hall conductance - has to be zero when the Hamiltonian is *symmetric with respect to time reversal*.

Insisting on neglecting spin there is only one possible way to obtain a non-trivial insulator from the Hamiltonian in section 3.2.2: introducing new hopping terms that *break time reversal symmetry*. This is Haldane's conclusion that lead to the physically meaningful terms [7] that shall be discussed hereafter.

3.5.1 SECOND-NEAREST-NEIGHBOR HOPPING

We start from the same modeling assumptions as in section 3.2.2, M and t -terms. Now the second-nearest neighbor hopping is assumed to be non-zero and complex, where the sign of the phase depends on whether the hopping occurs clockwise (positive) or counter-clockwise (negative) as depicted in Fig. 3.11. This hopping always connects points on the same sublattice and thus will contribute to diagonal terms in the Hamiltonian.

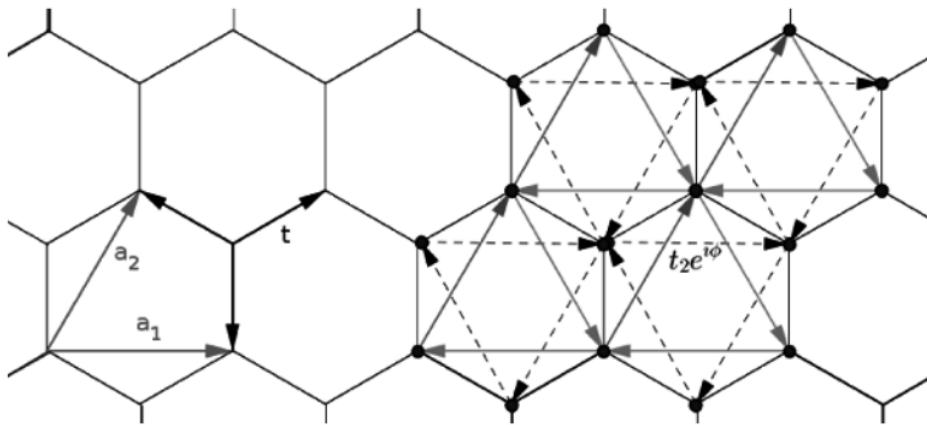


Figure 3.11: Complex second-nearest neighbour hopping in Haldane's model where arrows indicate sign of the phase.

Before writing down all the elements specifically, it is important to consider the physical argument that justifies these terms in the first place. Time reversal symmetry is typically broken by magnetic fields, since *e.g.* the direction of Lorentz force acting on a particle is dependent on the sign of the particle's velocity. We already know that magnetic fields in the lattice model cause complex phases since a transition along a closed circle in a magnetic field gives a phase factor $\exp(i \oint_{\gamma} \vec{A} \cdot d\vec{s}) = \exp(i\phi)$, where \vec{A} is the magnetic vector potential and ϕ the

flux through $\text{int}(\gamma)$. We want to achieve one important aim: we want zero net flux through the cell because we know from the Hofstadter problem that non-zero net flux breaks the translational invariance and requires introducing a bigger unit cell to restore it [13]. The choice Haldane made was to have a staggered magnetic field [7] so that the smallest six triangle areas within a hexagonal cell have flux ϕ with alternating sign as can be seen in Fig. 3.12.

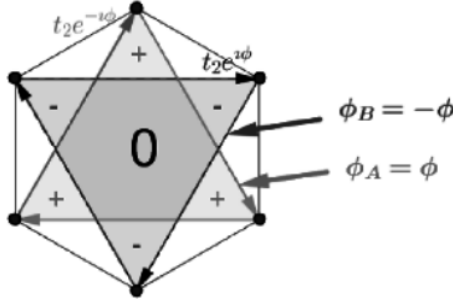


Figure 3.12: Physical realization of Haldane hopping terms using a superposition of two magnetic fields.

Carefully tracking all hopping between neighboring unit cells and the respective phase signs shows that the hopping elements are

$$\begin{aligned} t_{\vec{\delta}}^{AA} &= -t_2 e^{+\imath\phi} & t_{\vec{\delta}}^{BB} &= -t_2 e^{-\imath\phi}, & \vec{\delta} &\in \{\vec{a}_2, -\vec{a}_1, \vec{a}_1 - \vec{a}_2\} \\ t_{\vec{\delta}}^{A\bar{A}} &= -t_2 e^{-\imath\phi} & t_{\vec{\delta}}^{\bar{B}B} &= -t_2 e^{+\imath\phi}, & \vec{\delta} &\in \{-\vec{a}_2, \vec{a}_1, -\vec{a}_1 + \vec{a}_2\} \end{aligned}$$

The new Bloch operator can now be written as sum of the old one from section 3.2.2, here denoted $h^{\text{NN}}(\vec{k})$ and one constructed from these new term, denoted $h^{\text{NNN}}(\vec{k})$ which only contains diagonal entries:

$$\begin{aligned} h_H(\vec{k}) &= h^{\text{NN}}(\vec{k}) + h^{\text{NNN}}(\vec{k}) \\ &= d_0(\vec{k}) \mathbb{1} + \vec{d}_{(\vec{k})} \cdot \vec{\sigma} \end{aligned} \quad (3.41)$$

where the decomposition now requires a \vec{k} -dependent identity term and has the coefficients as in Eq. 3.42.

$$d_1(\vec{k}) = -t \left[1 + \cos(\vec{k} \cdot \vec{a}_1) + \cos(\vec{k} \cdot \vec{a}_2) \right] \quad (3.42a)$$

$$d_2(\vec{k}) = t \left[\sin(\vec{k} \cdot \vec{a}_1) + \sin(\vec{k} \cdot \vec{a}_2) \right] \quad (3.42b)$$

$$d_3(\vec{k}) = M - 2t_2 \sin(\phi) \left[\sin(\vec{k} \cdot \vec{a}_1) - \sin(\vec{k} \cdot \vec{a}_2) - \sin(\vec{k} \cdot (\vec{a}_1 - \vec{a}_2)) \right] \quad (3.42c)$$

$$d_0(\vec{k}) = -2t_2 \cos(\phi) \left[\cos(\vec{k} \cdot \vec{a}_1) + \cos(\vec{k} \cdot \vec{a}_2) + \cos(\vec{k} \cdot (\vec{a}_1 - \vec{a}_2)) \right] \quad (3.42d)$$

3.5 Chern Insulator

3.5.2 BAND STRUCTURE AND DIRAC NODES

In analogy to section 3.2.2 we calculate the band structure for Haldane's model using Eq. 3.14, where we now have additional parameters t_2 and ϕ to describe the complex hopping terms. Looking at different settings as in Fig. 3.13 reveals interesting behavior: when on-site potentials are zero the band structure is gapped evenly at K and K' like in the case $t_2 = 0$, $M > 0$ (*pure on-site term case*) from before and when both $t_2 > 0$ and $M > 0$ (*mixed case*) we obtain that the gap is still dominated by the behavior around K and K' because of C_3 symmetry, just like before. But now the two contributions seem to be different at K and K' points which allows for different phases where the bands are fully gapped. These phases are separated by gap-closing and reopening transitions at either K or at K' (or both for the exotic cases $M = 0$, and $\phi = 0, \pi$).

Analyzing the *insulator phases* and their transitions with respect to topology will be the next course of action.

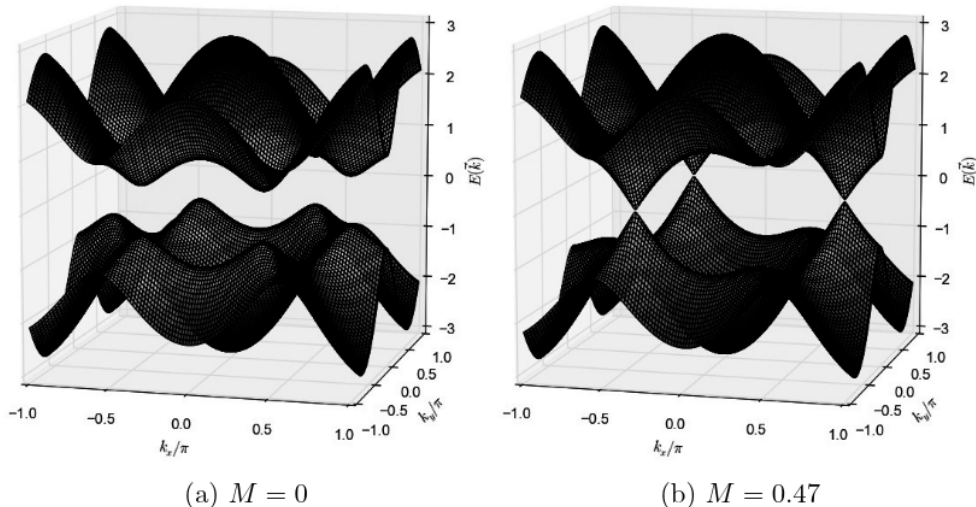


Figure 3.13: Band structure for Haldane's model ($t = 1$, $\phi = \frac{\pi}{2}$).

As the gap behavior is still given at K and K' (Dirac) points we again make a low-energy expansion around Fermi level $E = 0$ for $|\vec{\kappa} \cdot \vec{a}_{1,2}| \ll 1$:

$$\begin{aligned} h(\vec{K} + \vec{\kappa}) &\approx \frac{3}{2}t(\kappa_y\sigma_x - \kappa_x\sigma_y) + (M + 3\sqrt{3}t_2 \sin \phi)\sigma_z \\ &= \kappa_i \mathcal{A}_{ij}^+ \sigma_j + m^+ \sigma_z \end{aligned}$$

$$h(\vec{K}' + \vec{\kappa}) \approx -\frac{3}{2}t(\kappa_y\sigma_x + \kappa_x\sigma_y) + (M - 3\sqrt{3}t_2 \sin \phi)\sigma_z \quad (3.43)$$

$$= \kappa_i \mathcal{A}_{ij}^- \sigma_j + m^- \sigma_z \quad (3.44)$$

where we systematically suppressed the term $3t_2 \cos \phi \mathbb{1}$ because constant terms only shift the spectrum (which if necessary could be corrected introducing a chemical potential) and made the definitions

$$\mathcal{A}^\pm := \frac{3}{2}t \begin{pmatrix} 0 & -1 \\ \pm 1 & 0 \end{pmatrix}, \quad m^\pm := M \pm 3\sqrt{3}t_2 \sin \phi \quad (3.45)$$

to recover the same form as in Eq. 3.35. Now we can immediately apply Eq. 3.38 by calculating

$$\operatorname{sgn}(\det \mathcal{A}^\pm) = \operatorname{sgn}\left(\pm \frac{9}{4}t^2\right) = \pm 1 \quad (3.46)$$

and

$$\operatorname{sgn}(m^\pm) = \operatorname{sgn}\left(M \pm 3\sqrt{3}t_2 \sin \phi\right) \quad (3.47)$$

which now enables us to track topological phase transitions as explained in section 3.3.2.

3.5.3 TOPOLOGICAL PHASE TRANSITIONS

For a particular choices of parameters M, t_2, ϕ we can now find topologically non-trivial phases by considering the change in Chern numbers of the low-energy approximation Dirac Hamiltonian. In fact for this simple case this *relative* Chern number is obtained by summing both contributions:

$$\begin{aligned} \nu &= \nu_K + \nu_{K'} & (3.48) \\ &= \frac{1}{2} (\operatorname{sgn}(m^+) \operatorname{sgn}(\det \mathcal{A}^+) + \operatorname{sgn}(m^-) \operatorname{sgn}(\det \mathcal{A}^-)) \\ &= \frac{1}{2} (\operatorname{sgn}(M + 3\sqrt{3}t_2 \sin \phi) - \operatorname{sgn}(M - 3\sqrt{3}t_2 \sin \phi)) \\ &= \frac{\operatorname{sgn} t_2}{2} \left(\operatorname{sgn}\left(\frac{M}{t_2} + 3\sqrt{3} \sin \phi\right) - \operatorname{sgn}\left(\frac{M}{t_2} - 3\sqrt{3} \sin \phi\right) \right) \end{aligned}$$

To get some insight into this expression the best idea would be to draw the critical lines of the two sgn functions and to calculate the Chern numbers once within each region as depicted in Fig. 3.14. This simple picture now contains all information about our topological phase transitions.

3.6 Graphene ribbons in Haldane model

However, changes without a reference state with known Chern number are still unsatisfactory. This is why we consider the case $M > 0$, $t_2 \rightarrow 0$ which takes us to the time-reversal symmetric insulator with $\nu = 0$ which means that in this particular case the *absolute* Chern number is given by the *relative* one in Eq. 3.48.

Note that we implicitly assumed $t_2 > 0$ throughout. If changes in sign of t_2 are allowed then the sign of the Chern number in Eq. 3.48 also changes which would require Fig. 3.14 to be modified accordingly by interchanging the signs of ν .

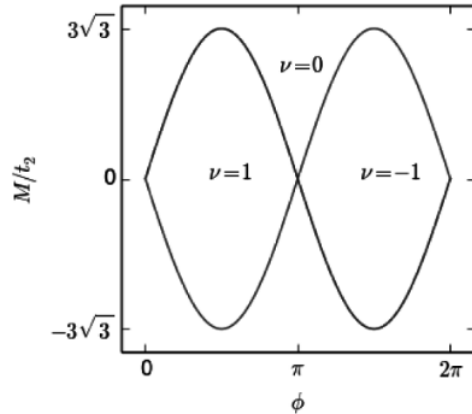


Figure 3.14: Topological phase diagram in Haldane's model for $t_2 > 0$.

3.6 GRAPHENE RIBBONS IN HALDANE MODEL

Similar to the NN hopping case we only consider a Graphene ribbon with zigzag edge. Analog to the section for NN hopping the Hamiltonian for a Graphene ribbon is constructed by using x and y labels and then performing a Fourier transform on the x-variable only. This yields:

$$H^{\text{Haldane}} = \sum_{k_x} H_{k_x}^{\text{NN}} + H_{k_x}^{\text{NNN}}$$

where:

$$\begin{aligned}
 H_{k_x}^{\text{NNN}} = & \sum_y^{N_y-1} it_2 \delta_{y \bmod 4, 0} (c_{k_x, y-2}^\dagger c_{k_x, y} e^{ik_x} + c_{k_x, y}^\dagger c_{k_x, y} e^{ik_x} + c_{k_x, y+2}^\dagger c_{k_x, y} e^{ik_x}) \\
 & + \sum_y^{N_y-1} it_2 \delta_{y \bmod 4, 1} (-c_{k_x, y-2}^\dagger c_{k_x, y} e^{ik_x} + c_{k_x, y}^\dagger c_{k_x, y} e^{ik_x} - c_{k_x, y+2}^\dagger c_{k_x, y}) \\
 & + \sum_y^{N_y-1} it_2 \delta_{y \bmod 4, 2} (c_{k_x, y-2}^\dagger c_{k_x, y} e^{ik_x} - c_{k_x, y}^\dagger c_{k_x, y} e^{ik_x} + c_{k_x, y+2}^\dagger c_{k_x, y}) \\
 & + \sum_y^{N_y-1} it_2 \delta_{y \bmod 4, 3} (-c_{k_x, y-2}^\dagger c_{k_x, y} e^{ik_x} + c_{k_x, y}^\dagger c_{k_x, y} e^{ik_x} - c_{k_x, y+2}^\dagger c_{k_x, y} e^{ik_x}) \\
 & + \text{h.c.}
 \end{aligned}$$

After constructing the Hamiltonian we take a mesh for k_x and solve for the eigenvalues of this matrix to obtain the energybands. One notices that the look of the energybands is different depending on the value of $\frac{M}{t_2}$. Several examples are shown in Fig. 3.15.

Now there are different things to note: first of all we still see some out-of-the bulk energystates. But in difference to the NN hopping case, we know see that they can cross/touch each other. To check if these out-of-the bulk energies are still corresponding to edgestates we have a look at the wavefunctions again and see, where they are localised. In Fig. 3.16 we see the absolute value squared of the corresponding wavefunctions as a function of y . Indeed one confirms the corresponding wavefunctions are still localized on the edge of the ribbon. Hence they are still edgestates. Another important question to investigate is, whether the edgestate energies cross each other or if they just touch (if they do). We therefore look at the localisation of the corresponding wavefunctions again for both possibilities. See Fig. 3.17. In Fig. 3.17 we can see that if the left column (i.e. touching energybands) would be the case, the localisation of the wavefunctions of the edgestates would have to jump from one edge to the other edge at the k_x where the energies touch. This is not physical. A small change in k_x should not lead to a huge change in the wavefunction. The physical way to look at it would be the right column: i.e. we have two edgestates, one on each edge, for all k_x . The energies corresponding to these edgestates cross the bulk gap as well as each other. One of them has positive slope and the other one negative. This brings us to the next interesting point: in contrary to the case where we only allowed for NN hopping, we now have non-vanishing slopes! One slope corresponding to one edge and one slope corresponding to the other! This means the wavefunctions

3.6 Graphene ribbons in Haldane model

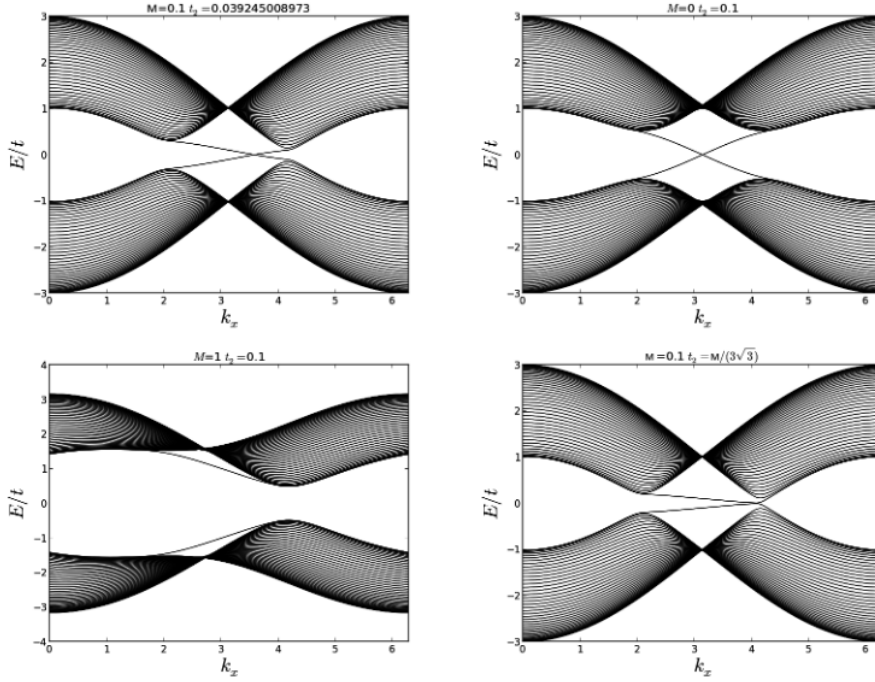


Figure 3.15: We see a plot of the energybands for the haldane Hamiltonian of a zigzag ribbon of Graphene. The four different plots correspond to different M , t_2 combinations.

have some group velocity in x-direction with opposite signs. In the section on edgestates considering NN hopping it was reasoned that for $k_x = \pi$ the electrons localized at $y = 0$ and $y = N_y$ can not hop to a different y value and hence can not hop at all. The first part is still true considering NNN hopping but the second part is not! If we look at a zigzag edge and allow for NNN hoppings it is also possible to hop in horizontal direction (which means only the x-label is changing). This gives a intuitive reason why the edgestates now travel along the edge. The situation is illustrated in Fig. 3.18. If t_2 is negative the direction of the velocities is reversed.

3.6.1 STABILITY OF THE EDGE STATES

In Fig. 3.15 we see that the edge states do not necessarily have to cross (they do not in the bottom left picture). But if they do not cross each other, there are no edge states around the Fermi level (which is located between the bulk bands) we just have a normal insulator. So a question of interest is: where is the transition between not-crossing and crossing edge states happening. This

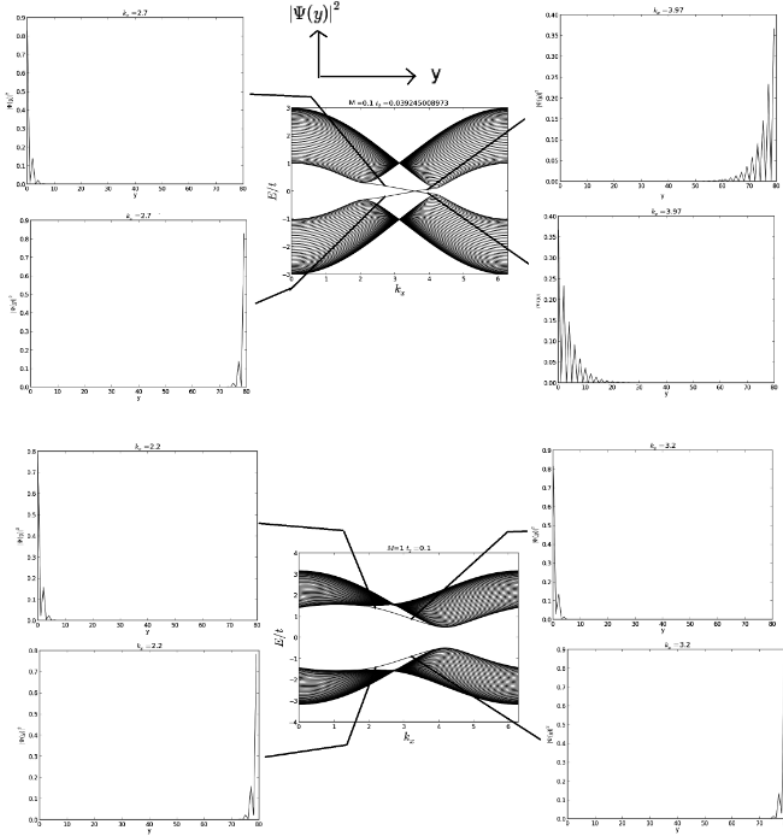


Figure 3.16: Absolute value squared of the wavefunctions corresponding to the out-of-the-bulk energies as a function of y .

transition is happening exactly where the bulk bands close at one of the dirac points i.e. where $t_2 = \pm \frac{M}{3\sqrt{3}}$ (at + the K points are touching and at - the K' points). Where $|t_2| > \frac{M}{3\sqrt{3}}$ the edge states cross. In the section on phase transitions we saw that this is exactly the region where our system is topological! This is no coincidence but it is manifested in a theorem: The *Bulk-Edge correspondance* [14] and [15]:

Theorem 1. (Bulk-Edge correspondance) *The bulk chern number is equal to the number of crossings of the Fermi-level of an edge state. To remove an edge state one hence has to change the chern number of the bulk.*

In this sense, the crossing edge states are stable now. They can not be gapped out by some small perturbation! To gap them out one has to change the chern number of the bulk. So our edge states, our being topological is protected by

3.6 Graphene ribbons in Haldane model

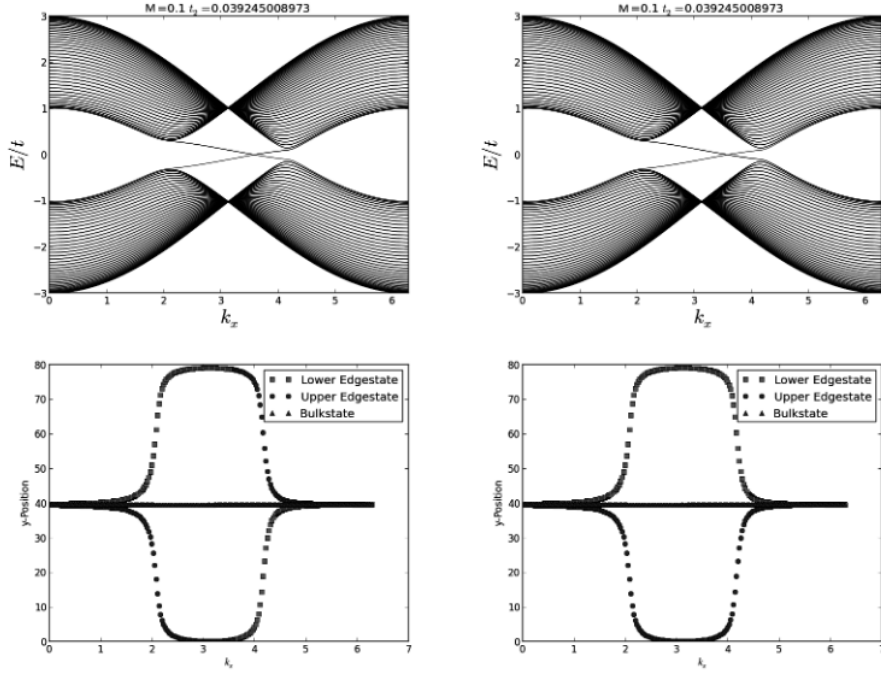


Figure 3.17: Localisation of the wavefunctions of the edgestates. Left column: we see the energybands of the two edgestates touch and below the corresponding localisation of the corresponding wavefunctions. Right column: we see the energybands of the two edgestates cross each other and below the corresponding localisation of the corresponding wavefunctions.

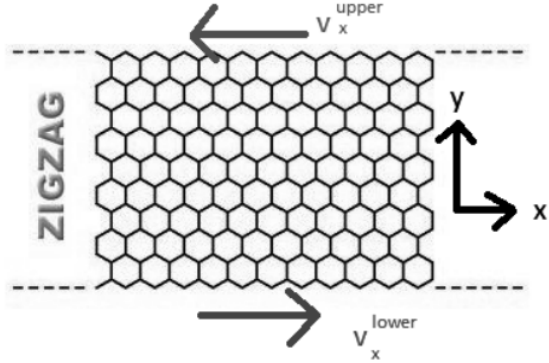


Figure 3.18: The two edgestates which appear in Haldane model travel in different directions on the opposite edges.

the bulk gap (because we saw the chern number is changing when the dirac-cones touch)! This is why here, in contrary to the NN hopping case we call the edgestates stable. Experimentally however, Haldane model is difficult to realize, also because it breaks time reversal symmetry.

3.7 KANE MELE MODEL

3.7.1 THE KANE MELE HAMILTONIAN

Haldane model gave as nice and interesting properties such as edgestates protected by the bulk band gap as well as edge-currents and topologically non-trivial insulators. But it broke time reversal symmetry. Now we ask the question whether it is possible to keep all the nice physics, but obey time reversal symmetry. An answer to this question was proposed by Charles L. Kane and Eugene J. Mele in 2005 [16]. The idea is to introduce spin on top of Haldane model, so that time reversal (TR) symmetry is obeyed. To do this, one takes two copies of Haldane model one for spin up and one for spin down. In order to conserve TR symmetry in one of the copies one changes $t_2 \rightarrow -t_2$. Before explicitly writing down the Kane-Mele Hamiltonian, let us introduce some notation which will simplify our future calculations:

$$\begin{aligned} H_{\mathbf{k}} &:= H_{\mathbf{k}}(t_2) := H_{\mathbf{k}}^{\text{Haldane}}(t_1, t_2, M) \\ H_{\mathbf{k}}^* &:= H_{\mathbf{k}}^*(t_2) := H_{\mathbf{k}}^{\text{Haldane}*}(t_1, t_2, M) \end{aligned}$$

where one could show the simple mathematical relation

$$H_{\mathbf{k}}(-t_2) = H_{-\mathbf{k}}^*(t_2) = H_{-\mathbf{k}}^*.$$

The Kane Mele Hamiltonian is then given by

$$H_{\mathbf{k}}^{KM} = \begin{pmatrix} H_{\mathbf{k}}(t_2) & \\ & H_{\mathbf{k}}(-t_2) \end{pmatrix} = \begin{pmatrix} H_{\mathbf{k}} & \\ & H_{-\mathbf{k}}^* \end{pmatrix} \quad (3.49)$$

where $H_{\mathbf{k}}$ is the Haldane Hamiltonian. Keeping in mind, that for spin systems the TR operator is given by

$$T = i\sigma_y \kappa = \begin{pmatrix} 0 & \mathbb{1} \\ -\mathbb{1} & 0 \end{pmatrix} \kappa \quad (3.50)$$

and hence

$$TH_{\mathbf{k}}^{KM}T^{-1} = H_{-\mathbf{k}}^{KM} \quad (3.51)$$

3.7 Kane Mele Model

which shows that TR symmetry is indeed obeyed.

Now we want to have a look at the energies of a Graphene ribbon in Kane-Mele model. Since we now that the Kane-Mele Hamiltonian just consists of two Haldane Hamiltonians (one having negative t_2) we have the solutions already. $H_{\mathbf{k}}^{KM\uparrow} = H_{\mathbf{k}} = H_{\mathbf{k}}(t_2)$ gives us the same plots as before in Haldane model. In $H_{\mathbf{k}}^{KM\downarrow} = H_{-\mathbf{k}}^* = H_{\mathbf{k}}(-t_2)$ we changed $t_2 \rightarrow -t_2$ how does this affect the energies? Let us have a look at Fig. 3.19 and Fig. 3.20. We see that at each edge there

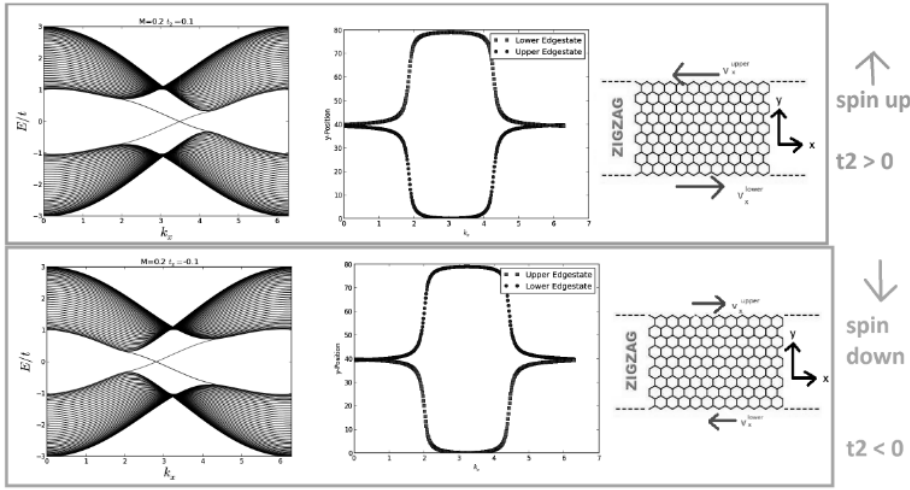


Figure 3.19: The top panel (framed green) is showing solutions for the spin up part, and the bottom panel (framed orange) is showing solutions for the spin down part. The left column is showing the energybands including the edgestates. The edgestate with positive group velocity (v_x) is coloured red, the one with negative group velocity ($-v_x$) is coloured blue. The middle column is displaying the localisation of the wavefunctions belonging to the edgestates of the same colour in the left column. The right column shows the group velocity of the respecting edgestates. We see that the edgecurrent flows in opposite directions for opposite spins.

are two edgestates. One for each spin. Furthermore the group velocities (and hence the edgecurrent) point in opposite direction. This means, looking at one edge only (let us say the upper one) we have two currents, the spin up electrons move along negative x -direction and the spin down electrons move along positive x -direction. Visa versa for the lower edge. This is remarkable because it means that if an impurity on the edge, wanted to backscatter an electron (hence leading to resistance) it also had to flip the spin, or jump to the other edge (which is highly improbable for a ribbon which is wise compared to the correlation length of the electrons). If one on the other hand reduces the ribbon to be narrow (i. e.

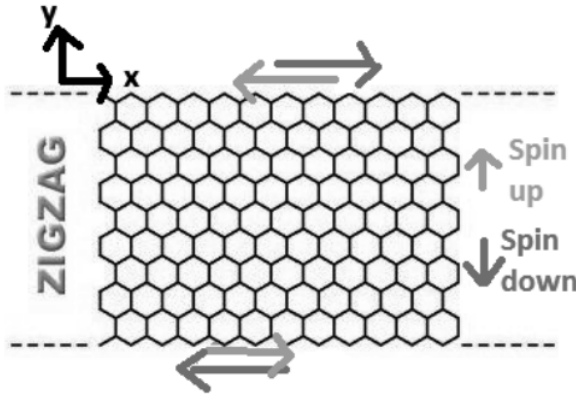


Figure 3.20: Edgecurrents in Kane-Mele model. One each edge there are two currents belonging to the two opposite spins flowing in two opposite directions

N_y to be close to 1), it becomes possible for the particle to jump from one edge to the other and it can hence be scattered back by non-spin-flipping impurities. An extreme example is the 1d chain.

3.7.2 Z_2 INVARIANCE

Let us now look at only one edge and small energies. The only energy states around the fermi level are the edge states, one for spin up and one for spin down. See Fig. 3.21. Now we want to find out, if there is a way that a perturbation

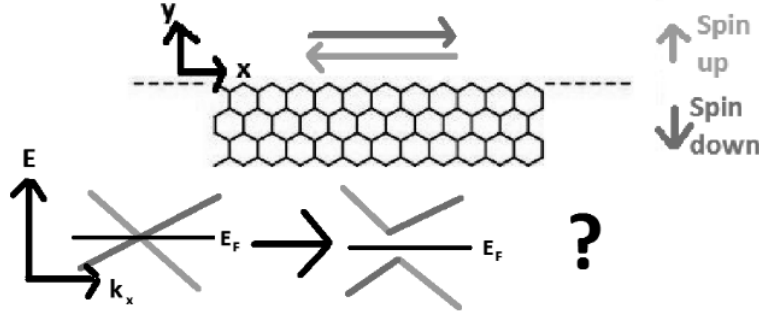


Figure 3.21: Edgecurrents in Kane-Mele model. At one edge we have two spin currents flowing in opposite directions. Their energy bands cross at $k_x = \pi$. We are asking the question, if they can be gapped out by a TR symmetry obeying perturbation

leads to a energygap. If this would be possible, the Fermi level could be shifted

3.7 Kane Mele Model

into that gap, which, considering the Bulk-Edge correspondence, would lead to a trivial insulator. To address this question we consider a corollary of Kramers Theorem [17] stating that TR symmetry obeying perturbations can not remove the degeneracy of an energy eigenstate of a TR symmetry obeying Hamiltonian. In our system, we have a degeneracy at $k_x = \pi$, where the two edge states cross. According to Kramers Theorem this crossing is protected by TR symmetry which means the energies of one pair of edge states at one edge of a Graphene ribbon can not be gapped out. To see why there initially is a degeneracy at $k_x = \pi$, notice:

$$H_{\pi}^{KM\uparrow} = H_{\pi} = H_{-\pi} = H_{\pi}^{KM\downarrow*}$$

Where the second equality is because $e^{i\pi} = e^{-i\pi}$. Since $H_{\pi}^{KM\downarrow*}$ and $H_{\pi}^{KM\downarrow}$ yield the same eigenvalues, $E_{\text{pi}}^{\uparrow} = E_{\text{pi}}^{\downarrow}$. So we have seen that for one pair of edge states at one edge, TR symmetry is protecting our edge states to be gapped out and is hence protecting our insulator from being a topologically trivial one (though Bulk-Edge correspondence as explained above).

What would happen if there would be two pairs of edge states at each edge? Would it then be possible to gap out the edge states and, at the same time, still respect TR symmetry? The situation in question is displayed in Fig. 3.22. The

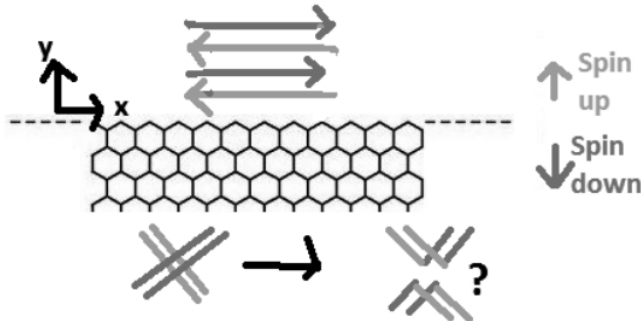


Figure 3.22: Edge currents in Kane-Mele model. At one edge we have four spin currents flowing in opposite directions (two edge states having the same spin, moving into the same direction). Their energy bands cross at $k_x = \pi$. We are asking the question, if they can be gapped out by a TR symmetry obeying perturbation

answer is *yes!* This can be shown by just giving an explicit example of such a perturbation (taken from [18]): For four spin currents along one edge, the

Hamiltonian expanded around $k_x = \pi$ is given by

$$H_{\mathbf{k}}^{KM} = \begin{pmatrix} v_1 k & & & \\ & v_2 k & & \\ & & -v_1 k & \\ & & & -v_2 k \end{pmatrix}.$$

Now we add the following perturbation to the system:

$$H^{pert} = \begin{pmatrix} & & & m \\ & & -m & \\ & -m & & \\ m & & & \end{pmatrix}$$

which does obey TR symmetry. So does the total Hamiltonian

$$H_{\mathbf{k}}^{tot} = H_{\mathbf{k}}^{KM} + H^{pert}$$

because we can easily calculate that

$$TH_{\mathbf{k}}^{tot}T^{-1} = H_{-\mathbf{k}}^{tot}$$

where T is now given by 3.50. Now we want to have a look at the eigenvalues of $H_{\mathbf{k}}^{tot}$. For simplicity we now take $v_1 = v_2$ (for $v_1 \neq v_2$ the qualitative results would stay the same). We obtain $E_{\mathbf{k}} = \pm \sqrt{m^2 + kv_1^2}$ each with a degeneracy of two. The upper and the lower energybands do not touch or cross, this means the system is now gapped out and we have a topologically trivial case. Hence we saw that, for two spin pairs on one edge TR symmetry is no longer protecting the system from being topologically trivial, even a small perturbation $m \neq 0$ will lead to the topologically trivial case. We hence call a system with one spin pair on one edge topological and a system with two spin pairs on one edge non-topological. This can be generalized to even and odd numbers of spin-pairs [9]. This generalization will not be explained here.

3.7.3 IS THE KANE MELE MODEL PHYSICALLY IMPLEMENTABLE?

Yes it is! This actually is probably the way how Kane and Mele obtained the Kane Mele Hamiltonian in first place [16] back in 2005. To see the physical sense of Kane Mele model one has to consider spin orbit (SO) interaction. Including SO interaction in our Hamiltonian we obtain

$$H = H_0 + H_{SO}$$

3.7 Kane Mele Model

where H_0 is given by:

$$H_0 = -i\hbar v_F \psi^\dagger (\sigma_x \tau_z \partial_x + \sigma_y \partial_y) \psi \quad (3.52)$$

where σ and τ are Pauli matrices with $\sigma_z = \pm 1$ describing states on the A(B) sublattice and $\tau_z = \pm 1$ describing states at the K(K') points. H_{SO} is then given by:

$$H_{SO} = \Delta_{SO} \psi^\dagger \sigma_z \tau_z s_z \psi \quad (3.53)$$

where s_z is a Pauli matrix representing the electron's spin. It respects all the symmetries of graphene. Looking at our Kane-Mele Hamiltonian we basically had:

$$H = \sum_{< i,j > \alpha} t_1 c_{i\alpha}^\dagger c_{j\alpha} + \sum_{<< i,j >> \alpha\beta} it_2 \nu_{ij} s_{\alpha\beta}^z c_{i\alpha}^\dagger c_{j\beta} \quad (3.54)$$

Where the first term is H^{NN} and the second is H^{NNN} where $\nu_{ij} = -\nu_{ji} = \pm 1$ (+ if the electron makes a left- and - if the electron makes a right turn to get to the NNN). For low temperatures 3.54 reduces exactly to 3.52 and 3.53 with $\Delta_{SO} = 3\sqrt{3}t_2$. So we see that considering SO interaction and doing low temperature approximation leads to nothing else than the Kane-Mele Hamiltonian 3.49. This makes Kane-Mele model to something bigger than a mathematical game, it makes it (and therefore the QSH effect in graphene) experimentally realizable (in principle). The magnitude of Δ_{SO} can be estimated considering the microscopic SO interaction in first order perturbation theory:

$$V_{SO} = \frac{\hbar}{4m^2c^2} \mathbf{s}(\nabla V \times \mathbf{p}) \quad (3.55)$$

Argument completely taken from [16]. The downside is, that in the case of graphene, the SO interaction is too weak to measure this effect [19]. But it was shown that QSHE could indeed be realized experimentally in HgTe Quantum Wells [20] (theoretical argument), [21] (experiment) and [22] (review of both).

BIBLIOGRAPHY

- [1] Y. Yao, F. Ye, X.-L. Qi, S.-C. Zhang, and Z. Fang, *Spin-orbit gap of graphene: First-principles calculations*, Physical Review B **75**, 041401 (2007).
- [2] B. A. Bernevig, *Topological Insulators and Topological Superconductors* (Princeton University Press, 2013).
- [3] K. v. Klitzing, G. Dorda, and M. Pepper, *New method for high-accuracy determination of the fine-structure constant based on quantized hall resistance*, Phys. Rev. Lett. **45**, 494 (1980).
- [4] K. Novoselov, A. K. Geim, S. Morozov, D. Jiang, M. Katsnelson, I. Grigorieva, S. Dubonos, and A. Firsov, *Two-dimensional gas of massless dirac fermions in graphene*, nature **438**, 197 (2005).
- [5] P. R. Wallace, *The band theory of graphite*, Physical Review **71**, 622 (1947).
- [6] G. W. Semenoff, *Condensed-matter simulation of a three-dimensional anomaly*, Phys. Rev. Lett. **53**, 2449 (1984).
- [7] F. Haldane, *Model for a quantum hall effect without landau levels: Condensed-matter realization of the parity anomaly*, Physical Review Letters **61**, 2015 (1988).
- [8] E. Kogan and V. Nazarov, *Symmetry classification of energy bands in graphene*, arXiv preprint arXiv:1201.5045 (2012).
- [9] C. L. Kane and E. J. Mele, *Z_2 topological order and the quantum spin hall effect*, Physical review letters **95**, 146802 (2005).
- [10] M. Oshikawa, *Quantized hall conductivity of bloch electrons: Topology and the dirac fermion*, Phys. Rev. B **50**, 17357 (1994).

BIBLIOGRAPHY

- [11] *Graphene simulations hint at future electronics @ONLINE* (2007), URL nanotechweb.org/cws/article/indepth/31360.
- [12] K. Nakada, M. Fujita, G. Dresselhaus, and M. S. Dresselhaus, *Edge state in graphene ribbons: Nanometer size effect and edge shape dependence*, Phys. Rev. B **54**, 17954 (1996).
- [13] D. R. Hofstadter, *Energy levels and wave functions of bloch electrons in rational and irrational magnetic fields*, Phys. Rev. B **14**, 2239 (1976).
- [14] Y. Hatsugai, *Chern number and edge states in the integer quantum hall effect*, Phys. Rev. Lett. **71**, 3697 (1993).
- [15] Y. Hatsugai, *Edge states in the integer quantum hall effect and the riemann surface of the bloch function*, Phys. Rev. B **48**, 11851 (1993).
- [16] C. L. Kane and E. J. Mele, *Quantum spin hall effect in graphene*, Physical Review Letters **95**, 226801 (2005).
- [17] H. A. Kramers, *General theory of paramagnetic rotation in crystals*, Proceedings Koninklijke Akademie van Wetenschappen 33 (1930).
- [18] K. Sun, *Lecture notes for the course physics 620 at the university of michigan* (2014), URL http://www-personal.umich.edu/~sunkai/teaching/Fall_2012/chapter5_part1.pdf.
- [19] Y. Yao, F. Ye, X.-L. Qi, S.-C. Zhang, and Z. Fang, *Spin-orbit gap of graphene: First-principles calculations*, Phys. Rev. B **75**, 041401 (2007).
- [20] B. A. Bernevig, T. L. Hughes, and S.-C. Zhang, *Quantum spin hall effect and topological phase transition in hgte quantum wells*, Science **314**, 1757 (2006).
- [21] M. Knig, S. Wiedmann, C. Brne, A. Roth, H. Buhmann, L. W. Molenkamp, X.-L. Qi, and S.-C. Zhang, *Quantum spin hall insulator state in hgte quantum wells*, Science **318**, 766 (2007).
- [22] M. Koenig, H. Buhmann, L. W. Molenkamp, T. L. Hughes, C.-X. Liu, X.-L. Qi, and S.-C. Zhang, *The quantum spin hall effect: Theory and experiment* (2008), arXiv/0801.0901.

CHAPTER 4

TOPOLOGICAL INSULATORS IN 2D AND 3D: THE QUANTUM SPIN HALL EFFECT IN HGTE QUANTUM WELLS AND A SHORT INTRODUCTION TO 3D TOPOLOGICAL INSULATORS

ERIK CHEAH

SUPERVISOR: ALEXEY SOLUYANOV

Certain materials may host a phase that is different from the conventional metal/insulator classification: a topological insulating phase. Topological insulators are insulating in the bulk yet show conducting edge or surface states that are protected by time-reversal symmetry. The Quantum Spin Hall Effect (QSH), that describes the edge states in 2D systems, was predicted and experimentally observed in HgTe/CdTe quantum wells. In this report the 4×4 Bernevig-Hughes-Zhang model for HgTe/CdTe quantum well structures is described. Group theory allows to construct an effective model from symmetry considerations alone. The topological phase transition is discussed in detail. Transport experiments on HgTe quantum well structures are also discussed. Finally, a short introduction to 3D topological insulators and their classification is given.

4.1 Introduction

4.1 INTRODUCTION

The Quantum Spin Hall state is distinguished from the quantum Hall effect by counter-propagating (helical) spin-polarized edge transport channels that are protected by time-reversal symmetry [1].

In contrast to the quantum Hall effect, this phase is not driven by an external field but is intrinsic to certain materials – Topological insulators (TI).

In the following, a few models are presented in order to understand why spin-orbit (SO) interaction and time-reversal symmetry play a major role in the discussion of TI (Some of them are discussed in detail in previous chapters of this Proseminar series).

The first one is due to Haldane, who in 1988 introduced a honeycomb-lattice tight-binding model, where complex hopping corresponded to locally non-zero magnetic fluxes. However, the net flux through the unit cell vanishes. This model described quantum Hall effect without external magnetic field, and, hence, Landau levels [2].

In 2004, [3] theoretically predicted zero-gap and narrow band-gap semiconductors with large SO coupling to exhibit dissipationless spin-Hall effect. One year later, right after the experimental discovery of single-layer graphite sheets [4], graphene was proposed to host a new topological phase that exhibits the QSH effect. In the work of [1], the authors made use of Haldane’s model, and showed that spin-orbit interactions can lead to a gap at the Dirac points and helical edge transport channels upon introduction of time-reversal symmetry into the model. The energy spectrum takes the form (compare to the previous chapter in this series): $E_k = \pm\sqrt{(\hbar v_F k)^2 + \Delta_{SO}^2}$, where Δ_{SO} is the spin-orbit induced gap [5]. Violation of inversion symmetry, that is, a difference between the two atoms in the unit cell, also leads to a gapping spectrum, however, such a state corresponds to an ordinary band insulator [6].

Later on it was argued that the spin-orbit induced gap in graphene is too small to give access to the QSH effect in experiments [7, 8]. In fact, calculations of Ref. [8] showed that the gap at the Dirac points is of the order of 10^{-3} meV so that in graphene the QSH effect should only be observable well below 0.01 K.

4.2 ROLE OF SPIN-ORBIT COUPLING IN TOPOLOGICAL INSULATORS

Going a step further and taking the electron spin into account, the work of [1] suggested a TRS model based on two copies of Haldane model for spin-up and spin-down species. It was also shown in that work that introducing a SO interaction term can lead to a graphene system that is gapped at the Dirac points but does not break TR symmetry and exhibits counter-propagating and spin-polarized edge states [1, 5].

In the quest for finding the QSH effect in real materials it is therefore worth looking for materials where SO coupling is large. i.e. $E_{gap} < E_{SO}$. As the strength of the SO coupling scales roughly with Z^4 [9], Z the atomic number, elements or compounds with larger atomic number are of interest. Furthermore, to circumvent the treatment of d -orbitals that give rise to strongly correlated effects it makes sense to look at the lower right corner of the periodic table.

Following this reasoning, HgTe was found to be a 2D topological insulator. Also, inverted type II semiconductor structures have been proposed [10] to host this phase. Generalizing the QSH state to three dimensions, several materials (bismuth-antimony alloys ($\text{Bi}_{1-x}\text{Sb}_x$), strained HgTe, α -Sn [11]) were proposed as candidates. In 2009, ARPES measurements on bismuth-selenide $\text{Bi}_{1-x}\text{Sb}_x$ revealed a topological phase in this material [12] as predicted earlier by first-principles calculations in the work of [13].

In this report, the main focus is on the description of the low-energy electronic properties and band structure of HgTe and HgTe/CdTe quantum wells (QW). Quantum confinement induced by a QW is used to drive a transition to the topological phase [14]. To understand the band structure and the symmetries involved, the main features of the group theoretical concept of 'double groups' is introduced. In a further step a 4-band Bernevig-Hughes-Zhang (BHZ) model is presented and its symmetries are discussed. Finally, two transport measurements are presented.

4.3 SEMICONDUCTOR BAND STRUCTURES AROUND THE Γ -POINT AND THE CONCEPT OF DOUBLE GROUPS

In this section the group theoretical concept of double groups is introduced briefly. Double groups will be useful to understand the band structure symmetries which

4.3 Semiconductor band structures around the Γ -point and the concept of double groups

are important for the low energy physics of the presented materials. For more information readers are referred to the book of [9]. A good overview is also found in the lecture notes of Ref. [15], as well as in Ref. [16]. An introduction to the basic group theory is also given the first chapter of this series.

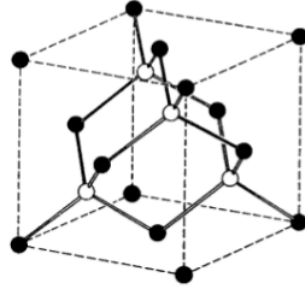


Figure 4.1: The zinc-blende crystal structure. Black and white depict two different atomic species and for identical species the diamond structure is obtained. From [9])

Here we are mainly concerned with HgTe. It is a II-VI semiconductor with zinc-blende structure (see Fig. 4.1). The space group of the a crystal with zinc-blende structure is symmorphic, i.e. all operations are the point group operations plus the translation operations of the underlying Bravais lattice. The crystallographic point group associated with the zinc-blende structure is the cubic crystal system T_d (Schönflies notation), the symmetry of a regular tetrahedron [9, 16]. Further down, some simplifications to justify the BHZ model are made. Therefore the symmetries of the diamond lattice, corresponding to the point group O_h (cubic group = O + inversion I) are mainly discussed here. See Tab. 4.1 and 4.2 for an overview of the mentioned crystallographic point groups and their elements.

Another application of group theory is that to the splitting of atomic energy levels, i.e. lifting of degeneracies, when the atom is incorporated in a crystal lattice potential. Starting from the full rotational symmetry of the atom, it can be shown that the spherical harmonics $Y_{l,m}(\theta, \phi)$, which are angular momentum eigenfunctions, yield odd-dimensional, irreducible representations of the rotation group: The $l = 0$ (s-like) rep. is one-dimensional, the $l = 1$ ($m = -1, 0, 1$; p-like) is three-dim. and so on. Eventually one arrives at the representation $D^{(l)}(\alpha)$ for

TI IN 2D AND 3D: THE QUANTUM SPIN HALL EFFECT IN HGTE
QUANTUM WELLS AND A SHORT INTRO. TO 3D TI [ERIK CHEAH]

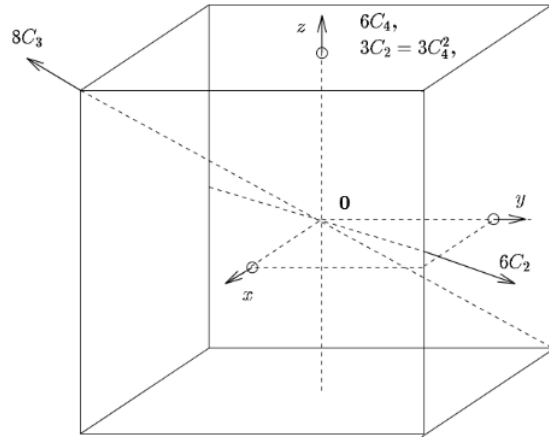


Figure 4.2: Symmetry operations of the crystal point group \mathcal{O}_h . From [9]

a rotation C_α around an angle α .

$$D^{(l)}(\alpha) = \begin{pmatrix} e^{-il\alpha} & & & 0 \\ & e^{-i(l-1)\alpha} & & \\ & & \ddots & \\ 0 & & & e^{-ila} \end{pmatrix} \quad (4.1)$$

(note: the character is directly given by the trace.)

Point group	classes	nr. of elements	lattice
\mathcal{O}	5: $E, 8C_3, 3C_2, 6C_4, 6C'_2$	24	cubic
$\mathcal{O}_h = \mathcal{O} \otimes \mathcal{I}$	10	48	diamond
\mathcal{T}_d	5: $E, 8C_3, 3C_2, 6S_4, 6\sigma_d$	24	zinc-blende

E : identity,
 C_n : n-fold ($2\pi/n$) rotation,
 S_n : improper rotation $C_n \otimes \sigma_h$
 σ_h : "horizontal" plane reflection
 σ_d : "diagonal" plane reflection

Table 4.1: Overview of the relevant crystal point groups. From [9].

As the crystal point group has a finite number of rotation symmetries, above representation is usually reducible, thus the $(2l+1)$ -fold degeneracy will be to some extent lifted. The decomposition to irreducible representations gives then the level splitting,

4.3 Semiconductor band structures around the Γ -point and the concept of double groups

\mathcal{O}_h	E	$3C_4^2$	$6C_4$	$6C_2$	$8C_3$	I	$3IC_4^2$	$6IC_4$	$6IC_2$	$8I C_3$
Γ_1^\pm	1	1	1	1	1	± 1	± 1	± 1	± 1	1
Γ_2^\pm	1	1	-1	-1	1	± 1	± 1	∓ 1	∓ 1	1
Γ_{12}^\pm	2	2	0	0	-1	± 2	± 2	0	0	∓ 1
Γ_{15}^\pm	3	-1	1	-1	0	∓ 3	± 1	∓ 1	± 1	0
Γ_{25}^\pm	3	-1	-1	1	0	∓ 3	± 1	± 1	∓ 1	0

Table 4.2: Character table of \mathcal{O}_h . Γ^\pm denote irreduc. rep. with even or odd parity. From [9].

however not the order of the energy levels.

By combining $\mathbf{k} \cdot \mathbf{p}$ perturbation with group theory the form of the band structure can be found. A result from group theory is that the Γ -point, $\mathbf{k} = 0$, in reciprocal space displays the full point group symmetry of the crystal [9]. Usually, without SO coupling, the symmetries of bands at Γ are denoted by Γ_1, Γ_{15} and Γ_{12}, Γ_{25} for s-, p- and d-states correspondingly. The Γ^\pm stands for even or odd parity, when inversion symmetry is present. A typical band ordering near the Γ -point (for example Si, Ge, GaAs) without SO coupling is shown in Fig. 4.3.

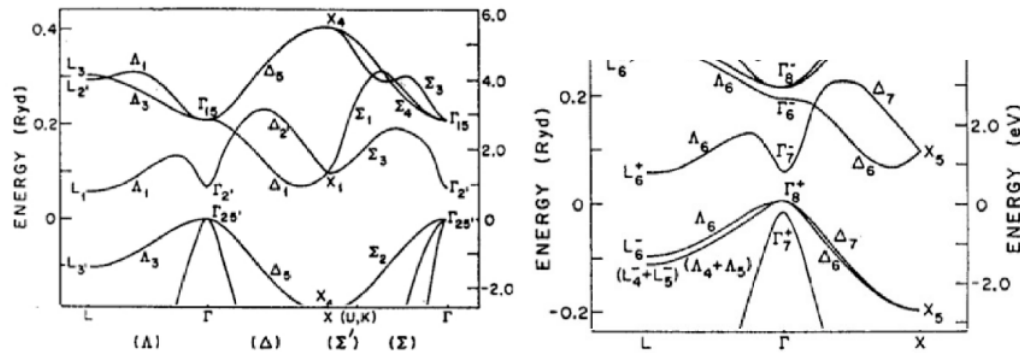


Figure 4.3: Band structure of Ge. Left: Without SOC. Right: Including SOC, zoom on Γ -point. From [9]

So far, only the symmetries of the crystal played a role. If now the electron spin is added to the discussion, we have to reconsider, since a rotation in spin space by 2π leads to a phase factor -1 . This has to be accounted for in the irreducible representations of the electron wave functions. In zinc-blende crystals, the point group at the Γ -point contains 24 elements, taking spin into account the number of elements increases to 48. On the other hand, the number of classes is not necessarily doubled. Let \mathcal{R} be a rotation by 2π in spin $1/2$ space. This rotation

TI IN 2D AND 3D: THE QUANTUM SPIN HALL EFFECT IN HGTE
QUANTUM WELLS AND A SHORT INTRO. TO 3D TI [ERIK CHEAH]

yields a phase factor of $e^{i\pi} = -1$

For a class A_i in the original point group, $\mathcal{R}A_i$ forms a new class (except for a rotation by 2π (C_2 and $\mathcal{R}C_2$ lie in the same class)). This also leads to additional irreducible representations. As an example: The Double group of \mathcal{O} has eight classes, 3 "new" ones → three new irred. rep. $\Gamma_6, \Gamma_7, \Gamma_8$ with dimension 2, 2, 4, see Tab. 4.3.

\mathcal{O}_h	E	\mathcal{R}	...
Γ_1^\pm	1	...	
Γ_2^\pm	1	...	
Γ_{12}^\pm	2	...	
Γ_{15}^\pm	3	...	
Γ_{25}^\pm	3	...	
Γ_6^\pm	2	...	
Γ_7^\pm	2	...	
Γ_8^\pm	4	...	

Table 4.3: Double group extension of the character table of \mathcal{O}_h

Extending the spherical harmonics with spin rotation one eventually arrives at the additional double group representations for \mathcal{O} by taking the direct product of the spatial wave function representation with the electron spin function representation: $\Gamma_i \otimes D_{1/2}$. One denotes $\Gamma_1 \otimes D_{1/2} = \Gamma_6$ ($j_z=1/2$), s-like), and $\Gamma_{15} \otimes D_{1/2} = \Gamma_7$ ($j_z=1/2$) + Γ_8 ($j_z=3/2$), p-like, where . For the case of a diamond lattice, the parity has also to be taken into account in the equations.

Including spin-orbit interaction, one can show that the common band ordering near the Γ -point is as in Fig. 4.4 [16]. Away from $k = 0$, the Γ_8 splits into a heavy hole (HH) band and a light hole (LH) band (stronger curvature), see also Fig. 4.4.

In general, computer simulations and comparison to experimental data are needed to fit the values of the parameters for the band structure.

4.4 Band Structure of HgTe

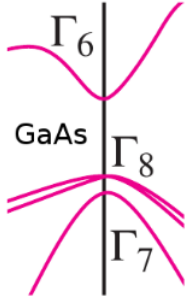


Figure 4.4: Representative: Calculated band structure for GaAs close to the Γ -point. Γ_6 is the lowest conduction band, Γ_7 the SO split-off band and Γ_8 the highest valence band. From [16].

4.4 BAND STRUCTURE OF HGTE

In HgTe, the hybridized sp^3 bonds that define the physics of this compound, being the closest to the Fermi level, are composed of 6s states of Hg atom and 5p states of the Te [17, 18]. In contrast to the band ordering of other semiconductors with similar structure, as in Fig. 4.4, SO coupling caused by the heavy Hg leads to "inverted" position of the bands: The s-type - spin 1/2 band (Γ_6) band is energetically below the p-type - spin 3/2 band (Γ_8), with a gap of ~ 300 meV [19]. In Fig. 4.5 it can be seen, that bulk HgTe is a semimetal [19].

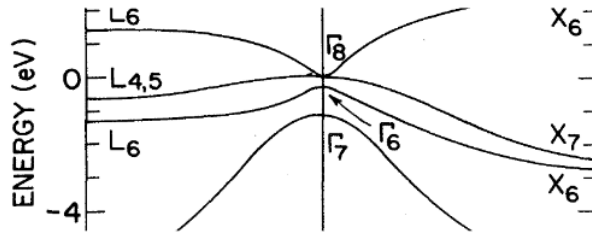


Figure 4.5: Calculated band structure for HgTe. The band structure is "inverted", i.e. the Γ_6 lies below the Γ_8 band. From [19].

Important for the quantum well structure is the difference in the symmetries of the highest valence and lowest conduction band compared to CdTe near the Γ -point, shown schematically in Fig. 4.7. For CdTe the energy at the Γ -point of the Γ_6 band lies above the Γ_8 band. As the thickness of the HgTe layer is increased, the band properties of the HgTe bulk become more pronounced, i.e. energetically the Γ_8 lies above the Γ_6 band. Eventually, at a critical thickness this results in a level crossing at the interfaces.

4.5 HGTE QUANTUM WELLS AND THE BERNEVIG-HUGHES-ZHANG MODEL

In 2006, a model was proposed by Bernevig, Hughes, and Zhang [14] to describe thin layers of HgTe in quantum wells with CdTe as barrier. This model identified such QWs as a candidate system to find the QSH effect. In order to drive HgTe through a topological phase transition one needs to remove the semimetallic character at the Γ -point. As mentioned, lifting the degeneracies of the Γ_8 band can be achieved through lowering of the point group symmetry [20, 17]. Experimentally this can be obtained by strain [18].

HgTe/CdTe QW's belong to the type III heterostructures [21], see Fig. 4.6.

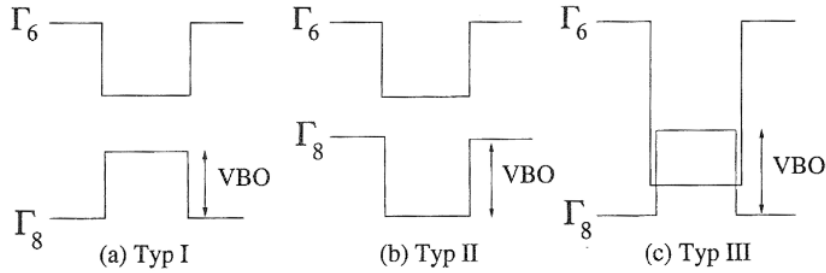


Figure 4.6: Band-offset classification of semiconductor heterostructures. From [21].

Spatially confining the electrons by barriers in, say, z -direction leads to energy quantization and formation of subbands. In QWs the energy of these newly formed subbands depends on the width of the well. As the symmetries of the low-energy bands of HgTe are inverted compared to CdTe it was argued that by controlling the symmetry/order of the QW subbands via the well width, one would be able to drive the thin film of HgTe into a topological phase.

To capture the low energy physics in HgTe/CdTe quantum wells it is important to know, which bands play a major role and how they couple. The important bands are the s-like Γ_6 and the LH Γ_7 and HH Γ_8 band. To describe the coupling between these bands the Kane model was used [21, 22]. It was found that the split-off Γ_7 band can be omitted as it couples weakly (< 5% [21, 14]) to the other subband states. Therefore, [14] reduced the problem to a 6x6 Kane Hamiltonian resp. 6-band Hamiltonian with the basis $| \Gamma_6, +1/2 \rangle$, $| \Gamma_6, -1/2 \rangle$, $| \Gamma_8, +3/2 \rangle$, $| \Gamma_8, +1/2 \rangle$, $| \Gamma_8, -1/2 \rangle$, $| \Gamma_8, -3/2 \rangle$. Their Hamiltonian preserves bulk inversion symmetry (BIA) [23]; resp. neglects zinc-blende induced BIA. Further in the work of Ref. [14] it is stated, that the first electron subband, E_1 , which

4.5 HgTe Quantum Wells and the Bernevig-Hughes-Zhang model

consists of hybridized states of the electron and LH bands ($j_z = 1/2$), has mainly Γ_6 character. The LH subband, L_1 , is argued to be far off in energy. So the subbands of interest are the $E_1, j_z = 1/2$ subband and the $H_1, j_z = 3/2$ subband. For a detailed derivation it is referred to Refs. [14, 23].

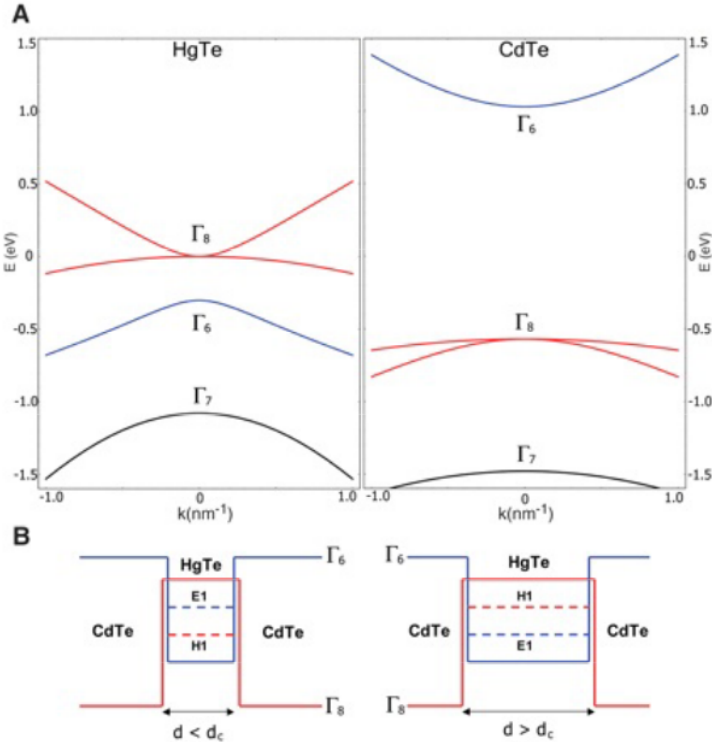


Figure 4.7: Top: Schematic band structure around the Γ -point for HgTe and CdTe bulk. Bottom: Schematic of the lowest subband situation in a HgTe/CdTe quantum well. For a critical thickness, the subbands are inverted. From [14].

The BHZ model is made out of these four states, describe the low-energy physics: $|E_1, +1/2\rangle, |H_1, +3/2\rangle, |E_1, -1/2\rangle, |H_1, -3/2\rangle$, which are two Kramer's pairs [5]. Finally, the effective BHZ Hamiltonian is claimed to be of the form

$$\begin{pmatrix} h(k) & 0 \\ 0 & h^*(-k) \end{pmatrix} \text{ in the above ordered basis:}$$

$$H_{BHZ}(k) =$$

TI IN 2D AND 3D: THE QUANTUM SPIN HALL EFFECT IN HGTE
QUANTUM WELLS AND A SHORT INTRO. TO 3D TI [ERIK CHEAH]

$$\begin{pmatrix} \epsilon(k) + M(k) & A(k_x + ik_y) & 0 & 0 \\ A(k_x - ik_y) & \epsilon(k) - M(k) & 0 & 0 \\ 0 & 0 & \epsilon(k) + M(k) & -A(k_x - ik_y) \\ 0 & 0 & -A(k_x + ik_y) & \epsilon(k) - M(k) \end{pmatrix} \quad (4.2)$$

$\epsilon(k) = C - D(k_x^2 + k_y^2)$, $M(k) = M - B(k_x^2 + k_y^2)$ A, B, C, D and M are QW parameters.

4.5.1 GENERAL 4-BAND HAMILTONIAN FOR THE 2D SYSTEM

Knowing the basis of the 4x4 Hamiltonian, the next task is to derive the most general Hamiltonian, that satisfies the important symmetries of the HgTe QW system. Thus, we will explain the appearance of the Hamiltonian above.

In 2D, a full set of basis matrices are the Pauli matrices

$$\sigma_x = \begin{pmatrix} 0 & 1 \\ 1 & 0 \end{pmatrix}, \sigma_y = \begin{pmatrix} 0 & -i \\ i & 0 \end{pmatrix}, \sigma_z = \begin{pmatrix} 1 & 0 \\ 0 & -1 \end{pmatrix} \text{ with the}$$

unit matrix I_{2x2} .

By taking the Kronecker product of these matrices, one arrives at a complete basis for a 4x4 matrix space. These are 15 basis matrices in total and build the Clifford Algebra and are sometimes called Dirac matrices [5].

The Hamiltonian to be derived should have all symmetries of the HgTe lattice structure. However a number of simplifications, partially used already, are made:

- Obviously, we already assume that only 4 bands play a major role in the low-energy physics.
- Neglect the two different atomic species in the unit cell \rightarrow generalize the zinc-blende to the diamond structure: $\mathcal{T}_d \rightarrow \mathcal{O}_h$, i.e. BIA is neglected
- The symmetries are further reduced by the two dimensional nature of the QW \rightarrow Basis functions in k_x and k_y

With these assumptions, the only symmetries left to consider are therefore: Inversion I , Time reversal \mathcal{T} , C_2 and C_4 rotation and the in-plane reflection σ_d . Remember, with spin, for the symmetry operations the following must hold:

4.5 HgTe Quantum Wells and the Bernevig-Hughes-Zhang model

$$I^2 = 1, T^2 = -1, C_4^4 = -1, C_2^2 = -1, \sigma_d^2 = -1$$

Considering the basis is ordered as s-, p-, s-, p-like, $I = \text{diag}(1, -1, 1, -1)$. $T = i(\sigma_y \otimes I) \cdot \hat{K}$, where \hat{K} is hermitian conjugate. The C_n are given by Eq. 4.1.

In Tab. 4.4 the symmetries of the basis matrices are summarized. Similarly, for the general basis functions in k_x and k_y up to second order, the symmetry properties are shown in Tab. 4.5.

Matrix	I	T	C_2	C_4	σ_d
$I \otimes \tau_x$	-	+	-	$-\sigma_z \otimes \tau_y$	$\sigma_z \otimes \tau_y$
$I \otimes \tau_y$	-	-	-	$\sigma_z \otimes \tau_x$	$-\sigma_z \otimes \tau_x$
$I \otimes \tau_z$	+	+	+	+	+
$\sigma_x \otimes I$	+	-	-	$\sigma_y \otimes \tau_z$	$-\sigma_x \otimes \tau_x$
$\sigma_x \otimes \tau_x$	-	-	+	-	$\sigma_y \otimes \tau_x$
$\sigma_x \otimes \tau_y$	-	+	+	-	$\sigma_y \otimes \tau_y$
$\sigma_x \otimes \tau_z$	+	-	-	$\sigma_x \otimes \tau_y$	$-I \otimes \tau_z$
$\sigma_y \otimes I$	+	-	-	$-\sigma_x \otimes \tau_x$	$\sigma_y \otimes \tau_z$
$\sigma_y \otimes \tau_x$	-	-	+	-	$\sigma_x \otimes I$
$\sigma_y \otimes \tau_y$	-	+	+	-	$\sigma_x \otimes \tau_x$
$\sigma_y \otimes \tau_z$	+	-	-	$-I \otimes \tau_z$	$\sigma_x \otimes \tau_y$
$\sigma_z \otimes I$	+	-	+	+	-
$\sigma_z \otimes \tau_x$	-	-	-	$-I \otimes \tau_y$	$-I \otimes \tau_y$
$\sigma_z \otimes \tau_y$	-	+	-	$I \otimes \tau_x$	$I \otimes \tau_x$
$\sigma_z \otimes \tau_z$	+	-	+	+	-

Table 4.4: Summary of the investigated symmetry properties of the 4x4 basis matrices.

basis function	I	T	C_2	C_4	σ_d
const.	+	+	+	+	+
k_x	-	-	-	$-k_y$	k_y
k_y	-	-	-	$+k_x$	k_x
k_x^2	+	+	+	k_y^2	k_y^2
k_y^2	+	+	+	k_x^2	k_x^2
$k_x^2 + k_y^2$	+	+	+	+	+
$k_x k_y$	+	+	+	-	+

Table 4.5: Summary of the investigated symmetry properties of the basis functions in k_x and k_y up to second order.

TI IN 2D AND 3D: THE QUANTUM SPIN HALL EFFECT IN HGTE QUANTUM WELLS AND A SHORT INTRO. TO 3D TI [ERIK CHEAH]

Taking the basis functions with the same symmetry properties as the basis matrices, the general form of the 4x4 Hamiltonian can be derived. E.g. under a C_4 rotation $k_x \rightarrow k_y$, $k_y \rightarrow -k_x$; whereas $\sigma_z \otimes \tau_x \rightarrow -I \otimes \tau_y$ and $I \otimes \tau_y \rightarrow \sigma_z \otimes \tau_x$. No other matrices share exactly the same symmetry properties so we can write a first building block of our Hamiltonian: $k_x \cdot I \otimes \tau_y + k_y \cdot \sigma_z \otimes \tau_x$. Continuing with this procedure, one eventually arrives at the Hamiltonian, H_{gen} :

$$H_{gen} =$$

$$c_1 \cdot I_{4 \times 4} + c_2 k_x \cdot I \otimes \tau_y + c_3 k_y \cdot \sigma_z \otimes \tau_x + c_4 (k_x^2 + k_y^2) \cdot I \otimes \tau_z \quad (4.3)$$

c_i are constants.

Comparing this matrix to the BHZ Hamiltonian and choosing the same coefficients, it follows that H_{gen} is equal to H_{BHZ} up to an energy shift by $\epsilon(k)$. So the BHZ Hamiltonian already is the most general H that satisfies the required symmetries.

4.5.2 EIGENSTATES AND PARITY

In the previous parts of this collection, it was shown that in systems with inversion symmetry, the Z_2 invariant can be expressed as a Pfaffian. In the paper by [11] the Pfaffian was proofed to be related to the parity eigenvalues at the four time-reversal invariant momenta (TRIM). In fact, each TRIM would be a candidate for the opening of a gap and would have its own effective Hamiltonian. However, as only low energy physics are considered, only the Γ -point is critical [20], i.e. we have no change in parity at the other TRIM's as we change the thickness of the QW. Also, H_{BHZ} commutes with I : $[H_{BHZ}, I] = 0$.

To see now what material parameter influences a topological phase transition at $\mathbf{k} = 0$, we solve H_{BHZ} for its eigenenergies and the parity eigenvalues. The eigenenergies are calculated straightforwardly:

$$E_{\pm} = \epsilon(k) \pm \sqrt{A^2(k_x^2 + k_y^2) + M^2(k)} \quad (4.4)$$

A gap of magnitude $2M$ has appeared, $\epsilon(k)$ can be regarded as an arbitrary energy shift. From the above equation it can already be seen that close to the Γ -point the material parameter M is important. Calculating and normalizing

4.5 HgTe Quantum Wells and the Bernevig-Hughes-Zhang model

the eigenvectors the parity of the states was eigenvalues analyzed. They indeed turn out to be either +1 or -1 for either E_+ or E_- and change their sign under a sign change of M . When M changes sign the subband states also change their relative energy, the parity of the higher and lower energy states have changed. This means that the two subbands must have crossed for $M = 0$ and together with the Pfaffian argument from Ref. [11] one can deduce that a topological phase transition must have occurred. Which parameter regime now represents the QSH state is not clear yet, so further considerations are needed.

4.5.3 EDGE STATES

A simplified tight binding model that should describe the most important topological features was also proposed in the work of Refs. [14, 20]. By comparing the tight binding Hamiltonian to work done on the quantum anomalous Hall effect and the Hall conductance of the massive Dirac model, the following criterion is derived: If $M/2B < 0$ there is no Hall conductance, hence this is the normal regime. For $0 < M/2B < 2$ the two different blocks describe to two independent quantum Hall systems with counter-propagating edge states. The upper boundary is said to be fulfilled as the gap $2M$ is small. Comparing to numerical data, the topological non-trivial phase should occur in the inverted regime.

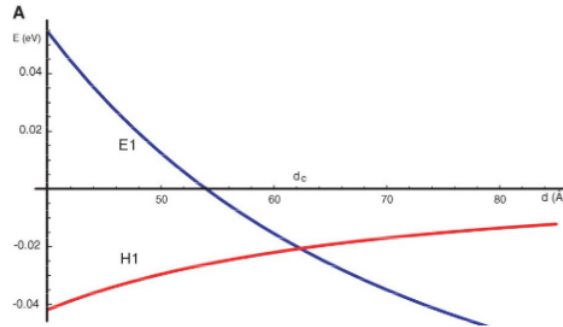


Figure 4.8: Calculated sub-band energies as function of QW thickness. From [14].

Numerical calculations pointed out that the band inversion occurs a HgTe layer thickness $d_c \approx 6.3$ nm, see Fig. 4.8. The material parameters in the vicinity of this value are given in Tab. 4.6.

TI IN 2D AND 3D: THE QUANTUM SPIN HALL EFFECT IN HGTE
QUANTUM WELLS AND A SHORT INTRO. TO 3D TI [ERIK CHEAH]

d [nm]	A [eV]	B [eV]	C [eV]	D [eV]	M [eV]	$\frac{M}{2B}$ [10^{-4}]
5.8	-3.62	-18.0	-0.018	-0.594	0.00922	-2.56
7.0	-3.42	16.9	-0.023	0.514	-0.00686	2.02

Table 4.6: Numerical values for HgTe/CdTe QW material parameters. From [14]

An exact solution was given in the paper by [24] in 2008 and proofed to be consistent with experimental results.

To obtain a rough estimate of the energy scales and the dimensions, one can calculate:

Energy difference of the two lowest QW states in the infinite well approximation for $L_{QW} = 70$ Å and $m^* = 0.03 m_e$ (from: [25])

$$\Delta E = \frac{3\hbar^2\pi^2}{2m^*L_{QW}^2} \approx 0.4 \text{ meV}$$

Typical kinetic energy with $v_F = 10^5$ m/s and $k = 2\pi/5$ Å:

$$E_{kin} = \frac{\hbar^2 k^2}{2m_e} = v_F \hbar k \approx 0.8 \text{ meV}$$

By comparing the level spacing ΔE to a typical kinetic energy E_{kin} , one can see that they are of the same order of magnitude. So one should also be cautious with the 2D approximation as the numbers suggest that the system is on the verge of becoming 3D. With temperatures below 100 mK only the ground state of the QW should be occupied and there should be no excitations over the small band gap.

4.6 EXPERIMENTS

In this section two transport measurements on HgTe QWs are presented. The first work was published only one year after the proposal of the BHZ model by [26] with first evidence of quantized QSH conductance and the expected behavior in magnetic field. The second work was published in 2009 by [27], where they made use of the Landauer-Büttiker formalism to predict the edge current flow for two geometries when different Voltage configurations are applied.

4.6 Experiments

HgTe/CdTe quantum wells are grown by molecular beam epitaxy and a schematic can be seen in Fig. 4.9. Common for quantum Hall conductance measurements is the Hall-bar geometry.

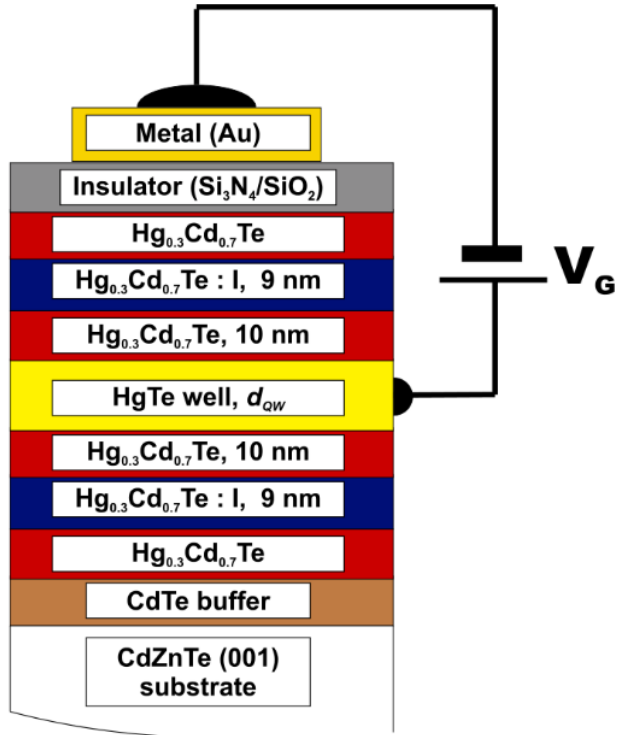


Figure 4.9: Schematic of the experimental QW structure. From [20].

4.6.1 QUANTIZED EDGE CHANNEL TRANSPORT

Before going over to the actual observations, a quick introduction to the Landauer-Büttiker formalism is given in order to understand the experiments.

In contrast to Ohm's law, in this formalism the current-voltage relation is given by:

$$I_i = e^2/h \sum_j (T_{ji}V_i - T_{ij}V_j) \quad (4.5)$$

where I_i is the current flowing out of the i th contact, T_{ij} is the transmission probability from contact $i \rightarrow j$. Charge conservation yields $\sum_i I_i = 0$. The voltage V_j

TI IN 2D AND 3D: THE QUANTUM SPIN HALL EFFECT IN HGTE
QUANTUM WELLS AND A SHORT INTRO. TO 3D TI [ERIK CHEAH]

of a voltage lead is defined through drawing zero net current. For TR invariant systems $T_{ij} = T_{ji}$ holds.

For a general 2D sample equation Eq. 4.5 is not easily solvable. However, assuming edge channel transport, one can rather straightforwardly predict the quantized multi-terminal resistance for simple multi-terminal geometries.

Two counter-propagating edge channels of the QSH state lead to transmission matrix elements $T_{i+1,i} = T_{i,i+1} = 1$; for the QH effect only $T_{i+1,i} = 1$. Consider a Hall-bar as shown in the inset of Fig. 4.12 Driving a current from lead 1 to 4 and having voltage on leads 2,3,5 and 6 one finds $I_1 = -I_4 \equiv I_{14}$, $V_2 - V_3 = 0$ and $V_1 - V_4 = (h/e^2)I_{14}$. This leads to a four-terminal resistance $R_{14,23} = 2 e^2/h$ ($R_{kl,ij} = \frac{V_i - V_j}{I_{kl}}$).

In the QSH state the 2D topological insulator, should have a finite conductance due to the spin polarized edge channels. The helical nature of the edge states has the consequence that one should observe twice the conductance quantum per channel pair: $2 e^2/h$.

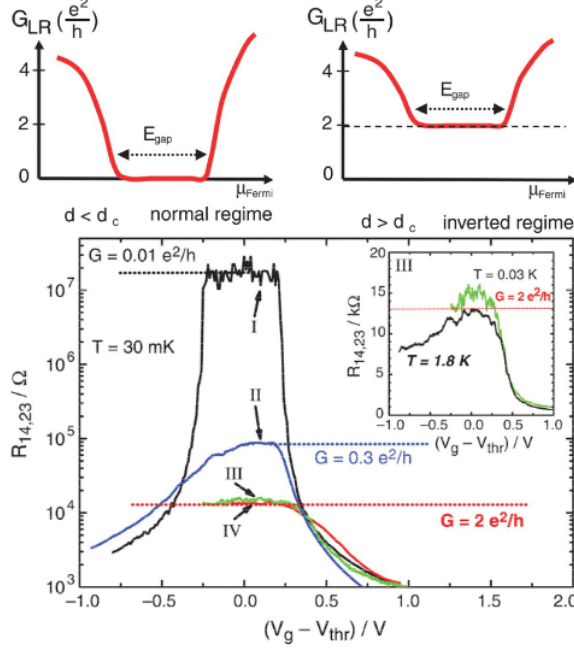


Figure 4.10: Top: Theoretical prediction of the four-terminal resistance. Bottom: Measured values for different sample sizes. From [14] (top), [26] (bottom).

4.6 Experiments

To observe a transition around the predicted critical thickness $d_c \approx 6.3$ nm samples with a QW width of 4.5 to 12.0 nm were investigated. At room temperature, they showed a n-type carrier density from $1.3 - 3.5 \times 10^{11}$ and mobilities up to $1.5 \times 10^5 \text{ cm}^2 \text{ V}^{-1} \text{ s}^{-1}$. The measurements were done at 30 mK.

In Fig. 4.10, bottom, the measurement of the four-probe longitudinal resistance $R_{14,23}$ is shown for different QW widths. For a thickness of $d_{QW}=7.3$ nm $> d_c$ a plateau at the predicted conductance value is observed for two thick enough samples, one of them half as broad as the other ($L \times W = 1.0 \times 1.0$ resp. $0.5 \mu\text{m}$). These two facts are a first evidence of the robust QSH channels. On the other hand, also ballistic transport could play a role in such small structures. For a large sample ($20.0 \times 13.3 \mu\text{m}$), the conductance plateau is at a higher value which is explained by the inelastic mean free path - even though the electrons cannot scatter back elastically, inelastic scatterers can lead to dissipation [26].

4.6.2 LANDAU LEVEL BEHAVIOR

For the same QWs as mentioned above, also measurements in external magnetic fields were conducted. This is of interest because the Landau levels (LL) of the inverted band structure exhibit a peculiar LL dispersion: The lowest level of the valence band (electron like) and conduction band (hole like) cross [26, 21]. Hence, the carrier type (n or p) is related to the Fermi level (tuned by gate voltage) and an external magnetic field. In Fig. 4.12 conductance measurements at varying B-field were obtained. Via magnetic field, inversion can be achieved and as mentioned before one can drive the system from a conducting n-type regime through a non-conducting region close to the Fermi energy to a p-type regime and vice versa. This gives rise to different regimes, see Fig. 4.13.

As a last proof, in the work of Ref. [26] it was shown, that for a sample that exhibited the QSH the conductance is destroyed when a longitudinal magnetic field is applied, i.e. TR symmetry is actively broken, see Fig. 4.14.

TI IN 2D AND 3D: THE QUANTUM SPIN HALL EFFECT IN HgTe
QUANTUM WELLS AND A SHORT INTRO. TO 3D TI [ERIK CHEAH]

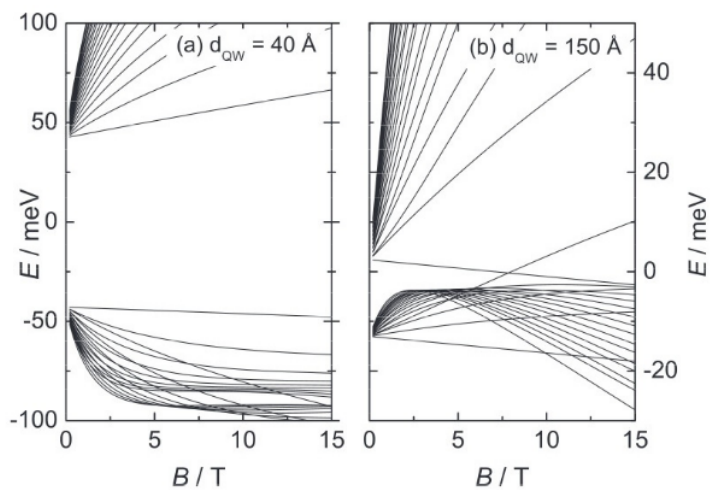


Figure 4.11: Landau level dispersion calculations for HgTe/CdTe QW. QW width is 40 Å (left) and the inverted case is visible for 150 Å (right). From [21].

4.6 Experiments

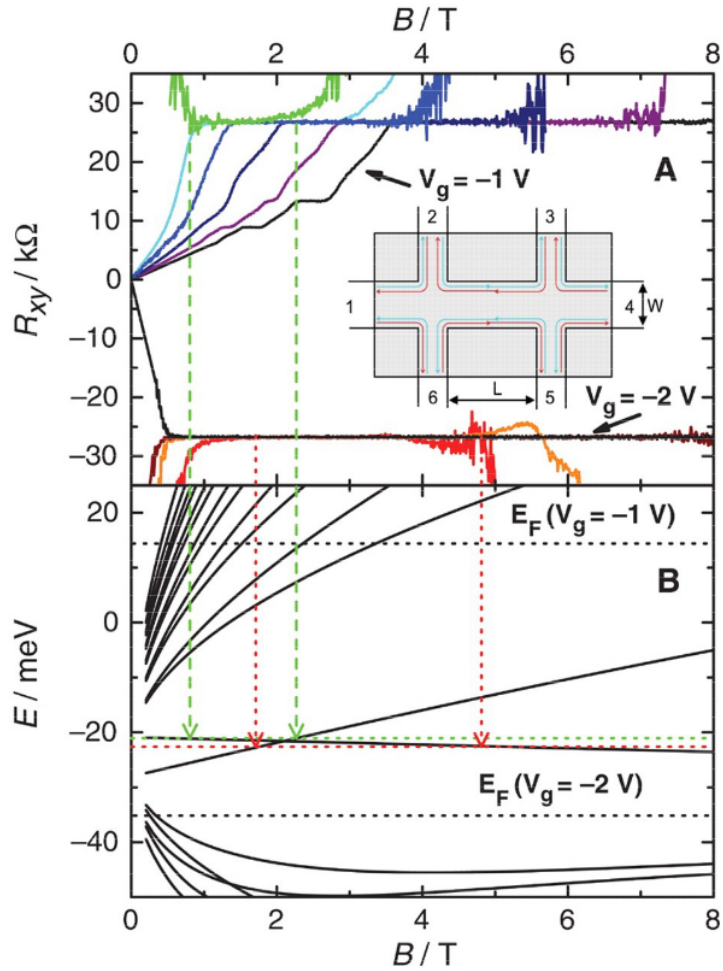


Figure 4.12: Top: Gate voltage dependent resistance. A change in carrier type can be seen: For $V_g = -1 \text{ V}$ we have n-type conductance. For $-1.4 \text{ V} < V_g < 1.9 \text{ V}$ the insulating regime is reached (Fermi level is in band gap) and lowering the gate voltage leads to p-type conductance. Bottom: The corresponding regions in the presence of magnetic field for the inverted case. From [26]

TI IN 2D AND 3D: THE QUANTUM SPIN HALL EFFECT IN HGTE
QUANTUM WELLS AND A SHORT INTRO. TO 3D TI [ERIK CHEAH]

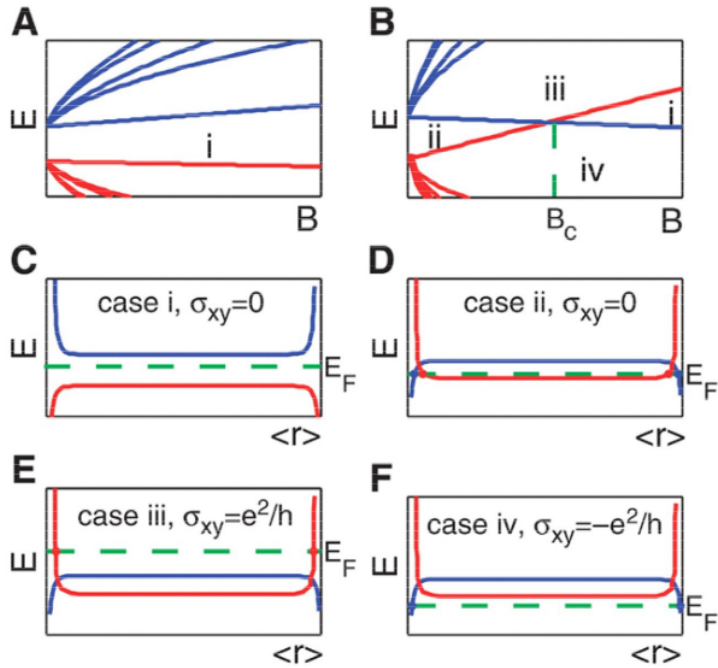


Figure 4.13: An increasing longitudinal magnetic field leads to a LL crossing. Regions i to iv give rise to different conductance regimes for the inverted case. From [26]

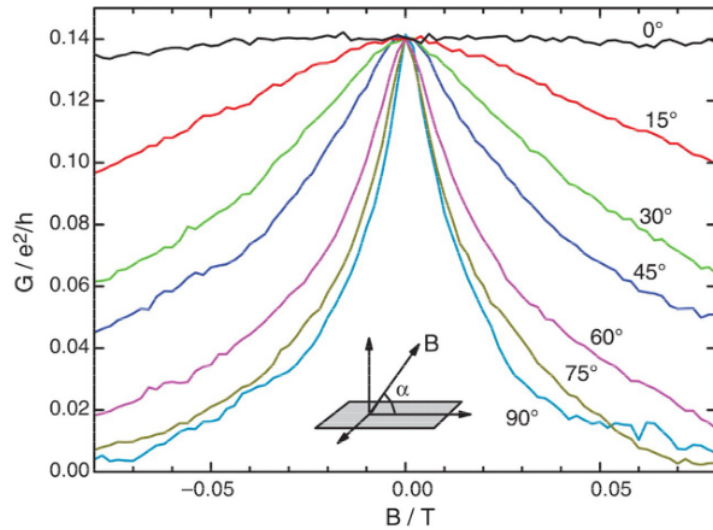


Figure 4.14: Increasing the perpendicular magnetic field destroys the quantized conduction plateau. From [26].

4.6 Experiments

4.6.3 NON-LOCAL TRANSPORT

The above presented transport measurements by [27] on a Hall-bar and an "H"-bar revealed a conductance of $\approx 2 e^2/h$, which would be expected for the QSH effect. However, for such small structures also ballistic transport could lead to the conductance value, see Fig. 4.15.

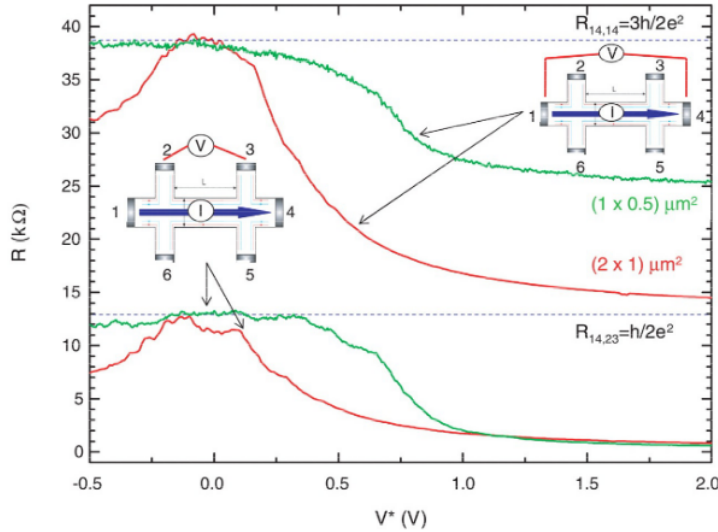


Figure 4.15: Two and four-terminal resistance measurements for two sample geometries. The smaller sample exhibits a value different value closer to the expected $R_{14,14}$. From [27].

So as to proof the existence of the QSH edge channels in topological HgTe QWs, [27] used the Landauer-Büttiker quantum transport formalism for multi-terminal measurement.

In their transport experiments the predicted value for the longitudinal four-terminal resistance was experimentally confirmed. In contrast to the QH effect, $R_{14,23}$ is finite for the QSH states, i.e. there is dissipation at the contacts [27, 17]. The metallic contacts contain an almost infinite number of low energy degrees of freedom that breaks TR symmetry. Being at the same energy (chemical potential) in the leads, the two channels can mix and eventually the phase coherence of corresponding wave function is lost over the contact. There is loss at contacts due to dephasing.

Furthermore, whereas in the QH state or for diffusive transport the longitudinal resistance remain at the same conductance value when voltage leads are changed

TI IN 2D AND 3D: THE QUANTUM SPIN HALL EFFECT IN HGTE
QUANTUM WELLS AND A SHORT INTRO. TO 3D TI [ERIK CHEAH]

[17], the QSH states exhibit different conductances. In particular, driving current from contact 1 to 3 and measuring the voltage over contacts 5 and 4 yields $R_{13,54} = h/3e^2$ and $R_{13,13} = 4h/3e^2$. Figure 4.16 shows this behavior for a Hall bar geometry schematically and the related experiment.

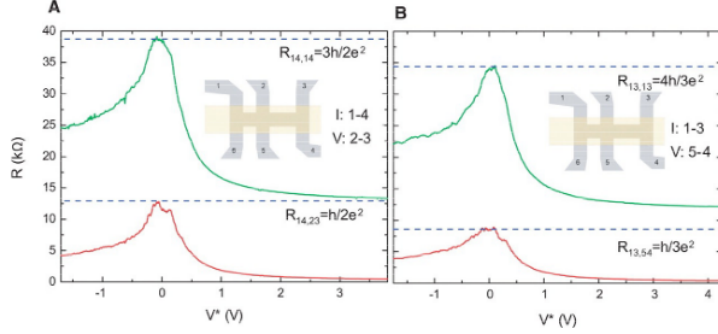


Figure 4.16: Two and four-terminal resistance measurements for different current and voltage lead configuration. From [27].

The last experimental result to mention is the increase of the resistance in the $2 - 3$ arm of the H-bar (inset in Fig. 4.17) when current is driven through the $1 - 4$ arm. Without edge states one would expect no voltage drop across the arm. In the experiments however, a resistance $R_{14,23} = h/4e^2$ when the Fermi level is tuned into the gap. This value can be derived again from the Landauer-Büttiker formula and the experiments are a direct evidence of the QSH in HgTe QWs.

4.7 Inverted type II semiconductor

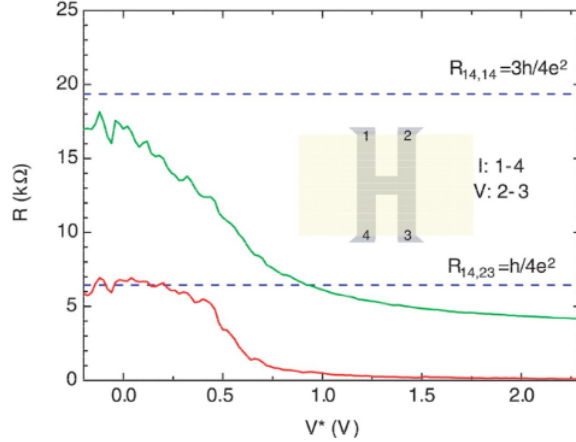


Figure 4.17: Transport measurements on a "H-bar" geometry. For gate voltages where the sample is the n-type and metallic regime two- and four-terminal resistance tend to zero. For the Fermi level in the gap, finite quantized resistances are measured. From [27].

4.7 INVERTED TYPE II SEMICONDUCTOR

Similar to the situation in HgTe/CdTe QWs, the type-II semiconductor QWs can theoretically also exhibit an inverted band structure [10]. In these structures also the E_1 and H_1 are the key sub-bands. However, the main difference is that the bands are situated at different sites in the structure; inversion symmetry is broken [28].

The situation can also be described by a BHZ model Hamiltonian with additional BIA and SIA terms.

4.8 3D TOPOLOGICAL INSULATORS - A BRIEF INTRODUCTION

For completeness of this Proseminary series, a brief summary on 3D topological insulators is given here.

4.8.1 CLASSIFICATION OF 3D TOPOLOGICAL INSULATORS NEW VERSION

So far, time-reversal-symmetric, two dimensional systems were classified by a \mathbb{Z}_2 -invariant. T-symmetry also bear pairs of Kramer's degenerate band at T-

TI IN 2D AND 3D: THE QUANTUM SPIN HALL EFFECT IN HGTE
QUANTUM WELLS AND A SHORT INTRO. TO 3D TI [ERIK CHEAH]

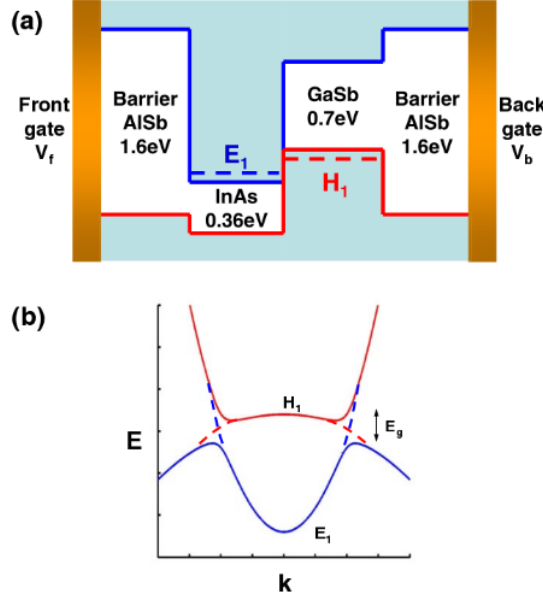


Figure 4.18: Schematic band structure of an asymmetric AlSb/InAs/GaSb type-II quantum well. From [10].

invariant points in \mathbf{k} -space where each is described by a unique \mathbb{Z}_2 invariant.

For 3D systems, it can be shown, that in the band structure can eventually be characterized by four \mathbb{Z}_2 -invariants.

Following the work of [29] and Ref. [30], consider in 3D the Brillouin Zone to be a three dimensional torus T^3 with coordinates $-\pi/a$ to π/a in each dimension. In the time-reversal-symmetric case, 6 planes are inequivalent, where each plane can be described by a 2D \mathbb{Z}_2 -invariant. For instance the k_xk_y plane is the same for $k_z = \pm\pi/a$ but different for $k_z=0$. The same applies for the k_yk_z , k_zk_x planes.

However, for other values of k_z in the xy case, where TRS is violated, there is no 2D equivalent and therefore all xy planes have to be described by at least two \mathbb{Z}_2 -invariants, one for $k_z = 0$ and $k_z = \pm\pi/a$. In total this would yield six \mathbb{Z}_2 -invariants. Yet, it can be shown, that if in one direction the phase changes from "odd" to "even", the same follows for the other two directions. Such a topological change in any direction corresponds to a "strong" topological insulator and is described by the number ν_0 .

All in all a 3D band can be described by four \mathbb{Z}_2 -invariants: $(\nu_0; \nu_1\nu_2\nu_3)$, where the later three are called "weak" topological invariants referring to the reference directions.

4.8 3D Topological Insulators - A brief Introduction

$\nu_0 = 0$ denotes a *weak* TI and can be thought of as a stacking of 2D quantum spin hall insulator layers. However, the surface states are not protected by TRS but can be localized by disorder [31].

$\nu_0 = 1$ denotes a *strong* TI and describes a different phase, where the surface Fermi circle encloses an odd number of Kramers degenerate points [31]. This has also the consequence, that only a single Dirac point can be intersected by the Fermi energy, see Fig. 4.19.

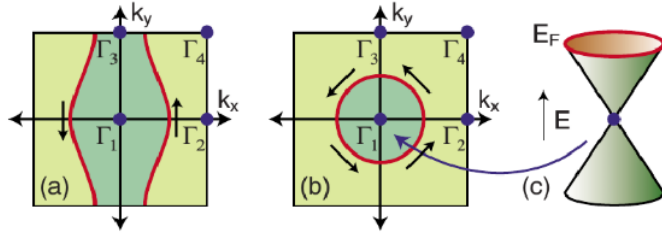


Figure 4.19: Possible Fermi surface circle intersection (red line, blue shade) in the BZ for (a) a weak TI, (b) strong TI with a corresponding single Dirac cone. From [31].

4.8.2 EXPERIMENTS

[12] published the first direct evidence of a 3D TI by measuring the band dispersion with ARPES. One year later in 2009 [13] published also a 4x4 effective model which predicts 3D topological insulating phase in Bi_2Se_3 , Bi_2Te_3 and Sb_2Te_3 . An ARPES measurement on Bi_2Se_3 from the same year is shown in Fig. 4.20.

As a final remark, also transport measurements on Bi_2Se_3 nano ribbons were conducted. In an Aharonov-Bohm (AB) interference experiment by [33], a dominant signal of the h/e AB oscillations was found, which was stable up to large B-fields and a temperature of the order of 20K.

TI IN 2D AND 3D: THE QUANTUM SPIN HALL EFFECT IN HGTE
QUANTUM WELLS AND A SHORT INTRO. TO 3D TI [ERIK CHEAH]

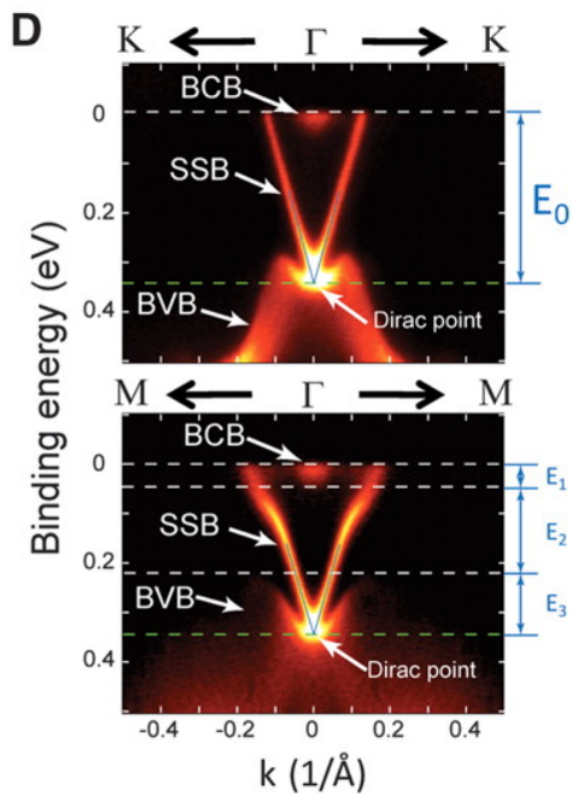


Figure 4.20: Possible surface Fermi surface circle intersection in the BZ for (a) a weak TI, (b) strong TI with a corresponding single Dirac cone. BCB (Bulk Conduction Band), BVB (Bulk Valence Band) and SSB (Surface State Band). From [32].

4.9 Summary

4.9 SUMMARY

In the first part of this report, the role of Spin-Orbit coupling to obtain a gapped system was discussed. Then the concept of crystal double groups was introduced to describe the symmetries of bands in the band structure of materials. Especially the case for CdTe/HgTe quantum wells was discussed, where the "inverted" band structure of HgTe can lead to a crossing of the two lowest energy sub bands in the quantum well.

The simplified 4x4 model suggested by [14] was compared to the most general Hamiltonian that captured all the symmetries of the QW structure. It was shown, that the BHZ model is the most general model for the HgTe/CdTe model when the zinc-blende structure is generalized to the diamond structure and we reduce the symmetries to a 2D system. Furthermore, two transport measurements were presented that confirm the quantum spin Hall effect in the HgTe quantum wells. As an outlook a brief summary of inverted type II semiconductors and 3D topological insulator was presented.

BIBLIOGRAPHY

- [1] C. L. Kane and E. J. Mele, *Quantum spin hall effect in graphene*, Phys. Rev. Lett. **95**, 226801 (2005).
- [2] F. D. M. Haldane, *Model for a quantum hall effect without landau levels: Condensed-matter realization of the "parity anomaly"*, Phys. Rev. Lett. **61**, 2015 (1988).
- [3] S. Murakami, N. Nagaosa, and S.-C. Zhang, *Spin-hall insulator*, Phys. Rev. Lett. **93**, 156804 (2004).
- [4] K. S. Novoselov, A. K. Geim, S. V. Morozov, D. Jiang, Y. Zhang, S. V. Dubonos, I. V. Grigorieva, and A. A. Firsov, *"electric field effect in atomically thin carbon films"*, "Science" **306**, 666 ("2004").
- [5] B. A. Bernevig and T. L. Hughes, *"Topological Insulators and topological superconductors"* ("Princeton University Press", "41 William Street, Princeton, New Jersey 08540", "2013").
- [6] C. Kane, *Chapter 1 - topological band theory and the 2 invariant*, in *Topological Insulators*, edited by M. Franz and L. Molenkamp (Elsevier, 2013), vol. 6, pp. 3 – 34.
- [7] H. Min, J. E. Hill, N. A. Sinitsyn, B. R. Sahu, L. Kleinman, and A. H. MacDonald, *Intrinsic and rashba spin-orbit interactions in graphene sheets*, Phys. Rev. B **74**, 165310 (2006).
- [8] Y. Yao, F. Ye, X.-L. Qi, S.-C. Zhang, and Z. Fang, *Spin-orbit gap of graphene: First-principles calculations*, Phys. Rev. B **75**, 041401 (2007).
- [9] M. S. Dresselhaus, G. Dresselhaus, and A. Jorio, *"Group Theory"* ("Springer-Verlag", "Berlin Heidelberg", "2008").

BIBLIOGRAPHY

- [10] C. Liu, T. L. Hughes, X.-L. Qi, K. Wang, and S.-C. Zhang, *Quantum spin hall effect in inverted type-ii semiconductors*, Phys. Rev. Lett. **100**, 236601 (2008).
- [11] L. Fu and C. L. Kane, *Topological insulators with inversion symmetry*, Phys. Rev. B **76**, 045302 (2007).
- [12] D. Hsieh, D. Qian, L. Wray, Y. Xia, Y. S. Hor, R. J. Cava, and M. Z. Hasan, *A topological dirac insulator in a quantum spin hall phase*, Nature **452**, 970 (2008).
- [13] H. Zhang, C.-X. Liu, X.-L. Qi, X. Dai, Z. Fang, and S.-C. Zhang, *Topological insulators in bi₂se₃, bi₂te₃ and sb₂te₃ with a single dirac cone on the surface*, Nature Physics **5**, 438 (2009).
- [14] B. A. Bernevig, T. L. Hughes, and S.-C. Zhang, *Quantum spin hall effect and topological phase transition in hgte quantum wells*, Science **314**, 1757 (2006).
- [15] P. D. G. Blatter, *Festkörperphysik*, Lecture notes (2006).
- [16] P. Y. Yu and M. Cardona, *"Fundamentals of Semiconductors"* ("Springer-Verlag", "Heidelberg Dordrecht London New York", "2010"), "fourth" ed.
- [17] C. Brüne, H. Buhmann, and L. Molenkamp, *Chapter 5 - quantum spin hall state in hgte*, in *Topological Insulators*, edited by M. Franz and L. Molenkamp (Elsevier, 2013), vol. 6, pp. 125 – 142.
- [18] C. Liu and S. Zhang, *Chapter 3 - models and materials for topological insulators*, in *Topological Insulators*, edited by M. Franz and L. Molenkamp (Elsevier, 2013), vol. 6, pp. 59 – 89.
- [19] K. C. Hass, H. Ehrenreich, and B. Velický, *Electronic structure of hg_{1-x}cd_xte*, Phys. Rev. B **27**, 1088 (1983).
- [20] M. König, H. Buhmann, L. W. Molenkamp, T. Hughes, C.-X. Liu, X.-L. Qi, and S.-C. Zhang, *The quantum spin hall effect: Theory and experiment*, Journal of the Physical Society of Japan **77**, 031007 (2008).
- [21] A. "Pfeuffer-Jeschke, Ph.D. thesis, " University of Würzburg, Germany" ("2000").

BIBLIOGRAPHY

- [22] E. G. Novik, A. Pfeuffer-Jeschke, T. Jungwirth, V. Latussek, C. R. Becker, G. Landwehr, H. Buhmann, and L. W. Molenkamp, *Band structure of semi-magnetic $hg_{1y}mn_yte$ quantum wells*, Phys. Rev. B **72**, 035321 (2005).
- [23] D. G. Rothe, R. W. Reinthalter, C.-X. Liu, L. W. Molenkamp, S.-C. Zhang, and E. M. Hankiewicz, *Fingerprint of different spin-orbit terms for spin transport in hgte quantum wells*, New Journal of Physics **12**, 065012 (2010).
- [24] B. Zhou, H.-Z. Lu, R.-L. Chu, S.-Q. Shen, and Q. Niu, *Finite size effects on helical edge states in a quantum spin-hall system*, Phys. Rev. Lett. **101**, 246807 (2008).
- [25] Authors and editors of the volumes III/17B-22A-41B, *Landolt-Börnstein - group iii condensed matter*, in *SpringerMaterials - The Landolt-Börnstein Database*, edited by O. Madelung, U. Rössler, and M. Schulz (Springer, copyright 1999), vol. 41B, chap. Mercury telluride (HgTe) effective masses.
- [26] M. König, S. Wiedmann, C. Brüne, A. Roth, H. Buhmann, L. W. Molenkamp, X.-L. Qi, and S.-C. Zhang, *Quantum spin hall insulator state in hgte quantum wells*, Science **318**, 766 (2007).
- [27] A. Roth, C. Brüne, H. Buhmann, L. W. Molenkamp, J. Maciejko, X.-L. Qi, and S.-C. Zhang, *Nonlocal transport in the quantum spin hall state*, Science **325**, 294 (2009).
- [28] S.-Q. Shen, "Topological Insulators - Dirac Equations in Condensed Matters" ("Springer-Verlag", "Heidelberg New York Dordrecht London", "2012"), "first" ed.
- [29] J. E. Moore and L. Balents, *Topological invariants of time-reversal-invariant band structures*, Phys. Rev. B **75**, 121306 (2007).
- [30] J. E. Moore, *Chapter 2 - theory of three-dimensional topological insulators*, in *Topological Insulators*, edited by M. Franz and L. Molenkamp (Elsevier, 2013), vol. 6, pp. 35 – 57.
- [31] M. Z. Hasan and C. L. Kane, *Colloquium*, Rev. Mod. Phys. **82**, 3045 (2010).
- [32] Y. L. Chen, J. G. Analytis, J.-H. Chu, Z. K. Liu, S.-K. Mo, X. L. Qi, H. J. Zhang, D. H. Lu, X. Dai, Z. Fang, et al., *Experimental realization of a three-dimensional topological insulator, bi2te3*, Science **325**, 178 (2009).

BIBLIOGRAPHY

- [33] H. Peng, K. Lai, D. Kong, S. Meister, Y. Chen, X.-L. Qi, S.-C. Zhang, Z.-X. Shen, and Y. Cui, *Aharonov-bohm interference in topological insulator nanoribbons*, Nature Materials **9**, 225 (2010).

CHAPTER 5

TOPOLOGICAL INSULATORS

JOHAN ANDBERGER

SUPERVISOR: ALEXEY SOLUYANOV

In this chapter a formula for a \mathbb{Z}_2 index will be derived that distinguishes the two possible phases of a normal insulator and a topological one in the case of a time-reversal invariant system. It will also be shown that with the additional presence of inversion symmetry this formula can be simplified.

5.1 INTRODUCTION

A term "topological insulator" refers to a time-reversal (TR) invariant band insulator, in which edge/surface states are gapless unless a TR-breaking perturbation is added. The edge states of TR-symmetric insulators always come in pairs due to TR symmetry. This is a fact known as Kramers degeneracy theorem[1], and these pairs are known as Kramers pairs. In 2D, for example, TR-symmetric insulators can host odd or even numbers of gapless counterpropagating Kramers pairs of edge states [2]. TR-symmetry does not allow to gap the edge if and only if there the number of such pairs is odd [3]. In this case the insulator is to be called a "topological insulator", to distinguish it from a regular insulator with an even number of pairs of edge states. The reason for this is that since an even number of pairs of edge states is not protected, they are easily gapped by the presence of impurities, for example.[4] This division into two categories of insulators implies the existence of a \mathbb{Z}_2 -type index, i.e. an index that takes on one value (e.g. 1) if the system is a topological insulator and another (e.g. 0) if the system is a regular insulator. In this chapter it will be shown that by imposing symmetries on a system, it is possible to derive formulas to determine if

5.1 Introduction

the system is a topological insulator or not. Concretely, time-reversal symmetry will be imposed on a system and then, in addition, inversion symmetry.

It will be shown that for a system with time-reversal symmetry only, a \mathbb{Z}_2 invariant is given by a contour integral with a path enclosing half the Brillouin zone,

$$I = \frac{1}{2\pi i} \oint_C d\vec{k} \cdot \nabla_{\vec{k}} \log P(\vec{k}).$$

where

$$P(\vec{k}) = \text{Pf} \left[\left(\langle u_i(\vec{k}) | T | u_j(\vec{k}) \rangle \right)_{i,j} \right] := \sqrt{\det \left[\left(\langle u_i(\vec{k}) | T | u_j(\vec{k}) \rangle \right)_{i,j} \right]}$$

and "half" is defined in such a way that for each pair of points $\pm\vec{k}$ where the Pfaffian vanishes, only one is inside of the contour[2]. Pf denotes the so-called *Pfaffian*, defined as the square root of the determinant. For a skew-symmetric $(2n+1) \times (2n+1)$ matrix the Pfaffian disappears and for a skew-symmetric $2n \times 2n$ matrix the Pfaffian is a polynomial. Because of the Kramers doublets in the system, if there are more bands in the system, this matrix consists of blocks. This makes the Pfaffian equal to a product of components. $|u_i(\vec{k})\rangle$ denotes the Bloch wavefunctions of the occupied bands, i.e. the index i is an enumeration of all occupied bands, and T denotes the time-reversal operator.

For a system with both time-reversal symmetry and inversion symmetry it will be shown that the \mathbb{Z}_2 invariant is given by the product of

$$\delta_\Gamma = \prod_{m=1}^N \xi_{2m}(\Gamma)$$

where Γ is one of the four time-reversal invariant (and thus also inversion symmetric) points in the Brillouin zone in the case of two dimensions. $\xi_{2m}(\Gamma)$ denotes the parity eigenvalue of the $2m$ -th occupied energy band at the point Γ , it can therefore only take on the values ± 1 . The formula for the \mathbb{Z}_2 invariant therefore looks like

$$(-1)^\nu = \prod_\Gamma \delta_\Gamma$$

In the discussion below only systems described by 4×4 Hamiltonians will be considered, which corresponds to systems with 2 bands. These are the smallest systems that can be considered for time-reversal invariant two-dimensional topological insulators, because of the pairing caused by the Kramers degeneracy theorem. The discussion for these Hamiltonians can be easily generalized to systems with more bands because of this pairing. Under the assumption that the system has a gap, only occupied eigenstates will be considered and these will be denoted by $|u_{i=1,2}(\vec{k})\rangle$.

5.2 \mathbb{Z}_2 INDEX FOR SYSTEMS WITH TIME-REVERSAL SYMMETRY

In this section systems with time-reversal symmetry will be considered, this means that in momentum space the Hamiltonian $h(\vec{k})$ obeys the following relation with respect to the time-reversal operator T

$$Th(\vec{k})T^{-1} = h(-\vec{k}).$$

It's worth noting that the points $\vec{k} = \vec{0}, \frac{\vec{G}}{2}$ are invariant under this relation, where \vec{G} denotes a reciprocal lattice vector. These points are known as time-reversal invariant momenta (TRIM points). One notes that $T|u(\vec{k})\rangle$ is an eigenstate of $h(-\vec{k})$ with $E(\vec{k}) = E(-\vec{k})$ because of the above relation, this can be easily seen through the derivation

$$h(-\vec{k})T|u(\vec{k})\rangle = Th(\vec{k})T^{-1}T|u(\vec{k})\rangle = Th(\vec{k})|u(\vec{k})\rangle = TE(\vec{k})|u(\vec{k})\rangle = E(\vec{k})T|u(\vec{k})\rangle$$

Because of time-reversal symmetry, consider the matrix

$$(\langle u_i(\vec{k}) | T | u_j(\vec{k}) \rangle)_{i,j}. \quad (5.1)$$

It is not immediately clear why this matrix would be useful, the reason is that with it the time-reversal symmetry of the system can be exploited. Therefore it will be used as an ansatz for the derivation of the \mathbb{Z}_2 invariant. This matrix is antisymmetric for every \vec{k} in the Brillouin zone because of the properties of T , which means vanishing diagonal entries. This fact can be seen by considering that in general $T = UK$ with U being unitary and antisymmetric and K being the conjugation operator. Then

$$\langle u_i(\vec{k}) | T | u_j(\vec{k}) \rangle = (u_i(\vec{k}))_m^* U_{mn} (u_j(\vec{k}))_n^* = -(u_j(\vec{k}))_n^* U_{nm} K (u_i(\vec{k}))_m = -\langle u_j(\vec{k}) | T | u_i(\vec{k}) \rangle \quad (5.2)$$

for all \vec{k} on the Brillouin zone torus. On this matrix the *Pfaffian* $P(\vec{k})$ is defined through

$$P(\vec{k}) = \text{Pf}[\langle u_i(\vec{k}) | T | u_j(\vec{k}) \rangle] := \sqrt{\det(\langle u_i(\vec{k}) | T | u_j(\vec{k}) \rangle)}.$$

In the case of two occupied bands $|u_i(\vec{k})\rangle$, the matrix above would look like

$$\begin{pmatrix} \langle 0 & \langle u_1(\vec{k}) | T | u_2(\vec{k}) \rangle \\ -\langle u_1(\vec{k}) | T | u_2(\vec{k}) \rangle & 0 \end{pmatrix}$$

because of antisymmetry. It's easy to see that in this case the Pfaffian takes the shape

$$P(\vec{k}) = \langle u_1(\vec{k}) | T | u_2(\vec{k}) \rangle,$$

5.2 \mathbb{Z}_2 index for systems with time-reversal symmetry

i.e. it merely picks out one components. This relation holds in the case of more bands as well, although in this case the Pfaffian would be a product of components.

Now $U(1)$ and $U(2)$ gauge transformations will be considered for $P(\vec{k})$. The knowledge about gauge freedom will later be useful for the derivations. For $R \in U(2)$, consider

$$|u'_i(\vec{k})\rangle = R_{ij}(\vec{k})|u_j(\vec{k})\rangle.$$

It then follows that

$$\begin{aligned} P'(\vec{k}) &= \sqrt{\det\langle u'_i(\vec{k})|T|u'_j(\vec{k})\rangle} \\ &= \sqrt{\det[\langle u_m(\vec{k})|(R^*)_{im}T(R^*)_{nj}^T|u_n(\vec{k})\rangle]} \\ &= \sqrt{\det(R^*)\det(R^H)\det\langle u_i(\vec{k})|T|u_j(\vec{k})\rangle} \\ &= \det(R^*)P(\vec{k}), \end{aligned}$$

i.e. the Pfaffian is not gauge invariant under arbitrary $U(2)$ transformations. For $U(1)$ transformations, $|u'_i(\vec{k})\rangle = e^{i\phi}|u_i(\vec{k})\rangle$ and therefore

$$\begin{aligned} P'(\vec{k})\sqrt{\det[\langle u'_i(\vec{k})|T|u'_j(\vec{k})\rangle]} &= \sqrt{\det[\langle u_i(\vec{k})|e^{-i\phi}Te^{i\phi}|u_j(\vec{k})\rangle]} \\ &= \sqrt{e^{-4i\phi}\det[\langle u_i(\vec{k})|T|u_j(\vec{k})\rangle]} \\ &= e^{-2i\phi}P(\vec{k}). \end{aligned}$$

The Pfaffian is thus in addition not gauge invariant under $U(1)$ transformations. It's worth noting however that $|P(\vec{k})|$ is gauge invariant under both $U(1)$ and $U(2)$ transformations!

To use this first note that due to time-reversal symmetry, two important subspaces of Hamiltonians can be identified, each classified by the below two cases

$$\begin{aligned} |u_n^I(-\vec{k})\rangle &= -T|u_n^{II}(\vec{k})\rangle \\ |u_n^{II}(-\vec{k})\rangle &= T|u_n^I(\vec{k})\rangle. \end{aligned}$$

For these cases the Pfaffian will take on an absolute value of 0 and 1 and respectively. In addition note that $P(-\vec{k}) = P^*(\vec{k})$, this fact can be seen by using that $T|u_i(\vec{k})\rangle$ is an eigenstate of the Hamiltonian $h(-\vec{k})$. This means that if $P(\vec{k})$ is zero, then so is $P(-\vec{k})$! With these properties it can now be claimed that an index classifying the system can be constructed by only considering half the Brillouin

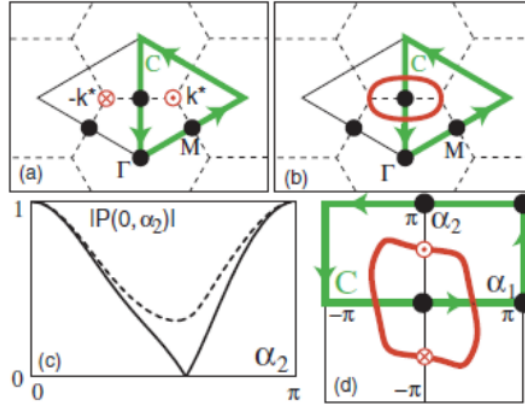


Figure 5.1: (a) show the zeros $\pm\vec{k}^*$ of the Pfaffian $P(\vec{k})$ on a honeycomb lattice. The green outline with the arrows show the contour C that encloses half the Brillouin zone, which is marked with the thin line. The dots show the TRIM points, called Γ and M . (b) shows another possible case, sometimes the zeros of the Pfaffian occur along lines instead of at discrete points, here the Pfaffian is zero on the red oval. (c) shows a plot of the Pfaffian in 1D for a zigzag strip, the solid line shows the system in a topologically insulating phase and the dashed one shows the system when it has been gapped by a staggered sublattice potential, it's then a regular insulator. (d) shows the same system as in (c) but this time in two dimensions, with the Pfaffian zeros falling on a line.

zone. Concretely, the \mathbb{Z}_2 invariant can be defined through the winding number of $\nabla_{\vec{k}} \log P(\vec{k})$,

$$\frac{1}{2\pi i} \int_C d\vec{k} \cdot \nabla_{\vec{k}} \log P(\vec{k}),$$

where C is a contour around half the Brillouin zone, in a manner such that it encloses at most one of the Pfaffian zeros $P(\vec{k})$ and $P(-\vec{k})$. By using the theory of complex analysis, more specifically the residue theorem, that states that

$$\oint_C \frac{f'(z)}{f(z)} dz = 2\pi i \sum_{\vec{k}: P(\vec{k})=0} I(C, \vec{k}) \text{Res}(\vec{k})$$

where \vec{k} is a zero of the Pfaffian and thus a simple pole of $\nabla_{\vec{k}} \log P(\vec{k})$, it can be seen that because of the minus sign, $P(-\vec{k})$ will have an additional minus in front of the residue, i.e. the residue would be equal to -1 instead of 1 , and the sum will therefore evaluate to zero. Integrating over the entire Brillouin zone would thus make the integral zero. By only taking half, the integral is assured

5.3 \mathbb{Z}_2 index for systems with time-reversal symmetry and inversion symmetry

to be non-zero. It is also not possible to use gauge freedom to join the points $P(\pm\vec{k})$ somewhere inside the Brillouin zone, since to do this one would need to move through one of the time-reversal invariant points, which would break the time-reversal symmetry. What if there are more zeros in the Brillouin zone, e.g. at $\pm\vec{k}_1$ and at $\pm\vec{k}_2$? Now it's possible to use the gauge freedom to move $\pm\vec{k}_1$ and $\mp\vec{k}_2$ together without going through any TRIM points. Thinking in terms of residues, the integral will evaluate to zero in this case. This argument can be generalized to arbitrarily many zeros, if there are an even number of pairs of them, the integral will evaluate to zero and if there are an odd number the integral will be nonzero. This gives the \mathbb{Z}_2 invariant.

5.3 \mathbb{Z}_2 INDEX FOR SYSTEMS WITH TIME-REVERSAL SYMMETRY AND INVERSION SYMMETRY

In the previous section it was seen that a \mathbb{Z}_2 index could be defined through the winding number. This formula is however for practical purposes not very useful, even for numerical purposes. In order to derive a simpler formula, an additional symmetry is imposed on the system, inversion symmetry. Let P be the inversion operator (also called parity operator) and also suppose that $\vec{r} = 0$ is an inversion center of the Hamiltonian. Then the Hamiltonian in momentum space satisfy the relation $h(-\vec{k}) = Ph(\vec{k})P^{-1}$. One notes that for a wavefunction $|u_i(\vec{k})\rangle$, $P^2 = 1$ and therefore $P^2|u_i(\vec{k})\rangle = |u_i(\vec{k})\rangle$, i.e. the inversion operator P must have the eigenvalues ± 1 . In addition, $P^\dagger P = 1$. At the TRIM points Γ , $Ph(\Gamma)P^{-1} = h(\Gamma)$, which implies that $[P, h(\Gamma)] = 0$. An eigenstate of $h(\Gamma)$ is thus also an eigenstate of P . Since the eigenstates of $h(\vec{k})$ are the $|u_i(\vec{k})\rangle$'s, it can be concluded that

$$P|u_i(\Gamma)\rangle = \xi_i(\Gamma)|u_i(\Gamma)\rangle \quad (5.3)$$

with $\xi_i(\Gamma) \in \{\pm 1\}$.

Consider the Berry curvature $\mathcal{F}(\vec{k})$, it must be odd under time-reversal and even under inversion, i.e. $\mathcal{F}(\vec{k}) = 0$ at these globally. Because

$$\mathcal{F}(\vec{k}) = \nabla_{\vec{k}} \times \mathcal{A}(\vec{k}) = -i\nabla_{\vec{k}} \times \sum_{n=1}^{2N} \langle u_n(\vec{k}) | \nabla_{\vec{k}} | u_n(\vec{k}) \rangle,$$

for a system with $2N$ occupied bands, there should be a globally continuous gauge for which $\mathcal{A}(\vec{k}) = 0$. To find this gauge the same approach will be used as for the case of time-reversal symmetry only, i.e. the matrix

$$v_{mn}(\vec{k}) = \langle u_m(\vec{k}) | PT | u_n(\vec{k}) \rangle \quad (5.4)$$

is looked at. This time both P and T are present since both these symmetries are present in the system. This $2N \times 2N$ matrix is antisymmetric because of time-reversal symmetry, this can be shown using a similar derivation as in equation 5.2. Because $[PT, H(\vec{k})] = 0$, $v(\vec{k})$ is in addition unitary, which means that the determinant has unit magnitude. The Pfaffian of $v(\vec{k})$ is therefore well-defined and it also has unit magnitude. The phase of $\text{Pf}[v(\vec{k})]$ depends on the gauge and its gradient is related to $\mathcal{A}(\vec{k})$,

$$\mathcal{A}(\vec{k}) = -\frac{i}{2} \text{Tr}[v(\vec{k})^\dagger \nabla_{\vec{k}} v(\vec{k})] = -i \nabla_{\vec{k}} \log \text{Pf}[v(\vec{k})].$$

The first equality follows by differentiating the matrix $v(\vec{k})$ (5.4) and using that it is unitary and the second one follows by using the definition of the Pfaffian and that $\nabla_{\vec{k}} \log \det[v(\vec{k})] = \text{Tr}[\nabla_{\vec{k}} \log v(\vec{k})] = \text{Tr}[v^\dagger(\vec{k}) \nabla_{\vec{k}} v(\vec{k})]$. To set $\mathcal{A}(\vec{k}) = 0$, adjust the phase of $|u_n(\vec{k})\rangle$ to make $\text{Pf}[v(\vec{k})] = 1$ by using a $U(1)$ transformation, i.e. $\text{Pf}[v(\vec{k})] \mapsto \text{Pf}[v(\vec{k})] e^{-i\theta(\vec{k})}$ with $\theta(\vec{k}) \in \mathbb{R}$. Note that due to the above relation, if $\mathcal{A}(\vec{k}) \equiv 0$, then the Pfaffian $\text{Pf}[v(\vec{k})] \equiv 1$.

Because a \mathbb{Z}_2 invariant is defined through[5]

$$(-1)^\nu = \prod_i \delta_i$$

where

$$\delta_i = \frac{\sqrt{\det[w(\Gamma_i)]}}{\text{Pf}[w(\Gamma_i)]}$$

and Γ_i denotes a time-reversal invariant point. The matrix $w(\vec{k})$ is defined as

$$w(\vec{k}) = \left(\langle u_m(-\vec{k}) | T | u_n(\vec{k}) \rangle \right)_{m,n}$$

and is antisymmetric at the TRIM points, in comparison with the matrix 5.1 defined at the beginning, which is antisymmetric everywhere. The problem of potentially having a zero in the denominator is eliminated, since the magnitude is always equal to one for all \vec{k} . This can be seen by noting that

$$v(-\vec{k}) = w(\vec{k}) v(\vec{k})^* w(\vec{k})^T, \quad (5.5)$$

which can be shown through straight-forward calculation. If the determinant is taken on both sides, this relation implies that $\text{Pf}[w(\Gamma_i)] = 1$, since $\text{Pf}[v(\vec{k})] = 1$. $\text{Pf}[w(\Gamma_i)]$ can be evaluated by noting that at the TRIM points $|u_m(-\Gamma_i)\rangle = |u_m(\Gamma_i)\rangle$ and that $P^2 = 1$, then

$$w_{mn}(\Gamma_i) = \langle u_m(\Gamma_i) | P^2 T | u_n(\Gamma_i) \rangle = \xi_m \langle u_m(-\Gamma_i) | PT | u_n(\Gamma_i) \rangle = \xi_m v_{mn}(\Gamma_i)$$

5.4 Graphene

implies that

$$w_{mn}(\Gamma_i) = \xi_m(\Gamma_i)v_{mn}(\Gamma_i)$$

since $[H, P] = 0$. This is useful since

$$\text{Pf}[w(\Gamma_i)]^2 = \det[w(\Gamma_i)] = \det[v(\Gamma_i)] \prod_{n=1}^{2N} \xi_n(\Gamma_i).$$

The product contains an even number of terms because of Kramers degeneracy at the TRIM points and because of the pairing each parity eigenvalue occurs twice, making the square root of this expression well-defined. If $\xi_{2n-1}(\Gamma) = \xi_{2n}(\Gamma)$, it can be concluded that

$$\text{Pf}[w(\Gamma)] = \text{Pf}[v(\Gamma)] \prod_{n=1}^N \xi_{2n}(\Gamma).$$

Since the sign of the square root is ambiguous, $w(\Gamma_i) = v(\Gamma_i)$ is chosen in the case when $\xi_{2n} = 1$ for all occupied bands n . Putting everything together using that $\sqrt{\det[w(\Gamma_i)]} = 1$ and $\text{Pf}[w(\Gamma_i)] = \prod_{n=1}^N \xi_{2n}(\Gamma_i)$ in the chosen gauge, the result

$$\delta_i = \frac{\sqrt{\det[w(\Gamma_i)]}}{\text{Pf}[w(\Gamma_i)]} = \prod_{n=1}^N \xi_{2n}(\Gamma_i)$$

is achieved and the formula for the \mathbb{Z}_2 invariant simplifies to

$$(-1)^\nu = \prod_i \prod_{n=1}^N \xi_{2n}(\Gamma_i),$$

in essence nothing else than the product of parity eigenvalues of the occupied bands at the TRIM points. For example if the product on the right-hand side is equal to -1 , then $\nu = 1$ and the system is a topological insulator. On the other hand, if the product is positive, equal to 1 , then $\nu = 0$.

5.4 GRAPHENE

As an example employing the derived \mathbb{Z}_2 invariants a tight-binding model of graphene with unit cell as shown in figure 5.2 will be used. The momentum space Hamiltonian of this model is given by [2][3]

$$h = t \sum_{\langle ij \rangle} c_i^\dagger c_j + i\lambda_{\text{SO}} \sum_{\langle\langle ij \rangle\rangle} \nu_{ij} c_i^\dagger s^z c_j$$

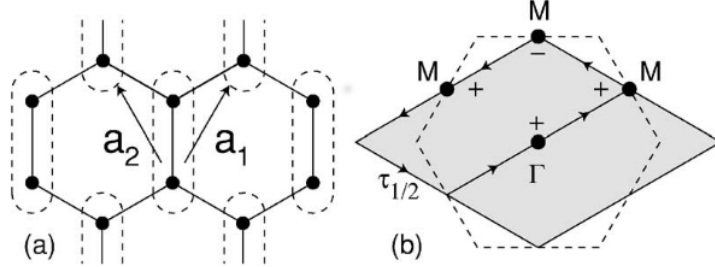


Figure 5.2: The dashed lines in (a) indicates the unit cell of the graphene lattice with lattice vectors $a_1 = \frac{1}{2}(3, \sqrt{3})^T$ and $a_2 = \frac{1}{2}(3, -\sqrt{3})^T$ (for example) and (b) shows the Brillouin zone with the TRIM points Γ and M , the signs indicate the value of δ_i . $\tau_{1/2}$ is the contour used to calculate the first \mathbb{Z}_2 index. Figure taken from [6].

which in the form of a matrix can be written as

$$h(\vec{k}) = t[1 + \cos x_1 + \cos x_2] \begin{pmatrix} 0 & 0 & 1 & 0 \\ 0 & 0 & 0 & 1 \\ 1 & 0 & 0 & 0 \\ 0 & 1 & 0 & 0 \end{pmatrix} + it[\sin x_1 + \sin x_2] \begin{pmatrix} 0 & 0 & -1 & 0 \\ 0 & 0 & 0 & -1 \\ 1 & 0 & 0 & 0 \\ 0 & 1 & 0 & 0 \end{pmatrix} + 2\lambda_{SO}[\sin x_1 - \sin x_2 - \sin(x_1 - x_2)] \begin{pmatrix} 1 & 0 & 0 & 0 \\ 0 & -1 & 0 & 0 \\ 0 & 0 & -1 & 0 \\ 0 & 0 & 0 & 1 \end{pmatrix}$$

with $x_l = \vec{k} \cdot \vec{a}_l = n_l \pi$, $l = 1, 2$ and $n_l = 0, 1$. [6]

In order to calculate the values of the δ_i , one notes that at the time-reversal invariant points Γ_i , only one of the matrices in the above Hamiltonian is even under both the parity operator P and the time-reversal operator T , the first one. This means that the parity eigenvalues are the eigenvalues of this matrix. Under the assumption there is an energy gap in the Brillouin zone, then the formula

$$\delta_i = -\text{sgn}(d_1(\vec{k} = \Gamma_i)) \quad (5.6)$$

holds. Applying this on the four combinations for x_l , $(x_1, x_2) = (0, 0), (0, \pi), (\pi, 0), (\pi, \pi)$, one get $\delta_{(0,0)} = \delta_{(1,0)} = \delta_{(0,1)} = -1$ and $\delta_{(1,1)} = 1$. The product of these four num-

5.5 Concluding remarks

bers is negative, which means that $\nu = 1$. One concludes therefore that the system is a topological insulator.

To apply the integral approach, it must first be ascertained how many zeros of the Pfaffian occur inside the Brillouin zone, or half of it. This highlights the problem of only having time-reversal symmetry in the system, since it is not as easy to calculate. The existence of one pair of zeros for this system was shown in [3]. Using the residue theorem to calculate the integral over half the Brillouin zone and choosing the half with positive vorticity,

$$I = \frac{1}{2\pi i} \oint_{\tau_{1/2}} d\vec{k} \cdot \nabla_{\vec{k}} \log P(\vec{k}) = 1.$$

This indicates that the system is a topological insulator.

5.5 CONCLUDING REMARKS

In this chapter it has been shown that by imposing time-reversal on a system yields a formula that can be used to determine if the system is a topological insulator or not. This formula turned out to be nothing else than the winding number

$$I = \frac{1}{2\pi i} \int_C d\vec{k} \cdot \nabla_{\vec{k}} \log P(\vec{k})$$

with $P(\vec{k})$ being the Pfaffian and C being a loop around half the Brillouin zone in such a way that for each pair of points $\pm\vec{k}$ with $P(\pm\vec{k}) = 0$, both of them are not inside the loop. $P(\vec{k})$ was defined as

$$P(\vec{k}) = \text{Pf} \left[\left(\langle u_i(\vec{k}) | T | u_j(\vec{k}) \rangle \right)_{i,j} \right] := \sqrt{\det \left[\left(\langle u_i(\vec{k}) | T | u_j(\vec{k}) \rangle \right)_{i,j} \right]}$$

with $|u_i(\vec{k})\rangle$ being the wavefunctions of the occupied bands at point \vec{k} in the Brillouin zone and T being the time-reversal operator.

Imposing an additional symmetry, inversion symmetry, a simpler formula was derived. This formula only depends on the parity eigenvalues at the time-reversal invariant and inversion symmetric points, the TRIM points,

$$(-1)^\nu = \prod_i \prod_{m=1}^N \xi_{2m}(\Gamma_i).$$

The way to use this formula is to calculate the right-hand side, which can take on the values ± 1 , and if the value is for example 1 then $\nu = 0$, meaning the

TOPOLOGICAL INSULATORS [JOHAN ANDBERGER]

system is not a topological insulator. The two approaches are very different, with the Pfaffians of different matrices being used. These matrices had different properties, so care needs to be taken to keep them apart.

Finally, the two results were applied to a tight-binding model of graphene. The two approaches gave the same answer, but the result for the first index had to be calculated numerically, in comparison with the second, which had an analytic answer.

5.5 Concluding remarks

BIBLIOGRAPHY

- [1] H. Kramers and G. Ittmann, *Zur quantelung des asymmetrischen kreisels. iii*, Zeitschrift fr Physik **60**, 663 (1930), ISSN 0044-3328.
- [2] C. L. Kane and E. J. Mele, *\mathbb{Z}_2 topological order and the quantum spin hall effect*, Phys. Rev. Lett. **95**, 146802 (2005).
- [3] C. L. Kane and E. J. Mele, *Quantum spin hall effect in graphene*, Phys. Rev. Lett. **95**, 226801 (2005).
- [4] C. Wu, B. A. Bernevig, and S.-C. Zhang, *Helical liquid and the edge of quantum spin hall systems*, Phys. Rev. Lett. **96**, 106401 (2006).
- [5] L. Fu and C. L. Kane, *Time reversal polarization and a \mathbb{Z}_2 adiabatic spin pump*, Phys. Rev. B **74**, 195312 (2006).
- [6] L. Fu and C. L. Kane, *Topological insulators with inversion symmetry*, Phys. Rev. B **76**, 045302 (2007).

BIBLIOGRAPHY

CHAPTER 6

TOPOLOGICAL FIELD THEORY FOR TOPOLOGICAL INSULATORS

FLORIAN JOHNE

SUPERVISOR: ADEL BENLAGRA

We investigate topological insulators by using topological field theory. Starting from the Quantum Hall effect in (2+1)-D we investigate the effect of integrating out fermions from a (2+1)-D or (4+1)-D field theory with interacting gauge and fermions fields. The resulting Chern - Simons terms are topological. For insulators, the topological invariants of these theories can be calculated by using Berry curvature.

Using the so-called dimensional reduction procedure, we derive \mathbb{Z}_2 - classifications descending from the (2+1)-D and (4+1)-D theory and we show that the Chern numbers inherit a topological invariant under certain symmetry assumptions. In the case of time - reversal invariant (3+1)-D systems we show some physical consequences and the modification of Maxwell's equations.

Finally we give a brief outlook to Chern - Simons theories in higher dimensions.

6.1 INTRODUCTION

Many phenomena in physics are successfully described by field theories. Some examples for this are classical electrodynamics, models in continuum mechanics and theories in particle physics (Quantum Electrodynamics, Standard model). The main building component of these field theories is the action, equivalently

6.2 Topological Field Theory in (2+1)-D

the Lagrangian, from which the equation of motions and the response equation to external fields can be derived. Note however that a field theory does not necessarily have a description by an action principle.

The approach to topological insulators is possible by “topological band theory”, within which topological characteristics such as the Chern number of the bands can be determined, or by “topological field theory”, where we can compute all measurable topological effects.

The topological field theories (TFTs) we consider will be derived by integrating out fermions from the Dirac Lagrangian in various dimensions, in other words we are not interested in the detailed effects of the fermionic degrees of freedom, but only on their overall effect. We will focus on topological field theories in (2+1)-D and (4+1)-D. In (2+1)-D we will use a topological invariant, the response coefficient M_1 , to construct, by dimensional reduction, an \mathbb{Z}_2 - invariant for particle-hole symmetric insulators in (1+1)-D. In (4+1)-D we will use the topological invariant M_2 to construct a \mathbb{Z}_2 - invariant for time-reversal invariant insulators in (3+1)-D.

For the higher dimensional Chern-Simons theories general remarks about the structure of such theories will be given.

Calculations corresponding to some results in the body of the paper are given in the appendix.

6.2 TOPOLOGICAL FIELD THEORY IN (2+1)-D

In this section we will show how to obtain a description of topological phenomena in (2+1)-D from a field theory perspective. First we will motivate an action principle from the response equation of the Quantum Hall effect. However this action can also be derived by integrating out fermions from a Dirac Lagrangian. Finally we will show how to obtain a classification of (1+1)-D particle-hole symmetric insulators by dimensional reduction from a field theory in (2+1)-D.

In the Quantum Hall effect the response (“Hall current”) to the external field A^μ is given by

$$j^i = \sigma_H \epsilon^{ij} E_j, \quad (6.1)$$

where $E_i = -\partial_i A_0 - \partial_0 A_i$. Using the charge conservation equation $\partial_t \rho + \text{div} \vec{j} = 0$ and the covariant formulation $j^\mu = (\rho, j^i)$, we obtain

$$j^\mu = \sigma_H \epsilon^{\mu\nu\rho} \partial_\nu A_\rho. \quad (6.2)$$

From this we can guess that the Lagrangian of an action principle should satisfy

$$\mathcal{L} \propto \epsilon^{\mu\nu\rho} A_\mu \partial_\nu A_\rho, \quad (6.3)$$

to obtain the above response equation by functional differentiation with respect to the field A^μ .

Starting from an action with the Lagrangian of quantum electrodynamics in (2+1)-D,

$$\mathcal{L} = -F_{\mu\nu}F^{\mu\nu} + \bar{\psi}(i\gamma^\mu\partial_\mu - m)\psi - e\bar{\psi}\gamma^\mu A_\mu\psi, \quad (6.4)$$

and integrating out the fermions, we obtain the Chern - Simons action in (2+1)-D

$$S_{2+1}[A] = \frac{M_1}{4\pi} \int dt d^2x \epsilon^{\mu\nu\rho} A_\mu \partial_\nu A_\rho. \quad (6.5)$$

In the above expression the response coefficient M_1 is given by [1, 2],

$$M_1 = \frac{\pi}{3} \int \frac{d\omega d^2k}{(2\pi)^3} \text{Tr} \left[\left(G \frac{\partial G^{-1}}{\partial k^\mu} \right) \left(G \frac{\partial G^{-1}}{\partial k^\nu} \right) \left(G \frac{\partial G^{-1}}{\partial k^\rho} \right) \right], \quad (6.6)$$

where G denotes the bare Green's function of the fermions in the above Lagrangian (6.4).

Observe that this Lagrangian is not time - reversal invariant, because we have under time reversal \mathcal{T} that $A^0 \rightarrow A^0$ and $A^i \rightarrow -A^i$.

The idea of integrating out the fermions in the action is that we are not interested in an exact description of the phenomena associated explicitly with the fermions, but only in their overall contribution. The resulting effective action,

$$\exp(i\hat{S}_{\text{Eff}}[A]) = \int \mathcal{D}\psi \mathcal{D}\bar{\psi} \exp \left(-i \int dt d^2x \mathcal{L} \right), \quad (6.7)$$

incorporates all fermionic effects without explicitly having fermions in the action. In this path integral, the kinetic term of the field A^μ is constant with respect to the integration variables ψ and $\bar{\psi}$ and therefore stays unchanged in the new effective action. The remaining terms in the Lagrangian are linear in $\bar{\psi}$ and ψ and therefore we can use properties of Berezin integration given in the appendix, to deduce that

$$\exp(iS_{\text{Eff}}[A]) = \mathcal{N} \det(i\partial_\mu\gamma^\mu - eA_\mu\gamma^\mu - m), \quad (6.8)$$

where \mathcal{N} is a constant.

The object on the right-hand side is called a functional determinant and in general the evaluation of such an object is hard. One can simplify the evaluation by taking the logarithm of (6.8) and use the relation $\log \det = \text{Tr} \log$. After dropping constants, the object we have to evaluate is

$$S_{\text{Eff}}[A] = \text{Tr} \log(i\partial_\mu\gamma^\mu - eA_\mu\gamma^\mu - m). \quad (6.9)$$

6.2 Topological Field Theory in (2+1)-D

There are two ways to derive (6.5) from the last expression: The first way [3] is a direct perturbative expansion of the logarithm in which we only keep the quadratic terms in the field A^μ . From this we need to extract the completely antisymmetric term in μ, ν and ρ , as in the action (6.5).

The second way is a method developed by Schwinger [4] and applied by Redlich [5] to (2+1)-D quantum electrodynamics. The idea is to evaluate the functional determinant for a simple choice of the gauge field A^μ , such that the field strength $F^{\mu\nu}$ is constant. Using a trick of Schwinger, one can evaluate the functional determinant by calculating the trace of a differential operator. This is done by finding all eigenstates, which is possible for the above simple form of the gauge field interaction.

For the application of topological field theory to insulators we use a reformulation of the response coefficient M_1 . Topological effects for insulators can be described by the Chern number, which can be calculated from the the Berry curvature associated to the band structure. In fact one can show [6], that for insulators the response coefficient M_1 equals the first Chern number C_1 and is given by [7],

$$M_1 = C_1 = \frac{1}{2\pi} \int d^2k f_{xy}(k), \quad (6.10)$$

where the Berry curvature $f_{xy}(k)$ is calculated from the Berry potential $a_i(k)$,

$$f_{xy}(k) = \frac{\partial a_y(k)}{\partial k_x} - \frac{\partial a_x(k)}{\partial k_y}, \quad (6.11)$$

and the Berry potential is given for a band insulator with band index α by

$$a_i(k) = -i \sum_{\alpha \text{ occupied}} \left\langle \alpha k \left| \frac{\partial}{\partial k_i} \right| \alpha k \right\rangle. \quad (6.12)$$

The derivation is similar to the derivation in the (4+1)-D case, which is guided by the calculation in [7] and given in the appendix.

6.2.1 DIMENSIONAL REDUCTION TO (1+1)-D

Chern - Simons theories can only arise in even spatial dimensions and are natural topological theories. It seems that topological field theories in (1+1)-D are difficult to get in a direct and straightforward manner.

Here we will show that these kind of theories can be derived using a dimensional reduction from (2+1)-D to (1+1)-D.

A generic insulator can be described by a Hamiltonian $H = \sum_k c_k^\dagger h(k_x, k_y) c_k$, where c_k and c_k^\dagger are annihilation and creation operators for electrons.

In the procedure of dimensional reduction, periodic boundary conditions in the y -direction are used to compactify the model (this means we curl up the y -direction, such that the plane is curled up into a cylinder). The compactified dimension along k_y will serve as a parametrization, with a parameter $\theta \in [0, 2\pi]$, of a collection of (1+1)-D Hamiltonians and we can then rewrite our Hamiltonian H as $H = \sum_{\theta} H_{(1+1)-D}(\theta)$.

The Hamiltonian $H_{(1+1)-D}(\theta)$ describes an effective (1+1)-D system depending on the external parameter θ . It is given by $H_{(1+1)-D} = \sum_{k_x} c_{k_x, \theta}^{\dagger} h(k_x, \theta) c_{k_x, \theta}$. Integrating out the fermions in the path integral associated to the above (1+1)-D Hamiltonian, we obtain an action principle with a response coefficient $G_1(\theta)$. This response coefficient is related to the response coefficient M_1 (which for insulators equals the Chern number C_1) through

$$\int G_1(\theta) d\theta = M_1. \quad (6.13)$$

To each (1+1)-D Hamiltonian can be associated a charge polarization $P_1(\theta)$ which can be related to the response coefficient $G_1(\theta)$ through the equation $\partial_{\theta} P_1(\theta) = G_1(\theta)$. The properties of the charge polarization P_1 will be used in the next section to define a \mathbb{Z}_2 -invariant for particle-hole symmetric systems.

6.2.2 CLASSIFICATION OF PARTICLE-HOLE SYMMETRIC INSULATORS IN (1+1)-D

The Chern number C_1 , which can be associated to insulators in (2+1)-D by formula (6.10), is a topological invariant. A natural question is to ask whether the topological nature of this coefficient is preserved under the procedure of dimensional reduction. The argument presented in this subsection is from Qi, Hughes and Zhang [7].

Particle-hole symmetry exchanges particles with holes: it acts in momentum space by the mapping $c_k \mapsto \mathcal{C}c_{-k}^{\dagger}$, so a particle with momentum k is mapped to a hole with momentum $-k$.

An insulator is called particle-hole symmetric, if its Hamiltonian $H = \sum_k c_k^{\dagger} h(k) c_k$ fulfills the requirement $\mathcal{C}^{\dagger} h(k) \mathcal{C} = -h^t(k)$.

In order to build a classification of particle-hole symmetric insulator in (1+1)-D, we consider the family of transformations between two particle-hole symmetric Hamiltonians $h_1(k)$ and $h_2(k)$. The properties of these transformations together with the sum rule (6.13) will determine, as we will see, a topological invariants for the systems under study.

6.2 Topological Field Theory in (2+1)-D

A transformation between $h_1(k)$ and $h_2(k)$ is any function $h(k, \theta)$, where θ is a parameter, such that $h(k, 0) = h_1(k)$ and $h(k, \pi) = h_2(k)$. We require any (1+1)-D Hamiltonian $h(\cdot, \theta)$, i.e for a fixed $\theta \in [0, \pi]$, to be gapped.

Using particle-hole symmetry, we can extend the definition of a transformation $h(k, \theta)$ to $\theta \in [0, 2\pi]$ using $h(k, \theta) = -[\mathcal{C}^{-1}h(-k, 2\pi - \theta)\mathcal{C}]^t$. Notice that $h(k, 0) = h(k, 2\pi) = h_1(k)$. We have thus constructed a (2+1)-D Hamiltonian $h(k, \theta)$ in a space where the 2nd spatial dimension is compactified.

This (2+1)-D Hamiltonian $h(k, \theta)$ has a band structure and one can calculate the Berry connection and the Berry curvature. By formula (6.10) we can assign a Chern number C_1 as a topological invariant to the Hamiltonian $h(k, \theta)$.

The charge polarization P_1 , which fullfills $\int \partial_\theta P_1 d\theta = M_1 = C_1$, can be expressed in the particle-hole symmetric case by [7],

$$P_1(\theta) = \int \frac{dk_x}{2\pi} \sum_{E_\alpha(k) < 0} (-i) \langle k_x, \theta; \alpha | \partial_{k_x} | k_x, \theta; \alpha \rangle, \quad (6.14)$$

where α is a band index and $E_{\alpha(k)} < 0$ means we sum over all filled bands at momentum k .

One important question: What is the relation between the Chern numbers numbers $C_1[h]$ and $C_1[h']$, associated to different transformations h, h' between $h_1(k)$ and $h_2(k)$?

Two different transformations $h(k, \theta)$ and $h'(k, \theta)$ in general will lead to different Chern numbers C_1 , however, as we will show below, the difference of this Chern numbers is constrained by particle - hole symmetry,

$$C_1[h] - C_1[h'] = 2n \text{ for } n \in \mathbb{Z}. \quad (6.15)$$

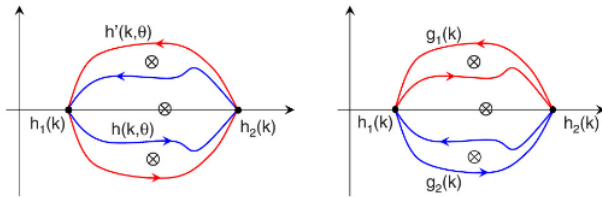


Figure 6.1: Pictorial representation of (2+1)-D Hamiltonian, [7]

In figure (6.1) points symbolize (1+1)-D Hamiltonians in an abstract plane. Reflection on the horizontal axis represents particle - hole symmetry and therefore points on the horizontal axis symbolize particle - hole symmetric insulators in (1+1)-D. The closed curves are parametrized by the control parameter θ and

symbolize a (2+1)-D Hamiltonian for which there is a well defined first Chern number C_1 . We can see that the constructed (2+1)-D Hamiltonian is mapped under particle - hole symmetry to itself and therefore it is particle - hole symmetric. To show equation (6.15), we will construct two new (2+1)-D Hamiltonians out of the two given transformations $h(k, \theta)$ and $h'(k, \theta)$ and show that their Chern numbers C_1 are equal.

For this we define the transformations g_1 and g_2 in picture (6.1) by

$$g_1(k, \theta) = \begin{cases} h(k, \theta) & \theta \in [0, \pi] \\ h'(k, 2\pi - \theta) & \theta \in [\pi, 2\pi] \end{cases}, \quad (6.16)$$

$$g_2(k, \theta) = \begin{cases} h'(k, 2\pi - \theta) & \theta \in [0, \pi] \\ h(k, \theta) & \theta \in [\pi, 2\pi] \end{cases}. \quad (6.17)$$

Using the sum rule (6.13) for Chern numbers and the representation of the coefficient G_1 by the polarization P_1 , we can establish the following expression for the Chern number associated to the transformation g_1 ,

$$C_1[g_1] = \int_0^\pi d\theta (\partial_\theta P_1 - \partial_\theta P'_1), \quad (6.18)$$

where P_1 and P'_1 are the polarizations associated to h and h' . The same expression is valid for the transformation g_2 with the integration range 0 to π replaced by the integration range π to 2π . The crucial point is the use of particle-hole symmetry to establish that the contribution from both integration ranges is the same, this means $\int_0^\pi dP_1(\theta) = \int_\pi^{2\pi} dP_1(\theta)$.

To establish this more rigorously one can prove the equation $P_1(\theta) = -P_1(2\pi - \theta)$, from which our results follow by integration from 0 to π and a change of variables $2\pi - \theta \rightarrow \theta$ on the right-hand side. For this remember the definition of the polarization $P_1(\theta)$ as summing over occupied states. The rigorous calculation is provided in [7].

Thanks to relation (6.15), we can unambiguously define the “Relative First Chern Parity”

$$N_1[h_1, h_2] = (-1)^{C_1[h]} = (-1)^{C_1[h']}, \quad (6.19)$$

which depends on the $(1 + 1) - D$ insulator Hamiltonians $h_1(k)$ and $h_2(k)$. This is indeed well defined as it is independent of the choice of interpolation $h(k, \theta)$. Observe that this is a \mathbb{Z}_2 - invariant depending on two insulator Hamiltonians $h_1(k)$ and $h_2(k)$.

The “Relative First Chern Parity” fulfills the transitivity relation

$$N_1[h_1(k), h_2(k)] N_1[h_2(k), h_3(k)] = N_1[h_1(k), h_3(k)]. \quad (6.20)$$

6.3 Topological Field Theory in (4+1)-D

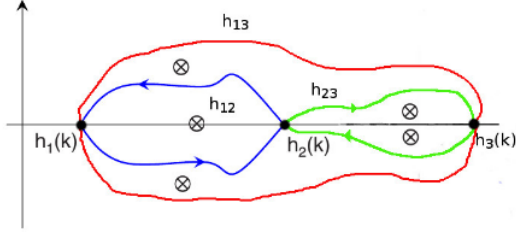


Figure 6.2: Equivalence relation for First Relative Chern Parity, Modified from [7]

as shown graphically below.

The argument for this last relation is pictorial, given (1+1)-D Hamiltonians $h_1(k)$, $h_2(k)$ and $h_3(k)$ we can define interpolations h_{12} , h_{23} and h_{13} . Observe that by construction the “gluing” of the interpolations h_{12} and h_{23} is also a possible interpolation between $h_1(k)$ and $h_3(k)$, denote it by h'_{13} , then we know that $C_1[h_{13}] - C_1[h'_{13}] = 2n$ for $n \in \mathbb{Z}$ and by the fact that the Chern number C_1 of the glued transformation h'_{13} is the sum of the Chern numbers of its components h_{12} and h_{23} , this means $C_1[h_{12}] + C_1[h_{23}] = C_1[h'_{13}]$, we get the claimed transitivity relation.

Given this relation, it is possible to assign a \mathbb{Z}_2 - invariant to a single particle - hole symmetric insulator $h_1(k)$ by fixing a reference Hamiltonian $h_0(k)$ which can conveniently be considered to be independent of the momentum k . Then one can define the “Absolute First Chern Parity” by

$$N_1[h_1] = N_1[h_1, h_0]. \quad (6.21)$$

Insulators with $N_1[h_1] = 1$ are called \mathbb{Z}_2 - trivial insulators and insulators with $N_1[h_1] = (-1)$ are called \mathbb{Z}_2 - nontrivial insulators.

6.3 TOPOLOGICAL FIELD THEORY IN (4+1)-D

In this section we will study a topological field theory in (4+1)-D, using the techniques introduced above.

Again we will integrate out fermions from an action associated with the (4+1)-D Dirac Lagrangian to obtain the Chern - Simons action in (4+1)-D. Dimensional reduction will result in a classification of time-reversal invariant insulators in (3+1)-D.

The Chern - Simons action in (4+1)-D is given by [7, 1]

$$S_{4+1}[A] = \frac{M_2}{24\pi^2} \int dt d^4x \epsilon^{\mu\nu\rho\sigma} A_\mu \partial_\nu A_\rho \partial_\sigma A_\tau \quad (6.22)$$

The response coefficient M_2 in this action is given by [7, 1]

$$M_2 = -\frac{\pi^2}{15} \epsilon^{\mu\nu\rho\sigma\tau} \int \frac{d\omega d^4k}{(2\pi)^5} \text{Tr} \left[\left(G \frac{\partial G^{-1}}{\partial k^\mu} \right) \left(G \frac{\partial G^{-1}}{\partial k^\nu} \right) \left(G \frac{\partial G^{-1}}{\partial k^\rho} \right) \left(G \frac{\partial G^{-1}}{\partial k^\sigma} \right) \left(G \frac{\partial G^{-1}}{\partial k^\tau} \right) \right], \quad (6.23)$$

where G denotes the bare Green's function of the fermions in the Lagrangian of (4+1)-D quantum electrodynamics.

Observe that this action is time - reversal invariant, we have $\mathcal{T}S_{4+1} = S_{4+1}$. For the derivation of this expression we expand the functional determinant up to third order. Observe that there is no term similar to the action (6.5) from the second order of the expansion (compare with the appendix "Integrating out fermions").

As in the (2+1)-D case for insulators the response coefficient M_2 can be related to the non - abelian Berry curvature. Using the non - abelian Berry curvature, where α, β denote band labels for an insulator,

$$f_{ij}^{\alpha\beta}(k) = \partial_i a_j^{\alpha\beta}(k) - \partial_j a_i^{\alpha\beta}(k) + i[a_i, a_j]^{\alpha\beta}(k). \quad (6.24)$$

derived from the Berry potential $a_i(k)$, which is defined as before, we obtain

$$M_2 = C_2 = \frac{1}{32\pi^2} \int d^4k \epsilon^{ijkl} \text{Tr}[f_{ij} f_{kl}]. \quad (6.25)$$

The derivation of this formula is given in the appendix.

The physical response of the above system to a variation in A^μ is given by

$$j^\mu = \frac{\delta S_{(4+1)-D}[A]}{\delta A^\mu} = \frac{C_2}{8\pi^2} \epsilon^{\mu\nu\rho\sigma\tau} \partial_\nu A_\rho \partial_\sigma A_\tau. \quad (6.26)$$

Observe that in comparison to the response in (2+1)-D the equation is non - linear in the external field A^μ .

6.3.1 DIMENSIONAL REDUCTION TO (3+1)-D

The idea of the dimensional reduction from (4+1)-D to (3+1)-D is similar to the case (2+1)-D to (1+1)-D. We impose periodic boundary conditions on the fourth spatial dimension. Then the momentum k^4 is a good quantum number. After the

6.3 Topological Field Theory in (4+1)-D

calculation of the effective (3+1)-D action [8], we obtain a response coefficient $G_3(\theta)$ fulfilling the sum rule

$$\int G_3(\theta) d\theta = M_2, \quad (6.27)$$

and with $G_3(\theta) = \partial_\theta P_3(\theta)$ we introduce the “magneto-electric polarization” P_3 , a three - dimensional polarization. This quantity is a pseudo - scalar which couples in a nonlinear way to $\vec{E} \cdot \vec{B}$ [8] and it depends on the coordinates t, x^1, x^2, x^3 through the control parameter θ .

The effective (3+1)-D action can be written in terms of the magneto-electric polarization P_3 as [7],

$$S_{(3+1)-D} = \frac{1}{4\pi} \int dx^0 d^3x \epsilon^{\mu\nu\rho\tau} P_3(x, t) \partial_\mu A_\nu \partial_\rho A_\sigma. \quad (6.28)$$

From the action in (3+1)-D we can derive the following response equation,

$$j^\mu = \frac{1}{2\pi} \epsilon^{\mu\nu\rho\sigma} \partial_\nu P_3 \partial_\rho A_\sigma. \quad (6.29)$$

A possible consequence of this response equation can be observed in the following setup [7]:

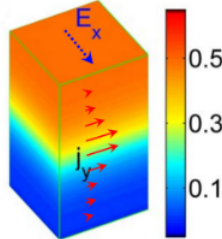


Figure 6.3: System with spatial gradient in P_3 , [7]

In figure (6.3) we have an (3+1)-D insulator, which has a polarization $P_3 = P_3(z)$. Then the above response equation simplifies to

$$j^\mu = \frac{\partial_z P_3}{2\pi} \epsilon^{\mu\nu\rho} \partial_\nu A_\rho. \quad (6.30)$$

This response equation looks very similar to the response equation (6.2) of the Quantum Hall effect, however here we have no quantization condition on $\sigma_H = \frac{\partial_z P_3}{2\pi}$.

6.3.2 CLASSIFICATION OF TIME - REVERSAL INVARIANT INSULATORS

As before we ask whether there is a topological invariant associated to the (3+1)-D system and how it is related to the response coefficient M_2 . The answer and derivation is very similar to the reduction case from (2+1)-D to (1+1)-D, again we will use a symmetry to study the transformations between two (3+1)-D insulator Hamiltonians. However this time we will use time-reversal symmetry instead of the particle-hole symmetry. Recall that the time - reversal constraint for a (3+1)-D Hamiltonian is given by

$$\mathcal{T}^\dagger h(-k)\mathcal{T} = h^t(k). \quad (6.31)$$

Then for any (3+1)-D time-reversal invariant insulator Hamiltonians $h_1(k)$ and $h_2(k)$, we can define a (4+1)-D Hamiltonian $h(k, \theta)$ in the following way: Prescribe $h(k, 0) = h_1(k)$ and $h(k, \pi) = h_2(k)$, next define $h(k, \theta)$ for $\theta \in [0, \pi]$ by any continuous transformation. To complete the definition of $h(k, \theta)$ for $[\pi, 2\pi]$ define $\mathcal{T}^\dagger h(-k, 2\pi - \theta)\mathcal{T} = h^t(k, \theta)$.

Similar to the case in (2+1)-D we have that the “Relative Second Chern Parity”

$$N_2[h_1(k), h_2(k)] = (-1)^{C_2[h]}, \quad (6.32)$$

is well defined for two given time-reversal invariant insulator Hamiltonians in (3+1)-D and the transformation $h(k, \theta)$ constructed above..

By fixing a reference vacuum Hamiltonian $h_0(k)$, we can define by similar arguments as for the (2+1)-D case the “Absolute Second Chern Parity”,

$$N_2[h_1(k)] = N_2[h_1(k), h_0(k)]. \quad (6.33)$$

Insulators with $N_2 = 1$ are called \mathbb{Z}_2 trivial and insulators with $N_2 = -1$ are called \mathbb{Z}_2 nontrivial.

This notion of trivial and non-trivial time - reversal invariant insulators discussed here was introduced by Qi, Hughes and Zhang [7] and is different from the classification of other authors based on topological band theory. For example the “strong topological insulators” discussed by Fu, Kane and Mele [9] correspond to the the \mathbb{Z}_2 non - trivial insulators in (3+1)-D discussed here. The “weak topological insulators” discussed in [9] are (2+1)-D insulators and therefore are not effected by the \mathbb{Z}_2 - classification in (3+1)-D.

As an example consider the following setup taken from [7]: For $z \leq 0$ we take vacuum and there the magneto-electric polarization P_3 is 0 and for $z > 0$ we take a \mathbb{Z}_2 - nontrivial topological insulator. For a \mathbb{Z}_2 - nontrivial insulator we have [7]

6.3 Topological Field Theory in (4+1)-D

$P_3 = \frac{2n+1}{2}$ for $n \in \mathbb{Z}$. Thus we have that the magnetoelectric polarization takes the form, $P_3 = \frac{2n+1}{2}\Theta(z)$, where Θ is the Heaviside step function. If we assume that the external field A^μ is only non - zero in a small spatial region, we can perform integration by parts and we obtain no boundary terms in this process. Observing that $\partial_z P_3 = \frac{2n+1}{2}\delta(z)$, we can simplify formula (6.28) by performing the integration with respect to the variable z to obtain an action defined on the $z = 0$ surface given by

$$S_{z=0} = -\frac{2n+1}{8\pi} \int dt d^2x \epsilon^{3\nu\rho\sigma} A_\nu \partial_\rho A_\sigma.$$

This action looks similar to the Chern - Simons action in (2+1)-D and it is not time - reversal symmetric, therefore we can make an interesting observation: Although the bulk of the \mathbb{Z}_2 non - trivial topological insulator and the vacuum have time - reversal symmetry, we see that the time - reversal symmetry needs to be broken on the surface between topological insulators belonging to different classes. Furthermore this action describes an Hall effect on the surface with a Hall conductance $\sigma_H = \frac{2n+1}{2}$.

6.3.3 MODIFIED MAXWELL EQUATIONS

If we want to describe the electrodynamics of a time-reversal invariant topological insulator in (3+1)-D by an action principle, we should include the Maxwell term and the Chern - Simons term and arrive at the action principle,

$$S[A] = \int dx^0 d^3x \frac{1}{16\pi} F_{\mu\nu} F^{\mu\nu} + \frac{1}{2} F_{\mu\nu} \mathcal{P}^{\mu\nu} - \frac{1}{c} j^\mu + \frac{\alpha}{16\pi} P_3, \quad (6.34)$$

where $F_{\mu\nu}$ is the field - strength tensor, $\mathcal{P}^{\mu\nu}$ is the polarization tensor (covariant formulation of magnetization and electric polarization) , j^μ an external source and P_3 is the magneto-eletre polarization, which is quantized for time - reversal invariant topological insulators.

By Hamilton's principle ($\delta S[A] = 0$) we can derive the following equations [1] from action (6.34), which are the Maxwell equations modified by the magneto-electric polarization P_3 ,

$$\nabla \cdot \vec{D} = 4\pi\rho + 2\alpha (\nabla P_3 \cdot \vec{B}), \quad (6.35)$$

$$\nabla \times \vec{H} - \frac{1}{c} \partial_t \vec{D} = \frac{4\pi}{c} \vec{j} - 2\alpha \left((\nabla P_3 \times \vec{E} + \frac{1}{c} (\partial_t P_3) \vec{B}) \right), \quad (6.36)$$

$$\nabla \times \vec{E} + \frac{1}{c} \partial_t \vec{B} = 0, \quad (6.37)$$

$$\nabla \cdot \vec{B} = 0, \quad (6.38)$$

and we have the supplementing relations $\vec{D} = \vec{E} + 4\pi\vec{P}$ and $\vec{H} = \vec{B} - 4\pi\vec{M}$. Since the Maxwell term and the Chern - Simons term have the same scaling behavior, they are equally important at low energies [1]. These equations describe how electrodynamic properties are affected by the topological properties of the system.

6.4 TOPOLOGICAL FIELD THEORIES IN HIGHER DIMENSIONS

We have observed that we can formulate a Chern - Simons action in (2+1)-D and (4+1)-D. One can ask whether there is Chern - Simons action in higher dimensions and why there is no Chern - Simons action in the case (3+1)-D. For every space-time with an even number of spatial dimensions, it is possible to formulate a Chern - Simons theory by [7],

$$S_{(2n+1)-D} = \frac{C_n}{(n+1)!(2\pi)^n} \int dt d^{2n}x \epsilon^{\mu_1 \dots \mu_{2n+1}} \times A_{\mu_1} \partial_{\mu_2} A_{\mu_3} \dots \partial_{\mu_{2n}} A_{\mu_{2n+1}}, \quad (6.39)$$

where the Chern number C_n is given for insulators by

$$C_n = \frac{1}{n!2^n(2\pi)^n} \int d^{2n}k \epsilon^{i_1 \dots i_{2n}} \text{Tr} [f_{i_1 i_2} \dots f_{i_{2n-1} i_{2n}}]. \quad (6.40)$$

We observe that this actions have time - reversal symmetry in dimensions (4n+1)-D and break time - reversal symmetry in (4n-1)-D.

As before we can ask whether we can use the Chern number C_n to derive associated topological invariants by the process of dimensional reduction. This is possible and depending on the dimension of the fundamental topological field theory, we need particle - hole symmetry or time - reversal symmetry.

An overview over the higher dimensional Chern Simons theories is given in figure (6.4). On the trunk the fundamental topological field theories in even spatial dimensions are indicated by black. \mathbb{Z}_2 - classifications obtained by dimensional reduction with the use of particle - hole symmetry by blue boxes and blue circles, and a \mathbb{Z}_2 - index from time - reversal symmetry is indicated by red boxes and red circles.

The non-existence of a Chern - Simons term in (3+1)-D (and by a similar argument in general even spacetime dimensions) can be seen by the calculation “Integrating out fermions” in the appendix. In this calculation we obtain a completely antisymmetric term from the trace of Dirac matrices. Therefore recall that

6.5 Conclusion

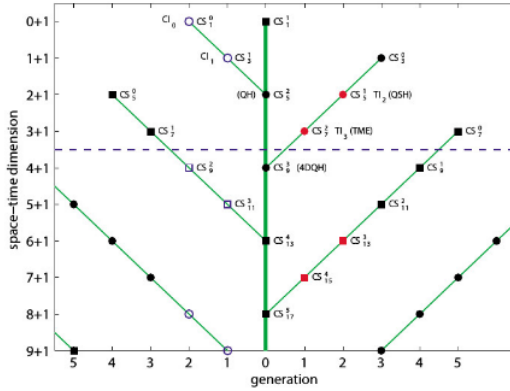


Figure 6.4: Family tree of topological field theories, [7]

in $(n+1)$ -D we have $(n+1)$ Dirac matrices and furthermore that Dirac matrices in $(n+1)$ -D with n even can be obtained by using Dirac matrices in $(n-1+1)$ -D and adding the matrix $\gamma^0 \cdots \gamma^{n-1}$ (possibly with a prefactor to account for normalization) to this collection of Dirac matrices. Then no trace of Dirac matrices in even spacetime dimension is completely antisymmetric, however in odd spacetime dimensions the trace of all $(n+1)$ Dirac matrices is completely antisymmetric.

6.5 CONCLUSION

In conclusion we have seen how the Chern - Simons terms arise by evaluating a functional determinant. For (2+1)-D systems we used particle - hole symmetry to derive a \mathbb{Z}_2 classification for (1+1)-D particle - hole symmetric insulators derived by dimensional reduction. This method was used in the (4+1)-D case to get a similar classification of (3+1)-D time - reversal invariant in terms of a \mathbb{Z}_2 invariant. We investigated some properties of the non - trivial topological insulator in (3+1)-D with the use of the associated effective action.

In the appendix we show two calculations from the literature, which are important for our topic – integrating out fermions and the evaluation of the response coefficient M_2 in terms of Berry curvature.

6.6 APPENDIX

6.6.1 CONVENTIONS

In this work we use the following conventions. The variable t denotes time and $x = (x^1, \dots, x^n)$ denotes n spatial coordinates. Greek letters $\mu, \nu, \rho, \sigma, \tau$ refer to the collection of all space-time indices, this means for example $x^\mu = (x^0 = t, x^1, \dots, x^n)$. Small Latin letters i, j, k, l refer to the spatial coordinates (x^1, \dots, x^n) only.

The Dirac matrices γ^μ in (2+1)-D are determined by the anti-commutation relations $\{\gamma^\mu, \gamma^\nu\} = 2g^{\mu\nu}$, where we use the convention $g^{\mu\nu} = \text{diag}(1, -1, -1)$. In the Dirac representation they are given by the Pauli matrices [3] ,

$$\begin{aligned}\gamma^0 &= \sigma^3 = \begin{pmatrix} 1 & 0 \\ 0 & -1 \end{pmatrix} \\ \gamma^1 &= i\sigma^1 = \begin{pmatrix} 0 & i \\ i & 0 \end{pmatrix} \\ \gamma^2 &= i\sigma^2 = \begin{pmatrix} 0 & 1 \\ -1 & 0 \end{pmatrix},\end{aligned}$$

For the evaluation of traces involving Dirac matrices in (2+1)-D the following relations are useful,

$$\begin{aligned}\gamma^\mu \gamma^\nu &= g^{\mu\nu} \text{Id} - i\epsilon^{\mu\nu\rho} \gamma^\rho \\ \text{Tr} \gamma^\mu &= 0 \\ \text{Tr} \gamma^\mu \gamma^\nu &= 2g^{\mu\nu} \\ \text{Tr} \gamma^\mu \gamma^\nu \gamma^\rho &= -2i\epsilon^{\mu\nu\rho} \\ \text{Tr} \gamma^\mu \gamma^\nu \gamma^\rho \gamma^\sigma &= 2g^{\mu\nu} g^{\rho\sigma} - 2\epsilon^{\mu\nu\tau} \epsilon^{\rho\sigma\tau}.\end{aligned}$$

In contrast to the (3+1)-D case the trace of three Dirac matrices is not zero.

6.6.2 INTEGRATING OUT FERMIONS

For the derivation of the functional determinant in equation (6.8), we use the following fact about Berezin integration [10]: Given two vectors of Grassmann variables $\xi = (\xi^1, \dots, \xi^n)$ and $\theta = (\theta^1, \dots, \theta^n)$, we have

$$\int d\xi d\theta \exp(-\xi^t A \theta) = \det A, \quad (6.41)$$

where A is a $n \times n$ matrix. This fact generalizes to path integrals.

6.6 Appendix

Here we will evaluate the functional determinant by expansion in the gauge field A^μ . For this we start with equation (6.9) and observe that this equation can be rewritten,

$$S_{\text{Eff}}[A] = \text{Tr} \log(i\partial_\mu \gamma^\mu - m)(1 - e(i\partial_\mu \gamma^\mu - m)^{-1} A_\mu \gamma^\mu). \quad (6.42)$$

Now we can use the rule $\log ab = \log a + \log b$ and the relation $\log(1 - x) = -\sum_{n \geq 1} \frac{x^n}{n}$ for $|x| < 1$ to expand this effective action up to quadratic terms in A ,

$$\begin{aligned} S_{\text{Eff}}[A] &= \text{Tr} \log(i\partial_\mu \gamma^\mu - m) + e \text{Tr} \left(\frac{1}{i\partial_\rho \gamma^\rho - m} A_\mu \gamma^\mu \right) \\ &\quad - \frac{e^2}{2} \text{Tr} \left(\frac{1}{i\partial_\rho \gamma^\rho - m} A_\mu \gamma^\mu \frac{1}{i\partial_\sigma \gamma^\sigma - m} A_\nu \gamma^\nu \right), \end{aligned} \quad (6.43)$$

Since the Chern Simons action in (2+1)-D is quadratic in the gauge field, we will only keep this term. The above trace Tr involves taking a matrix trace (denoted by tr) and performing an integration over space-time, thus we have

$$S_{\text{Eff}}^{\text{Quad}} = -\frac{e^2}{2} \int dx \text{tr} \left\langle x \left| \frac{1}{i\partial_\rho \gamma^\rho - m} A_\mu \gamma^\mu \frac{1}{i\partial_\sigma \gamma^\sigma - m} A_\nu \gamma^\nu \right| x \right\rangle. \quad (6.44)$$

By using the completeness relation $\text{id} = \int dy^0 dy^2 |y\rangle \langle y|$, $\langle y| A^\mu |x\rangle = \delta(x-y) A^\mu(x)$ and some manipulations we obtain,

$$S_{\text{Eff}}^{\text{Quad}}[A] = \frac{e^2}{2} \int dx_1 dx_2 A_\mu(x_2) A_\nu(x_1) \times \text{tr} S_F(x_1 - x_2) \gamma^\mu S_F(x_2 - x_1) \gamma^\nu, \quad (6.45)$$

where $S_F(x - y)$ is the fermion propagator in position space. To evaluate this expression we perform the substitution $\bar{x} = \frac{x_1 + x_2}{2}$ and $x = x_1 - x_2$, to obtain

$$S_{\text{Eff}}^{\text{Quad}}[A] = \frac{e^2}{2} \int d\bar{x} dx A_\mu \left(\bar{x} - \frac{x}{2} \right) A_\nu \left(\bar{x} + \frac{x}{2} \right) \times (\text{tr} S_F(x) \gamma^\mu S_F(-x) \gamma^\nu). \quad (6.46)$$

This expression can be related to a Feynman diagram by expressing A_μ , A_ν and the fermion propagators in momentum space. Then we have in total six integrations and by applying $\int dk \exp(-ikx) = \delta(x)$ and performing the δ -integration, we are left with two integrations.

Then the quadratic term is given by

$$S_{\text{Eff}}^{\text{Quad}}[A] = \frac{e^2}{2} \int dp^0 d^2 p \hat{A}_\mu(-p) \Gamma^{\mu\nu}(p) \hat{A}_\nu(p), \quad (6.47)$$

where $\Gamma^{\mu\nu}(p)$ is the contribution of the Feynman diagram in figure (6.5). In the Feynman diagram (6.5) a curly line denotes a photon propagator and a straight line with arrow denotes a fermion propagator.

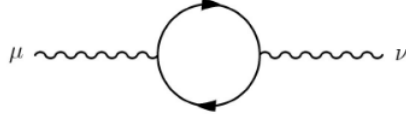


Figure 6.5: Fermion loop with two external gauge fields [3]

The contribution $\Gamma^{\mu\nu}(p)$ is given by

$$\Gamma^{\mu\nu}(p) = \int dk^0 d^2k \text{Tr} \left[\gamma^\mu \frac{p_\rho \gamma^\rho + k_\sigma \gamma^\sigma - m}{(p+k)^2 - m^2} \gamma^\nu \frac{k_\sigma \gamma^\sigma}{k^2 - m^2} \right]. \quad (6.48)$$

The next step is to observe that the Chern-Simons action (6.5) is completely antisymmetric in the indices μ, ν and ρ . Therefore we need to extract a term proportional to $\epsilon^{\mu\nu\rho}$ from the above trace. By the special structure of the Dirac matrices in (2+1)-D such a term is given by a trace of exactly three Dirac matrices. From the 6 possible terms in the trace, only three terms have the right number of Dirac matrices: $m\gamma^\mu\gamma^\nu\gamma^\rho p_\rho$, $m\gamma^\mu\gamma^\nu\gamma^\sigma k_\sigma$ and $m\gamma^\mu\gamma^\sigma\gamma^\nu k_\sigma$.

But since $\epsilon^{\mu\nu\rho}$ is antisymmetric, the last two terms cancel each other.

Therefore we need to evaluate the integral,

$$\Gamma_{\text{Antisym}}^{\mu\nu}(p) = -2\epsilon^{\mu\nu\rho} p_\rho \int dk^0 d^2k \frac{1}{(p+k)^2 - m^2} \frac{1}{k^2 - m^2}. \quad (6.49)$$

The integral on the right-hand side can be evaluated using Wick rotation. Observe that the integrand actually has no poles on the real line, because we did not carry the necessary deformations $+i\delta$ in the propagators obtained from figure (6.5). After evaluation of this integral we only keep the leading term in the limit $p \rightarrow 0$ and $m \rightarrow \infty$.

Hence we have

$$S_{\text{Eff}}^{\text{Quad} + \text{Antisym}} \propto \epsilon^{\mu\nu\rho} \int dp^0 d^2p \hat{A}_\mu(-p) p_\rho \hat{A}_\nu(p). \quad (6.50)$$

To rewrite this in coordinate space, we use the convolution theorem, $(f \cdot g) = \hat{f} * \hat{g}$ and apply it to $\hat{f} = \hat{A}_\mu(p)$ and $\hat{g} = p_\rho \hat{A}_\nu(p)$, then

$$\int dx^0 d^2x A_\mu(x)(\partial_\rho A_\mu)(x) \exp(ixk) = \int dp^0 d^2p \hat{A}_\mu(k-p) p_\rho \hat{A}_\nu(p), \quad (6.51)$$

and evaluating at $k = 0$ we obtain the result.

6.6 Appendix

Thus we have established that by integrating out fermions we obtain a term in the effective action of the form

$$S_{\text{Eff}}[m, A] = c_{CS} \int dx^0 d^2x A_\mu(x) (\partial_\rho A_\mu)(x), \quad (6.52)$$

however the dimensionless coefficient c_{CS} is not calculated yet. This coefficient c_{CS} can be calculated [2] by looking again at the fermion bubble and using the Ward identity to rewrite the expression such that we obtain $c_{CS} = M_1$, where M_1 is the response coefficient given in expression (6.6).

The calculation in (4+1)-D is very similar. The action (6.22) is obtained from the third order term in the expansion of the functional determinant. Similar to the steps (6.43) to (6.45) we find the expression

$$S_{Cubic} = \frac{e^3}{3} \int dp dp' \hat{A}_\mu(-p) \hat{A}_\nu(-p') \hat{A}_\rho(p+p') \Gamma^{\mu\nu\rho}(p, p'), \quad (6.53)$$

where $\Gamma^{\mu\nu\rho}$ is the fermion bubble with three external legs. The idea is again to extract the completely antisymmetric part similar to equation (6.50). However one has to be careful in the evaluation of the trace – one has to take the Dirac matrices in (4+1)-D.

What happens with the quadratic term in the expansion of the functional determinant (6.42) in the (4+1)-D case? Up to equation (6.48) the result is the same except multiplicative constants, integration over (4+1)-D instead of integration over (2+1)-D and the use of Dirac matrices in (4+1)-D. However in the evaluation of the trace in expression (6.48) – due to the Dirac matrices in (4+1)-D – three of the six terms vanish, and the three other terms are not antisymmetric in μ, ν, ρ as in the Chern - Simons action in (2+1)-D in equation (6.5).

6.6.3 RESPONSE COEFFICIENT C_2 AND BERRY CURVATURE

In this section we will follow the calculation of [7] for the relation of the response coefficient M_2 and the Berry curvature f_{ij} for insulators. The calculation here will provide some more details than in the original reference.

The argument consists of three steps, in the first step, we will show that the response coefficient M_2 is indeed a topological invariant, in the second step we will show that any Hamiltonian of a insulator can be connected to a flat band insulator and in the third step, we will explicitly calculate the response coefficient M_2 for this model.

To show the topological invariance, we will observe that small changes in the Green's function G of the insulator should not affect the response coefficient M_2 , this means $\delta M_2 = 0$ for a small transformation δG .

First we will analyze the main building block in the response coefficient M_2 given by (6.23),

$$\begin{aligned}\delta(G\partial_\mu G^{-1}) &= (\delta G)\partial_\mu G^{-1} + G\partial_\mu(\delta G^{-1}) \\ &= (\delta G)\partial_\mu G^{-1} - G\partial_\mu(G^{-1}\delta GG^{-1}) \\ &= -\partial_\mu(\delta G)G^{-1} - G(\partial_\mu G^{-1})(\delta G)G^{-1}.\end{aligned}\quad (6.54)$$

In this calculation we used the product rule in the first equality, for the second equality we calculated δG^{-1} from $1 = GG^{-1}$ by applying δ on both sides, in the last equality we expanded.

In the next step we want to calculate δM_2 , the idea is to express this quantity as a divergence term, which then vanishes. The variation δM_2 is given by

$$\delta M_2 = -\frac{\pi^2}{15}\epsilon^{\mu\nu\rho\sigma\tau}\int \frac{d^4kd\omega}{(2\pi)^5} \delta\text{Tr}[(G\partial_\mu G^{-1})\cdots(G\partial_\tau G^{-1})]. \quad (6.55)$$

Because of the symmetry properties of $\epsilon^{\mu\nu\rho\sigma\tau}$ and the cyclicity of the trace we only need to consider the term, where δ acts on the first term in the trace. Using the identity derived above, we have the first equality below,

$$\begin{aligned}-\text{Tr}[\delta(G\partial_\mu G^{-1})\cdots(G\partial_\tau G^{-1})] &= \text{Tr}[\partial_\mu(\delta G)G^{-1}\cdots(G\partial_\tau G^{-1})] + \text{Tr}[G(\partial_\mu G^{-1})(\delta G)G^{-1}\cdots(G\partial_\tau G^{-1})] \\ &= \text{Tr}[\partial_\mu(G^{-1}\delta G)\cdots(\partial_\tau G^{-1}G)],\end{aligned}\quad (6.56)$$

where we used the observation that $G\partial_\mu(G^{-1}\delta G)G^{-1} = G(\partial_\mu G^{-1})(\delta G)G^{-1} + GG^{-1}\partial_\mu(\delta G)G^{-1}$ and the cyclicity of the trace to bring the Greens function G on the left to the end of the expression in the trace, this changes the order of $\partial_\mu G^{-1}$ and G in the four terms without the μ -index in the last expression.

The next step is to take out the partial derivative ∂_μ from the trace, then we are left with the following,

$$\begin{aligned}\text{Tr}[\partial_\mu(G^{-1}\delta G)\cdots(\partial_\tau G^{-1}G)] &= \partial_\mu\text{Tr}[(G^{-1}\delta G)\cdots] - \text{four terms Tr}[(G^{-1}\delta G)\cdots(\partial_\mu)(\partial_\tau G^{-1}G)].\end{aligned}\quad (6.57)$$

The first term is our divergence term and the other four terms vanish due to the antisymmetry of the Levi - Civita tensor $\epsilon^{\mu\nu\rho\sigma\tau}$.

The next step in our argument is that any gapped insulator can be connected to a flat two-band insulator. The flat two - band insulator Hamiltonian is given by

$$h_0(k) = \epsilon_G P_G(k) + \epsilon_E P_E(k), \quad (6.58)$$

where P_G is the projection operator on the occupied bands and P_E is the projection operator on the unoccupied bands.

6.6 Appendix

So we want to find a continuous transformation $H(k, s)$ with $s \in [0, 1]$, such that we have $H(k, 0) = h(k)$ and $H(k, 1) = h_0(k)$. For this we diagonalize the Hamiltonian $h(k) = U(k)D(k)U^\dagger(k)$, where $U(k)$ is a unitary transformation and $D(k)$ is a diagonal matrix with

$$D(k) = \text{diag} [\epsilon_1(k), \dots, \epsilon_n(k)], \quad (6.59)$$

where we assumed that our Hamiltonian $h(k)$ has n bands. We can assume that the eigenvalues $\epsilon_i(k)$ are sorted and $\epsilon_i(k) < 0$ for all filled bands and $\epsilon_i(k) > 0$ for all unfilled bands by shifting the Fermi level and multiplying by permutation matrices to sort the energy eigenvalues.

Then we can define, if we assume that we have M filled bands the following energy interpolation,

$$E_i(k, t) = \begin{cases} \epsilon_i(k)(1 - t) + \epsilon_G t & 1 \leq i \leq M \\ \epsilon_i(k)(1 - t) + \epsilon_E t & M + 1 \leq i \leq N \end{cases}, \quad (6.60)$$

which lifts all energies of filled bands to ϵ_G and all energies of the unfilled bands to ϵ_E . This interpolation of energies can be stored in a diagonal matrix, $D_0(k, t) = \text{diag}[E_1(k, t), \dots, E_N(k, t)]$.

This matrix stays “gapped” for all $t \in [0, 1]$, whenever we have $\epsilon_G < 0 < \epsilon_E$. Now we can define,

$$h(k, t) = U(k)D_0(k, t)U^\dagger(k) \quad (6.61)$$

and we get the interpolation we want.

Now we have shown the topological invariance of χ_2 and the fact that any band insulator can be connected to a flat two-band insulator, we will compute the quantity M_2 for such a flat band model.

First we want to list some properties of the flat two-band Hamiltonian and the associated Greens function G_0 . Since P_G and P_E are projectors, we need to have that $P_G + P_E = 1$ and thus $P_G = 1 - P_E$.

Furthermore since P_E and P_G are projectors, we have $P_E = P_E^2$ and $P_G = P_G^2$ and hence, $P_E P_G = P_E(1 - P_E) = P_E - P_E^2 = 0$.

For the calculation the following projector relations are useful,

$$P_E \partial_{k_i} P_G = -\partial_{k_i} P_E P_G = \partial_{k_i} P_G P_G \quad (6.62)$$

$$P_G \partial_{k_i} P_G = -P_G \partial_{k_i} P_E = P_E \partial_{k_i} P_G. \quad (6.63)$$

For the derivation of these equations observe that $0 = \partial_{k_i} 0 = \partial_{k_i}(P_E P_G)$ and as above $P_E = 1 - P_G$.

From this relations we derive further that

$$(P_E \partial_{k_i} P_G) P_E = (\partial_{k_i} P_G) P_G P_E = 0 \quad (6.64)$$

$$(P_G \partial_{k_i} P_G) P_G = (\partial_{k_i} P_G) P_E P_G = 0 \quad (6.65)$$

by applying the above projector relations and the $P_E P_G = P_G P_E = 0$. This observation will reduce the number of terms in the latter calculation.

For the Greens function $G_0 = [\omega + i\delta - h(k)]^{-1}$ associated to the Hamiltonian $h(k)$ the properties of the projectors imply that

$$\partial_\omega G_0^{-1} = 1 \text{ and } \partial_{k_i} G_0^{-1} = (\epsilon_E - \epsilon_G) \partial_{k_i} P_G(k). \quad (6.66)$$

Furthermore we notice that

$$G_0(\omega, k) = \frac{P_G(k)}{\omega + i\delta - \epsilon_G} + \frac{P_E(k)}{\omega + i\delta - \epsilon_E}, \quad (6.67)$$

which can be verified by calculating $G_0(\omega, k)G_0^{-1}(\omega, k)$ with projector relations. So our first step in the calculation of the response coefficient M_2 will be the elimination of the frequency in the trace expression. From the properties of the Levi - Civita tensor $\epsilon^{\mu\nu\rho\sigma\tau}$ we observe that we have 5 identical expressions and hence,

$$M_2 = -\frac{\pi^2}{3} \int \frac{d\omega d^4 k}{(2\pi)^5} \epsilon^{ijkl} \text{Tr} [G_0(G_0 \partial_{k_i} G_0^{-1}) \times (G_0 \partial_{k_j} G_0^{-1})(G_0 \partial_{k_k} G_0^{-1})(G_0 \partial_{k_l} G_0^{-1})]. \quad (6.68)$$

With the formula for the flat two-band Greens function, we can evaluate the $G_0 G_0$ term in the above expression using projector relations to give,

$$M_2 = -\frac{\pi^2}{3} \int \frac{d\omega d^4 k}{(2\pi)^5} \epsilon^{ijkl} \sum_{n=1}^2 \frac{1}{(\omega + i\delta - \epsilon_n)^2} \text{Tr} [(P_n \partial_{k_i} G_0^{-1})(G_0 \partial_{k_j} G_0^{-1})(G_0 \partial_{k_k} G_0^{-1})(G_0 \partial_{k_l} G_0^{-1})], \quad (6.69)$$

where we introduced the abbreviated notation $\epsilon_{G,E} = \epsilon_{1,2}$ and $P_{G,E} = P_{1,2}$. Now we can use (6.66) to expand this expression further, we then obtain a summation over 16 terms,

$$M_2 = -\frac{\pi^2}{3} \int \frac{d\omega d^4 k}{(2\pi)^5} \epsilon^{ijkl} \sum_{n,m,s,t=1}^2 \frac{(\epsilon_E - \epsilon_G)^4}{(\bar{\omega} - \epsilon_n)^2 (\bar{\omega} - \epsilon_m)(\bar{\omega} - \epsilon_s)(\bar{\omega} - \epsilon_t)} \times \text{Tr} [(P_n \partial_{k_i} P_G)(G_0 \partial_{k_j} P_G)(G_0 \partial_{k_k} P_G)(G_0 \partial_{k_l} P_G)], \quad (6.70)$$

6.6 Appendix

where we used the abbreviation $\bar{\omega} = \omega + i\delta$. However now we can use the projector relations (6.64) and (6.65) to observe that from the 16 terms only terms with $n \neq m, m \neq s, s \neq t$ are non - vanishing, we thus obtain the expression,

$$M_2 = -\frac{\pi^2}{3} \int \frac{d\omega d^4k}{(2\pi)^5} \epsilon^{ijkl} (\epsilon_E - \epsilon_G)^4 \left(\frac{\text{Tr} P_E(\partial_i P_G) P_E(\partial_j P_G) P_G(\partial_k P_G) P_E(\partial_l P_G)}{(\omega + i\delta - \epsilon_G)^3 (\omega + i\delta - \epsilon_E)^2} \right. \\ \left. + \frac{P_E(\partial_i P_G) P_G(\partial_j P_G) P_E(\partial_k P_G) P_G(\partial_l P_G)}{(\omega + i\delta - \epsilon_G)^2 (\omega + i\delta - \epsilon_E)^3} \right) \quad (6.71)$$

The next step is to perform the frequency integration. For this we use contour integration with a contour on the real line, which is closed in the lower half plane. Recall that the integration is over all frequencies, but the momenta integration region is the Brillouin zone.

Observe that there are no poles on the real line, because the denominator is deformed by $+i\delta$. Exchanging the terms in the trace with use of the projector identities, we arrive at

$$M_2 = \frac{1}{8\pi^2} \int d^4k \epsilon^{ijkl} \text{Tr} P_E(\partial_i P_G)(\partial_j P_G) P_E(\partial_k P_G)(\partial_l P_G). \quad (6.72)$$

The last step is to evaluate the Berry curvature $\text{Tr} f_{ij} f_{kl}$ for the flat - band Hamiltonian (6.58) and observing that this is equal to the above expression. Therefore $M_2 = C_2$.

BIBLIOGRAPHY

- [1] X.-L. Qi and S.-C. Zhang, *Topological insulators and superconductors*, Revues of Modern Physics **83**, 1057 (2011).
- [2] M. F. Golterman, K. Jansen, and D. B. Kaplan, *Chern-simons currents and chiral fermions on the lattice*, Phys.Lett. **B301**, 219 (1993), [hep-lat/9209003](#).
- [3] G. Dunne, *Aspects of chern-simons theory*, in *Aspects topologiques de la physique en basse dimension. Topological aspects of low dimensional systems*, edited by A. Comtet, T. Jolicur, S. Ouvry, and F. David (Springer Berlin Heidelberg, 1999), vol. 69 of *Les Houches - Ecole d'Ete de Physique Theorique*, pp. 177–263.
- [4] J. Schwinger, *On gauge invariance and vacuum polarization*, Phys. Rev. **82**, 664 (1951).
- [5] A. N. Redlich, *Parity violation and gauge noninvariance of the effective gauge field action in three dimensions*, Phys. Rev. D **29**, 2366 (1984).
- [6] Z. Wang, X.-L. Qi, and S.-C. Zhang, *Topological order parameters for interacting topological insulators*, Phys. Rev. Lett. **105**, 256803 (2010).
- [7] X.-L. Qi, T. L.Hughes, and S.-C. Zhang, *Topological field theory of time-reversal invariant insulators*, Physical Review B **78** (2008).
- [8] A. B. Bernevig and T. Hughes, *Topological Insulators and Topological Superconductors* (Princeton University Press, 2010).
- [9] L. Fu, C. L. Kane, and E. J. Mele, *Topological insulators in three dimensions*, Phys. Rev. Lett. **98**, 106803 (2007).
- [10] S. Weinberg, *The Quantum Theory of Fields, Volume 1: Foundations* (Cambridge University Press, 2010), 10th ed.

BIBLIOGRAPHY

CHAPTER 7

BCS THEORY OF SUPERCONDUCTIVITY

PAOLO MOLIGNINI
SUPERVISOR: ADRIEN BOUHON

First a review of standard BCS theory of superconductivity will be given, including the discussion of Cooper pairing mechanism and of mean field theory. In this context thermodynamic quantities of interest like the critical temperature T_C will be obtained. Subsequently an introduction to generalized BCS mean field theory will be presented, leading to a discussion of the Bogoliubov-de Gennes Hamiltonian. Finally, the most relevant results will be summarized and highlighted. The purpose of this report is to illustrate and summarize the topics discussed during my talk as part of the theoretical proseminar titled “Topological insulators and topological superconductors”, which was organized by Prof. Gianni Blatter at the Federal Institute of Technology (ETH) in Zurich during the spring semester 2014.

7.1 OUTLINE

This report is structured in four sections. The first section serves as an introduction in the theme of superconductors. Their main macroscopic properties will be presented and a connection to microscopic BCS theory will be made. This latter theory will be more thoroughly discussed in section two: the concept of Cooper pairs will be introduced and possible mechanisms leading to their formation will be analyzed. After that, the mathematical formalism of mean field

7.2 Introduction

theory for superconductivity will be presented for the simplest case of s-wave spin singlet pairing. In the framework of mean field theory the consistency with the Cooper pair formulation will be shown and to that end some macroscopic quantities will be derived. In section three the mean field approach will be generalized to system with arbitrary spin configurations, essentially following the same path already traced in section two. Finally, the discussion in section four will summarize and link the main results previously obtained.

7.2 INTRODUCTION

Superconductivity is a new state of matter occurring in certain materials when they are cooled down below a critical temperature T_c . Upon reaching this critical value the electrical resistivity ρ drops to an unmeasurably small value (as graphically shown in figure 7.1) and currents start to flow without dissipation: the material begins to superconduct. Since in the majority of cases the value of the critical temperature is of the order of a few Kelvin, this peculiar phenomenon was discovered only in 1911 by H. K. Onnes while he was working at a cryogenics experiment involving mercury cooled down by liquid helium[1]. In his experiment Onnes observed that upon lowering the temperature below 4.2 K, the resistance of the mercury sample suddenly disappeared. In the following years similar experiments were conducted with other elements and many were found to superconduct at temperatures around the critical temperature of mercury. In 1941 NbN was found to superconduct below 16 K[2] and subsequently many other superconducting alloys were discovered[3]. To this day the majority of transition metals, many other metallic and non-metallic elements and dozens of alloys are known to present a superconducting phase[4].

In 1933 the understanding of superconductivity was enriched with the discovery by Meissner and Ochsenfeld that magnetic fields are spontaneously ejected from the bulk of a material in its superconducting phase[6]. This effect is nowadays called *Meissner-Ochsenfeld effect* - honoring the scientists who first observed it - and forms the basis for superconducting levitation[7]. A graphic depiction of this phenomenon is shown in figure 7.2.

The existence of the Meissner-Ochsenfeld effect allows a clear distinction between a superconductor and an ideal conductor with $\rho = 0$ below a critical temperature T_c and undoubtedly characterizes superconductivity as a thermodynamic change of state, *i.e.* a phase transition. As figure 7.3 points out, when an ideal conductor is cooled down below critical temperature, and subsequently an external magnetic

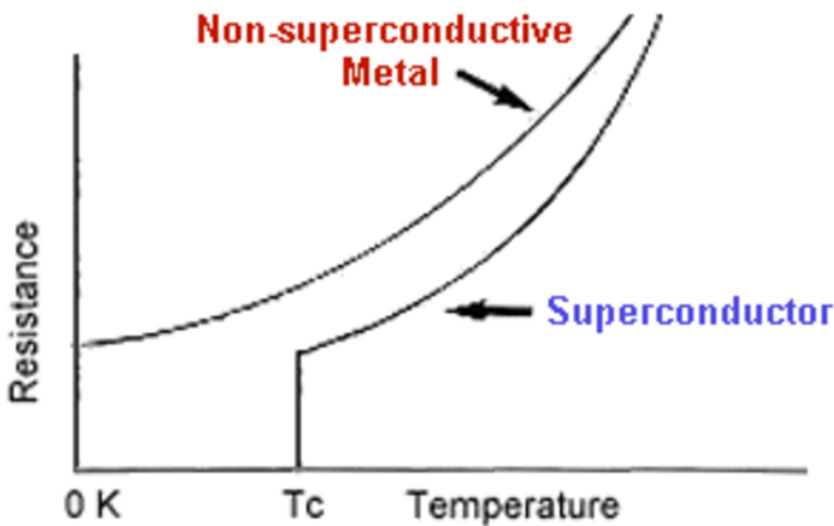


Figure 7.1: Behavior of resistance in a superconductor as a function of temperature. Ref. [5]

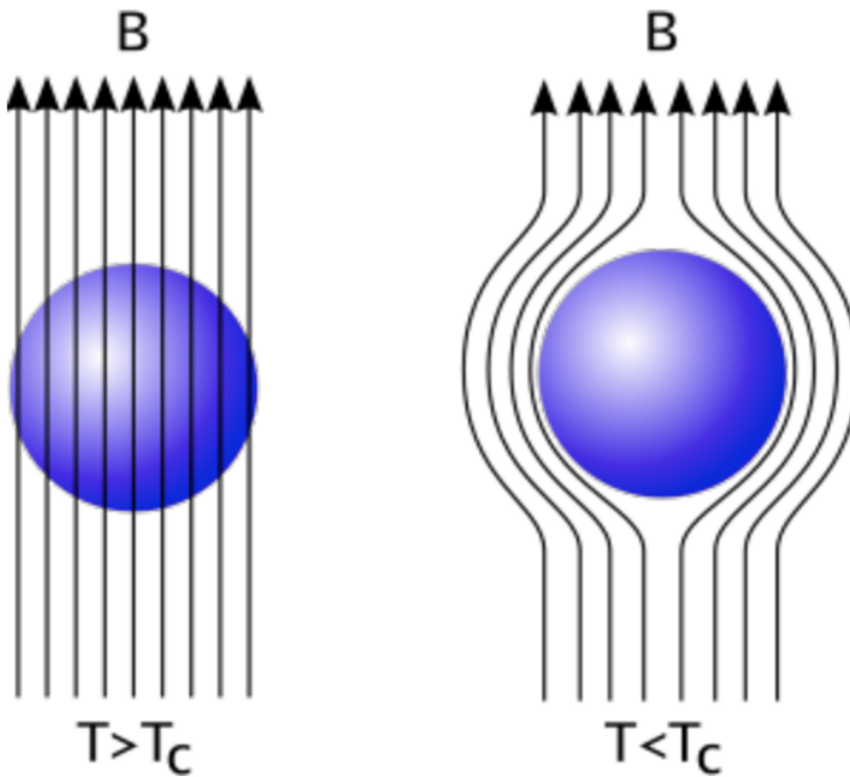


Figure 7.2: Schematic depiction of the Meissner-Ochsenfeld effect in a superconductor. Image taken from Wikimedia Commons.

7.2 Introduction

field \mathbf{B}_{ext} is turned on, the resistance-free bulk prevent the magnetic field lines to penetrate in the material. When the magnetic field is turned off, the bulk remains field-free. On the other hand, if the sample is first subjected to the external field, and only later cooled down below T_c , the outcome by turning off the magnetic field is different: a vanishing resistance implies via Faraday's law that the magnetic flux through the surface of the sample can not change, so that the internal field is maintained even after lifting the external one. As opposed to the two possible outcomes for an ideal conductor, the final state of a superconductor does not depend on the succession of the events and the magnetic field line are ejected from the bulk in both cases. The independence of the path by which the final state is reached characterizes the crossover between normal and superconducting state as a phase transition. In this sense, the superconducting phase can be viewed as a perfect diamagnetic phase with $\mathbf{M} = -\mathbf{H}_{ext}$.

By 1935 the phenomenology of the Meissner-Ochsenfeld effect could already be explained by the London brothers through a modification of the Maxwell equations of electrodynamics[8]. By manipulating Faraday's and Ampère's laws they were able to obtain two wave equations of the magnetic field and current, and whose solutions decay exponentially with a decay constant Λ_L , called *London penetration depth*. The phenomenological London theory was therefore able to reproduce the main features of the Meissner-Ochsenfeld effect, in particular the absence of magnetic fields in the interior of the superconductor. Nevertheless, a microscopic theory of superconductivity was still missing.

It took scientists another twenty years to come up with a microscopic theory of superconductivity that could reproduce the features observed experimentally. In 1956 L. N. Cooper had already shown that the Fermi surface of an electron gas at zero temperature is unstable under even the smallest attractive interaction and tends to spontaneously form *Cooper pairs*, *i.e.* pairs of bound electrons which behave like bosons and can carry the quantized supercurrent measured in tunneling experiments[9, 10]. In 1957 Bardeen, Cooper and Schrieffer proposed a quantum mechanical theory of superconductivity based on electron-phonon interaction using a variational method applied to the ground state of the Cooper pairs. In 1958 N.N. Bogoliubov extended the theory to include a derivation of the BCS wave function through mean field theory and canonical transformation applied to the Hamiltonian[11]. This exhaustive theoretical framework is known today as *conventional BCS theory of superconductivity*.

Up until the beginning of the Seventies, BCS theory was only applied to s-wave pairing Cooper pairs, *i.e.* with vanishing ($l=0$) relative orbital angular momentum and spin singlet configuration. In 1971, with the discovery of superfluidity in ^3He , the electron pairing mechanism underlying BCS theory was then extended

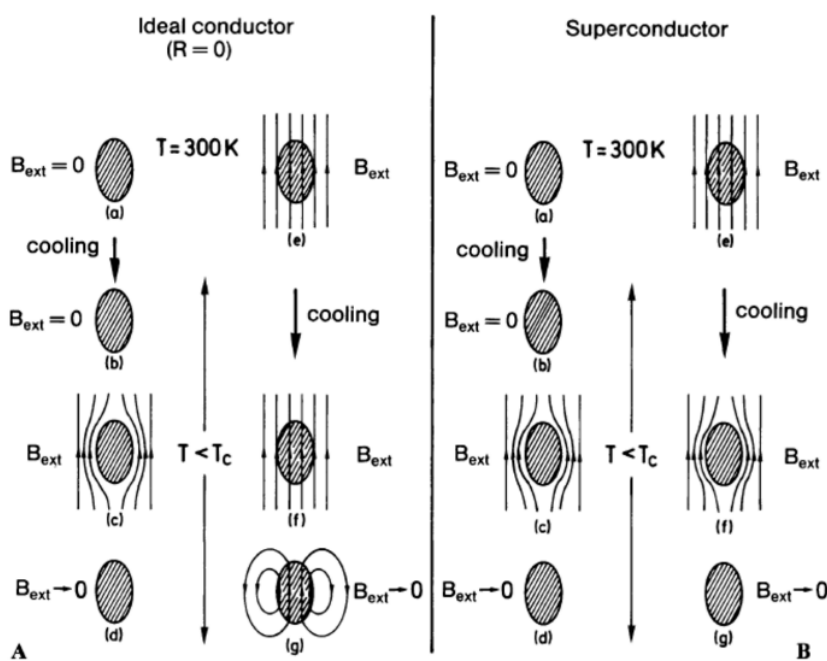


Figure 7.3: Difference in magnetic behavior under T_c between an ideal conductor and a superconductor. For an ideal conductor with zero resistance below T_c , Faraday's law leads to two possible outcomes depending on the presence or absence of the external field. In a superconductor the final state is independent of the path chosen to achieve it, which is a characterizing feature of a phase transition. Image taken from Ref. [4]

7.2 Introduction

to describe other pairing mechanisms with lower symmetry, such as Cooper pairs in spin triplet configuration (p-wave pairing)[12]. Another example of the application of this *unconventional BCS theory* revolves around a new class of high temperature superconductors (HTSC) discovered a decade later in ceramic materials. In 1986, while working at the IBM Research Facilities in Rüschlikon (CH), J. G. Bednorz and K. A. Müller discovered that a barium-doped compound of lanthanum and copper oxide (LaBaCuO) exhibited superconducting properties at a temperature around 35 K[13]. Within a decade a whole new range of materials with even higher transition temperature were discovered[?]. To this day, the exact microscopic mechanism that leads to the peculiar properties of HTSC is still under debate, albeit several theoretical[14, 15] and experimental[16, 17, 18, 19] works point to an orbital d-wave pairing of Cooper pairs.

Following the structure developed by M. Tinkham in chapter three of Ref. [20], this report is going to focus on the theoretical framework developed by Bardeen, Cooper and Schrieffer to describe superconductivity due to Cooper pairing of electrons in s-wave and spin singlet state. In a second step the BCS theory will be generalized to other spin configurations as shown in the work of M. Sigrist (Ref. [?]). First of all, a simple model of a Fermi sea with two additional electrons will be discussed: the introduction of an attractive potential between the electrons will entail the condensation of Cooper pairs shown in Ref. [9]. Furthermore, the possible origin of the interaction potential will be briefly discussed. After that, starting from the pair-interaction Hamiltonian, the mean field theory of BCS superconductivity will be developed. To obtain an explicit form for the gapped excitation spectrum, a diagonalization procedure known as Bogoliubov transformation will be necessary. This approach will naturally lead to the definition of a self-consistency gap equation, which will be solved in the limit of a vanishing gap to obtain a closed formula for the critical temperature. The gap equation will be also considered in the zero temperature limit to derive an explicit form for the gap, which will turn out to be linearly dependent on the critical temperature. Subsequently, the whole mean field approach applied to s-wave pairing will be revisited for arbitrary spin configurations. In particular, the Bogoliubov-de Gennes form for the electronic Hamiltonian will be derived and various examples of gap functions will be presented. In the final discussion, the salient results developed in the previous sections will be summarized and connected to the phenomenology of superconductivity briefly mentioned in this introduction.

7.3 STANDARD BCS THEORY

In this section the conventional BCS theory for superconductivity will be presented, following the exposition given in Ref. [20]. The main idea behind its theoretical formulation lies in the fact that an attractive interactions between the electrons can induce - at low enough temperatures - an energetically favorable formation of two-particle bound states, called Cooper pairs. Since Cooper pairs consists of two fermions, they obey Bose-Einstein statistics and can be accumulated in arbitrary number in their ground state. In the superconducting state, Cooper pairs are the charge carriers which are responsible for the transport of the electric current. This statement can be proved by means of experiments involving the quantization of the magnetic flux, which is measured to be an integer multiple of $\Phi_0 = \frac{h}{2e}$.

7.3.1 COOPER PAIRS

The assumptions made by Cooper in his approach are quite simple[9]. Two electrons are added to a Fermi sea at zero temperature (see figure 7.4). At $T = 0$ the Fermi surface is a very sharp defined sphere with fully occupied states below the Fermi vector k_F and because of the Pauli exclusion principle, the two extra free electrons can only occupy momentum states corresponding to energies with $E_{free} > E_F$ each. Apart from being subjected to the Pauli exclusion principle, an additional requirement for the two electrons is that they also interact with each other - but not with the rest of the Fermi sea - through a potential V .

A natural question is if this configuration could allow a bound state of the electrons, *i.e.* a state whose energy is smaller than twice the energy of the free particles: $E_{bound} < 2E_F$. To investigate this possibility, the lowest energy state with zero momentum is considered. Its orbital wave function can then be expressed as a Fourier series in k -space:

$$\psi_0(\vec{r}_1, \vec{r}_2) = \sum_{\vec{k}} g_{\vec{k}} e^{i\vec{k}\cdot\vec{r}_1} e^{-i\vec{k}\cdot\vec{r}_2} \quad (7.1)$$

Here $g_{\vec{k}}$ are the Fourier coefficients of the expansion. Pauli exclusion principle constrains the wave function to be totally antisymmetric, such that two cases are possible:

$$\begin{cases} \psi_{0,S} = \sum_{k>k_F} g_{\vec{k}} \cos(\vec{k} \cdot (\vec{r}_1 - \vec{r}_2)) & \text{for spin singlet} \\ \psi_{0,T} = \sum_{k>k_F} g_{\vec{k}} \sin(\vec{k} \cdot (\vec{r}_1 - \vec{r}_2)) & \text{for spin triplet} \end{cases} \quad (7.2)$$

Because of the cosinusoidal dependence of the orbital part, the spin singlet state is expected to have a higher probability for the two electrons to be found close

7.3 Standard BCS Theory

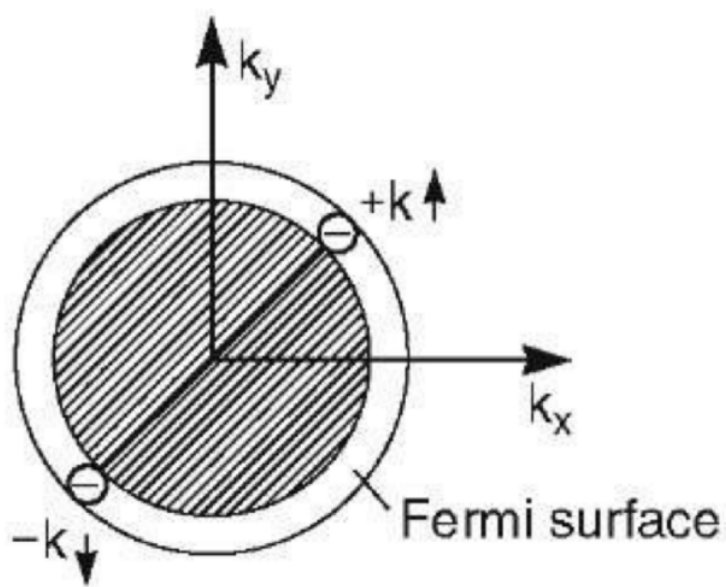


Figure 7.4: Illustration of the problem proposed by Cooper: two electrons with $E > E_F$ are added above the Fermi surface at $T = 0$. The energy of their possible bound state is investigated. Online image taken from <http://what-when-how.com>.

to each other and their energy will then be smaller than for the spin triplet case.

The rest of the section will therefore focus on spin singlet pairing only.

The Schrödinger equation for the two-electron problem has the form[21]:

$$-\frac{\hbar^2}{2m} (\nabla_1^2 + \nabla_2^2) \psi_0(\vec{r}_1, \vec{r}_2) + V(\vec{r}_1 - \vec{r}_2) \psi_0(\vec{r}_1, \vec{r}_2) = E \psi_0(\vec{r}_1, \vec{r}_2) \quad (7.3)$$

and can be transformed to the c.o.m. system (note $E = \Delta + 2E_F$):

$$\left[-\frac{\hbar^2}{2\mu} \nabla^2 + V(r) \right] \psi_0(r) = E \psi_0(r) \quad \text{with } \vec{r} \equiv \vec{r}_1 - \vec{r}_2 \quad (7.4)$$

Inserting the ansatz (7.1) in (7.4), multiplying through by $e^{i\vec{k}' \cdot \vec{r}}$ and integrating over the real space leads to a condition on the coefficients $g_{\vec{k}}$:

$$(E - 2\epsilon_{\vec{k}}) g_{\vec{k}} = \sum_{k' > k_F} V_{\vec{k}\vec{k}'} g_{\vec{k}'} \quad (7.5)$$

where $\epsilon_{\vec{k}} = \frac{\hbar^2 \vec{k}^2}{2m}$ is the free electron energy and $V_{\vec{k}\vec{k}'} = \frac{1}{\Omega} \int d\vec{r} V(\vec{r}) e^{i(\vec{k}' - \vec{k}) \cdot \vec{r}}$ is the matrix element of the interacting potential in k -space. Equation (7.5) determines the possible set of coefficients for the bound state: if a set $\{g_{\vec{k}}\}$ with energy $E < 2E_F$ exists, then a bound state can be found.

Since equation (7.5) is not in a closed form, some extra knowledge about the potential is required to extract the information contained in it. Cooper's approximation[9] consisted in defining an attractive potential of the following type ($V > 0$):

$$V_{\vec{k}\vec{k}'} = \begin{cases} -V & \text{for } |\epsilon_{\vec{k}} - E_F| < \hbar\omega_c \\ 0 & \text{for } |\epsilon_{\vec{k}} - E_F| > \hbar\omega_c \end{cases} \quad (7.6)$$

This approximation relies on the fact that the underlying mechanism which mediates the interaction is active only in a relatively small shell around the Fermi surface up to a certain cutoff frequency ω_c . For the conventional s-pairing considered here, the mediating interaction will turn out to be phonon exchange between the electrons, which exists only up to the characteristic Debye frequency ω_D of the material. Because in this approximation $V_{\vec{k}\vec{k}'}$ becomes k -independent, it can be taken out of the sum on the right hand side of equation (7.5):

$$g_{\vec{k}} = \frac{V}{2\epsilon_{\vec{k}} - E} \sum_{\vec{k}' > k_F} g_{\vec{k}'} \quad (7.7)$$

Summation over k on both sides leads to cancellation of the $g_{\vec{k}}$ dependence (because the dummy index plays no role in the sum):

$$\frac{1}{V} = \sum_{k > k_F} \frac{1}{2\epsilon_{\vec{k}} - E} \quad (7.8)$$

7.3 Standard BCS Theory

Assuming a very large number of k -states, the summation can be replaced by an integral in the continuum limit:

$$\frac{1}{V} = \sum_{k>k_F} \delta(\epsilon - \epsilon_{\vec{k}}) \frac{1}{2\epsilon - E} \quad (7.9)$$

$$\iff \frac{1}{V} = \int_{E_F}^{E_F + \hbar\omega_c} N(\epsilon) \frac{d\epsilon}{2\epsilon - E} \quad (7.10)$$

$$\iff \frac{1}{V} = N(E_F) \int_{E_F}^{E_F + \hbar\omega_c} \frac{d\epsilon}{2\epsilon - E} \quad (7.11)$$

$$\implies \frac{1}{V} = \frac{1}{2} N(E_F) \ln \left(\frac{2E_F - E + 2\hbar\omega_c}{2E_F - E} \right) \quad (7.12)$$

where in the third line the approximation $N(\epsilon) \approx N(E_F)$ due to the integration boundaries was made. This expression can be rearranged to obtain an explicit form for E :

$$E = 2E_F - 2\hbar\omega_c \frac{e^{-2/N(E_F)V}}{1 - e^{-2/N(E_F)V}} \quad (7.13)$$

In most superconductors $N(E_F)V \lesssim 0.3$ and the exponential in the denominator of equation (7.13) can be neglected. This approximation is known as *weak coupling approximation*, because it assumes a small value of V compared to the (usually very high) density of states at the Fermi surface $N(E_F)$ for metals. Under these assumptions, the energy of the bound state is:

$$E = 2E_F - 2\hbar\omega_c e^{-2/N(E_F)V} < 2E_F \quad (7.14)$$

It should be noted that the second term on the r.h.s. of equation (7.14) is strictly negative for any choice of the attractive potential $-V$. For any arbitrary small potential V , there will always be a two-electron bound state - named Cooper pair - possessing an energy smaller than twice the energy of the free electrons taken separately. In this sense, the Fermi sea presents an instability with respect to any attractive potential $-V$. The mathematical origin of this instability lies in the divergence of the integrand $\frac{1}{2\epsilon - E}$. The integral can be rewritten as:

$$\frac{1}{N(E_F)V} = \int_0^{\hbar\omega_c} \frac{d\xi}{2\xi + (2E_F - E)} \quad (7.15)$$

By tuning E from 0 to $2E_F$, the value of the integral will increase but it will always be compensated by a decrease of the magnitude of the interaction potential V . Even upon reaching infinity at $E = 2E_F$ on the r.h.s., the equation will still hold by setting $V = 0$ on the l.h.s. No matter how small the attractive potential is, the formation of Cooper pairs will always be favorable.

BCS THEORY OF SUPERCONDUCTIVITY [PAOLO MOLIGNINI]

As a side note, it is interesting to gauge the distance separating the two electrons forming the Cooper pair. In order to do that, the uncertainty relation $\Delta r \Delta p \sim \hbar$ can be of use. By solving with respect to the distance and inserting all the relevant dimensionalities of the problem, one obtains:

$$\Delta r \sim \hbar v_F / \Delta E \sim \hbar v_F / k_B T_c \sim \frac{10^{-16} \text{ eV} \cdot \text{s}}{1 \text{ meV}} \frac{10^5 \text{ ms}^{-1}}{\text{eV}} \sim 1000 \text{ \AA} \quad (7.16)$$

The distance separating the electrons is therefore three orders of magnitude bigger than the average lattice spacing in a crystalline structure. Clearly, there must be an underlying mediation mechanism for the attraction between electrons, because two such distant particles can not directly interact with each other in a material. As the next subsection will show, this mediating interaction will turn out to be electron-phonon coupling.

7.3.2 ATTRACTIVE POTENTIALS

While Cooper's approximation (eq. (7.10)) explicitly required a short range attractive interaction, it did not make any assumptions on its origins. A natural question arises whether the ubiquitous Coulomb repulsion could somehow lead to an effective attractive force between electronic pairs at long range, thereby allowing condensation of Cooper pairs. In materials, the Coulomb interaction takes the form

$$V(\vec{r}) = \frac{e^2}{\epsilon r} \quad (7.17)$$

where $\epsilon(\vec{q}, \omega)$ is known as the *dielectric function* and represents the screening effect due to the electrons in a solid[22]. In the Thomas-Fermi approximation (static limit $\omega \rightarrow 0$) the dielectric function can be written as $\epsilon(\vec{q}) = 1 + \frac{k_s^2}{q^2}$, with the screening length $\frac{1}{k_s} \approx 1 \text{ \AA}$. Therefore, plugging equation (7.17) into the

7.3 Standard BCS Theory

definition of the reciprocal space interaction $V_{\vec{k}\vec{k}'}$, one obtains:

$$V_{\vec{k}\vec{k}'} = \Omega^{-1} \int d^3r V(\vec{r}) e^{i(\vec{k} - \vec{k}') \cdot \vec{r}} = \frac{e^2}{\Omega} \int d^3r \frac{e^{i\vec{q} \cdot \vec{r}}}{\epsilon r} = \frac{e^2}{\Omega} \int d^3r \frac{q^2}{q^2 + k_s^2} \frac{e^{i\vec{q} \cdot \vec{r}}}{r} \quad (7.18)$$

$$= \frac{e^2}{\Omega} \frac{q^2}{q^2 + k_s^2} \int dr r^2 \int_0^{2\pi} d\phi \int_{-1}^1 d(\cos \theta) \frac{e^{iqr \cos \theta}}{r} \quad (7.19)$$

$$= \frac{2\pi e^2}{\Omega} \frac{q^2}{q^2 + k_s^2} \int dr r^2 \left[\frac{e^{iqr} - e^{-iqr}}{iqr} \right] \quad (7.20)$$

$$= \frac{4\pi e^2}{\Omega} \frac{1}{q^2 + k_s^2} \int dr [q \sin(qr)] \quad (7.21)$$

$$= \frac{4\pi e^2}{\Omega(q^2 + k_s^2)} [-\cos(qr)]_0^{r_{max}} \quad (7.22)$$

$$= \frac{4\pi e^2}{\Omega(q^2 + k_s^2)} > 0 \quad (7.23)$$

Clearly, the matrix element $V(\vec{q}) = V_{\vec{k}\vec{k}'} = \frac{4\pi e^2}{\Omega(q^2 + k_s^2)}$ is positive, since it contains only positive constants and squared quantities; it does not fulfill the requirements of Cooper's approximation and therefore no attractive interaction would result from a purely Coulombic potential between electrons.

Although the calculation above does not work for the Coulomb potential, other mediated interactions do indeed return a negative matrix element. As an example, the electron-phonon coupling will be discussed next. In the jellium model¹ the potential receives an additional phonon contribution:

$$V(\vec{q}, \omega) = \frac{4\pi e^2}{q^2 + k_s^2} \left(1 + \frac{\omega_q^2}{\omega^2 - \omega_q^2} \right) \quad (7.24)$$

where ω_q is the phonon frequency and $\hbar\omega \equiv \xi_{\vec{k}} - \xi_{\vec{k}'}$ gives the energy difference between the two electrons expressed as a frequency. From equation (7.24) it is evident that the interaction is attractive whenever the term in brackets becomes negative, *i.e.* if $\omega_q > \omega$. Luckily enough, at low energies the acoustic branch of the phonon dispersion relation (shown in figure 7.5) always provides modes for which this condition is fulfilled.

¹The *jellium* or *uniform electron gas model* is a simplification of the internal structure of a solid, in which the interacting electrons are described by a homogeneous electronic density $\rho(\vec{r})$ embedded in a background of uniformly distributed positive charges $n(\vec{r})$. This model allows to focus on the intrinsic quantum mechanical properties of the electron gas without taking into account lattice effects.[23]

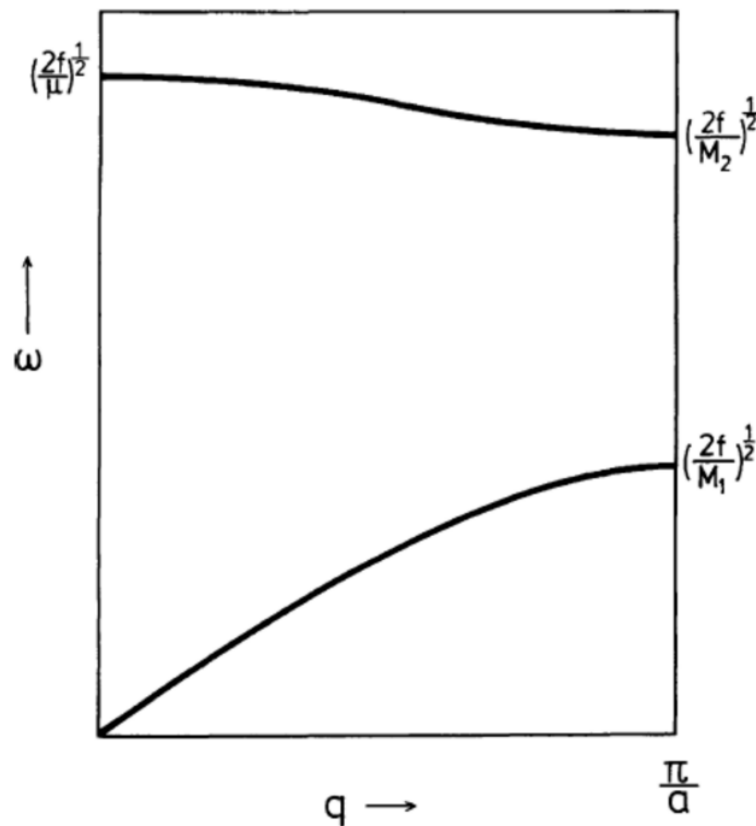


Figure 7.5: One dimensional phonon dispersion curves $\omega(\vec{q})$ in the model of a two-atom chain with different masses M_1 and M_2 . The upper line represents optic phonons (which exist only for $M_1 \neq M_2$). The lower line corresponds to acoustic phonons, which are relevant as mediators for the attractive electron interaction necessary for Cooper pair condensation. Image taken from Ref. [4].

7.3 Standard BCS Theory

In other words, for low enough energy difference $\hbar\omega$, the interaction between the electrons can be mediated by an exchange of phonons (as depicted in figure 7.6). Since in a solid the vibrational modes are disrupted at frequencies higher than the Debye frequency ω_D , this also represents the maximal difference in energy that the two electrons can have to condense into Cooper pairs. Retrospectively, this is the reason why Cooper chose to limit the range of the interaction V to a tiny shell around the Fermi surface. The cutoff frequency chosen in equation (7.6) corresponds to the Debye frequency of the material: for energy differences higher than the cutoff energy $\hbar\omega_D$, there is simply no possible mediation by phonons and the electrons cannot attract each other. A simple way to picture the process of interaction between the electrons and the lattice is given in figure 7.7 and was already discussed by Fröhlich in 1950[24]. On his way through the material, the electron attracts the positively charged ion cores in the immediate neighborhood of its path. Because of Coulomb attraction the lattice planes tend to come slightly closer together. If another electron happens to cross this lattice deformation it can become attracted by the positively charged ion cores, thereby leading to an effective attractive coupling with the first electron. Because of the huge difference in mass between the light and fast electrons and the heavy and slow ions, the accumulation of positive charges is retarded with respect to the passage of the first electron. Therefore, by the time the second electron approaches the positive trail, the first electron associated with it is already far away and Coulomb repulsion between the two particles becomes negligible. This qualitative picture also explains why the distance between electrons belonging to the same Cooper pair is of the order of 10^3 Å.

To conclude this brief excursion in the origin of the electron coupling, it should be noted that other mechanisms of interaction not involving phonons are possible, such as spin-fluctuation exchange[?]. These more exotic interactions can lead to electron pairing with lower symmetry, for instance p-wave (triplet state), d-wave, etc.

7.3.3 MEAN FIELD THEORY OF SUPERCONDUCTIVITY

In section 1 a simple model of two interacting electrons added to the Fermi sea was enough to derive some features of superconductivity, namely the existence of a two-particle bound state with energy $E < 2E_F$, denominated Cooper pair. In this section the discussion will be further developed in the language of second quantization in order to dig deeper in the properties of the superconducting state. The starting point of this analysis is the N-particle Hamiltonian in momentum

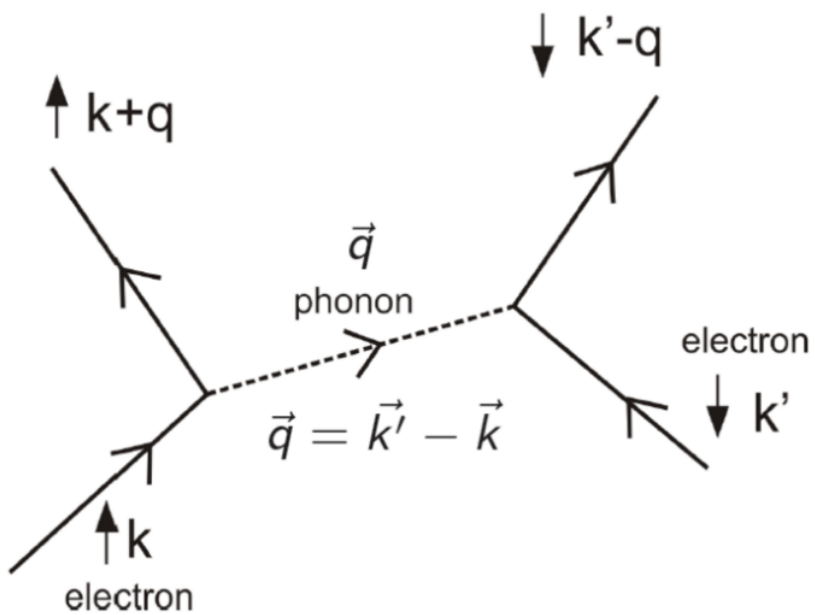


Figure 7.6: Feynman diagram of elastic electron-electron scattering involving the exchange of a phonon. Note that this mechanism conserves both momentum and energy. In particular energy conservation $\epsilon_{\vec{k}} + \epsilon_{\vec{k}'} = \epsilon_{\vec{k}+\vec{q}} + \epsilon_{\vec{k}'-\vec{q}}$ implies $\vec{q} = \vec{k} - \vec{k}'$. Image taken from Ref. [25].

7.3 Standard BCS Theory

space:

$$\mathcal{H} = \sum_{\vec{k}, s} \xi_{\vec{k}} c_{\vec{k}s}^\dagger c_{\vec{k}s} + \sum_{\vec{k}, \vec{k}', \vec{q}} V_{\vec{k}\vec{k}'} c_{\vec{k}+\vec{q}, \uparrow}^\dagger c_{\vec{k}'-\vec{q}, \downarrow}^\dagger c_{\vec{k}', \downarrow} c_{\vec{k}, \uparrow} \quad (7.25)$$

This Hamiltonian is the quantum mechanical operator associated with the energy of the system and is composed of a kinetic part described by the dispersion relation for the band structure (*e.g.* for a parabolic band $\xi_{\vec{k}} = \frac{\hbar^2}{2m}(\vec{k}^2 - k_F^2)$) and an interaction part involving a scattering matrix element $V_{\vec{k}\vec{k}'}$ for an attractive contact interaction between two particle (*e.g.* $V_{\vec{k}\vec{k}'} = \int d^3r V(\vec{r}) e^{i\vec{q}\cdot\vec{r}} = g$ for $V(\vec{r} - \vec{r}') = g\delta(\vec{r} - \vec{r}')$). In the first sum the index s refers to the possible spin orientations of the electrons. Recalling the property of Cooper pairs having vanishing total momentum, the Hamiltonian can be rearranged as

$$\mathcal{H} = \sum_{\vec{k}, s} \xi_{\vec{k}} c_{\vec{k}s}^\dagger c_{\vec{k}s} + \sum_{\vec{k}, \vec{k}'} V_{\vec{k}\vec{k}'} c_{\vec{k}, \uparrow}^\dagger c_{-\vec{k}, \downarrow}^\dagger c_{-\vec{k}', \downarrow} c_{\vec{k}', \uparrow} \quad (7.26)$$

In order to extract information - such as the eigenvalue spectrum - from this Hamiltonian, the ground state of the Cooper pairs has to be determined. In second quantization, the most general N -particle wave function of Cooper pairs takes the following form, which implements the Slater determinant form for fermions:

$$|\psi_N\rangle = \sum g(\vec{k}_i, \dots, \vec{k}_l) c_{\vec{k}_i, \uparrow}^\dagger c_{-\vec{k}_i, \downarrow}^\dagger \cdots c_{\vec{k}_l, \uparrow}^\dagger c_{-\vec{k}_l, \downarrow}^\dagger |0\rangle. \quad (7.27)$$

The sum is taken over all momenta \vec{k} of the band with M values, while \vec{k}_i and \vec{k}_l correspond to the first and last of these (occupied) values. The state $|0\rangle$ represents the vacuum with no particles present. The weighting factor $g(\vec{k}_i, \dots, \vec{k}_l)$ is the generalization of the coefficient present in the ansatz of equation (7.1). Since there are $\frac{M!}{(M-\frac{N}{2})!(\frac{N}{2})!} \approx 10^{10^{20}}$ ways of picking the $N/2$ electron pairs, the constraint of a fixed number of particles can be relaxed and the calculations can be performed in the grand canonical ensemble without the danger of incurring in big errors. In this approximation Bardeen, Cooper and Schrieffer showed that the ground state can be expressed as a phase-coherent superposition of Bloch states $\{|\vec{k} \uparrow\rangle \otimes |-\vec{k} \downarrow\rangle\}$:

$$|\psi_G\rangle = \prod_{\vec{k}=\vec{k}_1 \dots \vec{k}_M} (u_{\vec{k}} + v_{\vec{k}} c_{\vec{k}, \uparrow}^\dagger c_{-\vec{k}, \downarrow}^\dagger) |0\rangle \quad (7.28)$$

where $v_{\vec{k}}$ is the probability amplitude for an occupied pair $(\vec{k} \uparrow, -\vec{k} \downarrow)$ and $u_{\vec{k}}$ the corresponding probability amplitude for an empty pair of momenta, such that $|u_{\vec{k}}|^2 + |v_{\vec{k}}|^2 = 1$ must hold.

Given that the BCS ground state is a coherent state, expectation values of quantities involving only annihilation or only creation operators can be non-zero. For

instance:

$$b_{\vec{k}} \equiv \langle c_{-\vec{k}\downarrow} c_{\vec{k}\uparrow} \rangle \neq 0 \quad (7.29)$$

Because of this, the operators $c_{-\vec{k}\downarrow} c_{\vec{k}\uparrow}$ and $c_{\vec{k},\uparrow}^\dagger c_{-\vec{k},\downarrow}^\dagger$ can be substituted by their mean-field averaged counterpart. In other words, it is possible to express $c_{-\vec{k}\downarrow} c_{\vec{k}\uparrow} = b_{\vec{k}} + \delta b_{\vec{k}}$, with the small fluctuations $\delta b_{\vec{k}} = c_{-\vec{k}\downarrow} c_{\vec{k}\uparrow} - b_{\vec{k}}$. The same consideration applies of course to $c_{\vec{k},\uparrow}^\dagger c_{-\vec{k},\downarrow}^\dagger$ as well. Given the huge number of particles in the system, the correlation between fluctuations given by quartic terms $\delta b_{\vec{k}} \delta b_{\vec{k}'}$ can be neglected. With this mean-field approach the Hamiltonian then becomes:

$$\mathcal{H} = \sum_{\vec{k}, s} \xi_{\vec{k}} c_{\vec{k}s}^\dagger c_{\vec{k}s} + \sum_{\vec{k}, \vec{k}'} V_{\vec{k}\vec{k}'} c_{\vec{k},\uparrow}^\dagger c_{-\vec{k},\downarrow}^\dagger c_{-\vec{k}',\downarrow} c_{\vec{k}',\uparrow} \quad (7.30)$$

$$= \sum_{\vec{k}, s} \xi_{\vec{k}} c_{\vec{k}s}^\dagger c_{\vec{k}s} + \sum_{\vec{k}, \vec{k}'} V_{\vec{k}\vec{k}'} (b_{\vec{k}}^* + \delta b_{\vec{k}}^*) (b_{\vec{k}'} + \delta b_{\vec{k}'}) \quad (7.31)$$

$$= \sum_{\vec{k}, s} \xi_{\vec{k}} c_{\vec{k}s}^\dagger c_{\vec{k}s} + \sum_{\vec{k}, \vec{k}'} V_{\vec{k}\vec{k}'} (b_{\vec{k}}^* b_{\vec{k}'} + b_{\vec{k}}^* \delta b_{\vec{k}'} + b_{\vec{k}'} \delta b_{\vec{k}}^* + \underline{\delta b_{\vec{k}}^* \delta b_{\vec{k}'}}) \quad (7.32)$$

$$= \sum_{\vec{k}, s} \xi_{\vec{k}} c_{\vec{k}s}^\dagger c_{\vec{k}s} + \sum_{\vec{k}, \vec{k}'} V_{\vec{k}\vec{k}'} (b_{\vec{k}}^* b_{\vec{k}'} + b_{\vec{k}}^* c_{-\vec{k}'\downarrow} c_{\vec{k}'\uparrow} - b_{\vec{k}}^* b_{\vec{k}'} + b_{\vec{k}'} c_{\vec{k},\uparrow}^\dagger c_{-\vec{k},\downarrow}^\dagger - b_{\vec{k}'} b_{\vec{k}}^*) \quad (7.33)$$

$$= \sum_{\vec{k}, s} \xi_{\vec{k}} c_{\vec{k}s}^\dagger c_{\vec{k}s} + \sum_{\vec{k}, \vec{k}'} V_{\vec{k}\vec{k}'} (b_{\vec{k}'} c_{\vec{k},\uparrow}^\dagger c_{-\vec{k},\downarrow}^\dagger + c_{-\vec{k}',\downarrow} c_{\vec{k}',\uparrow} b_{\vec{k}}^* - b_{\vec{k}}^* b_{\vec{k}'}) \quad (7.34)$$

$$= \sum_{\vec{k}, s} \xi_{\vec{k}} c_{\vec{k}s}^\dagger c_{\vec{k}s} - \sum_{\vec{k}} (\Delta_{\vec{k}}^* c_{-\vec{k},\downarrow} c_{\vec{k},\uparrow} + \Delta_{\vec{k}} c_{\vec{k},\uparrow}^\dagger c_{-\vec{k},\downarrow}^\dagger - \Delta_{\vec{k}} b_{\vec{k}}^*) = \mathcal{H}_{MF} \quad (7.35)$$

where the interaction $V_{\vec{k}\vec{k}'}$ was assimilated in the *gap function* of the energy spectrum $\Delta_{\vec{k}}$:

$$\Delta_{\vec{k}} = - \sum_{\vec{k}'} V_{\vec{k}\vec{k}'} b_{\vec{k}'} \quad (7.36)$$

It should be noted that the approximation made in the third line (discarding the quartic term) has created a Hamiltonian \mathcal{H}_{MF} which does not conserve particle number anymore. This can be deduced by the appearance in the final form of addends consisting of only creation or only annihilation operators, consistent with the fact that the mean-field Hamiltonian is obtained by considering the problem in the grand-canonical ensemble. Indeed, because of the elimination of correlations between fluctuations, the two Hamiltonians \mathcal{H} and \mathcal{H}_{MF} can not possibly describe the exact same problem. Fortunately, the particle number N is so big that small fluctuations around its value do not pose a serious threat to the

7.3 Standard BCS Theory

consistence of this approximation and the mean-field Hamiltonian can be used to effectively describe the original system.

Nevertheless, in order to obtain the energy spectrum, it would be best to recast the mean-field Hamiltonian in a diagonal form which contains only particle number operators. This procedure is known as canonical or Bogoliubov transformation and will be presented in the next subsection.

7.3.4 BOGOLIUBOV TRANSFORMATION

The aim of the Bogoliubov transformation is to find an equivalent canonical anticommutation relation algebra which conserves the particle number in the Hamiltonian. To achieve this, the original creation and annihilation operators are expressed as a linear combination of new fermionic operators $\gamma_{\vec{k},i}$,

$$\begin{cases} c_{\vec{k}\uparrow} = u_{\vec{k}}^* \gamma_{\vec{k},1} + v_{\vec{k}} \gamma_{\vec{k},2}^\dagger \\ c_{-\vec{k}\downarrow}^\dagger = -v_{\vec{k}}^* \gamma_{\vec{k},1} + u_{\vec{k}} \gamma_{\vec{k},2}^\dagger \end{cases} \quad (7.37)$$

with the complex coefficients $u_{\vec{k}}$ and $v_{\vec{k}}$. Since $\gamma_{\vec{k},1}$ participates in annihilating a state $|\vec{k}, \uparrow\rangle$ or creating a state $|\vec{-k}, \downarrow\rangle$, it has the net effect of decreasing the total momentum by \vec{k} and reducing the spin by $\hbar/2$ and can be associated with a hole-like quasiparticle. Analogously the operator $\gamma_{\vec{k},2}$ presents electron-like features: it involves the annihilation of a state $|\vec{-k}, \downarrow\rangle$ or the creation of a state $|\vec{k}, \uparrow\rangle$, thereby increasing total momentum by \vec{k} and spin by $\hbar/2$. Furthermore, the requirement that the old operators satisfy the anticommutation relations

$$\{c_{\vec{k}\uparrow}, c_{\vec{k}\uparrow}^\dagger\} = 1, \quad \{c_{-\vec{k}\downarrow}, c_{-\vec{k}\downarrow}^\dagger\} = 1 \quad (7.38)$$

imposes the following condition on the transformation coefficients:

$$|v_{\vec{k}}|^2 + |u_{\vec{k}}|^2 = 1 \quad (7.39)$$

The mean-field Hamiltonian can now be rewritten in terms of the new quasipar-

ticle operators by plugging the definition (7.37) in equation (7.35):

$$\mathcal{H}_{MF} = \sum_{\vec{k}} \left\{ \xi_{\vec{k}} \left[\left(u_{\vec{k}} \gamma_{\vec{k},1}^{\dagger} + v_{\vec{k}}^* \gamma_{\vec{k},2} \right) \left(u_{\vec{k}}^* \gamma_{\vec{k},1} + v_{\vec{k}} \gamma_{\vec{k},2}^{\dagger} \right) + \left(-v_{-\vec{k}}^* \gamma_{\vec{k},1} + u_{-\vec{k}} \gamma_{\vec{k},2}^{\dagger} \right) \left(-v_{-\vec{k}} \gamma_{\vec{k},1}^{\dagger} + u_{-\vec{k}}^* \gamma_{\vec{k},2} \right) \right] \right. \\ \left. - \left[\Delta_{\vec{k}}^* \left(-v_{\vec{k}} \gamma_{\vec{k},1}^{\dagger} + u_{\vec{k}}^* \gamma_{\vec{k},2} \right) \left(u_{\vec{k}}^* \gamma_{\vec{k},1} + v_{\vec{k}} \gamma_{\vec{k},2}^{\dagger} \right) + \Delta_{\vec{k}} \left(u_{\vec{k}} \gamma_{\vec{k},1}^{\dagger} + v_{\vec{k}}^* \gamma_{\vec{k},2} \right) \left(-v_{\vec{k}}^* \gamma_{\vec{k},1} + u_{\vec{k}} \gamma_{\vec{k},2}^{\dagger} \right) \right] \right\} \quad (7.40)$$

$$= \sum_{\vec{k}} \left\{ \left[|u_{\vec{k}}|^2 \gamma_{\vec{k},1}^{\dagger} \gamma_{\vec{k},1} + u_{\vec{k}} v_{\vec{k}} \gamma_{\vec{k},1}^{\dagger} \gamma_{\vec{k},2}^{\dagger} + v_{\vec{k}}^* u_{\vec{k}}^* \gamma_{\vec{k},2} \gamma_{\vec{k},1} + |v_{\vec{k}}|^2 \gamma_{\vec{k},2} \gamma_{\vec{k},2}^{\dagger} + \right. \right. \\ \left. \left. + |v_{\vec{k}}|^2 \gamma_{\vec{k},1} \gamma_{\vec{k},1}^{\dagger} - v_{\vec{k}}^* u_{\vec{k}}^* \gamma_{\vec{k},1} \gamma_{\vec{k},2} - u_{\vec{k}} v_{\vec{k}} \gamma_{\vec{k},2}^{\dagger} \gamma_{\vec{k},1}^{\dagger} + |u_{\vec{k}}|^2 \gamma_{\vec{k},2} \gamma_{\vec{k},2}^{\dagger} \right] \right\} + \\ - \sum_{\vec{k}} \left\{ \Delta_{\vec{k}}^* \left[-v_{\vec{k}} u_{\vec{k}}^* \gamma_{\vec{k},1}^{\dagger} \gamma_{\vec{k},1} - v_{\vec{k}}^2 \gamma_{\vec{k},1}^{\dagger} \gamma_{\vec{k},2}^{\dagger} + (u_{\vec{k}}^*)^2 \gamma_{\vec{k},2} \gamma_{\vec{k},1} + u_{\vec{k}}^* v_{\vec{k}} \gamma_{\vec{k},2} \gamma_{\vec{k},2}^{\dagger} \right] + \right. \\ \left. \Delta_{\vec{k}} \left[-v_{\vec{k}}^* u_{\vec{k}} \gamma_{\vec{k},1}^{\dagger} \gamma_{\vec{k},1} + u_{\vec{k}}^2 \gamma_{\vec{k},1}^{\dagger} \gamma_{\vec{k},2}^{\dagger} - (v_{\vec{k}}^*)^2 \gamma_{\vec{k},2} \gamma_{\vec{k},1} + u_{\vec{k}} v_{\vec{k}}^* \gamma_{\vec{k},2} \gamma_{\vec{k},2}^{\dagger} \right] - \Delta_{\vec{k}} b_{\vec{k}}^* \right\} \\ = \sum_{\vec{k}} \left\{ \xi_{\vec{k}} \left[(|u_{\vec{k}}|^2 - |v_{\vec{k}}|^2) \left(\gamma_{\vec{k},1}^{\dagger} \gamma_{\vec{k},1} + \gamma_{\vec{k},2}^{\dagger} \gamma_{\vec{k},2} \right) + 2|v_{\vec{k}}|^2 + 2u_{\vec{k}} v_{\vec{k}} \gamma_{\vec{k},1}^{\dagger} \gamma_{\vec{k},2}^{\dagger} + 2u_{\vec{k}}^* v_{\vec{k}}^* \gamma_{\vec{k},2} \gamma_{\vec{k},1} \right] \right\} + \right. \\ \left. (7.41) \right.$$

$$+ \sum_{\vec{k}} \left\{ \Delta_{\vec{k}} u_{\vec{k}} v_{\vec{k}}^* \left(\gamma_{\vec{k},1}^{\dagger} \gamma_{\vec{k},1} - 1 + \gamma_{\vec{k},2}^{\dagger} \gamma_{\vec{k},2} \right) + \Delta_{\vec{k}}^* \left(\gamma_{\vec{k},1}^{\dagger} \gamma_{\vec{k},1} - 1 + \gamma_{\vec{k},2}^{\dagger} \gamma_{\vec{k},2} \right) + \right. \\ \left. + [-\Delta_{\vec{k}}^*(u_{\vec{k}}^*)^2 + \Delta_{\vec{k}}(v_{\vec{k}}^*)^2] \gamma_{\vec{k},2} \gamma_{\vec{k},1} + [-\Delta_{\vec{k}} u_{\vec{k}}^2 + \Delta_{\vec{k}}^* v_{\vec{k}}^2] \gamma_{\vec{k},1}^{\dagger} \gamma_{\vec{k},2}^{\dagger} + \Delta_{\vec{k}} b_{\vec{k}}^* \right\} \quad (7.42)$$

The Hamiltonian is diagonalized, *i.e.* only proportional to constants and number operators, if all terms containing $\gamma_{\vec{k},2} \gamma_{\vec{k},1}$ and $\gamma_{\vec{k},1}^{\dagger} \gamma_{\vec{k},2}^{\dagger}$ vanish, which are complex conjugate to each other. Coincidentally, in equation (7.42) the coefficient of $\gamma_{\vec{k},2} \gamma_{\vec{k},1}$ is exactly the complex conjugate of the coefficient of $\gamma_{\vec{k},1}^{\dagger} \gamma_{\vec{k},2}^{\dagger}$, so that the condition for the Hamiltonian to be diagonalized is summarized in one equation only:

$$2\xi_{\vec{k}} u_{\vec{k}} v_{\vec{k}} + \Delta_{\vec{k}}^* v_{\vec{k}}^2 - \Delta_{\vec{k}} u_{\vec{k}}^2 = 0 \quad (7.43)$$

By multiplying through with $\frac{\Delta_{\vec{k}}^*}{u_{\vec{k}}^2}$ and solving the quadratic equation in $(\Delta_{\vec{k}}^* \frac{v_{\vec{k}}}{u_{\vec{k}}})$ (only the positive root corresponding to a minimum of the energy is considered here), this condition becomes:

$$\Delta_{\vec{k}}^* \frac{v_{\vec{k}}}{u_{\vec{k}}} = E_{\vec{k}} - \xi_{\vec{k}} \quad (7.44)$$

where $E_{\vec{k}}$ is the quasiparticle energy $E_{\vec{k}} = \sqrt{\xi_{\vec{k}}^2 + \Delta_{\vec{k}}^2}$ and $2u_{\vec{k}}^* v_{\vec{k}} = \frac{\Delta_{\vec{k}}}{E_{\vec{k}}}$. If condition (7.44) is fulfilled, then the Hamiltonian takes the simpler form

$$\mathcal{H}_{Bog} = \sum_{\vec{k}} [\xi_{\vec{k}} - E_{\vec{k}} + \Delta_{\vec{k}} b_{\vec{k}}^*] + \sum_{\vec{k}} E_{\vec{k}} (\gamma_{\vec{k},1}^{\dagger} \gamma_{\vec{k},1} + \gamma_{\vec{k},2}^{\dagger} \gamma_{\vec{k},2}) \quad (7.45)$$

7.3 Standard BCS Theory

Thanks to the Bogoliubov transformation the whole interaction mechanism of the mean-field Hamiltonian is now encoded in a dispersion relation for two intermixing Fermi seas of quasiparticles, whose behavior is illustrated in figure 7.8. The most prominent feature of the superconducting spectrum is the opening of a k -dependent gap $\Delta_{\vec{k}}$, which is due to the superposition of the two (hole-like and electron-like) Fermi seas. It is important to mention that since the operators $\gamma_{\vec{k},1}^\dagger \gamma_{\vec{k},1}$ and $\gamma_{\vec{k},2}^\dagger \gamma_{\vec{k},2}$ pertain to quasiparticles with different characteristics, their expectation value will vanish for different values of \vec{k} . Since the two Fermi seas intersect, this is a crucial point to consider in order to associate the branches of the spectrum to one or the other quasiparticle. For instance - denoting the Fermi sea with $|FS\rangle$ - the expectation value $\langle FS| \gamma_{\vec{k},1}^\dagger \gamma_{\vec{k},1} |FS\rangle$ is zero for $k < k_F$, because below the Fermi level at $T = 0$ there are no holes to annihilate and $\gamma_{\vec{k},1}^\dagger |FS\rangle = 0$. Consequently, the lower (occupied) states have electron-like character. Analogously, the expectation value $\langle FS| \gamma_{\vec{k},2}^\dagger \gamma_{\vec{k},2} |FS\rangle$ is zero above the Fermi level $k > k_F$ and in this region the occupied states have hole-like character.

7.3.5 GAP EQUATION

The mean-field approach to the analysis of the superconducting Hamiltonian enables the derivation of other results besides the form of the energy spectrum. In this last subsection the critical temperature and the gap size at zero temperature will be calculated. The self-consistency equation (7.8) presented in section 2 is in fact a special case of a more general, temperature-dependent gap equation derived within the mean-field formalism. The starting point of this analysis is the definition of the gap function (equation (7.36)), in which the quasi-particle operators $\gamma_{\vec{k},i}$ can be substituted in lieu of the mean-field $b_{\vec{k}'} = \langle c_{-\vec{k}'\downarrow} c_{\vec{k}'\uparrow} \rangle$:

$$\Delta_{\vec{k}} = - \sum_{\vec{k}'} V_{\vec{k}\vec{k}'} b_{\vec{k}'} = - \sum_{\vec{k}'} V_{\vec{k}\vec{k}'} \langle c_{-\vec{k}'\downarrow} c_{\vec{k}'\uparrow} \rangle \quad (7.46)$$

$$= - \sum_{\vec{k}'} V_{\vec{k}\vec{k}'} \left\langle \left(-v_{\vec{k}'} \gamma_{\vec{k}',1}^\dagger + u_{\vec{k}'}^* \gamma_{\vec{k}',2} \right) \left(u_{\vec{k}'}^* \gamma_{\vec{k}',1} + v_{\vec{k}'} \gamma_{\vec{k}',2}^\dagger \right) \right\rangle \quad (7.47)$$

$$= - \sum_{\vec{k}'} V_{\vec{k}\vec{k}'} \left\langle v_{\vec{k}'} u_{\vec{k}'}^* \left(1 - \gamma_{\vec{k}',2}^\dagger \gamma_{\vec{k}',2} - \gamma_{\vec{k}',1}^\dagger \gamma_{\vec{k}',1} \right) \right\rangle \quad (7.48)$$

At finite temperature the expectation value of the number operator is given by the Fermi-Dirac distribution:

$$\langle \gamma_{\vec{k}}^\dagger \gamma_{\vec{k}} \rangle = f(E_{\vec{k}}) = \left(1 + \exp \left(\frac{E_{\vec{k}}}{k_B T} \right) \right)^{-1} \quad (7.49)$$

which is sketched in figure 7.9. Inserting equation (7.49) in (7.48) one obtains the self-consistent *gap equation*:

$$\Delta_{\vec{k}} = - \sum_{\vec{k}'} V_{\vec{k}\vec{k}'} v_{\vec{k}'} u_{\vec{k}'}^* (1 - 2f(E_{\vec{k}'})) \quad (7.50)$$

$$= - \sum_{\vec{k}'} V_{\vec{k}\vec{k}'} v_{\vec{k}'} u_{\vec{k}'}^* \left(\frac{e^{E_{\vec{k}}/k_B T} - 1}{e^{E_{\vec{k}}/k_B T} + 1} \right) \quad (7.51)$$

$$= - \sum_{\vec{k}'} V_{\vec{k}\vec{k}'} \frac{\Delta_{\vec{k}'}}{2E_{\vec{k}'}} \tanh \left(\frac{\beta E_{\vec{k}'}}{2} \right) \quad (7.52)$$

Moreover, if the interaction potential is not k -dependent - as for the Cooper approximation (equation (7.6)) - neither is the gap and the gap equation simplifies to:

$$\boxed{\frac{1}{V} = \frac{1}{2} \sum_{\vec{k}'} \frac{\tanh(\beta E_{\vec{k}'}/2)}{E_{\vec{k}'}}} \quad (7.53)$$

From this equation it is possible to derive the critical temperature at which the superconducting phase appears. First of all, the sum is converted to an integral in the continuum limit:

$$1 = V \int_{-\infty}^{+\infty} dE \frac{N(E)}{2E} \tanh \left(\frac{E}{2k_B T_c} \right) \quad (7.54)$$

Because the integrand diverges logarithmically at the boundaries an energy cutoff $\epsilon_c \ll E_F$ must be introduced (actually this cutoff naturally arises from the definition of V). Then the integral can be evaluated numerically as:

$$1 = VN(E_F) \int_{-\epsilon_c}^{+\epsilon_c} \frac{dE}{2E} \tanh \left(\frac{E}{2k_B T_c} \right) \approx VN_0 \ln \left(\frac{1.14\epsilon_c}{k_B T_c} \right) \quad (7.55)$$

where the approximation $N(E) \rightarrow N(E_F)$ was also made. Solving for $k_B T_c$, an explicit result for the critical temperature is obtained:

$$\boxed{k_B T_c = 1.14\epsilon_c e^{-1/VN(E_F)}} \quad (7.56)$$

The energy gap at $T = 0$ can also be calculated using the same energy cutoff, by noticing that $\tanh(E/k_B T) \xrightarrow{T \rightarrow 0} 1$ and using the definition of the energy spectrum $E = \sqrt{\xi^2 + \Delta^2}$:

$$1 = VN(E_F) \int_{-\epsilon_c}^{\epsilon_c} \frac{d\xi}{2E} \quad (7.57)$$

$$= VN(E_F) \int_0^{\epsilon_c} \frac{d\xi}{\sqrt{\xi^2 + \Delta^2}} \quad (7.58)$$

$$= VN(E_F) \sinh^{-1} \left(\frac{\epsilon_c}{\Delta} \right) \quad (7.59)$$

7.4 Generalized BCS theory

$$\Rightarrow \Delta(T = 0) \approx 2\epsilon_c e^{-1/VN(E_F)} \quad (7.60)$$

It is worth noting the similarity between the special case of the gap equation at $T = 0$ (equation (7.57)) and the result derived in section two with the Cooper approximation (equation (7.10)). Interestingly, the equation for the energy gap at zero temperature (7.60) has the same form as the equation for the critical temperature (7.56), which implies that the two quantities are linearly dependent:

$$\Delta(T = 0) \approx 1.764k_B T_c \quad (7.61)$$

This result makes perfect sense in the Cooper pair picture. The condensation of Cooper pairs becomes energetically favorable below T_c . For this reason, a higher critical temperature implies a bigger energy gain of the superconducting phase. To describe it differently, the higher the value of T_c is, the stronger the binding energy of the Cooper pairs must be to compensate thermal excitation. Furthermore, as seen in figure 7.8, the gap is a direct measure of the ground state energy lowering compared to the non-superconducting state: the gap quantifies the energy needed by a Cooper pair to dissociate. That the two quantities Δ and T_c are directly related should therefore not come as a surprise.

7.4 GENERALIZED BCS THEORY

The BCS theory discussed in section two was based on a k -space Hamiltonian which explicitly encoded only spin singlet pairing in its most symmetric form (s-wave). The aim of this section is to generalize the previous considerations to arbitrary spin configurations and less symmetric orbital wave functions, *i.e.* p-wave, d-wave and so on. Apart from the addition of extra degrees of freedom derived from the introduction of spin variables, the mathematics involved in this generalization will not differ greatly from those of the previous discussion. For this reason, many of the results previously obtained will be simply reused in the context of spin-dependent BCS theory without renewed derivation. From the outcome of the generalized BCS theory it will be clear that the pairing mechanism of electrons underlying superconductivity is very heterogeneous and can appear under various forms in different physical landscapes.

7.4.1 GENERALIZED MEAN FIELD THEORY

As for standard BCS theory, the pairing Hamiltonian is the starting point of the model. Nevertheless, to include all possible spin configurations in the mathematical description, the Hamiltonian will include an interaction part where the sum

BCS THEORY OF SUPERCONDUCTIVITY [PAOLO MOLIGNINI]

runs not only over momenta but also over spins[27]:

$$\mathcal{H} = \sum_{\vec{k}, s} \xi_{\vec{k}} c_{\vec{k}, s}^\dagger c_{\vec{k}, s} + \frac{1}{2} \sum_{\vec{k}, \vec{k}'} \sum_{s_1, s_2, s_3, s_4} V_{\vec{k}\vec{k}', s_1 s_2 s_3 s_4} c_{\vec{k}, s_1}^\dagger c_{-\vec{k}, s_2}^\dagger c_{-\vec{k}', s_3} c_{\vec{k}', s_4} \quad (7.62)$$

The matrix element is now $V_{\vec{k}\vec{k}', s_1 s_2 s_3 s_4} = \langle -\vec{k}, s_1; \vec{k}, s_2 | \hat{V} | -\vec{k}', s_3; \vec{k}', s_4 \rangle$ and because of the anticommutation relations for fermionic operators it changes sign upon swapping the initial or final states involved in the scattering:

$$V_{\vec{k}\vec{k}', s_1 s_2 s_3 s_4} = -V_{-\vec{k}\vec{k}', s_2 s_1 s_3 s_4} = -V_{\vec{k}, -\vec{k}', s_1 s_2 s_4 s_3} = V_{-\vec{k}, -\vec{k}', s_2 s_1 s_4 s_3} \quad (7.63)$$

Furthermore, it is also assumed that V is even in \vec{k} for singlet pairing and odd in \vec{k} for triplet pairing. Finally, as before, the weak-coupling approximation implies $V_{\vec{k}\vec{k}', s_1 s_2 s_3 s_4} \neq 0$ for $|\xi_{\vec{k}}| < \epsilon_c \ll E_F$.

The Hamiltonian will now be treated in a mean field fashion to obtain a more handy form. Defining the mean field $b_{\vec{k}, ss'} \equiv \langle c_{-\vec{k}s} c_{\vec{k}s'} \rangle$ and rewriting $c_{-\vec{k}s} c_{\vec{k}s'} = \langle c_{-\vec{k}s} c_{\vec{k}s'} \rangle + (c_{-\vec{k}s} c_{\vec{k}s'} - \langle c_{-\vec{k}s} c_{\vec{k}s'} \rangle) = b_{\vec{k}, ss'} + \delta b_{\vec{k}, ss'}$, the Hamiltonian can be expressed in terms of $b_{\vec{k}, ss'}$. This procedure is analogous to the calculation already performed in section two. Ignoring quadratic terms in $b_{\vec{k}, ss'}$ and in $\delta b_{\vec{k}, ss'}$ the mean-field Hamiltonian becomes:

$$\mathcal{H}_{MF} = \sum_{\vec{k}, s} \xi_{\vec{k}} c_{\vec{k}, s}^\dagger c_{\vec{k}, s} - \frac{1}{2} \sum_{\vec{k}, s_1, s_2} \left(\Delta_{\vec{k}, s_1 s_2} c_{\vec{k}, s_1}^\dagger c_{-\vec{k}, s_2}^\dagger + \Delta_{\vec{k}, s_1 s_2}^* c_{\vec{k}, s_1} c_{-\vec{k}, s_2} \right) \quad (7.64)$$

with the spin-dependent *generalized gap*:

$$\boxed{\Delta_{\vec{k}, ss'} = - \sum_{\vec{k}', s_3, s_4} V_{\vec{k}, \vec{k}', ss' s_3 s_4} b_{\vec{k}', s_3, s_4}} \quad (7.65)$$

Equation (7.64) can be written in a more compact form. For spin-1/2 the sum over spins can be interpreted as a matrix product in spin space, *i.e.* for the first summand:

$$\sum_{\vec{k}, s_1, s_2} \Delta_{\vec{k}, s_1 s_2} c_{\vec{k}, s_1}^\dagger c_{-\vec{k}, s_2}^\dagger = \begin{pmatrix} c_{\vec{k}\uparrow}^\dagger & c_{\vec{k}\downarrow}^\dagger \end{pmatrix} \underbrace{\begin{pmatrix} \Delta_{\vec{k}, \uparrow\uparrow} & \Delta_{\vec{k}, \uparrow\downarrow} \\ \Delta_{\vec{k}, \downarrow\uparrow} & \Delta_{\vec{k}, \downarrow\downarrow} \end{pmatrix}}_{\widehat{\Delta}_{\vec{k}}} \begin{pmatrix} c_{-\vec{k}\uparrow}^\dagger \\ c_{-\vec{k}\downarrow}^\dagger \end{pmatrix} \quad (7.66)$$

and for the second

$$\sum_{\vec{k}, s_1, s_2} \Delta_{\vec{k}, s_1 s_2}^* c_{\vec{k}, s_1} c_{-\vec{k}, s_2} = \begin{pmatrix} c_{\vec{k}\uparrow} & c_{\vec{k}\downarrow} \end{pmatrix} \underbrace{\begin{pmatrix} \Delta_{\vec{k}, \uparrow\uparrow}^* & \Delta_{\vec{k}, \uparrow\downarrow}^* \\ \Delta_{\vec{k}, \downarrow\uparrow}^* & \Delta_{\vec{k}, \downarrow\downarrow}^* \end{pmatrix}}_{\widehat{\Delta}_{\vec{k}}^*} \begin{pmatrix} c_{-\vec{k}\uparrow} \\ c_{-\vec{k}\downarrow} \end{pmatrix} \quad (7.67)$$

7.4 Generalized BCS theory

The *generalized gap function* $\widehat{\Delta}_{\vec{k}}$ is now a two-dimensional complex matrix in spin space. By exploiting the property of the band dispersion $\xi_{\vec{k}} = \xi_{-\vec{k}}$ and combining creation and annihilation operators together into an extended 4-dimensional notation the mean-field Hamiltonian is finally mapped to the so called *Bogoliubov-de Gennes Hamiltonian*:

$$\boxed{\mathcal{H}_{BdG} = \frac{1}{2} \sum_{\vec{k}} \mathbf{C}_{\vec{k}}^\dagger \widehat{\mathcal{E}}_{\vec{k}} \mathbf{C}_{\vec{k}}} \quad (7.68)$$

$$\text{where } \mathbf{C}_{\vec{k}} = \begin{pmatrix} c_{\vec{k}\uparrow} \\ c_{\vec{k}\downarrow} \\ c_{-\vec{k}\uparrow}^\dagger \\ c_{-\vec{k}\downarrow}^\dagger \end{pmatrix} \text{ and } \widehat{\mathcal{E}}_{\vec{k}} = \begin{pmatrix} \xi_{\vec{k}} \widehat{\mathbb{1}}_2 & \widehat{\Delta}_{\vec{k}} \\ \widehat{\Delta}_{\vec{k}}^\dagger & -\xi_{\vec{k}} \widehat{\mathbb{1}}_2 \end{pmatrix}.$$

7.4.2 BOGOLIUBOV-DE GENNES HAMILTONIAN

The final form of \mathcal{H}_{BdG} developed in the previous subsection might look compact and pretty, but in order to compute its spectrum the Hamiltonian must be diagonalized. The goal of the diagonalization procedure is to find a basis in which the Hamiltonian can be written as

$$\mathcal{H}'_{BdG} = \sum_{\vec{k}} \mathbf{A}_{\vec{k}}^\dagger \widehat{\mathcal{E}}_{\vec{k}} \mathbf{A}_{\vec{k}} \quad (7.69)$$

with a new set of (quasiparticle) operators:

$$\mathbf{A}_{\vec{k}} = \begin{pmatrix} a_{\vec{k}\uparrow} \\ a_{\vec{k}\downarrow} \\ a_{-\vec{k}\uparrow}^\dagger \\ a_{-\vec{k}\downarrow}^\dagger \end{pmatrix} \quad (7.70)$$

and a diagonal matrix

$$\widehat{\mathcal{E}}_{\vec{k}} = \begin{pmatrix} E_{\vec{k}_+} & 0 & 0 & 0 \\ 0 & E_{\vec{k}_-} & 0 & 0 \\ 0 & 0 & -E_{\vec{k}_+} & 0 \\ 0 & 0 & 0 & -E_{\vec{k}_-} \end{pmatrix}. \quad (7.71)$$

In the following discussion the problem will be restricted to unitary pairing, which ensures that the eigenvalues of the Hamiltonian only assume two values $\pm E_{\vec{k}}$. Similarly with what unveiled in section two, the mapping which brings the Hamiltonian into diagonal form is a Bogoliubov transformation. This time the

transformation must act on the 4-dimensional vector space, hence it is given by the (unitary) transformation matrix

$$\widehat{U}_{\vec{k}} = \begin{pmatrix} \widehat{u}_{\vec{k}} & \widehat{v}_{\vec{k}} \\ \widehat{v}_{-\vec{k}}^* & \widehat{u}_{-\vec{k}}^* \end{pmatrix} \quad (7.72)$$

such that $\mathbf{C}_{\vec{k}} = \widehat{U}_{\vec{k}} \mathbf{A}_{\vec{k}}$ and $\widehat{E}_{\vec{k}} = \widehat{U}^\dagger \widehat{\mathcal{E}}_{\vec{k}} \widehat{U}_{\vec{k}}$. These conditions imply that the 2×2 -block matrices within the 4×4 -Bogoliubov transformation matrix are:

$$\widehat{u}_{\vec{k}} = \frac{(E_{\vec{k}} + \xi_{\vec{k}})\mathbb{1}_2}{\sqrt{2E_{\vec{k}}(E_{\vec{k}} + \xi_{\vec{k}})}} \quad \text{and} \quad \widehat{v}_{\vec{k}} = \frac{-\widehat{\Delta}_{\vec{k}}}{\sqrt{2E_{\vec{k}}(E_{\vec{k}} + \xi_{\vec{k}})}}. \quad (7.73)$$

The energy is computed to be

$$E_{\vec{k}} = \sqrt{\xi_{\vec{k}}^2 + |\Delta_{\vec{k}}|^2} \quad (7.74)$$

and the spectrum is gapped with:

$$|\Delta_{\vec{k}}|^2 = \frac{1}{2} \text{Tr} \left(\widehat{\Delta}_{\vec{k}}^\dagger \widehat{\Delta}_{\vec{k}} \right) \quad (7.75)$$

These are the natural generalization of the “scalar” case of s-wave pairing, in which the extra spin dimensions are not involved in the calculations. Despite the different dimensionality of the problem, the quantities of interest (energy eigenvalues, gap and as shown in the next subsection the critical temperature as well) have the exact same structure found in the standard BCS theory. Therefore, all the considerations made in section two about the spectrum are still valid within the framework of generalized BCS theory.

7.4.3 GENERALIZED GAP EQUATION

As already seen in section 2.5, the mean field $b_{\vec{k},ss'} = \langle c_{-\vec{k}s} c_{\vec{k}s'} \rangle$ can be expressed in terms of the new quasiparticle operators $a_{\vec{k}s}$ and $a_{\vec{k}s}^\dagger$. At finite temperatures the expectation value of the quasiparticle number operators is given as $\langle a_{\vec{k}s}^\dagger a_{\vec{k}'s} \rangle = \delta_{\vec{k}\vec{k}'} \delta_{ss'} f(E_{\vec{k}})$, where $f(E_{\vec{k}})$ is the Fermi-Dirac distribution. The gap function then becomes:

$$\Delta_{\vec{k},s_1s_2} = - \sum_{\vec{k}',s_3s_4} V_{\vec{k},\vec{k}';s_1s_2s_3s_4} \frac{\Delta_{\vec{k}',s_4s_3}}{2E_{\vec{k}}} \tanh \left(\frac{E_{\vec{k}}}{2k_B T} \right) \quad (7.76)$$

Linearization leads to the critical temperature:

$$k_B T_c = 1.14 \epsilon_c e^{-1/\lambda} \quad (7.77)$$

7.5 Summary and Conclusion

The form of equation (7.77) is exactly the same of equation (7.56). The only difference between the two results is the parameter of the exponential: in the s-wave pairing case it is simply given by the product of the interaction potential and the density of states at the Fermi energy, while in the generalized case it is a dimensionless parameter obtained by solving an eigenvalue equation involving the angular average over the Fermi surface of components of the gap function². Nonetheless, considering that the gap function depends on the pairing interaction V , the exponentials in the two cases are ultimately different expressions of the same physical quantities. This and the other analogies discovered in this section prove that BCS theory is in fact quite general and applies to different pairing mechanisms equivalently well.

7.5 SUMMARY AND CONCLUSION

This report provided the basics for a microscopic theory of superconductivity. The discussion started with the analysis of a simple model involving two electrons of opposite spins added to the Fermi sea at zero temperature. The Fermi sea was shown to be unstable under an arbitrarily small attractive interaction $-V$ between the particles and to condensate in a bound state, called Cooper pair. In the weak-coupling approximation, that is for weak potentials, and for constant potentials around the Fermi surface, the Cooper pair was found to have an energy lower than twice the Fermi energy, *i.e.* the minimum energy of the free particles. The distance between the electrons in a Cooper pair was computed to be of the order of 10^3 Å, which prompted to exclude Coulomb interaction as the underlying mechanism leading to the attractive interaction among electrons. This hypothesis was further corroborated by the explicit calculation of the matrix element of the Coulomb potential in the Thomas-Fermi approximation, which was found to be strictly positive, therefore implying a repulsive interaction. Only with the introduction of another term, corresponding to interaction of electrons with the lattice, could the matrix element be led to assume negative values. One possible mechanism of interaction between the electrons was therefore identified with electron-phonon coupling.

Subsequently, the discussion of superconductivity was shifted to a microscopic description taking advantage of a Hamiltonian embedding the properties of Cooper pairs in s-wave, spin-singlet pairing. By rewriting the fermionic operators with their mean field averaged counterpart, the pairing Hamiltonian was

²The interested reader can find a more detailed explanation of the linearization procedure and the following eigenvalue problem in reference [?].

mapped to a mean-field Hamiltonian in the grand-canonical ensemble, written in terms of a gap function $\Delta_{\vec{k}}$. The necessity of a diagonalization procedure arose from the relaxation of particle number conservation, which was brought on by the reformulation of the Hamiltonian. This diagonalization was performed through a unitary Bogoliubov transformation which mapped the electronic operators to new fermionic operators, corresponding to Fermi seas of hole-like and electron-like quasiparticles. The positive energy eigenvalue of the Bogoliubov Hamiltonian was found to be $E_{\vec{k}} = \sqrt{\xi_{\vec{k}}^2 + \Delta_{\vec{k}}^2}$. The spectrum had both hole-like and electron-like character, depending on the branch, and it came out to be gapped with the k -dependent gap function. The new quasiparticle operators were also inserted in the definition of the gap function to obtain a self-consistent gap equation. Explicit expressions for the critical temperature and the energy gap at zero temperature were then calculated from the self-consistency equation for a constant interaction V with cutoff ϵ_c . Both the critical temperature and the energy gap at $T = 0$ were found to have an exponential dependence on the coupling: $k_B T_c = 1.14 \epsilon_c e^{-1/VN(E_F)}$ and $\Delta(T = 0) = 2\epsilon_c e^{-1/VN(E_F)}$. This result implied a linear dependence between the two quantities.

Finally, the form of the Hamiltonian was generalized to arbitrary spin pairings, allowing for a description of lower symmetric orbital parts of the electronic wave function, such as p-wave and d-wave pairing. For this purpose, an explicit sum over all possible spin- $\frac{1}{2}$ configurations was introduced. The Hamiltonian was again treated in a mean field fashion, but this time a spin-dependent gap function $\Delta_{\vec{k},ss'}$ appeared. A four-dimensional space of spin and creation/annihilation operators was defined, thereby reformulating the problem in terms of the compact Bogoliubov-de Gennes Hamiltonian. This 4×4 -matrix was then diagonalized by applying a Bogoliubov transformation and the same spectral features of standard BCS theory were retrieved. Rewriting the mean field in terms of the quasiparticle operators, a generalized gap equation was calculated and upon its linearization the critical temperature was determined. Its functional dependence was found to be the same already calculated in standard s-wave pairing, albeit with slightly generalized parameters. These results manifested the general character of the BCS framework, *i.e.* its applicability to systems with different pairing mechanisms than electron-phonon coupling.

7.5 Summary and Conclusion

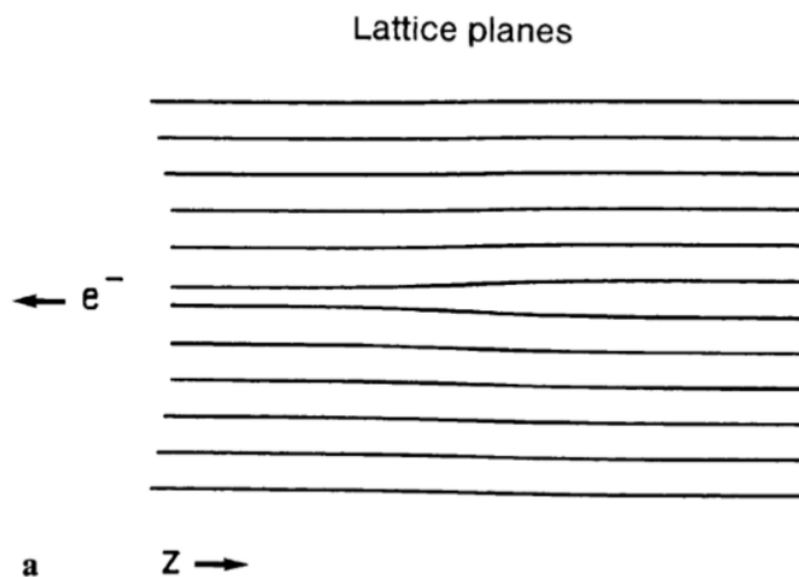


Figure 7.7: Pictorial depiction of the positively charged trail that an electron leaves upon crossing the bulk of a metal parallel to the lattice planes (not to scale). Image taken from Ref. [4].

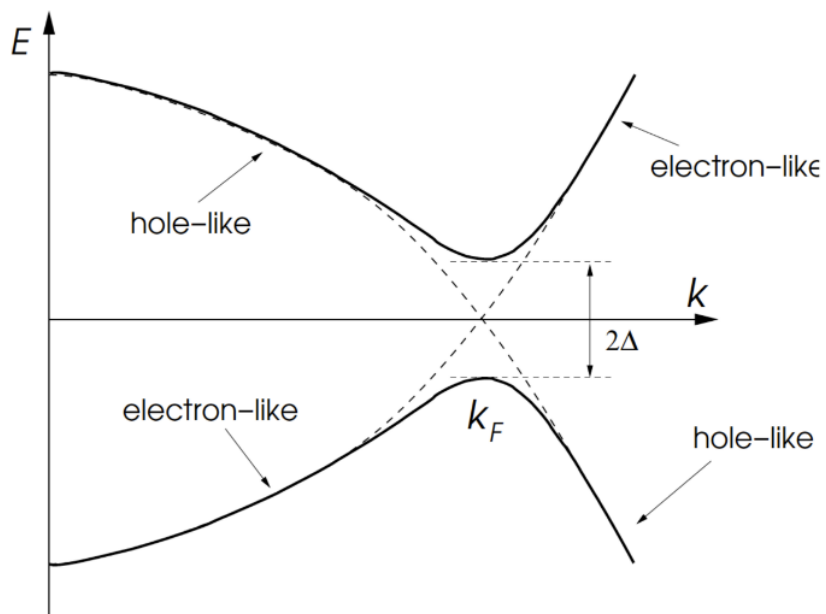


Figure 7.8: Graphic illustration of the quasiparticle spectrum in an s-wave superconductor. The solid line corresponds to a non-zero energy gap Δ , while the dashed line shows the spectrum of the trivial phase with $\Delta = 0$. States with negative energy are occupied, while states with $E > 0$ represent possible (empty) excited states. Note that the energy of the ground state is lower in the gapped case, indicating that Cooper pair condensation is energetically favorable. Image taken from Ref. [?].

7.5 Summary and Conclusion

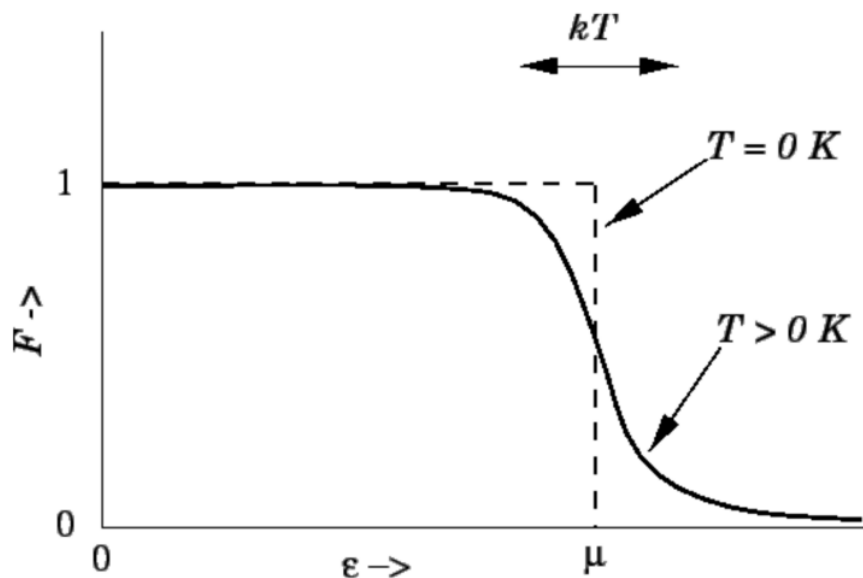


Figure 7.9: Plot of the Fermi-Dirac distribution $F(E)$ at zero temperature (dashed line) and at a small, finite temperature (solid line). The sharp edge at the chemical potential for the $T = 0$ case becomes rounded at higher temperatures. The “softening interval” in which the function is non-constant has an extension proportional to $k_B T$ and corresponds to the physical region where electrons are not clumped by the Pauli exclusion principle and can be excited to higher energies. Image taken from Ref. [26].

BIBLIOGRAPHY

- [1] H. K. Onnes, Commun. Phys. Lab. **12**, 120 (1911).
- [2] V. G. Ascherman, E. Friederich, E. Justi, and J. Kramer, Phys. Z. **42**, 349 (1941).
- [3] J. Eck (2014), URL <http://www.superconductors.org/Type2.htm>.
- [4] L. H. Ibach, H., *Solid State Physics* (Springer Verlag, Berlin, 2009).
- [5] F. P. Wheeler, F. (2001), URL <http://teachers.web.cern.ch/teachers/archiv/HST2001/ac>
- [6] W. Meissner and R. Ochsenfeld, Naturwissenschaften **21**, 44 (1933).
- [7] F. C. Moon, *Superconducting Levitation* (John Wiley and Sons, Inc, New York, 1993).
- [8] F. London and H. London, Proceedings of the Royal Society of London A **149**, 866 (1935).
- [9] L. N. Cooper, Phys. Rev. **104**, 1189 (1956).
- [10] J. M. Anderson P. W., Rowell, Phys. Rev. Lett. **10**, 230 (1963).
- [11] N. N. Bogoliubov, Zhurnal Eksperimental'noi i Teoreticheskoi Fiziki **34**, 58 (1958).
- [12] R. R. C. Osherooff, D. D. and D. M. Lee, Phys. Rev. Lett. **28**, 885 (1972).
- [13] M. K. A. Bednorz, J. G., Zeitschrift für Physik B **64**, 189 (1986).
- [14] B. A. V. Monthoux, P. and D. Pines, Phys. Rev. B **46 (22)**, 14803 (1992).
- [15] D. J. Scalapino, Phys. Rep. **250**, 329 (1995).
- [16] e. a. Tsuei, C. C., Nature **387 (6632)**, 481 (1997).

BIBLIOGRAPHY

- [17] C. C. Tsuei and J. R. Kirtley, Rev. Mod. Phys. **72**, 969 (2000).
- [18] J. R. e. a. Kirtley, Nature Physics **2** (3), 190 (2006).
- [19] J. R. e. a. Kirtley (2014), 1404.0362v2.
- [20] M. Tinkham, *Introduction to superconductivity* (McGraw-Hill, 1996).
- [21] S. K. L. L. D. Mineev, V. P., *Introduction to Unconventional Superconductivity* (CRC Press, 1999).
- [22] M. N. D. Ashcroft, N. W., *Solid State Physics* (Thomson Learning, Toronto, 1976).
- [23] E. N. Economou, *The physics of solids* (Springer Verlag, Berlin, 2010).
- [24] H. Fröhlich, Phys. Rev. **79**, 845 (1950).
- [25] D. Prananto, *Superconductivity* (2012), URL <http://simpliphy.wordpress.com/2012/05/06/superconductivity/>.
- [26] K. H. Kittel, C., *Thermal physics* (W. H. Freeman & co., New York, 1980).
- [27] U. K. Sigrist, M., Rev. Mod. Ph. **63** No. **2**, 239 (1991).

CHAPTER 8

TOPOLOGICAL SUPERCONDUCTORS

PAOLO MOLIGNINI

SUPERVISOR: ADRIEN BOUHON

As a starting point, the main features of the integer quantum Hall effect (IQHE) will be introduced and discussed, including the definition of the topological Chern number. The close similarities between the physics of the IQHE and of BCS superconductors will suggest the definition of an analogous topological number for the latter in terms of winding numbers. The winding numbers will be explicitly given for both real and complex 2×2 BdG Hamiltonians. They will be first rewritten as sums over occupied states of the Hilbert space and later reformulated using Green's functions. The Green's function formalism will be subsequently used to prove a special case of the bulk-edge correspondence, relating the number of zero-energy excitations ("edge states") on a one-dimensional interface to the difference of bulk topological indices. The purpose of this report is to illustrate and summarize the topics discussed during my talk as part of the theoretical proseminar titled "Topological insulators and topological superconductors", which was organized by Prof. Gianni Blatter at the Federal Institute of Technology (ETH) in Zurich during the spring semester 2014.

8.1 OUTLINE

This report is structured in four main sections. The first section will present an introduction in the concept of topology applied to solid state physics. In

8.2 Introduction

in this context the (integer) quantum Hall effect will be briefly discussed and the similarities between its quantum states and the superconducting states derived from BCS theory - such as the presence of a gap and bound states - will be highlighted. In the second section topological invariants for different classes of superconductors will be introduced as winding numbers and, using some mathematical identities, rewritten as sums over occupied states of the Hilbert space. The number of zero energy states will be related to the topological invariant in the form of an index theorem and contextually some concrete examples of superconductors satisfying the index theorem will be discussed. In the third section, the Green's function formalism developed by Volovik[1] will be presented. The topological indices introduced in section two will be first expressed in the language of Green's functions. Subsequently, borrowing some concepts from quantum field theory, the one-dimensional topological index N_1 will be recast as a sum over the energy spectrum. Thereafter, the bulk-edge correspondence will be formulated for a one-dimensional interface between two-dimensional topological superconductors with different topological indices; the bulk-edge correspondence for this special case will then be proved by taking advantage of Wigner transformations, Moyal product expansion and Gauss's theorem. Finally, a summary of the major findings of the previous chapters will conclude the report.

8.2 INTRODUCTION

In the last couple of decades, after the discovery of the quantum Hall effect in 1980[2], there has been quite a hype around topological insulators and topological superconductors in the scientific community. These are materials which present bulk gaps like ordinary insulators but are also characterized by the existence of gapless, conducting states on their boundaries (edges or surfaces). The peculiar feature of these edge states, is the fact that they are topologically protected, in the sense that they survive smooth changes in material parameters and can be disrupted only if the system undergoes a quantum phase transition[3, 4]. These properties of topological insulators make them on the one hand good candidates for future experimental applications of spintronics and quantum computation, but on the other hand offer another theoretical framework for the description of condensed matter systems based on the notion of *topological order*[5], as complementary to the one of spontaneous symmetry breaking based on the behavior of an order parameter[6, 7]. In mathematics, topological invariance is a tool used to categorize geometrical hypersurfaces into classes whose members can be smoothly deformed into each other, without creating “holes” or singularities in

the process[8]. In solid state physics, the main descriptive tool of microscopic systems is the Hamiltonian, which for insulators and superconductors intrinsically embed an energy gap. Thus, one defines physical topological equivalence classes in terms of smooth deformations which preserve the existence of such gap[9, 10]. Topological materials are however not simply confined to the world of theoretical physics, but have already been experimentally observed, for instance in HgTe and CdTe quantum wells[11, 12]. In the recent years many more materials which exhibit topological order have been theoretically predicted and some of them have been later experimentally observed[13, 14], making the theory of topological states of quantum matter a new and crawling subfield of condensed matter physics.

In this report the focus will be put on topological superconductors. These materials are characterized by the opening of a gap due to standard Cooper pair condensation, but which can close for certain zero-energy states located at the boundary between inequivalent topological phases. Since the description of their topological properties will be constructed on a similar manner as for the quantum Hall effect, this latter phenomenon will be first briefly introduced.

8.2.1 QUANTUM HALL STATES

The classical Hall effect was discovered at the end of the 19th century by Edwin Hall[15]: if a magnetic field B is applied perpendicular to a quasi two-dimensional sample (layer) through which an electric current I flows, a transverse electric field will be produced due to charge accumulation on the sides of the conductor. The electric field induces a voltage difference V_{Hall} , known as Hall voltage, which can be measured across the sample. A diagram showing the experimental setup is sketched in figure 8.1. The ratio of channel current and Hall voltage is called Hall conductivity σ_H .

Under standard conditions, the Hall resistivity $\rho_H = \frac{1}{\sigma_H}$, is a linear function of B and can assume a continuum of values depending on the strength of the magnetic field. In 1980, however, while working with high magnetic fields at very low temperatures (below 4 K) on a silicon-based sample, K. von Klitzing and colleagues made an astonishing discovery: the Hall conductivity was exactly quantized in integer values[2]:

$$\sigma_H = \frac{e^2}{h} C_1 \quad (8.1)$$

A plot of the behavior of transversal and longitudinal conductivity in the sample is shown in figure 8.2.

It did not take long time for physicists to come up with a solid theory justifying

8.2 Introduction

the experimental results of Klitzing. The phenomenon can be understood in terms of the quantization of the cyclotron orbits of the charge carriers (electrons) in the two-dimensional electron gas. The orbits of the electrons are discretized in so-called *Landau levels* and, because the filling factor of these orbits is proportional to integer multiples of the magnetic flux quantum $\Phi_0 = \frac{hc}{e}$, the quantization of σ_H is a direct consequence[16]:

$$\sigma_H = \frac{I_y}{E_x} = -\frac{en_0 v_y(k_y)}{E_x} = en_0 \frac{c}{B} = \frac{eC_1}{2\pi l^2} \frac{c}{B} = \frac{e^2}{h} C_1 \quad (8.2)$$

Here $v_y(k_y) = \frac{1}{\hbar} \frac{dE_{n=0}(k_y)}{dk_y} = -\frac{cE_x}{B}$ is the velocity of the electrons computed from the energy of the zeroth Landau level, which is turn is obtained by calculating the expectation value of the Hamiltonian. $C_1 = n_0 2\pi l^2 = \frac{n_0 hc}{eB}$ is the filling factor of the Landau level and l is the magnetic length for which $l^2 = \frac{hc}{|eB|}$.

From linear response theory, C_1 can also be calculated from the Kubo formula[17]:

$$\sigma_H = \frac{ie^2 \hbar}{A} \sum_{n>0} \frac{(\nu_1)_{0n} (\nu_2)_{n0} - (\nu_2)_{0n} (\nu_1)_{n0}}{(E_0 - E_n)^2} \quad (8.3)$$

where A is the area of the system and

$$\nu_1 = \sum_{i=1}^N \frac{1}{m} \left(-i\hbar \frac{\partial}{\partial x_i} \right) \quad (8.4)$$

$$\nu_2 = \sum_{i=1}^N \frac{1}{m} \left(-i\hbar \frac{\partial}{\partial y_i} - eBx_i \right) \quad (8.5)$$

are velocity operators (m is the mass of the electrons). Nevertheless, it turns out that C_1 can also be written as the winding number

$$C_1 = -\frac{1}{2\pi} \int_{T^2} d^2 k \epsilon^{ij} \partial_{k_i} \mathcal{A}_j(\vec{k}) \quad (8.6)$$

The integer C_1 is known as **Chern number** and is written as the integral of the so-called *Berry connection*

$$\mathcal{A}_i(\vec{k}) = i \sum_{E_n < E_F} \langle u_n(\vec{k}) | \partial_{k_i} u_n(\vec{k}) \rangle \quad (8.7)$$

over the Brillouin zone. Since in a two-dimensional periodic system like in the quantum Hall effect the Brillouin zone can be folded into a torus T^2 (as shown in figure 8.3), the Chern number can be understood as the winding number for the mapping $T^2 \rightarrow S^1$ induced by the wave functions of the occupied states $|u_n(\vec{k})\rangle$ of

the Hilbert space $U(1) \cong S^1$, which can be described by a complex phase. Being a winding number, the Chern number must be integer-valued. Summarizing, the quantization of the Hall conductance is a direct consequence of the quantization of the Chern number.

It must be pointed out that in the quantum Hall effect the states are gapped in the bulk because of the interference of the Landau levels. Nevertheless, the gap closes at the boundary, where chiral edge states are found. The deeper reasons for this behavior will not be highlighted here, but a good discussion of the phenomenon can be found in Ref. [19] and Ref. [20].

8.2.2 TOPOLOGICAL SUPERCONDUCTORS

The characteristics highlighted in previous paragraph are not to be found exclusively in the quantum Hall effect: over the past two decades a number of scientific publications - such as Ref. [9, 1, 21, 22] - have highlighted similar behavior (gapped bulk, gapless edges) in other systems, most notably superconductors described by Bogoliubov-De Gennes (BdG) Hamiltonians. The analogy between these two systems prompted physicists to introduce a topological invariant for superconductors akin to the Chern number which arises in the description of the topological properties of the QHE. By the same token these systems are commonly referred to as “topological superconductors”. The similarities between QHE and topological superconductors are summarized in table 8.1.

How does the spectrum of a superconductor acquire a gap? In practice, the microscopic description of superconductors in terms of a generalized BCS theory leads to an effective 4×4 -matrix Hamiltonian which is acted on by 4-vectors of creation and annihilation operators for each of the spin orientations[24]. The full Hamiltonian can be then written as:

$$\mathcal{H}_{BdG} = \frac{1}{2} \sum_{\vec{k}} \mathbf{C}_{\vec{k}}^\dagger \hat{\mathcal{E}}_{\vec{k}} \mathbf{C}_{\vec{k}} \quad (8.8)$$

where $\mathbf{C}_{\vec{k}} = \begin{pmatrix} c_{\vec{k}\uparrow} \\ c_{\vec{k}\downarrow} \\ c_{-\vec{k}\uparrow}^\dagger \\ c_{-\vec{k}\downarrow}^\dagger \end{pmatrix}$ and $\hat{\mathcal{E}}_{\vec{k}} = \begin{pmatrix} \epsilon_{\vec{k}} \hat{\mathbb{1}}_2 & \hat{\Delta}_{\vec{k}} \\ \hat{\Delta}_{\vec{k}}^\dagger & -\epsilon_{\vec{k}} \hat{\mathbb{1}}_2 \end{pmatrix}$. The spectrum of the BdG-

Hamiltonian turns out to be gapped:

$$E_{\vec{k}} = \sqrt{\epsilon_{\vec{k}}^2 + |\Delta_{\vec{k}}|^2} \quad (8.9)$$

where the size of the gap is contained in the trace of the gap function:

$$|\Delta_{\vec{k}}|^2 = \frac{1}{2} \text{Tr} \left(\hat{\Delta}_{\vec{k}}^\dagger \hat{\Delta}_{\vec{k}} \right) \quad (8.10)$$

8.2 Introduction

The spectrum for the special case of a p -wave superconductor is depicted in figure 8.4.

Thus far the description of the system involved the bulk of the system and did not mention any boundaries. The Andreev bound states (ABS) located at the edges are derived by attempting to solve the BdG-Hamiltonian directly. In the following calculation, in order to simplify the problem, the Hamiltonian is considered real-gapped and is treated in real space in the semiclassical approximation[25, 26]. The eigenvalue equation of the real BdG-Hamiltonian is:

$$\begin{pmatrix} \frac{-\vec{\nabla}^2}{2m} - \mu & \Delta(\vec{r}) \\ \Delta(\vec{r}) & \frac{-\vec{\nabla}^2}{2m} + \mu \end{pmatrix} \begin{pmatrix} u_n(\vec{r}) \\ v_n(\vec{r}) \end{pmatrix} = E_n \begin{pmatrix} u_n(\vec{r}) \\ v_n(\vec{r}) \end{pmatrix} \quad (8.11)$$

where the chemical potential is fixes the Fermi energy: $\mu = \frac{\hbar^2 k_F^2}{2m}$ and the two-dimensional eigenvectors are denoted with $\Psi_n(\vec{r}) = \begin{pmatrix} u_n(\vec{r}) \\ v_n(\vec{r}) \end{pmatrix}$. Since in BCS theory Cooper pair condensation occurs only around the Fermi surface, the electronic wavelength k_F^{-1} is the characteristic length scale of the system and the quasiparticle momentum $\hbar k_F$ is a good quantum number. Thereby, the wave function $\Psi_n(\vec{r})$ can be expanded in the semiclassical approximation as

$$\Psi_n(\vec{r}) = e^{i\hbar\vec{k}\cdot\vec{r}} \Psi_{\vec{k}}(\vec{r}) \quad (8.12)$$

consisting of a strongly oscillating, plane wave part $e^{i\hbar\vec{k}\cdot\vec{r}}$ and a slowly varying envelope $\Psi_{\vec{k}}(\vec{r})$. The semiclassical approximation therefore grants a relabeling of the state quantum number n to the wave vector \vec{k} . The differential operator applied to this function yields:

$$\left(\pm \frac{\vec{\nabla}^2}{2m} \pm \mu \right) e^{i\hbar\vec{k}\cdot\vec{r}} \Psi_{\vec{k}}(\vec{r}) = \pm \frac{1}{2m} \left[\vec{\nabla} \left(i\vec{k} e^{i\hbar\vec{k}\cdot\vec{r}} \Psi_{\vec{k}}(\vec{r}) + e^{i\hbar\vec{k}\cdot\vec{r}} \vec{\nabla} \Psi_{\vec{k}}(\vec{r}) \right) + \hbar k_F^2 e^{i\hbar\vec{k}\cdot\vec{r}} \Psi_{\vec{k}}(\vec{r}) \right] \quad (8.13)$$

$$= \pm \frac{1}{2m} \left[-\hbar^2 \vec{k}^2 e^{i\hbar\vec{k}\cdot\vec{r}} \Psi_{\vec{k}}(\vec{r}) + 2i\hbar\vec{k} e^{i\hbar\vec{k}\cdot\vec{r}} \vec{\nabla} \Psi_{\vec{k}}(\vec{r}) + e^{i\hbar\vec{k}\cdot\vec{r}} \vec{\nabla}^2 \Psi_{\vec{k}}(\vec{r}) \right. \quad (8.14)$$

$$\left. + \hbar^2 k_F^2 e^{i\hbar\vec{k}\cdot\vec{r}} \Psi_{\vec{k}}(\vec{r}) \right]$$

$$= e^{i\hbar\vec{k}\cdot\vec{r}} \left[\pm \frac{i\hbar k_F}{m} \vec{\nabla} \pm \frac{\vec{\nabla}^2}{2m} \right] \Psi_{\vec{k}}(\vec{r}) \quad (8.15)$$

By inserting ansatz (8.12) in the eigenvalue equation, using equation (8.15) and discarding quadratic terms in the differential operators, one obtains the *Andreev*

equation:

$$\begin{pmatrix} -i\hbar v_F \vec{\nabla} & \Delta(\vec{r}) \\ \Delta(\vec{r}) & i\hbar v_F \vec{\nabla} \end{pmatrix} \Psi_{\vec{k}}(\vec{r}) = E_{\vec{k}} \Psi_{\vec{k}}(\vec{r}) \quad (8.16)$$

where $v_F = \frac{k_F}{m}$ is the Fermi velocity. The Andreev equation is linear and is obtained on the assumption that the gap Δ is not too wide, *i.e.* for $\frac{v_F}{\Delta} k_F \gg 1$. This amounts to say that the coherence length of the system - which is roughly the length scale over which the quantum fluctuations are correlated and which is given by $\xi = \frac{\hbar v_F}{\Delta}$ - is much bigger than the lattice constant a . The eigenstates of the Andreev equation with eigenvalue $E = 0$ are termed *Andreev Bound States* (ABS) and will also be zero energy eigenstate of the BdG equation. Since this value lies in the middle of the gap it must be bound to a special location, such as the edge of the topological insulators where the gap must go to zero to fulfill continuity requirements. A concrete example of an ABS will be given in section two in connection with the index theorem.

8.3 TOPOLOGICAL INVARIANTS IN SUPERCONDUCTORS

Given the analogies between QHE and topological superconductors it is feasible to hypothesize the existence of equivalent “Chern numbers” for the latter. The construction and manipulation of these topological invariants will be the focus of the current section. Given a band theory description of a superconductor, the topological number should be somehow derived by Bloch wave functions (or more precisely their periodic part) $|u_n(\vec{k})\rangle$ or their derivatives. In fact, in the QHE, the occupied states map the Brillouin zone - which is isomorphic to the torus T^2 - to the Hilbert space H , depending on the phase of the Bloch wave function. As already stated in the introduction, the Chern number is given in terms of an integral over derivatives of the Berry connection (equation (8.6)) defined as $\mathcal{A}_i(\vec{k}) = i \sum_{E_n < E_F} \langle u_n(\vec{k}) | \partial_{\vec{k}_i} u_n(\vec{k}) \rangle$ and can be rewritten as the winding number of the aforementioned mapping between T^2 and H . In order to complete the analogy with the QHE, the key element of this section will therefore be the definition of a bulk topological number for superconductors as the winding number of the image of the Brillouin zone under the mapping induced by the Bloch wave functions.

8.3.1 SUPERCONDUCTORS WITH REAL GAP FUNCTION

Following Ref. [23], the first example of topological number will be introduced for superconductors with a single-component, real gap, such as the conventional

8.3 Topological invariants in superconductors

s-wave superconductor, single component p -wave superconductors and high temperature cuprates (d -wave superconductors). The simplest case for this class is described by a real 2×2 BdG Hamiltonian:

$$\mathcal{H} = \sum_{\vec{k}} \begin{pmatrix} c_{\vec{k}\uparrow}^\dagger, c_{-\vec{k}\downarrow} \end{pmatrix} \mathcal{H}(\vec{k}) \begin{pmatrix} c_{\vec{k}\uparrow} \\ c_{-\vec{k}\downarrow}^\dagger \end{pmatrix} \quad (8.17)$$

with

$$\mathcal{H}(\vec{k}) = \begin{pmatrix} \epsilon(\vec{k}) & \Delta(\vec{k}) \\ \Delta(\vec{k}) & -\epsilon(\vec{k}) \end{pmatrix} \quad (8.18)$$

The spectrum is given by:

$$E(\vec{k}) = \sqrt{\epsilon(\vec{k})^2 + \Delta(\vec{k})^2} \quad (8.19)$$

Since the Hamiltonian is a real 2×2 -matrix, the corresponding eigenvectors spanning the Hilbert space are two-component real vectors. Because the eigenvectors can be chosen to have unit norm, they can be parametrized with sine and cosine functions:

$$|u(\vec{k})\rangle = \begin{pmatrix} \cos(2\alpha(\vec{k})) \\ \sin(2\alpha(\vec{k})) \end{pmatrix} \quad (8.20)$$

The parameter $\alpha(\vec{k}) \in [0, \pi]$ is an angle variable and leads to association of the Hilbert space with the unit circle S^1 . The physical eigenstate is parametrized with twice the angle variable because of a sign ambiguity in the occupied state which leads the physical state $|u(\vec{k})\rangle$ to coincide with $-|u(\vec{k})\rangle$.

At this point, in order to define a topological number, it is necessary to obtain a fully gapped system. In three dimensions the gap-closing condition $\Delta(\vec{k}) = 0$ is rather easily fulfilled at node points or lineneodes, where the notion of a winding number over occupied states becomes ill-defined¹. For this reason the momenta in the y - and z -directions will be now held fix such that the system under consideration becomes an effective one-dimensional superconductor. For a one-dimensional system the Brillouin zone is $-\pi < k_x \leq \pi$ and can be folded into a circle. The occupied states thus induce an isomorphism $S^1 \rightarrow S^1$ by means of the function $\alpha(\vec{k})$: $2\alpha(\vec{k})$ changes by 2π when the image of the Brillouin zone winds around S^1 (in the Hilbert space). On the basis of these observation it is reasonable to define the topological invariant as the following winding number:

$$N_1(k_y, k_z) = \frac{1}{2\pi} \int_{-\pi}^{\pi} dk_x \partial_{k_x}(2\alpha(\vec{k})) \quad (8.21)$$

¹When the bulk gap closes over a certain interval, the distinction between empty and occupied state ceases to exist because the occupied and empty bands of the insulator merge together.

This quantity really is a winding number because it involves the integration of an angle variable $d(2\alpha(\vec{k})) = \frac{\partial}{\partial k_x}(2\alpha(\vec{k}))dk_x$ and outputs only integers corresponding to the times the mapping is “wrapped” around the Hilbert space. In complex analysis, for instance, the winding number (or index) of a path has the exact same form:

$$n = \frac{1}{2\pi i} \oint_C \frac{dz}{z} = \frac{1}{2\pi i} \oint_C (d(\ln r) + id\theta) = \frac{1}{2\pi} \int_{-\pi}^{\pi} d\theta \quad (8.22)$$

The definition of the angle variable and the evaluation of the integral in equation (8.21) can be problematic. Luckily enough, the topological invariant can be rewritten as a sum over the zeros of the spectrum, which is a quantity that can be more easily measured or calculated.

$$N_1(k_y) = -\frac{1}{2} \sum_{k_x; \epsilon(\vec{k})=0} \text{sgn}(\Delta(\vec{k})) \cdot \text{sgn}(\partial_{k_x} \epsilon(\vec{k})) \quad (8.23)$$

In order to obtain equation (8.23), first the eigenvectors of $\mathcal{H}(\vec{k})$ have to be computed for occupied states (negative energies):

$$|u(\vec{k})\rangle = \frac{1}{2} \begin{pmatrix} \frac{\Delta(\vec{k})}{E(\vec{k})} \\ \frac{\epsilon(\vec{k})}{E(\vec{k})} + 1 \end{pmatrix} \quad (8.24)$$

The eigenvectors can be reparametrized with:

$$\cos(\theta(\vec{k})) = \frac{\epsilon(\vec{k})}{\sqrt{\epsilon(\vec{k})^2 + \Delta(\vec{k})^2}} \quad \sin(\theta(\vec{k})) = \frac{\Delta(\vec{k})}{\sqrt{\epsilon(\vec{k})^2 + \Delta(\vec{k})^2}} \quad (8.25)$$

to give:

$$|u(\vec{k})\rangle = \frac{1}{2} \begin{pmatrix} \sin(\theta(\vec{k})) \\ \cos(\theta(\vec{k})) + 1 \end{pmatrix} \quad (8.26)$$

Upon renormalization with $-\frac{1}{\cos(\theta/2)}$ and use of the trigonometric identities

$$\sin \theta = 2 \sin(\theta/2) \cos(\theta/2) \quad (8.27)$$

$$\cos^2(\theta/2) = \frac{1 + \cos \theta}{2} \quad (8.28)$$

$$\cos(\theta/2 - \pi/2) = \sin(\theta/2) \quad (8.29)$$

$$\sin(\theta/2 - \pi/2) = -\cos(\theta/2) \quad (8.30)$$

8.3 Topological invariants in superconductors

the eigenvectors are brought to the same form of equation (8.20):

$$|u(\vec{k})\rangle = \begin{pmatrix} \cos\left(\frac{\theta(\vec{k})-\pi}{2}\right) \\ \sin\left(\frac{\theta(\vec{k})-\pi}{2}\right) \end{pmatrix} \quad (8.31)$$

The two angle variables α and θ can therefore be related:

$$2\alpha(\vec{k}) = \theta(\vec{k}) - \pi \quad (8.32)$$

This relations, along with the definition of indexed functions

$$m_1(\vec{k}) = \frac{\epsilon(\vec{k})}{\sqrt{\epsilon(\vec{k})^2 + \Delta(\vec{k})^2}} \quad m_2(\vec{k}) = \frac{\Delta(\vec{k})}{\sqrt{\epsilon(\vec{k})^2 + \Delta(\vec{k})^2}} \quad (8.33)$$

allows the topological number to be rewritten as:

$$N_1(k_y) = \frac{1}{2\pi} \int_{-\pi}^{\pi} dk_x \epsilon^{ab} m_a(\vec{k}) \left(\partial_{k_x} m_b(\vec{k}) \right) \quad (8.34)$$

By applying some approximations[27, 28] the integral can then be evaluated as a sum. The gap $\Delta(\vec{k})$ is first rescaled by a factor a :

$$m_1(\vec{k}) = \frac{\epsilon(\vec{k})}{\sqrt{\epsilon(\vec{k})^2 + a^2\Delta(\vec{k})^2}} \quad m_2(\vec{k}) = \frac{a\Delta(\vec{k})}{\sqrt{\epsilon(\vec{k})^2 + a^2\Delta(\vec{k})^2}} \quad (8.35)$$

This procedure is possible because the integral is an integer topological number and thus stable with respect to perturbations. For $a \ll 1$, the functions m_a are constants except in neighborhoods of k_x^0 with $\epsilon(k_x^0, k_y) = 0$:

$$m_1(\vec{k}) \approx \pm 1 \quad m_2(\vec{k}) \approx 0 \quad (8.36)$$

This also suggests a Taylor expansion around the zeros of the energy:

$$\epsilon(\vec{k}) = \partial_{k_x} \epsilon(k_x^0, k_y)(k_x - k_x^0) + h.o. \quad \Delta(\vec{k}) = \Delta(k_x^0, k_y) + h.o. \quad (8.37)$$

Because of the presence of a derivative of m_a in the integrand, the only contributions to the integral are around k_x^0 and can be obtained by direct calculation of the Taylor-expanded product $\epsilon^{ab} m_a(\vec{k}) \left(\partial_{k_x} m_b(\vec{k}) \right)$ as:

$$-\frac{1}{2\pi} \int_{-\pi}^{\pi} dk_x \frac{a\epsilon(\vec{k})\Delta(k_x^0, k_y)}{[\partial_{k_x} \epsilon(k_x^0, k_y)]^2 (k_x - k_x^0)^2 + a^2 \Delta(k_x^0, k_y)^2} \quad (8.38)$$

By letting a go to zero (consistently with the above assumption $a \ll 1$) and evaluating the integral (arctangent function), the contributions become

$$\frac{1}{2} \operatorname{sgn} [\Delta(k_x^0, k_y)] \cdot \operatorname{sgn} [\partial_{k_x} \epsilon(k_x^0, k_y)] \quad (8.39)$$

By summing all the contributions of the zeros of $\epsilon(\vec{k})$ the topological invariant becomes

$$N_1(k_y) = -\frac{1}{2} \sum_{k_x^0; \epsilon(k_x^0, k_y)} \operatorname{sgn} [\Delta(k_x^0, k_y)] \cdot \operatorname{sgn} [\partial_{k_x} \epsilon(k_x^0, k_y)] \quad (8.40)$$

8.3.2 INDEX THEOREM

As shown in [23], in the particular case of a real-gapped Hamiltonian a connection between zero energy states and (bulk) topological invariant already emerges without the need to resort to the more general bulk-edge correspondence, which will be analyzed more closely in section three. The BdG Hamiltonian has chiral symmetry, which means:

$$\{\mathcal{H}(\vec{k}), \hat{\sigma}_y\} = 0 \quad (8.41)$$

where $\hat{\sigma}_y$ is the chiral operator given in the Pauli representation

$$\hat{\sigma}_y = \begin{pmatrix} 0 & -i \\ i & 0 \end{pmatrix} \quad (8.42)$$

whose eigenvalues are ± 1 with corresponding eigenstates

$$\sigma_y^+ = \begin{pmatrix} 1 \\ i \end{pmatrix} \quad \sigma_y^- = \begin{pmatrix} 1 \\ -i \end{pmatrix} \quad (8.43)$$

which, for simplicity, will be called the “positive” and the “negative” eigenstate. It can be shown[14] that the zero energy eigenstate of \mathcal{H} are precisely the eigenstates of $\hat{\sigma}_y$ with eigenvalues ± 1 and the number of zero energy states is related to the topological invariant through the so called *index theorem*:

$$N_1 = n_0^+ - n_0^- \quad (8.44)$$

In this equation n_0^+ (n_0^-) stands for the number of zero energy states corresponding to the positive (negative) eigenvalue of $\hat{\sigma}_y$.

The above equality will be now applied to a couple of concrete examples. First a two-dimensional d_{xy} -wave superconductor will be considered. This type of

8.3 Topological invariants in superconductors

superconductors belongs to the class previously discussed described by real BdG Hamiltonians, where $\epsilon(\vec{k})$ and $\Delta(\vec{k})$ are given as:

$$\epsilon(\vec{k}) = \frac{\vec{k}^2}{2m} - \mu \quad (8.45)$$

$$\Delta(\vec{k}) = \Delta_0 \frac{k_x k_y}{k^2} \quad (8.46)$$

with $\Delta_0 > 0$ and $\mu = \frac{k_F^2}{2m}$. The computation of the topological invariant yields:

$$N_1(k_y) = -\frac{1}{2} \sum_{k_x; \epsilon(\vec{k})=0} \text{sgn}[\Delta(\vec{k})] \cdot \text{sgn}[\partial_{k_x} \epsilon(\vec{k})] \quad (8.47)$$

$$= -\frac{1}{2} \sum_{k_x; k=\pm k_F} \text{sgn}[k_x k_y] \cdot \text{sgn}[k_x/m] \quad (8.48)$$

$$= -\frac{1}{2} \sum_{k_x; k=\pm k_F} \text{sgn}[k_y] \quad (8.49)$$

$$= -\text{sgn}[k_y] = \begin{cases} -1, & \text{for } 0 < k_y < k_F \\ 1, & \text{for } 0 > k_y > -k_F \end{cases} \quad (8.50)$$

On the other hand, the zero energy Andreev bound state is obtained by solving the BdG equation directly[29]. For a semi-infinite superconductor on $x > 0$ it is given as:

$$|u_0(x, k_y)\rangle = C \begin{pmatrix} 1 \\ -i\text{sgn}(k_y) \end{pmatrix} e^{ik_y y} \sin(k_x x) e^{-\frac{m\Delta_0 k_y x}{k_F^2}} \quad (8.51)$$

with a constant C and $k_x = \sqrt{k_F^2 - k_y^2}$. From the form of this wave function one can see that the solution obeys the semiclassical approximation, having a fast oscillating exponential depending on the good quantum number k_y and a fast decaying x -dependent part localized around $x = 0$.

From the form of the solution of the Andreev equation it is clear that the eigenstate is either σ_y^- for positive k_y or σ_y^+ for negative k_y , leading to $n_0^+ - n_0^- = 0 - 1 = -1$ for $0 < k_y < k_F$ or $n_0^+ - n_0^- = 1 - 0 = 1$ for $0 > k_y > -k_F$. The index theorem is therefore confirmed.

As a second example a two-dimensional p_x -wave superconductor will be considered. This type of superconductor is also described by a real BdG Hamiltonian,

but in this case the parameters are:

$$\epsilon(\vec{k}) = \frac{\vec{k}^2}{2m} - \mu \quad (8.52)$$

$$\Delta(\vec{k}) = \Delta_0 \frac{k_x}{\sqrt{\vec{k}^2}} \quad (8.53)$$

By inserting these quantities equation (8.23) the topological invariant can be computed:

$$N_1(k_y) = -\frac{1}{2} \sum_{k_x; \epsilon(\vec{k})=0} \text{sgn}[\Delta(\vec{k})] \cdot \text{sgn}[\partial_{k_x} \epsilon(\vec{k})] \quad (8.54)$$

$$= -\frac{1}{2} \sum_{k_x; k=\pm k_F} \text{sgn}[k_x] \cdot \text{sgn}[k_x/m] \quad (8.55)$$

$$= -\frac{1}{2} \cdot 2 = -1 \quad \text{for } |k_y| < k_F \quad (8.56)$$

For a semi-infinite superconductor on the $x > 0$ half-plane the solution to the Andreev equation is very similar to the previous case, but only the negative eigenstate of the chirality operator is present²:

$$|u_0(x, k_y)\rangle = C \begin{pmatrix} 1 \\ -i \end{pmatrix} e^{ik_y y} \sin(k_x x) e^{-\frac{m\Delta_0 x}{k_F}} \quad (8.57)$$

The index theorem $-1 = N_1 = n_0^+ - n_0^- = 0 - 1 = -1$ is then once again fulfilled³.

8.3.3 TRS BREAKING SUPERCONDUCTORS

This subsection will be devoted to another class of superconductors exhibiting topological properties, namely superconductors whose Hamiltonian breaks time reversal symmetry. Still following the approach of [23], the simplest representative of this type of system is described by a complex, spinless 2×2 -BdG Hamiltonian of the type

$$\mathcal{H} = \frac{1}{2} \sum_{\vec{k}} \left(c_{\vec{k}\uparrow}^\dagger, c_{-\vec{k}\uparrow} \right) \mathcal{H}(\vec{k}) \begin{pmatrix} c_{\vec{k}\uparrow} \\ c_{-\vec{k}\uparrow}^\dagger \end{pmatrix} \quad (8.58)$$

²For a semi-infinite superconductor on the $x < 0$ half-plane, on the other hand, only the positive eigenstate of $\hat{\sigma}_y$ appears.

³The case $|k_y| > k_F$ in both types (d_{xy} - and p_x -superconductor) always trivially fulfills the index theorem, since no zero energy states are present and the superconductor is in the non-topological phase.

8.3 Topological invariants in superconductors

with

$$\mathcal{H}(\vec{k}) = \begin{pmatrix} \epsilon(\vec{k}) & \Delta(\vec{k}) \\ \Delta^*(\vec{k}) & -\epsilon(\vec{k}) \end{pmatrix} \quad (8.59)$$

The spectrum of the superconductor is given by:

$$E(\vec{k}) = \sqrt{\epsilon(\vec{k})^2 + |\Delta(\vec{k})|^2} \quad (8.60)$$

and is also gapped with the norm of the complex-valued gap function. It is straightforward to show that the matrix Hamiltonian is not time reversal invariant. The time inversion operator \mathcal{T} is given in the Pauli representation as $\mathcal{T} = i\sigma_y \mathcal{C}$, where \mathcal{C} denotes complex conjugation and σ_y is the Pauli matrix. In this case, because of the particular form of the Hamiltonian, complex conjugation is equivalent to transposition. With this in mind, one can check if the Hamiltonian breaks time reversal symmetry, and in fact:

$$\mathcal{T}\mathcal{H}^T\mathcal{T}^{-1} = (i\sigma_y)\mathcal{H}^T(-i\sigma) \quad (8.61)$$

$$= i \begin{pmatrix} 0 & -i \\ i & 0 \end{pmatrix} \begin{pmatrix} \epsilon(\vec{k}) & \Delta^*(\vec{k}) \\ \Delta(\vec{k}) & -\epsilon(\vec{k}) \end{pmatrix} i \begin{pmatrix} 0 & i \\ -i & 0 \end{pmatrix} \quad (8.62)$$

$$= \begin{pmatrix} 0 & 1 \\ -1 & 0 \end{pmatrix} \begin{pmatrix} \epsilon(\vec{k}) & \Delta^*(\vec{k}) \\ \Delta(\vec{k}) & -\epsilon(\vec{k}) \end{pmatrix} \begin{pmatrix} 0 & -1 \\ 1 & 0 \end{pmatrix} \quad (8.63)$$

$$= \begin{pmatrix} 0 & 1 \\ -1 & 0 \end{pmatrix} \begin{pmatrix} \Delta(\vec{k})^* & -\epsilon(\vec{k}) \\ -\epsilon(\vec{k}) & -\Delta(\vec{k}) \end{pmatrix} \quad (8.64)$$

$$= \begin{pmatrix} -\epsilon(\vec{k}) & -\Delta(\vec{k}) \\ -\Delta^*(\vec{k}) & \epsilon(\vec{k}) \end{pmatrix} = -\mathcal{H} \quad (8.65)$$

Since in general $\mathcal{H} \neq -\mathcal{H}$, time invariance is not preserved.

The occupied eigenstate of the Hamiltonian is a complex vector with two angle parameters and two phases (twice as many variables) but because of the $U(1)$ -symmetry of the wave function one phase can be eliminated to obtain the following form:

$$|u(\vec{k})\rangle = \begin{pmatrix} \cos(\alpha(\vec{k}))e^{-i\beta(\vec{k})} \\ \sin(\alpha(\vec{k})) \end{pmatrix} \quad (8.66)$$

From the general form of the eigenstate it can be shown by calculating the expectation value of the Pauli matrices[23], that the Hilbert space is isomorphic to the two-dimensional sphere S^2 . The minimal dimension for the realization of such types of superconductors is two and for two-dimensional periodic lattices the Brillouin zone can be folded twice to form a torus T^2 (as seen in the introduction).

Therefore the occupied states $|u(\vec{k})\rangle$ in this case form a mapping $BZ \cong T^2 \rightarrow S^2$. Following a procedure similar to the case of real BdG Hamiltonian, the next step in the topological characterization consists in defining the winding number of this mapping. On the two-dimensional sphere the surface element is given by⁴:

$$d\Omega = \sin(2\alpha)d(2\alpha)d\beta \quad (8.67)$$

The generalization of the concept of the winding number in two-dimension then leads to:

$$N_3 = \frac{1}{4\pi} \int_{-\pi}^{\pi} \int_{-\pi}^{\pi} dk_x dk_y \epsilon^{ij} \sin[2\alpha(\vec{k})] \partial_{k_i} [2\alpha(\vec{k})] \partial_{k_j} [\beta(\vec{k})] \quad (8.68)$$

Following an analogous calculation as the 1D case, N_3 can be recast into a sum[23, 27]:

$$N_3 = -\frac{1}{2} \sum_{(k_x, k_y); \Delta(\vec{k})=0} \text{sgn}[\epsilon(\vec{k})] \text{sgn}[\det(\partial_{k_i} \Delta_j(\vec{k}))] \quad (8.69)$$

with $\Delta_1(\vec{k}) = \text{Re}[\Delta(\vec{k})]$ and $\Delta_2(\vec{k}) = \text{Im}[\Delta(\vec{k})]$. It should be noted that the form of equation (8.69) is remarkably different than the formula obtained for N_1 . Intuitively the distinction is due to the intrinsic different nature of the mappings $S^1 \rightarrow S^1$ and $T^2 \rightarrow S^2$ which connect topologically inequivalent spaces. Curiously, the N_3 invariant is however topologically equivalent to the Chern number developed for the QHE and the two quantities can be mapped into each other. The deeper mathematical understanding of this phenomenon is to research in homotopy theory of algebraic topology and will not be discussed further in the context of this report. The interested read may refer to standard literature in topology, such as Ref. [8, 30].

8.4 GREEN'S FUNCTION FORMALISM

In section two the main properties of topological superconductors have been outlined with the introduction of the topological invariants N_1 and N_3 . Under certain conditions it has also been hinted that the number of gapless zero energy (edge) states can be related to the bulk topological invariant. The aim of this section is to further generalize this relation to obtain a more meaningful bulk-edge correspondence. This will be achieved by manipulating the topological invariants

⁴Analogously to the previous case, there is a sign ambiguity in the value of the wave function that can be solved by either substituting $\alpha \rightarrow 2\alpha$ or restricting the angle parameter to the interval $0 \leq \alpha(\vec{k}) < \pi/2$.

8.4 Green's function formalism

in such a way that will make them match for a particular interface between two topologically inequivalent phases. In order to facilitate the development of the mathematical link between N_1 and N_3 , the problem will be reformulated in the language of Green's functions. The main reference of this section will be a series of papers published by G. R. Volovik in the Nineties which culminated in his book *The Universe in a Helium Droplet* (Ref. [1]).

8.4.1 HAMILTONIANS, SYMMETRIES AND GREEN'S FUNCTIONS

The first subsection is dedicated to the basic feature of the Green's function formalism and its utility in the proof of the bulk-edge correspondence. For non-interacting systems the Green's function is defined as solutions of the operator equation

$$G(\Omega)[\Omega - \mathcal{H}] = \mathbb{1} \quad (8.70)$$

with formal solution:

$$G(\Omega, \vec{k}) = [\Omega - \mathcal{H}]^{-1} \quad (8.71)$$

It should be pointed out that, as a mean to avoid real singularities in the Green's function, the frequency Ω will be set to be purely imaginary, *i.e.*

$$\Omega = i\omega \quad (8.72)$$

with $\omega \in \mathbb{R}$. At zero frequency ($\Omega = 0$) the Green's function is simply the inverse of the Hamiltonian:

$$G(0, \vec{k}) = [-\mathcal{H}]^{-1} \quad (8.73)$$

For the case of a one-dimensional system of free electrons with Hamiltonian $\mathcal{H} = \frac{p^2}{2m}$ the Green's function is readily obtained by means of a Fourier transform:

$$(\Omega - \mathcal{H})G = \mathbb{1} \quad (8.74)$$

$$\iff (i\omega + \frac{\partial_x^2}{2m})G = 1 \quad (8.75)$$

$$\iff \frac{1}{2\pi} \int dp \left(i\omega + \frac{\partial_x^2}{2m} \right) G(p) e^{ipx} = \frac{1}{2\pi} \int dp e^{ipx} \quad (8.76)$$

$$\iff \int dp \left(i\omega - \frac{p^2}{2m} \right) G(p) e^{ipx} = \int dp e^{ipx} \quad (8.77)$$

$$\implies G(p) = \frac{1}{i\omega - \frac{p^2}{2m}} \approx \frac{1}{i\omega - v_F(p - p_F)} \quad (8.78)$$

where v_F is the Fermi velocity and p_F the Fermi momentum. As expected, equation (8.78) has the form of the formal solution (8.71).

Because of equation (8.73), all the symmetries of the Hamiltonian are directly inherited by its Green's function at zero frequency and can further extend to Green's functions at arbitrary frequency[31]. Going one step further, the symmetries of the Green's function remain valid even in the presence of interaction[31]; nevertheless, this report will always focus on superconductors where the interactions are negligible. The relevant generic discrete symmetries of the Hamiltonians of non-interacting topological insulating systems can be divided in three distinct categories, which correspond to as many physical constraints. All of these symmetries can be described by (antiunitary) operators which can be implemented as matrices satisfying $U^\dagger U = \pm 1$. Depending on the presence or absence of these symmetries and the sign of $U^\dagger U = \pm 1$ the Hamiltonian can be classified in ten distinct classes[22], which are reported in table 8.2. The first of these operations is time reversal symmetry (TRS) which is defined as:

$$U_T^\dagger \mathcal{H}^* U_T = \mathcal{H}, \quad \text{with } U_T^\dagger U_T = \pm 1 \quad (8.79)$$

The second is charge conjugation, also known as particle hole symmetry (PHS):

$$U_C^\dagger \mathcal{H}^* U_C = -\mathcal{H}, \quad \text{with } U_C^\dagger U_C = \pm 1 \quad (8.80)$$

The third and last symmetry is called chiral or sublattice symmetry (SLS). It takes its name from its realization as the symmetry operation of exchanging the sign of wave functions on all sites of a sublattice in a bipartite lattice and can be interpreted as the product of both TRS and PHS. Thus, it can be implemented as:

$$\Sigma^\dagger \mathcal{H} \Sigma = -\mathcal{H}, \quad \text{with } \Sigma = U_C^* U_T \quad (8.81)$$

Nevertheless, even in the absence of both TRS and PHS, SLS can still be present[22, 31]. As mentioned before, the Green's function are subjected to the same symmetries of the Hamiltonian. The constraints above applied to the Green's function $G(\Omega)$ then become[31]:

$$TRS : \quad U_T^\dagger G^T(\Omega) U_T = G(\Omega) \quad (8.82)$$

$$PHS : \quad U_C^\dagger G^T(-\Omega) U_C = -G(\Omega) \quad (8.83)$$

$$SLS : \quad \Sigma^\dagger G(-\Omega) \Sigma = -G(\Omega) \quad (8.84)$$

One is naturally led to wonder what the advantage of the Green's formulation is. The next subsection will answer this question by introducing topological invariants in terms of Green's functions: their mathematical form will then be used to prove a special case of the Bulk-Edge correspondence.

8.4 Green's function formalism

8.4.2 GREEN'S FUNCTIONS AND TOPOLOGICAL INVARIANTS

G. R. Volovik defined the topological invariant N_1 , in the general case of a matrix Hamiltonian with extra degrees of freedom such as spin indices, band indices etc., as[1, 31]:

$$N_1(k_y) = \text{Tr} \int_{-\infty}^{\infty} \frac{d\omega}{2\pi i} G^{-1} \partial_{\omega}(G) \quad (8.85)$$

where ω is a real variable such that $\Omega = i\omega$ and G^{-1} is the inverse of G : $\sum_j G_{ij}^{-1} G_{jl} = \delta_{il}$. The letters Tr indicate the full trace over states and spin or band indices. The quantity N_1 can be edited using some mathematical tools borrowed from quantum field theory:

$$N_1 = \text{Tr} \int_{-\infty}^{\infty} \frac{d\omega}{2\pi i} G^{-1} \partial_{\omega}(G) \quad (8.86)$$

$$= \text{Tr} \int_{-\infty}^{\infty} \frac{d\omega}{2\pi i} \partial_{\omega} [\log G] \quad (8.87)$$

$$= \int_{-\infty}^{\infty} \frac{d\omega}{2\pi i} \partial_{\omega} [\text{Tr}(\log G)] \quad (8.88)$$

$$= \int_{-\infty}^{\infty} \frac{d\omega}{2\pi i} \partial_{\omega} [\log(\det G)] \quad (8.89)$$

$$= \sum_n \int_{-\infty}^{\infty} \frac{d\omega}{2\pi i} \partial_{\omega} (\log \lambda_n) \quad (8.90)$$

$$= \frac{1}{2\pi i} \sum_n \log(\lambda_n) \Big|_{-\infty}^{+\infty} \quad (8.91)$$

In the second equality the integrand was rewritten as a logarithmic derivative. In the third equality the linearity of the trace and in the fourth the identity $\log(\det \hat{O}) = \text{Tr}(\log \hat{O})$ for an operator \hat{O} were used. In the fifth equality the determinant was rewritten in his spectral or Lehmann decomposition $\det G = \prod_n \lambda_n$ with the eigenvalues $\lambda_n = \frac{1}{\Omega - \epsilon_n}$, where ϵ_n are the energy eigenvalues of the Hamiltonian, exploiting equation (8.71).

Since the logarithm evaluated at infinity is not well-defined in the field of real numbers, the integral has to be interpreted as the limit of a path-integral on the complex plane. For negative energies $\epsilon_n < 0$ (bound states) the contour is closed in semicircle in the upper half plane, while for positive energies $\epsilon_n > 0$ the path is located in the lower half-plane. The integrand is

$$\partial_{\omega} \log \lambda_n = \partial_{\omega} [-\log(i\omega - \epsilon_n)] = -\frac{i}{-\omega - \epsilon_n} = -\frac{1}{\omega + i\epsilon_n} \quad (8.92)$$

and is holomorphic except for a pole at $\omega = -i\epsilon_n$. The path integral over the arch in figure 8.5 drops to zero in the limit of an infinite radius.

Nevertheless, the immediate application of the residue theorem is hindered by the slow decay of the integrand, which implies that the complex integral over the real axis is improper. Therefore, its Cauchy principal value has to be determined:

$$\mathcal{P} \left(-\frac{1}{2\pi i} \int_{\mathbb{R}} \frac{dz}{z + i\epsilon_n} \right) = -\frac{1}{2\pi i} \left(\oint_{\gamma(R)} \frac{dz}{z + i\epsilon_n} - \int_{\text{arc}} \frac{dz}{z + i\epsilon_n} \right) \quad (8.93)$$

The contour integral can be evaluated with the residue theorem:

$$-\frac{1}{2\pi i} \oint_{\gamma(R)} \frac{dz}{z + i\epsilon_n} = \frac{-1}{2\pi i} 2\pi i I(\gamma, -i\epsilon_n) \text{Res} \left(\frac{1}{z + i\epsilon_n}, -i\epsilon_n \right) \quad (8.94)$$

$$= -(-\text{sgn}[\epsilon_n]) = \text{sgn}[\epsilon_n] \quad (8.95)$$

where $I(\gamma, -i\epsilon_n)$ indicates the index (winding number) of the path γ which is either 1 or -1 depending on which half-plane the contour is closed in and the residue is computed as:

$$\text{Res} \left(\frac{1}{z + i\epsilon_n}, -i\epsilon_n \right) = \lim_{z \rightarrow -i\epsilon_n} (z + i\epsilon_n) \frac{1}{z + i\epsilon_n} = 1 \quad (8.96)$$

By parametrizing the arc as $[0, \pi] \rightarrow \mathbb{C}$, $t \mapsto z = Re^{it}$ for the contour integration in the upper-half plane ($\epsilon_n < 0$), the integral over the arc gives:

$$\frac{1}{2\pi i} \int_{\text{arc, UHP}} \frac{dz}{z + i\epsilon_n} = \frac{i}{2\pi i} \int_0^\pi \frac{dt}{1 + \frac{i\epsilon_n}{Re^{it}}} \xrightarrow{R \rightarrow \infty} \frac{1}{2\pi} \int_0^\pi dt = \frac{1}{2} \quad (8.97)$$

A similar parametrization $[0, \pi] \rightarrow \mathbb{C}$, $t \mapsto z = Re^{-it}$ for the arc in the lower-half plane ($\epsilon_n > 0$) gives:

$$\frac{1}{2\pi i} \int_{\text{arc, LHP}} \frac{dz}{z + i\epsilon_n} = \frac{-i}{2\pi i} \int_0^\pi \frac{dt}{1 + \frac{i\epsilon_n}{Re^{-it}}} \xrightarrow{R \rightarrow \infty} \frac{-1}{2\pi} \int_0^\pi dt = -\frac{1}{2} \quad (8.98)$$

Combining both cases into equation (8.93) one finally obtains:

$$-\frac{1}{2\pi i} \int_{-\infty}^{\infty} \frac{d\omega}{\omega + i\epsilon_n} = \mathcal{P} \left(-\frac{1}{2\pi i} \int_{\mathbb{R}} \frac{dz}{z + i\epsilon_n} \right) \quad (8.99)$$

$$= -\frac{1}{2\pi i} \left(\oint_{\gamma(R)} \frac{dz}{z + i\epsilon_n} - \int_{\text{arc}} \frac{dz}{z + i\epsilon_n} \right) \quad (8.100)$$

$$= \text{sgn}[\epsilon_n] - \frac{1}{2} \text{sgn}[\epsilon_n] \quad (8.101)$$

$$= \frac{1}{2} \text{sgn}[\epsilon_n] \quad (8.102)$$

so that the topological number N_1 can be rewritten as:

$$N_1(k_y) = \frac{1}{2} \sum_n \text{sgn}[\epsilon_n(k_y)] \quad (8.103)$$

8.4 Green's function formalism

i.e. as the net difference between positive- and negative-valued eigenvalues ϵ_n . Clearly the topological index can only be an integer. It is important to note that N_1 changes discontinuously only if a particular eigenvalue $\tilde{\epsilon}_n$ crosses zero as a function of some other parameter (e.g. k_y or external parameters). In a non-interacting, gapped system (e.g. superconductor) an increase in the number of positive eigenvalues (which can be interpreted as an excitation) forces the gap to close somewhere. These considerations can be visualized in figure 8.6 which shows a sketch of the energy spectrum for a topological superconductor with non-trivial topological number N_1 .

In terms of the Green's function the topological invariant N_3 takes the form[1, 31]:

$$N_3 = \frac{\epsilon_{\alpha\beta\gamma}}{6} \text{tr} \int_{-\infty}^{\infty} d\omega \int \frac{d^2k}{(2\pi)^2} G^{-1}(\partial_{k_\alpha} G) G^{-1}(\partial_{k_\beta} G) G^{-1}(\partial_{k_\gamma} G) \quad (8.104)$$

where now the trace tr is over matrix indices (spin etc.) of the Green's function in momentum space $G_{ab}(\Omega, \vec{k})$ and G^{-1} is a matrix inverse of G : $\sum_b G_{ab}^{-1}(\Omega, \vec{k}) G_{bc}(\Omega, \vec{k}) = \delta_{ac}$. The indices α, β, γ are to be chosen from $\{0, 1, 2\}$ and the frequency is rewritten as $k_0 = \omega$.

8.4.3 BULK-EDGE CORRESPONDENCE REVISITED

In this subsection a particular one-dimensional interface between two-dimensional superconducting regions of different topological numbers (but of described by the same Hamiltonian \mathcal{H}) will be considered. The superconductors will extend to infinity in the y -direction (so that translational invariance is preserved) and will be connected along the x -direction. For simplicity, the interface will be assumed to be located at $x = 0$. A sketch of this system is presented in figure 8.7. For this arrangement, the bulk-edge correspondence was formulated in 1992 by Volovik[1] as following:

If two domains separated by a straight 1D domain wall have different values of N_3 , then there are zero-energy excitations on the domain wall (“edge states”). Their “spectral flow” at different k_y values is related to the difference $N_3^L - N_3^R$:

$$N_1(\Lambda) - N_1(-\Lambda) = N_3^L - N_3^R \quad (8.105)$$

The introduction of a domain wall between the two neighboring superconductors has several consequences. First of all, the translational invariance is broken in the x -direction, so that the Hamiltonian \mathcal{H} , the corresponding Green's function

G and their parameters change (smoothly) with x . At large values of x , *i.e.* far away from the interface, the Hamiltonian and the Green's function return to their bulk values and become x -independent. Because of the broken translational invariance, the momentum k_x is no longer a good quantum number and the real inverse of the Green's function $\tilde{G}^{-1}(\Omega, -i\partial_x, k_y, x)$ is distinct from the “bulk” inverse $G^{-1}(\Omega, k_x, k_y, x)$. In particular, the inverse of the Green's function *at* the interface is not the same as the inverse of the Green's function inside the bulk, but the two coincide for big enough values of x : $\tilde{G}^{-1}(\Omega, \vec{k}, x) \xrightarrow{x \rightarrow \pm\infty} G^{-1}(\Omega, \vec{k})$. Furthermore, since topological invariants can only take integer values, the bulk topological number N_3 changes abruptly from N_3^L to N_3^R at the interface.

The topological invariant N_3 is defined in terms of the Green's function in momentum space, which is obtained from the real space Green's function by Fourier transforming in space and time. Nevertheless, the broken invariance in x -direction renders the transformation possible only for time and the y -coordinate of the position vector $\vec{r} = (x, y)$:

$$G(\underbrace{t_1 - t_2}_{\Delta t}, \vec{r}_1, \vec{r}_2) \xrightarrow{\mathcal{F}(\Omega)} G(\Omega, \vec{r}_1, \vec{r}_2) \xrightarrow{\mathcal{F}(k_y)} G(\Omega, x_1, x_2, k_y) \quad (8.106)$$

Here \mathcal{F} indicates the Fourier transform operator. In order to obtain a reciprocal space Green's function which is a function of the full momentum vector $\vec{k} = (k_x, k_y)$, the k_x coordinate must be somehow decoupled from the x -variable. This is achieved with the so called *Wigner transformation* \mathcal{W} :

$$G(\Omega, x_1, x_2, k_y) \xrightarrow{\mathcal{W}(k_x)} G(\Omega, \vec{k}, x) \quad (8.107)$$

which is realized as a Fourier transformation in the relative coordinate r between the x -coordinates of the vectors \vec{r}_1 and \vec{r}_2 , *i.e.*

$$G(\Omega, \vec{k}, x) = \int dr G\left(\Omega, x + \frac{r}{2}, x - \frac{r}{2}, k_y\right) e^{ik_x r} \quad (8.108)$$

where

$$\begin{cases} x = \frac{x_1 + x_2}{2} \\ r = x_1 - x_2 \end{cases} \quad (8.109)$$

The k_x coordinate (conjugate to r) can be thought of as periodic and assimilated with k_y in \vec{k} . With the newfound Green's function $G(\Omega, \vec{k}, x)$ now it is possible to define a *local*, x -dependent bulk topological invariant:

$$N_3(x) = \frac{\epsilon_{\alpha\beta\gamma}}{6} \text{tr} \int_{-\infty}^{\infty} d\omega \int \frac{d^2 k}{(2\pi)^2} G^{-1}(\partial_{k_\alpha} G) G^{-1}(\partial_{k_\beta} G) G^{-1}(\partial_{k_\gamma} G) \quad (8.110)$$

8.4 Green's function formalism

with $\sum_b G_{ab}^{-1}(\Omega, \vec{k}, x)G_{bc}(\Omega, \vec{k}, x) = \delta_{ac}$.

At this point, to prove the bulk-edge correspondence, the topology of the bulk, codified in N_3 , must be related to the zero-energy states at the boundary, which can be computed via N_1 thanks to equation (8.103). In fact, by constructing the difference

$$\Delta N_1 = [N_1(k_y = \Lambda) - N_1(k_y = -\Lambda)] \quad (8.111)$$

one can immediately see from figure 8.6 that if $\Delta N_1 \neq 0$ then a zero energy state must exist.

In order to relate N_1 to N_3 the former topological invariant must be brought in the same form as the latter. Assuming a weak x -dependence it is possible to relate \tilde{G}^{-1} and G^{-1} via their Wigner transforms using the *Moyal product expansion*:

$$\int dx_2 \tilde{G}^{-1}(x_1, x_2)G(x_2, x_3) = \delta(x_1 - x_3) \quad (8.112)$$

$$\xrightarrow{\text{Wigner transform}} 1 \stackrel{(*)}{=} \tilde{G}^{-1}(k_x, x)G(k_x, x) + \frac{1}{2i} \left(\partial_x \tilde{G}^{-1} \partial_{k_x} G - \partial_{k_x} \tilde{G}^{-1} \partial_x G \right) + h.o. \quad (8.113)$$

$$\partial_x (*) : 0 = \partial_x \tilde{G}^{-1} G + \tilde{G}^{-1} \partial_x G + h.o. \implies \partial_x \tilde{G}^{-1} \stackrel{(\star)^1}{=} -\tilde{G}^{-1} (\partial_x G) G^{-1} \quad (8.114)$$

$$\partial_{k_x} (*) : 0 = \partial_{k_x} \tilde{G}^{-1} G + \tilde{G}^{-1} \partial_{k_x} G + h.o. \implies \partial_{k_x} \tilde{G}^{-1} \stackrel{(\star)^2}{=} -\tilde{G}^{-1} (\partial_{k_x} G) G^{-1} \quad (8.115)$$

By inserting $(\star)^1$ and $(\star)^2$ in $(*)$ and considering only dominant terms, one obtains a relation between the two inverses:

$$\boxed{\tilde{G}^{-1} = G^{-1} + \frac{1}{2i} (G^{-1} (\partial_x G) G^{-1} G (\partial_{k_x} G) G^{-1} - G^{-1} (\partial_{k_x} G) G^{-1} G (\partial_x G) G^{-1})} \quad (8.116)$$

Noting that the trace over the states with given k_y can be written as

$$\int dx \tilde{G}^{-1}(\Omega, x, k_y, x) \partial_\omega [G(\Omega, x, k_y, x)] = \int \frac{dx dk_x}{2\pi} \tilde{G}^{-1}(\Omega, k_x, k_y, x) \partial_\omega [G(\Omega, k_x, k_y, x)] \quad (8.117)$$

the product expansion of equation (8.116) can be then inserted in equation (8.85), leading to:

$$N_1(k_y) = \text{tr} \int \frac{dx dk_x d\omega}{8\pi^2} [G^{-1} (\partial_x G) G^{-1} G (\partial_{k_x} G) G^{-1} (\partial_\omega G) - G^{-1} (\partial_{k_x} G) G^{-1} G (\partial_x G) G^{-1} (\partial_\omega G)] \quad (8.118)$$

which can be more compactly written in index notation as:

$$N_1(k_y) = \sum_{\alpha\beta\gamma} \epsilon_{\alpha\beta\gamma} \text{tr} \int \frac{dx dk_x d\omega}{24\pi^2} G^{-1} \partial_\alpha G G^{-1} \partial_\beta G G^{-1} \partial_\gamma G \quad (8.119)$$

Now that both topological invariants have the same form, it is possible to relate them. For starters, N_1 and N_3 can be interpreted as fluxes over a three-dimensional surface in a four-dimensional space spanned by (ω, k_x, k_y, x) . For N_1 , k_y is held fix while the other variable are integrated over. On the other hand, the flux given by N_3 (equation (8.110)) is obtained by integrating over k_x , k_y and ω while keeping x fix. The situation is illustrated in figure 8.8. Since the infinite planes at $k_y = \Lambda$ and $k_y = -\Lambda$ (giving rise to the flux $\frac{1}{2}[N_1(\Lambda) - N_1(-\Lambda)]$) in the two-dimensional space spanned by x and k_y can be continuously deformed into the equivalent sphere $S(k_y, x)$, one can invoke Gauss's theorem (in four dimensions) and equate the fluxes through the two surfaces. The same construction can be done for the infinite planes at $x = L$ and $x = -L$ corresponding to the flux difference $N_3(L) - N_3(-L)$. Thus, the bulk-edge correspondence follows immediately from the equality of the fluxes:

$$|N_1(\Lambda) - N_1(-\Lambda)| = |N_3(L) - N_3(-L)| \quad (8.120)$$

The bulk-edge correspondence is a very useful tool for extracting information about the zero-energy modes from the bulk properties of a superconductor and vice versa. As an example, a topological superconductor on a lattice of N sites (whose spectrum is depicted in figure 4) can once again be considered. From equation (8.103) the spectral flow is computed to be

$$N_1(\Lambda) - N_1(-\Lambda) = \frac{1}{2} \sum_n \text{sgn}[\epsilon_n(\Lambda)] - \frac{1}{2} \sum_n \text{sgn}[\epsilon_n(-\Lambda)] \quad (8.121)$$

$$= \frac{1}{2}[N + 1 - (N - 1)] - \frac{1}{2}[N - N] \quad (8.122)$$

$$= \frac{1}{2}[1 - (-1)] = 1 \quad (8.123)$$

where (as shown in figure 8.6) one eigenvalue was brought up to the upper band for positive k_y ($+\Lambda$), while the eigenvalue distribution remains symmetric for negative k_y ($-\Lambda$). This is - strictly speaking - a forbidden procedure in a lattice theory because of the violation of the Nielsen-Ninomiya theorem[32, 33, 34], which forbids the creation of isolated chiral particles. Nevertheless, this is the standard procedure to compute the spectral flow.

8.5 Summary and Conclusion

In this case the bulk-edge correspondence predicts that such a zero energy mode can be obtained for an interface between two superconductors whose topological numbers differ by one. One possible configuration for a class described by a \mathbb{Z}_2 topological index would therefore be a boundary between a topologically non-trivial superconductor ($N_3 = 1$) and vacuum or a topological superconductor in its trivial phase ($N_3 = 0$).

The bulk-edge correspondence can however also be used in the opposite direction to determine the number of edge states for given bulk configuration around the domain wall. For instance, from the previous paragraph, it is clear the at the boundary of a topological superconductor with vacuum there can only be one mode crossing the zero-energy. In chiral p -wave superconductors it is customary to realize domain walls between topological phases with topological numbers $N_3^L = 3$ and $N_3^R = -3$ (or vice versa) such that there must be $N_3^L - N_3^R = 6$ edge states closing the gap between the bulks at the interface. In the same fashion, a chiral p -wave superconductor would host 3 edge states at its boundary with a non-topological material.

It must be pointed out, however, that the knowledge gained from the bulk-edge correspondence is limited to the number of modes crossing the zero-energy level and does not offer more insight in the actual behavior of these modes. The spectral flow for a zero-energy mode crossing the k_y axis once or three times is in fact the same, as it can be judged by looking at figure 8.9. Albeit with limitations, the bulk-edge correspondence is an important concept in the study of the zero-energy states in topological superconductors.

8.5 SUMMARY AND CONCLUSION

This report provided a brief insight in the physics of topological superconductors. First the phenomenon known as quantum Hall effect was introduced and briefly discussed. The experimentally observed quantization of the Hall conductance could be attributed to the existence of a discrete quantity - named Chern number C_1 - written as the integral over the Brillouin zone of the Berry curvature $\partial_{k_i} \mathcal{A}_j(\vec{k}) = i \sum_{E_n < E_F} \partial_{k_i} \langle u_n(\vec{k}) | \partial_{k_j} u_n(\vec{k}) \rangle$, which is a mapping induced by the occupied states $|u_n(\vec{k})\rangle$ of the system. The topological Chern number was found to have the form of a winding number, therefore assuming only integer values and being invariant under small perturbations. The analogy between the microscopic description of the QHE and BCS superconductors - specifically the presence of gapped bulk state and gapless edge states - suggested the extension of the concept of topological invariant to the latter.

TOPOLOGICAL SUPERCONDUCTORS [PAOLO MOLIGNINI]

Following the analogy with QHE, topological invariants N_1 and N_3 were defined for BdG superconductors with real and complex gap function, respectively. Both quantities were first written as winding numbers (*i.e.* integrals) of the mapping of the Brillouin zone to the Hilbert space given by the occupied states. Subsequently, with a series of mathematical manipulation, they could be recast as sums over node points of the spectrum. For the specific case of real-gapped Hamiltonians, an index theorem was formulated, relating the topological index N_1 to the difference in the number of eigenstates of the chirality operator with different eigenvalues. The validity of the index theorem was then confirmed for two different examples: a d_{xy} -wave superconductor and a p_x -wave superconductor. The index theorem was explained to be a particular case of a broader-encompassing bulk-edge correspondence, which claims that edge states are found whenever the topological number changes in space (*i.e.* at boundaries or topological defects). In the last section the Green's function formalism for topological superconductors was introduced with the aim of proving a special case of the bulk-edge correspondence. In the case at hand, two topologically inequivalent two-dimensional regions of a superconductor were separated by a straight one-dimensional domain wall located at $x = 0$. The spectral flow $\frac{1}{2}[N_1(\Lambda) - N_1(-\Lambda)]$ (number of zero-energy modes in the spectrum) at the boundary between the two topologically inequivalent phases of the superconductor was then claimed to be related to the bulk topological indices to the left and right of the interface with the help of the equation $\frac{1}{2}[N_1(\Lambda) - N_1(-\Lambda)] = N_3(L) - N_3(-L)$. In order to prove this formula, a redefinition of the topological invariants as integrals of Green's functions and their derivatives was necessary. Then some quantum field theoretical results were applied to transform the topological number N_1 to a form similar to that found using the winding number formalism. In this form the spectral flow was shown to characterize the presence of zero-energy states. In a second moment, Wigner transformations and Moyal product expansions were utilized to recast both topological numbers N_1 and N_3 as equivalent k_y -respectively x -dependent fluxes through three-dimensional planes in a four-dimensional space spanned by frequency ω , momentum \vec{k} and the x -coordinate. Exploiting Gauss's divergence theorem, eventually, the fluxes were shown to be identical and the bulk-edge correspondence could thereby be proved. To conclude the discussion, some uses - alongside examples - of the bulk-edge correspondence were presented, showing that it can be a very handy tool in determining the topological structure of a superconductor.

8.5 Summary and Conclusion

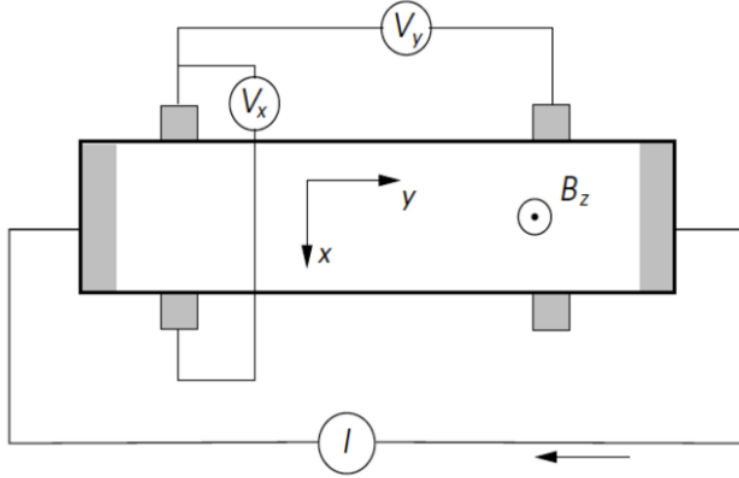


Figure 8.1: Schematics of an experimental setup used to probe the electric conductivity in the classical and quantum Hall effect. The current flows in the positive y -direction, while the magnetic field is applied perpendicularly in the z -direction. The Hall voltage V_x is measured across the sample. Image taken from Ref. [16]

	IQH state	superconducting state
Bulk	Gapped (Landau level)	Gapped (Cooper pair)
Edge	Chiral gapless edge state	Gapless Andreev Bound state

Table 8.1: Characteristics of quantum Hall and superconducting states in the two-dimensional bulk and at the edge (boundary). Both phenomena are described by a gapped spectrum in the bulk and by a gapless, bound state at the edge. Ref. [23].

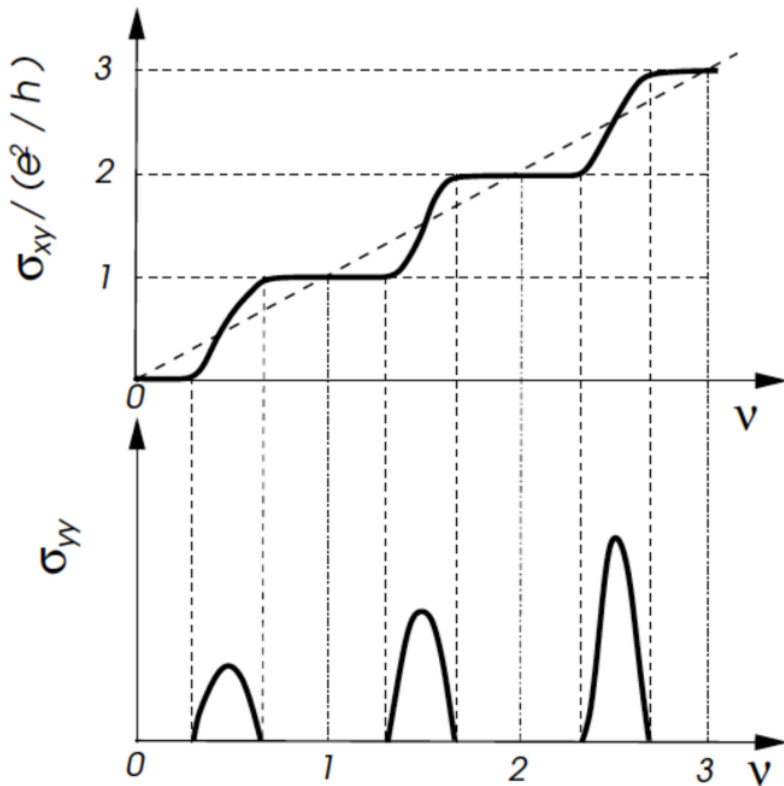


Figure 8.2: Graphical behavior of transversal (σ_{xy}) and longitudinal (σ_{yy}) conductivity as a function of the “filling factor” ν , which turns out to be the topological Chern number. The Chern number can be written as a winding number and is therefore forced by topological arguments to take integer values only. As a result, the Hall conductivity is quantized in integer values as well. Figure taken from Ref. [16]

8.5 Summary and Conclusion

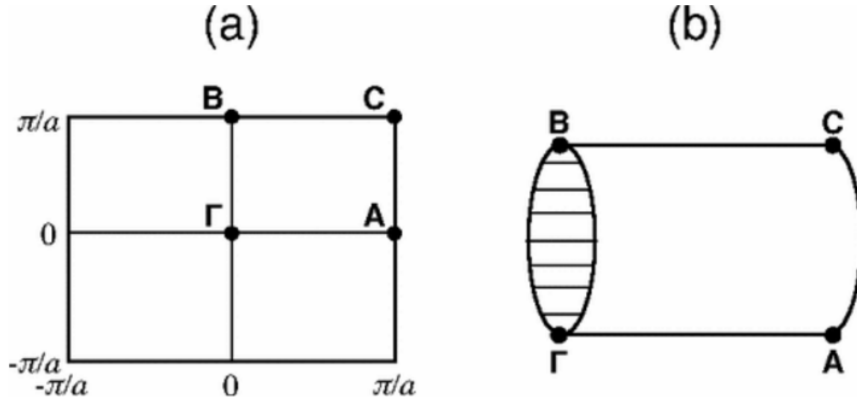


Figure 8.3: For a two-dimensional system, the doubly periodic Brillouin zone can be folded into a cylinder, which in turn can be closed to form a torus. Figure taken from Ref. [18]

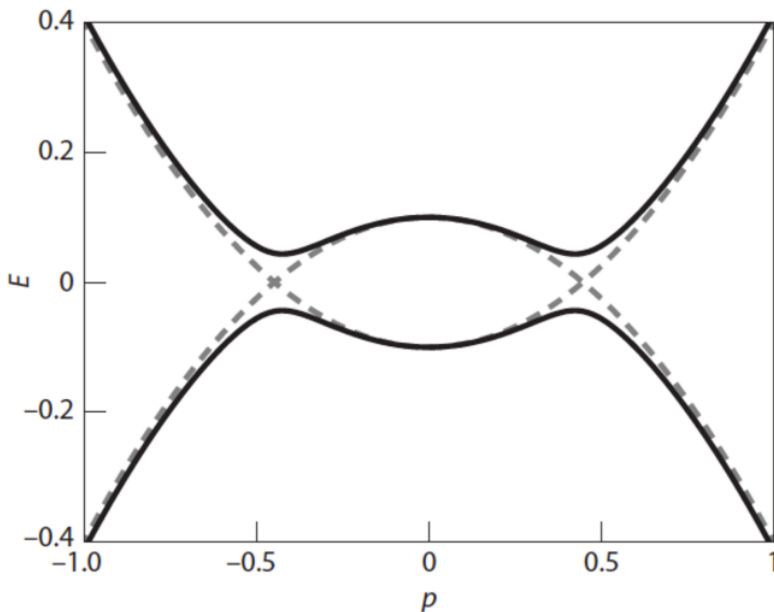


Figure 8.4: Graphs of the energy spectrum $E_{\pm}(p) = \sqrt{\epsilon(p)^2 + |\Delta|^2 p^2}$ for a p -wave superconductor described by a generalized BCS theory. The functions are written in terms of the momentum $p = \hbar k$. The dotted line depicts the case of a vanishing gap, while the solid line corresponds to a non-zero gap $|\Delta| = \mu = 0.1$. Figure taken from Ref. [19].

		TRS	PHS	SLS	d=1	d =2
Standar (Wigner-Dyson)	A (unitary)	0	0	0	-	\mathbb{Z}
	AI (orthogonal)	+1	0	0	-	-
	AII (symplectic)	-1	0	0	-	\mathbb{Z}_2
Chiral (sublattice)	AIII (chiral unitary)	0	0	1	\mathbb{Z}	-
	BDI (chiral orthogonal)	+1	+1	1	\mathbb{Z}	-
	CII (chiral symplectic)	-1	-1	1	\mathbb{Z}	-
BdG	D	0	+1	0	\mathbb{Z}_2	\mathbb{Z}
	BDI	0	-1	0	-	\mathbb{Z}
	DIII	-1	-1	1	\mathbb{Z}_2	\mathbb{Z}_2
	CI	+1	-1	1	-	-

Table 8.2: Classification of single particle Hamiltonians based on the presence or absence of time-reversal symmetry (TRS), particle-hole (or charge conjugation) symmetry (PHS) and sublattice (or chiral) symmetry (SLS). The presence of symmetries is characterized by either +1 for operators squaring to +1 or -1 for operators squaring to -1. The absence of the symmetry is denoted with a 0. The last two columns refer to the equivalence classes of topologically inequivalent ground states: for \mathbb{Z}_2 there are only two possible values of the topological invariant, while in the \mathbb{Z} case the topological invariant can assume all possible integer values. Ref. [22].

8.5 Summary and Conclusion

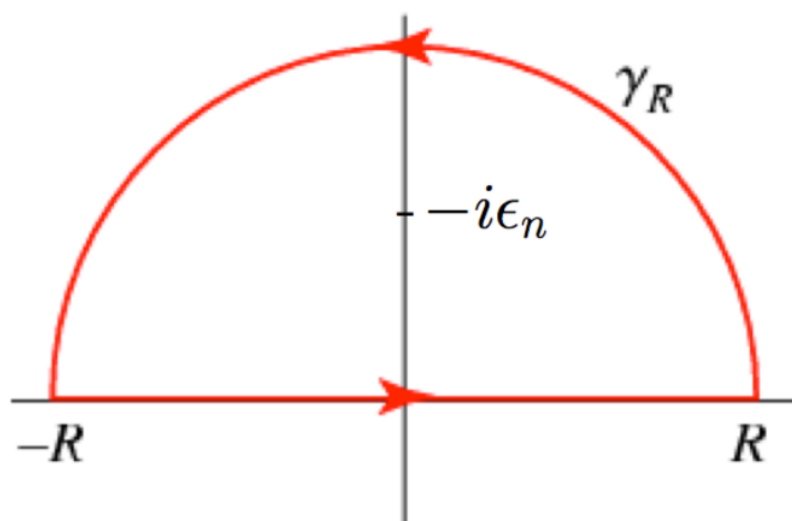


Figure 8.5: Graphical depiction of the contour integral used to evaluate equation (8.90) for the case of negative eigenvalues. For the case $\epsilon_n > 0$ the path γ_R must be closed in the lower half-plane.

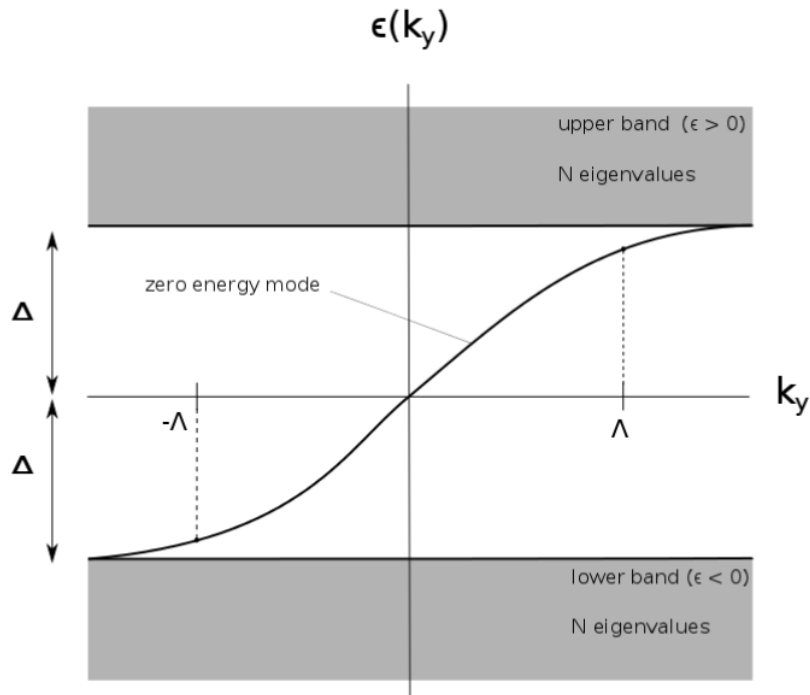


Figure 8.6: Sketch of a possible energy spectrum as a function of the momentum k_y for a non-trivial topological superconductor on a lattice of N sites. Because of the particle-hole description of the BdG Hamiltonian, there are $2N$ eigenvalues in total. If the system were non-topological, the eigenvalues would be equally distributed between positive- (excited states) and negative-valued (occupied states). For a non-trivial topological superconductor there must be an “excess” of positive or negative eigenvalues, which imply a non-zero topological invariant N_1 . Every mode is in principle a function of k_y and in the presence of zero-energy states at least one must cross (or touch) the $\epsilon = 0$ axis. If the topological N_1 is to change discontinuously as a function of k_y , then the edge mode can join the upper and the lower band together effectively closing the gap along its path.

8.5 Summary and Conclusion

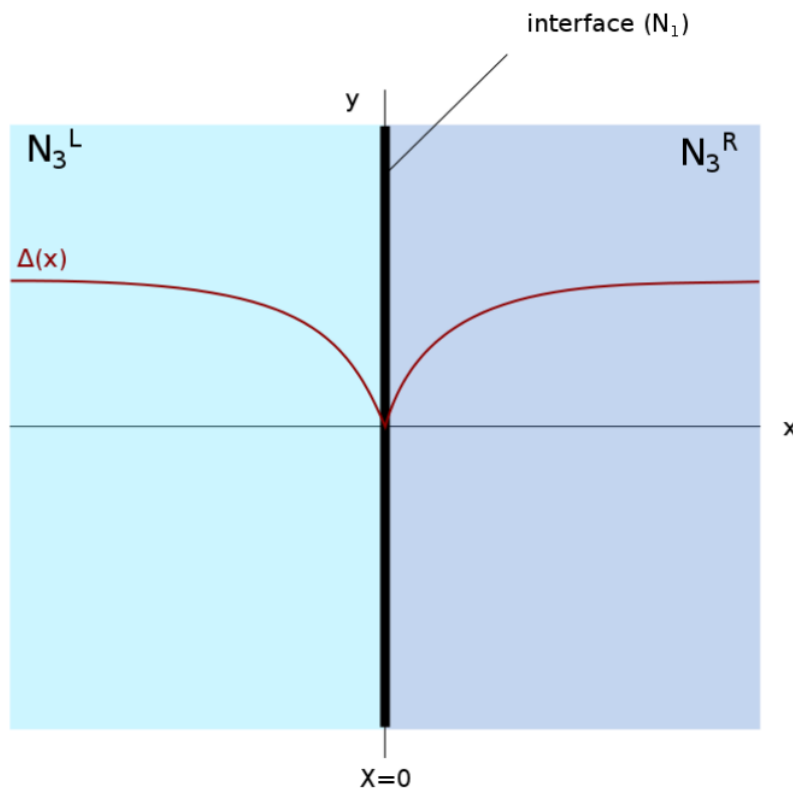


Figure 8.7: Sketch of the interface between two different topological phase of the same superconductor. The interface is a straight, one-dimensional line located at $x = 0$ and its topology is coded in the topological invariant N_1 . The regions to the left and right are the superconducting bulks and are characterized by topological numbers N_3^L and N_3^R , respectively. If $N_3^L \neq N_3^R$ the bulk-edge correspondence predicts the existence of zero energy states located at the domain wall, which forces the gap function $\Delta(x)$ to drop to zero at the interface.

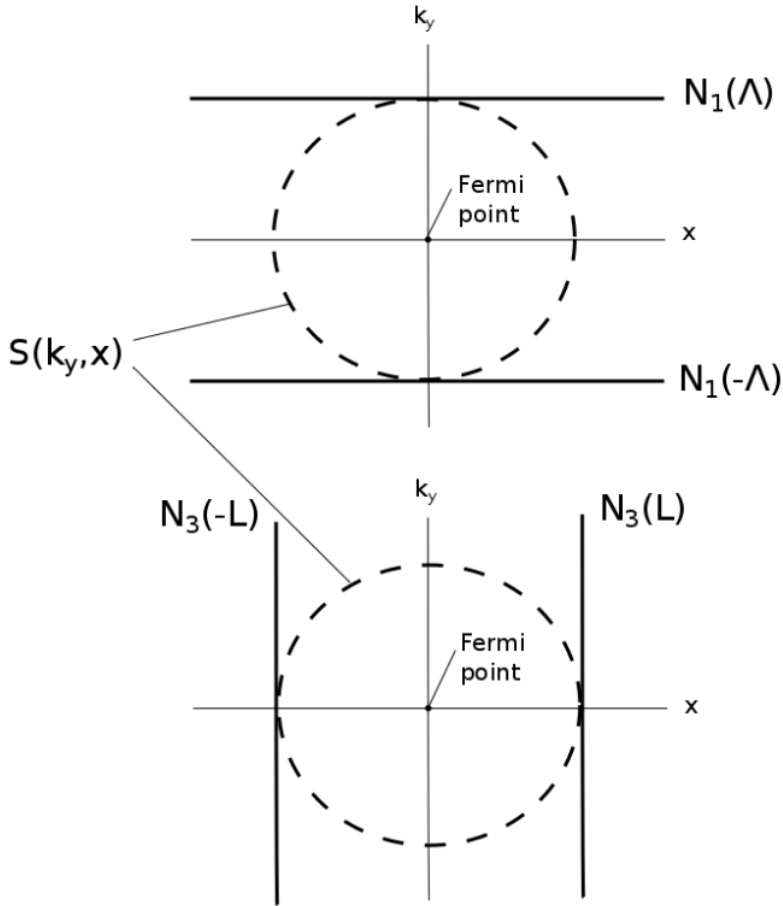


Figure 8.8: Graphical depiction of the topological invariants N_1 and N_3 as fluxes through three-dimensional surfaces in the four-dimensional (ω, k_x, k_y, x) space. The vertical lines in the first graph depict the surfaces which N_1 goes through, while the horizontal lines in the second graph represent the surfaces corresponding to the flux N_3 . The dimensions corresponding to the frequency ω and the momentum k_x are omitted since they are always integrated out. Because of Gauss's divergence theorem, the flux through the two vertical lines is the same as the flux through the sphere $S(k_y, x)$ around the Fermi point (singularity) $(\omega, k_x, k_y, x) = (0, 0, 0, 0)$. The same equality applies to the horizontal lines. In that way the fluxes N_1 and N_3 can be seen as equivalent.

8.5 Summary and Conclusion

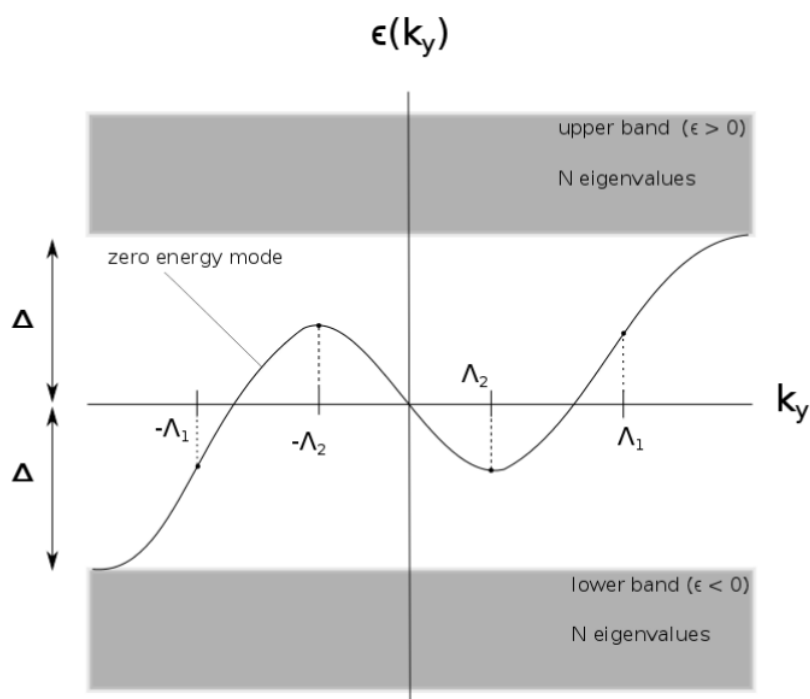


Figure 8.9: Sketch of another possible zero-energy mode for a topological superconductor at the boundary with vacuum or a non-topological material. Any choice of pairs $k_y = \Lambda$, $k_y = -\Lambda$ will lead to the same spectral flow. In the end, $|N_1(\Lambda) - N_1(-\Lambda)|$ is a quantity describing the difference in the number of zero crossings with positive and negative slope.

BIBLIOGRAPHY

- [1] G. E. Volovik, *The Universe in a Helium Droplet* (Oxford University Press, Oxford, 2003).
- [2] K. Klitzing, G. Dorda, and M. Pepper, Phys. Rev. Lett **45** (6), 494 (1980).
- [3] M. Z. Hasan and C. L. Kane, Rev. Mod. Phys. **82**, 3045 (2010).
- [4] X.-L. Qi and S.-C. Zhang, Physics Today **63** (1), 33 (2010).
- [5] D. J. Thouless, M. Kohmoto, M. P. Nightingale, and M. den Nijs, Phys. Rev. Lett **49**, 405 (1982).
- [6] P. W. Anderson, *Basic notions of condensed matter physics* (Westview press, Boulder, CO, 1997).
- [7] L. D. Landau and E. M. Lifshitz, *Statistical Physics* (Pergamon Press, Oxford, 1980).
- [8] J. R. Munkres, *Topology* (Prentice Hall, 1975).
- [9] X.-L. Qi and S.-C. Zhang, Rev. Mod. Phys. **83**, 1057 (2011).
- [10] S.-C. Zhang, Physics **1**, 6 (2008).
- [11] M. König, S. Wiedmann, C. Brüne, A. Roth, H. Buhmann, L. Molenkamp, X.-L. Qi, and S.-C. Zhang, Science **318**, 766 (2007).
- [12] A. Roth, C. Brüne, H. Buhmann, L. W. Molenkamp, J. Maciejko, X.-L. Qi, and S.-C. Zhang, Science **325**, 294 (2009).
- [13] Y. L. Chen, Phys. Rev. Lett. **105**, 266401 (2010).
- [14] T. Sato, K. Segawa, H. Guo, K. Sugawara, S. Souma, T. Takahashi, and Y. Ando, Phys. Rev. Lett. **105**, 136802 (2010).
- [15] E. Hall, Amer. J. Math. **2** (3), 287 (1879).

BIBLIOGRAPHY

- [16] M. Sigrist, *Solid state theory* (2014).
- [17] Q. Niu, D. J. Thouless, and Y.-S. Wu, Phys. Rev. B **31** (6), 3372 (1985).
- [18] A. M. Essin and J. E. Moore, Phys. Rev. B **76**, 165307 (2007).
- [19] B. A. Bernevig and T. L. Hughes, *Topological insulators and topological superconductors* (Princeton University Press, 2013).
- [20] D. Yoshioka, *The Quantum Hall Effect* (Springer Verlag, Berlin, 2002).
- [21] X.-L. Qi, L. Hughes, S. Raghu, and S.-C. Zhang, Phys. Rev. Lett. **102**, 187001 (2009).
- [22] A. P. Schnyder, S. Ryu, A. Furasaki, and L. A., Phys. Rev. B **78**, 195125 (2008).
- [23] Y. Tanaka, M. Sato, and N. Nagaosa, Journal of Phys. Soc. of Japan **81**, 011013 (2012).
- [24] M. Sigrist and K. Ueda, Rev. Mod. Phys. **63**, 239 (1991).
- [25] S.-K. Yip, Superlattices and Microstructures **25** (1999).
- [26] N. B. Kopnin, *Theory of superconductivity (lecture notes)*, Helsinki University of Technology (2004).
- [27] M. Sato, Y. Tanaka, K. Yada, and T. Yokoyama, Phys. Rev. B **83**, 224511 (2011).
- [28] M. Sato, Phys. Rev. B **79**, 214526 (2009).
- [29] C. R. Hu, Phys. Rev. Lett. **72**, 1526 (1994).
- [30] E. Spanier, *Algebraic Topology* (Springer Verlag, Berlin, 1994).
- [31] V. Gurarie, Phys. Rev. B **83**, 085426 (2011).
- [32] H. B. Nielsen and M. Ninomiya, Phys. Lett. B **105**, 219 (1981).
- [33] H. B. Nielsen and M. Ninomiya, Nucl. Phys. B **185**, 20 (1981).
- [34] H. B. Nielsen and M. Ninomiya, Nucl. Phys. B **193**, 173 (1981).

CHAPTER 9

TOPOLOGICAL SUPERCONDUCTORS

LENNART SCHMIDT

SUPERVISOR: ADRIEN BOUHON

This report takes a look at different aspects of topological superconductors. In a first part - using representation theory - the possible gap-functions for a superconductor on a square lattice are classified according to their behaviour under the symmetry of D_{4h} . In a second part the topological numbers for a simple tight-binding-like Hamiltonian for a 1D-Kitaev-chain and a 2D-square-lattice are calculated. The results are checked by numerically simulating these models. For the 1D-Kitaev-chain the point of view of Majorana fermions is discussed.

9.1 INTRODUCTION

Both symmetry and topology play an important role in modern physics. Symmetry, in particular, plays an important and useful role in solid state physics and has been used for a wide variety of phenomena - see the book by Dresselhaus [1].

In a first part this report will use representation theory and symmetry aspects to classify the possible forms of the gap function of general BCS theory following [2] and [3]. Here the example D_{4h} will be taken to illustrate the aspects of representation theory used in order to find general forms of gap functions that obey the symmetry of a square lattice.

In recent years topological states have been of particular interest in solid state

9.2 Symmetry classifications of gap functions

physics. Starting from the quantum hall effect and topological insulators physicists then also applied topological methods to the theory of superconductors.

This report will look at two example Hamiltonians: a 1D-Kitaev-chain and a 2D-model on a square lattice both with BCS-like superconducting terms whose Hamiltonians can be found in [4]. For both models the topological properties of the bulk are studied according to the formulas given in [5]. For the 1D-wire the connection to the existence of Majorana fermions - as was first proposed by Kitaev, see [6] - at the end of the chain is discussed. In both models a numerical implementation confirms the general structure that is predicted by topology.

9.2 SYMMETRY CLASSIFICATIONS OF GAP FUNCTIONS

The mathematics of group theory yield a very general and useful tool to classify physical systems according to their underlying symmetry. This has been especially true for solid state physics, where the point group of the of a given material determines the symmetry of the system. Using representation theory one can then make qualitative statements, i.e. label the eigenstates of the system according to the underlying symmetry. For quantitative information one however needs a physical model as symmetry alone does not determine these. In this section we want to explore the use of representation theory in the context of superconductors, in particular apply it to the gap function of general BCS theory.

9.2.1 EIGENFUNCTIONS AND REPRESENTATIONS

In order to motivate the use of representation theory we recap the well-known fact, that for an eigenvalue problem the eigenfunction spaces of all the eigenvalues form an irreducible representation of the symmetry group of the equation. As an example we use the familiar Schrödinger equation:

$$\mathcal{H}\varphi = E\varphi. \quad (9.1)$$

Let $\{\mathcal{R}_a\}$ be the symmetry group of the Hamiltonian, i.e. we have $[\mathcal{H}, \mathcal{R}_a] = 0$. Then applying an element of the symmetry group on the eigenvalue problem yields:

$$E(\mathcal{R}_a\varphi) = \mathcal{R}_a\mathcal{H}\varphi = \mathcal{H}(\mathcal{R}_a\varphi). \quad (9.2)$$

Thus the symmetry operator \mathcal{R}_a mixes the states φ with the same eigenvalue E . If the state φ is non-degenerate, then \mathcal{R}_a just adds a phase and it can immediately be seen - by applying multiple \mathcal{R}_i - that φ then spans a one-dimensional

irreducible representation of the symmetry group.

If however the eigenvalue E is l -fold degenerate, i.e. we have a vector of eigenfunctions $\varphi = (\varphi_1, \dots, \varphi_l)$, the symmetry operator \mathcal{R}_a now generally mixes between those states:

$$\mathcal{R}_a \varphi = \Gamma(\mathcal{R}_a) \varphi, \quad (9.3)$$

where $2\Gamma(\mathcal{R}_a)$ is a matrix describing the action of \mathcal{R}_a . Applying multiple \mathcal{R}_i again immediately shows that this forms a representation of the symmetry group, i.e. the span of φ_i forms a l -dimensional irreducible representation of the symmetry group of \mathcal{H} .

This connection between the eigenspaces of an eigenvalue problem and the representations of the underlying symmetry group can also be used in the context of gap functions and superconductivity. The linearized gap equation in general BCS theory is given by (see e.g. [2]):

$$\frac{1}{(1.14\beta_c\epsilon_c)} \Delta_{s_1 s_2} = - \sum_{s_3 s_4} \langle V_{s_1 s_2 s_3 s_4} \Delta_{s_4 s_3} \rangle. \quad (9.4)$$

This can be viewed as an eigenvalue problem with the gap function as the eigenfunction. Thus in complete analogy to the discussion above the gap functions live in irreducible representations of the group of the underlying symmetry of the superconductor. This will be discussed more closely later in this report.

9.2.2 PARAMETRIZATION OF GAP FUNCTION IN SPIN SPACE

The gap function in general BCS-theory is given by

$$\Delta_{\vec{k};ss'} = - \sum_{\vec{k}';s_3 s_4} V_{\vec{k}\vec{k}';ss's_3 s_4} b_{\vec{k}';s_3 s_4} \quad (9.5)$$

where $b_{\vec{k},s_3 s_4} = \langle c_{-\vec{k}s_3} c_{\vec{k}s_4} \rangle$ is the mean field of the cooper pairs and $V_{\vec{k}\vec{k}';ss's_3 s_4} = \langle -\vec{k}, s; \vec{k}, s' | \hat{V} | -\vec{k}', s_3; \vec{k}', s_4 \rangle$ is the pair scattering matrix element [2]. The gap function can therefore be written as a 2×2 -matrix in spin space:

$$\hat{\Delta}_{\vec{k}} = \begin{pmatrix} \Delta_{\vec{k},\uparrow\uparrow} & \Delta_{\vec{k},\uparrow\downarrow} \\ \Delta_{\vec{k},\downarrow\uparrow} & \Delta_{\vec{k},\downarrow\downarrow} \end{pmatrix}. \quad (9.6)$$

With this matrix we then obtain the energy spectrum $E_{\vec{k}} = \sqrt{\xi_{\vec{k}}^2 + |\Delta_{\vec{k}}|^2}$, where we have the magnitude of the gap

$$|\Delta_{\vec{k}}|^2 = \frac{1}{2} \text{Tr} \left(\hat{\Delta}_{\vec{k}}^\dagger \hat{\Delta}_{\vec{k}} \right). \quad (9.7)$$

9.2 Symmetry classifications of gap functions

For a more detailed derivation of this see [2].

In the following chapters we will distinguish between singlet- and triplet-pairing states for the cooper pairs in the gap function. We can do this since we look at systems with inversion symmetry and thus parity is well-defined. In order to find a useful parametrization of the gap matrix $\hat{\Delta}_{\vec{k}}$ we split its components into orbital and spin part of the wavefunction as usual:

$$\Delta_{\vec{k};ss'} = \Phi(\vec{k})\chi_{ss'}. \quad (9.8)$$

As the constituents of cooper pairs - i.e. the electrons - are fermions, we have to acquire an overall minus sign when exchanging them. Therefore:

$$-\Delta_{-\vec{k},s's} \stackrel{!}{=} \hat{\mathcal{P}}\Delta_{\vec{k},ss'} = \hat{\mathcal{P}}(\Phi(\vec{k})\chi_{ss'}) = \pm\Phi(-\vec{k})\hat{\mathcal{P}}(\chi_{ss'}), \quad (9.9)$$

where \mathcal{P} means permutation of the fermions and the \pm distinguishes between even and odd parity of the orbital part of the wavefunction. In order to satisfy this we obtain two separate cases:

- Even Parity: $\Phi(\vec{k}) = \Phi(-\vec{k}) \Leftrightarrow \chi_{s_3s_4}$ is singlet
- Odd Parity: $\Phi(\vec{k}) = -\Phi(-\vec{k}) \Leftrightarrow \chi_{s_3s_4}$ is triplet.

Let's now look at those two cases.

SINGLET-STATE PAIRING: Here we have $\Delta_{\vec{k},ss'} = -\Delta_{\vec{k},s's}$. This immediately means that the diagonal terms of our gap matrix have to be zero, i.e. $\Delta_{\vec{k},ss} = 0$. As this is a singlet we only have one degree of freedom $\Psi(\vec{k})$ in the off-diagonal entries of the gap matrix. We can therefore write:

$$\hat{\Delta}_{\vec{k}} = \begin{pmatrix} 0 & \Psi(\vec{k}) \\ -\Psi(\vec{k}) & 0 \end{pmatrix} = i\hat{\sigma}_y\Psi(\vec{k}),$$

(9.10)

where $\Psi(\vec{k}) = \Psi(-\vec{k})$ ensures the evenness in the orbital variable \vec{k} [2]. The gap magnitude (9.7) is then conveniently given by $|\Psi(\vec{k})|^2$. For singlet pairing we therefore only have to know $\Psi(\vec{k})$.

TOPOLOGICAL SUPERCONDUCTORS [LENNART SCHMIDT]

TRIPLET-STATE PAIRING: Here we have $\Delta_{\vec{k},ss'} = \Delta_{\vec{k},s's}$. Here the diagonal terms do not have to be zero and we have three degrees of freedom as we are in a triplet state [2]. A convenient choice of parametrization - one that transforms like a spin triplet under rotations - is given by:

$$\hat{\Delta}_{\vec{k}} = \begin{pmatrix} -d_x(\vec{k}) + id_y(\vec{k}) & d_z(\vec{k}) \\ d_z(\vec{k}) & d_x(\vec{k}) + id_y(\vec{k}) \end{pmatrix} = i \left(\vec{d}(\vec{k}) \cdot \hat{\vec{\sigma}} \right) \hat{\sigma}_y, \quad (9.11)$$

where $\vec{d}(\vec{k}) = -\vec{d}(-\vec{k})$ ensures oddness in the orbital variable \vec{k} [2]. Again the gap magnitude (9.7) is conveniently given by $|\vec{d}(\vec{k})|^2$. For a more detailed look at the reasons for this parametrization see [7].

The goal of this exercise is now to label the functions $\Psi(\vec{k})$ and $\vec{d}(\vec{k})$ according to the symmetry classes of the underlying. In order to do this we will use representation theory.

9.2.3 REPRESENTATION THEORY AND DOUBLE GROUP

In the following chapter we will use the square as a simple example to illustrate the features of representation theory. The point group of a square is denoted - in Schönflies notation - by D_{4h} .

THE GROUP D_{4h}

The point group for a square consists of all symmetry operations that leave a square invariant. It is easiest to see all these symmetry operations sequentially.

The most obvious form of transformations are the rotations about the axis normal to the basis plane (i.e. the \hat{z} -direction) through the center of the square. Here we can have four-fold rotations or a two-fold rotations, which leave the square including the colors in figure 9.1 invariant. This yields the group

$$C_4 = \{E, C_4(2), C_2\}. \quad (9.12)$$

When we ignore the colors and just want to leave the square as a whole invariant, we can include reflections along the planes σ_d and σ_v , which cut the base plane (see figure 9.1). This yields the group

$$C_{4v} = \{E, C_4(2), c_2, \sigma_v(2), \sigma_d(2)\}. \quad (9.13)$$

Alternatively we can rotate along the axis C'_2 and C''_2 that are traced by the previous planes of reflection (again see figure 9.1). (**Note:** This is only a different

9.2 Symmetry classifications of gap functions

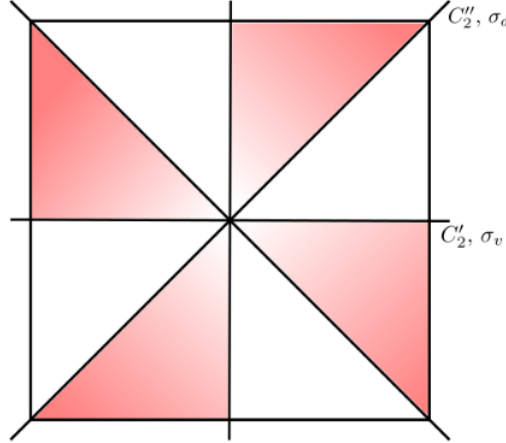


Figure 9.1: Visualization for the symmetry operations of a square; C_4 leaves this square invariant, including colors; neglecting the colors we can add reflections σ_d, σ_v and out of plane rotations C_2'', C_2'

operation to the reflections σ_d and σ_v when looking at out of plane vectors!) This group is then given by

$$D_4 = \{E, C_4(2), C_2, C_2'(2), C_2''(2)\}. \quad (9.14)$$

Either way we can obtain the desired group D_{4h} if we include a basal plane reflection σ_h or respectively the inversion operator I :

$$D_{4h} = C_{4v} \otimes \sigma_h = D_4 \otimes I \quad (9.15)$$

$$= \{E, C_4(2), C_2, C_2'(2), C_2''(2), I, S_4(2), \sigma_h, \sigma_v(2), \sigma_d(2)\}, \quad (9.16)$$

where S_n denotes an improper rotation defined via $S_n \equiv C_n \otimes \sigma_h$. Note that this is equivalent to saying that any improper rotation is some proper rotation times inversion, i.e. $S_n = C(\alpha) \otimes I$. However, in general, the proper rotation does not rotate by the same amount as the improper one (e.g. $S_6 = C_3^{-1} \otimes I!!$).

The group D_{4h} then contains all possible symmetry transformation of a square, i.e. **16** elements forming **10** conjugacy classes¹. This is the group that we will use as an illustrative example from now on.

REPRESENTATION THEORY - A QUICK RECAP

In order to study the structure of the group D_{4h} we look at its representations. For a comprehensive discussion of group theory in physics see [1]. Recall the

¹To quickly recap: the conjugacy classes of a group G are the equivalence classes of the equivalence relation $g_1 \sim g_2$ iff $g_1 = h^{-1}g_2h$ for some $h \in G$, i.e. they are related by conjugation.

definition of a group representation:

Definition:

A representation ρ of a group G on a vector space V is a linear map $\rho : G \rightarrow \text{Aut}(V)$ that maps every element $g \in G$ to a linear, invertible map on V , that respects the group operation, i.e.

$$\rho(g_1 \circ g_2) = \rho(g_1)\rho(g_2), \quad \rho(e) = \mathbb{1} \quad (9.17)$$

From now on we will suppress the ρ in our notation, but it is still implicitly there. Thus every representation of our group D_{4h} is associated with some finite-dimensional (called the dimension of the representation) vector space V . This vector space will be spanned by a set of basis functions, that behave according to the action of the representation. Then the gap function, which lives in such a representation (see section 9.2.1), will consist of those basis functions. Thus finding a suitable basis will give us a general form for our gap function.

If a representation V contains no proper vector subspace, that is invariant under the action of the group, it is called *irreducible*. It is a well-known fact, that any reducible representation of a *finite* group can be decomposed into a direct sum of irreducible representations. Thus it is enough to know the irreducible representations of a given group.

An important and useful formula to find said decomposition is the *projection formula*, given by

$$m_V^{(W)} = \frac{1}{|G|} \sum_{\mathcal{C}} |\mathcal{C}| \cdot \overline{\chi_V(\mathcal{C})} \cdot \chi_W(\mathcal{C}), \quad (9.18)$$

where $m_V^{(W)}$ denotes the multiplicity of irrep V in the rep W , \mathcal{C} are the conjugacy classes of G and χ is the character (i.e. trace of the linear map) in a given representation. A derivation of this formula can be found in Appendix A. Thus knowing the characters of all irreducible reps gives us all the information we need. These can be found in the so called character table and can be found for example in [8]. For D_{4h} we find (in [8]):

9.2 Symmetry classifications of gap functions

D_{4h}	E	$C_4(2)$	C_2	$C'_2(2)$	$C''_2(2)$	I	$S_4(2)$	σ_h	$\sigma_v(2)$	$\sigma_d(2)$
Γ_1^+	1	1	1	1	1	1	1	1	1	1
Γ_2^+	1	1	1	-1	-1	1	1	1	1	-1
Γ_3^+	1	-1	1	1	-1	1	-1	1	1	-1
Γ_4^+	1	-1	1	-1	1	1	-1	1	-1	1
Γ_5^+	2	0	-2	0	0	2	0	-2	0	0
Γ_1^-	1	1	1	1	1	-1	-1	-1	-1	-1
Γ_2^-	1	1	1	-1	-1	-1	-1	1	1	1
Γ_3^-	1	-1	1	1	-1	-1	1	-1	-1	1
Γ_4^-	1	-1	1	-1	1	-1	1	-1	1	-1
Γ_5^-	2	0	-2	0	0	-2	0	2	0	0

This table shows all 10 irreps of D_{4h} and their characters. The character table already exhibits some structure: As we have included the inversion operator in our group, we can label all irreducible representations by their parity, i.e. plus or minus. The plus-type irreps have the same character in the conjugacy classes containing proper rotations (first 5) as in the conjugacy classes containing improper rotations (last 5), whereas the minus-type irreps will acquire a minus sign in the characters of improper classes. Thus it is enough to know the top left quadrant (i.e. the character for the first five representations in the first five conjugacy classes) of the character table as the others are just copies of that quadrant with the proper minus signs attached. Additionally the first column denotes the dimension of the given representation, as this is just the trace of the identity matrix.

CHARACTERS FOR ORBITALS OF FULL ROTATION GROUP

The elemental quasiparticle in superconductors is the Cooper pair, which consists of two electrons. In the atomic limit these electrons live in orbitals which are a basis of irreps of $\mathcal{SO}(3)$, i.e. are given by spherical harmonics Y_l^m . Introducing the periodic potential lowers that symmetry and these irreps might now become reducible, as there are fewer symmetry operations. In order to know how these irreps break down in D_{4h} we need to know the characters of the orbital labeled by angular moment l .

In order to find a suitable formula we take a closer look at the spherical harmonics (see [1]). We know:

$$Y_l^m \propto P_l^m(\cos \theta) e^{im\phi}, \quad (9.19)$$

where P_l^m are the associated Legendre polynomials. Under a rotation the eigenkets $|l, m\rangle$ are mixed in m , but l stays fixed as rotations commute with L^2 , i.e.:

$$\hat{\mathcal{R}}Y_l^m = \sum_{m'} \underbrace{D^{(l)}(R)_{m'm}}_{\text{matrix of rep}} Y_l^{m'}. \quad (9.20)$$

We therefore need to find the trace of $D^{(l)}(R)_{m'm}$. As the quantization axis is arbitrary ([1]) we pick the \hat{z} -axis to be the axis of rotation, thus the rotation only affects ϕ . So for a rotation by angle α (i.e. rotating axis by $-\alpha$):

$$\hat{\mathcal{R}}_\alpha Y_l^m(\theta, \phi) = Y_l^m(\theta, \phi - \alpha) \stackrel{9.19}{=} e^{-im\alpha} Y_l^m(\theta, \phi), \quad (9.21)$$

i.e. in this basis $D^{(l)}(R)_{m'm}$ is just diagonal with entries $e^{-im\alpha}$. We take the trace:

$$\text{Tr} D^{(l)}(\alpha) = \sum_{m=-l}^l e^{-im\alpha} \quad (9.22)$$

$$= e^{-il\alpha} \sum_{m=0}^{2l} e^{im\alpha} \quad (9.23)$$

$$= e^{-il\alpha} \left(\frac{1 - e^{i(2l+1)\alpha}}{1 - e^{i\alpha}} \right) \quad (9.24)$$

$$= \frac{e^{i(l+\frac{1}{2})\alpha} - e^{-i(l+\frac{1}{2})\alpha}}{e^{i\frac{\alpha}{2}} - e^{-i\frac{\alpha}{2}}} \quad (9.25)$$

$$= \frac{\sin((l + \frac{1}{2})\alpha)}{\sin(\frac{\alpha}{2})}. \quad (9.26)$$

We also have to consider what happens for operations including the inversion operator I . Here we have:

$$IY_l^m(\theta, \phi) = Y_l^m(\pi - \theta, \pi + \phi) \quad (9.27)$$

$$\stackrel{9.19}{=} e^{im\pi} (-1)^{m+l} Y_l^m(\theta, \phi) \quad (9.28)$$

$$= (-1)^l Y_l^m(\theta, \phi). \quad (9.29)$$

This means that if we look at operations including inversion we have to add a factor of $(-1)^l$ to the trace. In total this yields for the character of orbital l for a rotation about angle α :

$$\chi_l(\alpha) = \frac{\sin((l + \frac{1}{2})\alpha)}{\sin(\frac{\alpha}{2})},$$

(9.30)

9.2 Symmetry classifications of gap functions

where we add a factor $(-1)^l$ for improper rotations, having previously determined the angle α via splitting $S_n = C(\alpha) \otimes I$ as explained above.

This formula also holds true for half-integer values of l ([1]), as can be seen by looking at the behaviour of spin spaces under rotation.

THE DOUBLE GROUP

The above character table above for D_{4h} only contains representations for integer values of orbital momentum. Since we are dealing with electrons - i.e. fermions - we need to expand our group to encompass half-integer representations as well: Looking at the above character formula for orbitals (9.30) under a 2π -rotation yields (see [1]):

$$\chi_l(\alpha + 2\pi) = \frac{\sin((l + \frac{1}{2})(\alpha + 2\pi))}{\sin(\frac{\alpha+2\pi}{2})} \quad (9.31)$$

$$= \frac{\sin((l + \frac{1}{2})\alpha) \cos((l + \frac{1}{2})2\pi)}{\sin(\frac{\alpha}{2}) \cos(\pi)} \quad (9.32)$$

$$= (-1)^{2l} \chi_l(\alpha). \quad (9.33)$$

Thus we get a minus-sign for half-integer values of l for a rotation by 2π . This is a manifestation of the well-known fact that fermions acquire a minus sign under a full rotation. This implies that for half-integer l a 2π -rotation is **not** the identity, but rather a 4π -rotation is. This means we can have more distinct symmetry operations in our group D_{4h} , as for example a rotation about 3π is not - as previously assumed - the same as a rotation about π . In fact these rotations and the representations associated with them are part of the full rotation group $O(3)$ and by restricting to D_{4h} we arbitrarily singled out the representations corresponding to integer values of l only. We can fix this by reverting this restriction and using the so called *double group* of D_{4h} .

We construct the double group in the following way:

Let \mathcal{R} denote a 2π -rotation, the double group is then given by:

$$G \otimes \mathcal{R} = \{g_1, \dots, g_n; \mathcal{R}g_1, \dots, \mathcal{R}g_n\}. \quad (9.34)$$

This group has by definition twice as many elements (hence the name). For integer values of l the additional elements in the group are redundant, but for half-integer values they are not. As we have a bigger group we will have more conjugacy classes - however not necessarily twice as many, as π -rotations usually do not yield a new class. For a more detailed view of this see [1]. As we have

TOPOLOGICAL SUPERCONDUCTORS [LENNART SCHMIDT]

more conjugacy classes we will necessarily have more irreps since the number of conjugacy classes is equal to the number of irreps (for a motivation of this see Appendix B).

From [8] we take the full character table for the double group:

D_{4h}	E	\overline{E}	$C_4(2)$	$\overline{C_4}(2)$	C_2	$C'_2(4)$	$C''_2(4)$	I	\overline{I}	$S_4(2)$	$\overline{S_4}(2)$	σ_h	$\sigma_v(4)$	$\sigma_d(4)$
Γ_1^+	1	1	1	1	1	1	1	1	1	1	1	1	1	1
Γ_2^+	1	1	1	1	1	-1	-1	1	1	1	1	1	1	-1
Γ_3^+	1	1	-1	-1	1	1	-1	1	1	-1	-1	1	1	-1
Γ_4^+	1	1	-1	-1	1	-1	1	1	1	-1	-1	1	-1	1
Γ_5^+	2	2	0	0	-2	0	0	2	2	0	0	-2	0	0
Γ_1^-	1	1	1	1	1	1	1	-1	-1	-1	-1	-1	-1	-1
Γ_2^-	1	1	1	1	1	-1	-1	-1	-1	-1	-1	-1	1	1
Γ_3^-	1	1	-1	-1	1	1	-1	-1	-1	1	1	-1	-1	1
Γ_4^-	1	1	-1	-1	1	-1	1	-1	-1	1	1	-1	1	-1
Γ_5^-	2	2	0	0	-2	0	0	-2	-2	0	0	2	0	0
Γ_6^+	2	-2	$\sqrt{2}$	$-\sqrt{2}$	0	0	0	2	-2	$\sqrt{2}$	$-\sqrt{2}$	0	0	0
Γ_7^+	2	-2	$-\sqrt{2}$	$\sqrt{2}$	0	0	0	2	-2	$-\sqrt{2}$	$\sqrt{2}$	0	0	0
Γ_6^-	2	-2	$\sqrt{2}$	$-\sqrt{2}$	0	0	0	-2	2	$-\sqrt{2}$	$\sqrt{2}$	0	0	0
Γ_7^-	2	-2	$-\sqrt{2}$	$\sqrt{2}$	0	0	0	-2	2	$\sqrt{2}$	$-\sqrt{2}$	0	0	0

As only non- π -rotations yield new conjugacy classes we only get 4 new classes in the double group of D_{4h} . This in turns yields 4 new irreducible representations corresponding to half-integer values of l . Of particular interest is the representation Γ_6^+ : One obtains this representation simply by plugging in $l = \frac{1}{2}$ into the formula for the characters (9.30). Thus this is how the spin- $\frac{1}{2}$ part behaves in the square. (Alternatively one can obtain the character for Γ_6^+ by looking at how rotations act on the 2-dimensional spin- $\frac{1}{2}$ -space, namely at the matrices $e^{\frac{-iS \cdot \hat{n}\phi}{\hbar}}$). The other additional irreps can be obtained via tensoring Γ_6^+ with any of the previous one-dimensional irreps, as this always yields another irrep. This process is repeated until one has 4 additional irreps as then everything has been determined.

9.2.4 CLASSIFICATION FOR POINT GROUP D_{4h}

With the above tools it is now possible to classify the possible types of gap functions according to the underlying symmetry and its representations. For

9.2 Symmetry classifications of gap functions

tables with the complete results for different groups - including D_{4h} - see [3]. We will first look at spin and orbital degrees of freedom separately. Then assuming a system with *strong spin-orbit coupling* we will tensor the representations of spin and orbital parts and find suitable linear combinations of basis functions for both parts.

SPIN DEGREES OF FREEDOM

As an example we will use representation theory to find the decomposition of the spin degrees of freedom in the representations of D_{4h} . A cooper pair consists out of two electrons, i.e. we have two spin- $\frac{1}{2}$ particles. For D_{4h} the spin- $\frac{1}{2}$ -representation - obtained by plugging in $l = \frac{1}{2}$ into the formula for characters (9.30) - is given by Γ_6^+ . As we have two electrons we tensor two Γ_6^+ -representations and find their decomposition into irreps of D_{4h} using the projection formula (9.18) and the character table above:

$$m_{\Gamma_1^+}^{(\Gamma_6^+ \otimes \Gamma_6^+)} = \frac{1}{32}(1 \cdot 4 + 1 \cdot 4 + 1 \cdot 2 \cdot 2 + 1 \cdot 2 \cdot 2) \quad (9.35)$$

$$+ 1 \cdot 4 + 1 \cdot 4 + 1 \cdot 2 \cdot 2 + 1 \cdot 2 \cdot 2) = 1 \quad (9.36)$$

$$m_{\Gamma_2^+}^{(\Gamma_6^+ \otimes \Gamma_6^+)} = \frac{1}{32}(1 \cdot 4 + 1 \cdot 4 + 1 \cdot 2 \cdot 2 + 1 \cdot 2 \cdot 2) \quad (9.37)$$

$$+ 1 \cdot 4 + 1 \cdot 4 + 1 \cdot 2 \cdot 2 + 1 \cdot 2 \cdot 2) = 1 \quad (9.38)$$

$$m_{\Gamma_5^+}^{(\Gamma_6^+ \otimes \Gamma_6^+)} = \frac{1}{32}(2 \cdot 4 + 2 \cdot 4 + 2 \cdot 4 + 2 \cdot 4) = 1. \quad (9.39)$$

$$(9.40)$$

Thus we get:

$$\boxed{\Gamma_6^+ \otimes \Gamma_6^+ = \Gamma_1^+ \oplus \Gamma_2^+ \oplus \Gamma_5^+.} \quad (9.41)$$

Thus the 4-dimensional representation $\Gamma_6^+ \otimes \Gamma_6^+$ splits into a sum of two 1-dimensional and a 2-dimensional irrep of D_{4h} . This correspond to the singlet- and triplet-pairings of two spin- $\frac{1}{2}$ -particles: The trivial representation Γ_1^+ corresponds to the singlet-state and the sum $\Gamma_2^+ \oplus \Gamma_5^+$ contains the triplet-state. Therefore we tensor with Γ_1^+ for even-parity-states and with $\Gamma_2^+ \oplus \Gamma_5^+$ for odd-parity-states.

Looking at the tables for the irreps of D_{4h} (e.g. in [8]) we find basis functions for the spin space. Γ_1^+ can just be described by a constant $\propto 1$, i.e. for singlet-pairing the spin part is trivial. $\Gamma_2^+ \oplus \Gamma_5^+$ is spanned by angular momentum components S_x, S_y and S_z , i.e. the basis functions behave like a pseudo-vector. In the parametrization of the gap-function for the triplet-state (9.11) we have chosen the \vec{d} -vector s.t. it transforms exactly like the spin triplet (see also [7]), thus the basis functions in spin space for the triplet just correspond to the different entries

of \vec{d} . Thus we have a basis in spin space: trivial for singlet-pairing and $\hat{z} \in \Gamma_2^+$, $\{\hat{x}, \hat{y}\} \in \Gamma_5^+$ for triplet-pairing.

ORBITAL DEGREES OF FREEDOM

For the orbital degrees of freedom we can apply the same machinery: The character for the representation with orbital momentum l (now full integer) is given by equation 9.30. We then use the character table from [8] in conjunction with the projection formula (9.18) to find the decompositions in terms of irreps of D_{4h} . For the first four orbitals this yields:

- **s-wave:** Γ_1^+
- **p-wave:** $\Gamma_2^- \oplus \Gamma_5^-$
- **d-wave:** $\Gamma_1^+ \oplus \Gamma_3^+ \oplus \Gamma_4^+ \oplus \Gamma_5^+$
- **f-wave:** $\Gamma_2^- \oplus \Gamma_3^- \oplus \Gamma_4^- \oplus \Gamma_5^{-\oplus 2}$

The appropriate choice of basis functions can again be found in the tables of [8]. As we assume strong spin-orbit coupling we can not treat the spin- and orbital degrees of freedom separately, but rather we have to tensor them and find suitable linear combinations of these basis functions to find a general form for the gap function.

RESULTS

D-WAVE: For d-wave we have even parity, i.e. we have a spin singlet. Thus we have after tensoring:

$$\Gamma^{\text{Singlet}} \otimes \Gamma^{\text{d-wave}} \cong \Gamma^{\text{d-wave}} = [\Gamma_1^+ \oplus \Gamma_3^+ \oplus \Gamma_4^+ \oplus \Gamma_5^+] \quad (9.42)$$

As the singlet representation is just trivial we do not really need to worry about spin-orbit coupling. In accordance with [3] a suitable set of basis functions (to lowest order in k) is then given by ([8]):

Representation	Basis Functions
Γ_1^+	C (const.)
Γ_3^+	$ k_x^2 - k_y^2 $
Γ_4^+	$k_x k_y$
Γ_5^+	k_x, k_y

9.2 Symmetry classifications of gap functions

Any of these would be a suitable choice for $\Psi(\vec{k})$ in the case of a d-wave-superconductor. In particular, the choice $\Psi(\vec{k}) \propto (k_x^2 - k_y^2)$ is realized in high temperature superconductors. These are then unconventional superconductors with a d-wave symmetry.

P-WAVE: For p-wave we have odd parity, i.e. we work with a spin triplet. Now the tensoring is not trivial and we obtain:

$$\Gamma^{\text{p-wave}} \otimes \Gamma^{\text{Triplet}} = (\Gamma_2^- \oplus \Gamma_5^-) \otimes (\Gamma_2^+ \oplus \Gamma_2^+) = [2\Gamma_1^- \oplus \Gamma_2^- \oplus \Gamma_3^- \oplus \Gamma_4^- \oplus 2\Gamma_5^-] \quad (9.43)$$

Finding suitable basis functions now requires finding linear combinations of products of the basis functions for spin and orbital parts that transform according to the representations of the tensor product. Finding these is essentially a problem of diagonalization. A guide on how to find the coupling coefficients can be found in the introduction of [8]. Alternatively they can be found in various coupling tables, which are listed in [8]. This yields the p-wave results in accordance with [3]:

Representation	Basis Functions
$2\Gamma_1^-$	$k_z \hat{z}$
	$\frac{1}{\sqrt{2}} (k_x \hat{x} + k_y \hat{y})$
Γ_2^-	$\frac{1}{\sqrt{2}} (k_x \hat{y} - k_y \hat{x})$
Γ_3^-	$\frac{1}{\sqrt{2}} (k_x \hat{x} - k_y \hat{y})$
Γ_4^-	$\frac{1}{\sqrt{2}} (k_x \hat{y} + k_y \hat{x})$
$2\Gamma_5^-$	$k_y \hat{z}, -k_x \hat{z}$ $k_z \hat{x}, -k_z \hat{y}$

Here $\hat{x}, \hat{y} & \hat{z}$ again denote the components of the \vec{d} -vector.

Looking - for example - at one of the Γ_5^- representations we can then ask which particular choice in that two-dimensional space is optimal. This can be found by plugging the Ansatz $\vec{d}(\vec{k}) = (\alpha k_x + \beta k_y) \cdot \hat{z}$ into the linearized gap equation of general BCS theory (see [2]):

$$\vec{d}(\vec{k}) = - \sum_{\vec{k}'} V(k \cdot k') \frac{\vec{d}(\vec{k}')}{\xi_{\vec{k}'}} \tanh \frac{\xi_{\vec{k}'}}{2k_b T_c} \quad (9.44)$$

This yields a value for $T_c = T_c(\alpha, \beta)$. The highest T_c corresponds to the biggest gap at zero temperature - as they are linearly related, see [2] - and therefore to

the most likely, optimal state². For this particular choice this calculation yields:

$$d_z(\vec{k}) = k_x \pm ik_y. \quad (9.45)$$

This example is called the *chiral p-wave-state superconductor*, which is believed to be realized in Sr_2RuO_4 .

9.3 TOPOLOGICAL ASPECTS AND NUMERICAL SIMULATIONS

In this chapter we want to consider the topology of the superconductor as a complement to the symmetry aspects. In this vein we use numerical simulations in order to study the topological properties of BCS-like Hamiltonians on a lattice first in 1D and then in 2D. In the following we assume a constant gap, i.e. we do not solve the self-consistent gap equation.

9.3.1 THE INDEX THEOREM

In the following chapters we will discuss the topological numbers in different regimes for specific 1D- and 2D-models of superconductivity. An important and general theorem that we will verify in these examples is the so-called index theorem (see e.g. [5]):

Every topological defect, i.e. boundaries where the topological number shifts, results in bound gapless edge states. The index theorem states that the difference in the topological number in the two different regimes at the topological defect is equal to the spectral flow of the gapless edge states. This means that the total number of edge states connecting the band below the gap with the band above the gap (i.e. increasing the spectral flow by 'one') or vice versa is determined by the topological number of the neighbouring regimes.

For example imagine a boundary between regimes with topological numbers 2 and 1 respectively. The difference in topological number is then 1 and we can expect gapless edge states, in total one more connecting the bottom with the top band and thus increasing the spectral flow by one accordingly.

In the following chapters we can verify this theorem in our numerical results.

²For a more rigorous treatment look at the free energy. Here the condensation energy contributes negatively, so when minimizing the free energy, we pick the state with the largest condensation energy, i.e. the largest gap.

9.3 Topological aspects and numerical simulations

9.3.2 1D: KITAEV-CHAIN

THE HAMILTONIAN

We imagine a 1D chain of lattice sites separated by a distance a and a BCS-like Hamiltonian with both s-wave- and p-wave-pairing (as in [4]):

$$\mathcal{H}_{1D}^{\text{BdG}} = -\mu \sum_{i\sigma} c_{i\sigma}^\dagger c_{i\sigma} - t \sum_{\langle i,j \rangle} c_{i\sigma}^\dagger c_{j\sigma} + V_0 \sum_i c_{i\uparrow}^\dagger c_{i\downarrow}^\dagger c_{i\uparrow} c_{i\downarrow} + \sum_{\langle i,j \rangle} V_{ij} c_{i\uparrow}^\dagger c_{j\downarrow}^\dagger c_{i\uparrow} c_{j\downarrow}. \quad (9.46)$$

From this we use the mean field approach, i.e. we define $\Delta_{ii} = V_0 (\langle c_{i\uparrow} c_{i\downarrow} \rangle + \langle c_{i\downarrow} c_{i\uparrow} \rangle)$ and $\Delta_{ij} = V_{ij} (\langle c_{i\uparrow} c_{j\downarrow} \rangle + \langle c_{i\downarrow} c_{j\uparrow} \rangle)$ and rewrite the BCS-terms in terms of the gap, akin to the calculations done in [2] and [4] in \vec{k} -space:

$$V_0 \sum_i c_{i\uparrow}^\dagger c_{i\downarrow}^\dagger c_{i\uparrow} c_{i\downarrow} \rightarrow \sum_{ij} \left(c_{i\uparrow}^\dagger c_{j\downarrow}^\dagger \Delta_{ii} + c_{i\uparrow} c_{j\downarrow} \Delta_{ii}^* \right) \delta_{ij} \quad (9.47)$$

$$\sum_{\langle i,j \rangle} V_{ij} c_{i\uparrow}^\dagger c_{j\downarrow}^\dagger c_{i\uparrow} c_{j\downarrow} \rightarrow \sum_{ij} \left(c_{i\uparrow}^\dagger c_{j\downarrow}^\dagger \Delta_{ij} + c_{i\uparrow} c_{j\downarrow} \Delta_{ij}^* \right) \delta_{i\pm 1j}. \quad (9.48)$$

Note that by definition we have a symmetric s-wave type gap and an antisymmetric p-wave type gap:

- commuting the fermions in the s-wave type gap yields:

$$\begin{aligned} \Delta_{ii} &= V_0 (\langle c_{i\uparrow} c_{i\downarrow} \rangle - \langle c_{i\downarrow} c_{i\uparrow} \rangle) \\ &= -V_0 (\langle c_{i\downarrow} c_{i\uparrow} \rangle - \langle c_{i\uparrow} c_{i\downarrow} \rangle) \\ &= \Delta_{ii} \end{aligned} \quad (9.49)$$

- whereas commuting the fermions in the p-wave type gap yields:

$$\begin{aligned} \Delta_{ij} &= V_{ij} (\langle c_{i\uparrow} c_{j\downarrow} \rangle + \langle c_{i\downarrow} c_{j\uparrow} \rangle) \\ &= -V_{ji} (\langle c_{j\downarrow} c_{i\uparrow} \rangle + \langle c_{j\uparrow} c_{i\downarrow} \rangle) \\ &= -\Delta_{ji} \end{aligned} \quad (9.50)$$

We then rewrite all the terms in (9.46) in terms of a 2D-spinor that represents a state in the particle-hole space:

- on-site term:

$$\begin{aligned} -\mu \sum_{i\sigma} c_{i\sigma}^\dagger c_{i\sigma} &= -\mu \sum_i c_{i\uparrow}^\dagger c_{i\uparrow} + c_{i\downarrow}^\dagger c_{i\downarrow} \\ &= -\mu \sum_{ij} \left(c_{i\uparrow}^\dagger c_{j\downarrow} + c_{j\downarrow}^\dagger c_{i\uparrow} \right) \delta_{ij} \\ &= \sum_{ij} \begin{pmatrix} c_{i\uparrow}^\dagger & c_{i\downarrow}^\dagger \end{pmatrix} \begin{pmatrix} -\mu \delta_{ij} & 0 \\ 0 & \mu \delta_{ij} \end{pmatrix} \begin{pmatrix} c_{j\uparrow} \\ c_{j\downarrow}^\dagger \end{pmatrix} \end{aligned}$$

- hopping term:

$$\begin{aligned}
 -t \sum_{\langle i,j \rangle \sigma} c_{i\sigma}^\dagger c_{j\sigma} &= -t \sum_{\langle i,j \rangle} \left(c_{i\uparrow}^\dagger c_{j\uparrow} + c_{i\downarrow}^\dagger c_{j\downarrow} \right) \\
 &= -t \sum_{i,j} \left(c_{i\uparrow}^\dagger c_{j\uparrow} + c_{i\downarrow}^\dagger c_{j\downarrow} \right) \delta_{i\pm 1j} \\
 &= \sum_{i,j} \begin{pmatrix} c_{i\uparrow}^\dagger & c_{i\downarrow} \end{pmatrix} \begin{pmatrix} -t\delta_{i\pm 1j} & 0 \\ 0 & t\delta_{i\pm 1j} \end{pmatrix} \begin{pmatrix} c_{j\uparrow} \\ c_{j\downarrow}^\dagger \end{pmatrix}
 \end{aligned}$$

- BCS s-wave term:

$$\sum_{ij} \left(c_{i\uparrow}^\dagger c_{j\downarrow}^\dagger \Delta_{ii} + c_{i\uparrow} c_{j\downarrow} \Delta_{ii}^* \right) \delta_{ij} = \sum_{ij} \begin{pmatrix} c_{i\uparrow}^\dagger & c_{i\downarrow} \end{pmatrix} \begin{pmatrix} 0 & \Delta_{ii} \delta_{ij} \\ \Delta_{ii}^* \delta_{ij} & 0 \end{pmatrix} \begin{pmatrix} c_{j\uparrow} \\ c_{j\downarrow}^\dagger \end{pmatrix}$$

- BCS p-wave term:

$$\sum_{ij} \left(c_{i\uparrow}^\dagger c_{j\downarrow}^\dagger \Delta_{ij} + c_{i\uparrow} c_{j\downarrow} \Delta_{ij}^* \right) \delta_{i\pm 1j} = \sum_{ij} \begin{pmatrix} c_{i\uparrow}^\dagger & c_{i\downarrow} \end{pmatrix} \begin{pmatrix} 0 & \Delta_{ij} \delta_{i\pm 1j} \\ \Delta_{ij}^* \delta_{i\pm 1j} & 0 \end{pmatrix} \begin{pmatrix} c_{j\uparrow} \\ c_{j\downarrow}^\dagger \end{pmatrix}$$

Putting this together yields the Bogoliubov-de-Gennes-Hamiltonian for a 1D-chain of lattice sites:

$$\mathcal{H}_{1D}^{\text{BdG}} = \sum_{ij} \begin{pmatrix} c_{i\uparrow}^\dagger & c_{i\downarrow} \end{pmatrix} \underbrace{\begin{pmatrix} -\mu\delta_{ij} - t\delta_{i\pm 1j} & \Delta_{ii}\delta_{ij} + \Delta_{ij}\delta_{i\pm 1j} \\ \Delta_{ii}^*\delta_{ij} + \Delta_{ji}^*\delta_{i\pm 1j} & \mu\delta_{ij} + t\delta_{i\pm 1j} \end{pmatrix}}_{=: h_{ij}} \begin{pmatrix} c_{j\uparrow} \\ c_{j\downarrow}^\dagger \end{pmatrix} \quad (9.51)$$

$$= \begin{pmatrix} c_{1\uparrow}^\dagger c_{1\downarrow} & \dots & c_{N\uparrow}^\dagger c_{N\downarrow} \end{pmatrix} \begin{pmatrix} h_{11} & \dots & \dots & h_{1N} \\ \vdots & \ddots & & \vdots \\ \vdots & & \ddots & \vdots \\ h_{N1} & \dots & \dots & h_{NN} \end{pmatrix} \begin{pmatrix} c_{1\uparrow} \\ c_{1\downarrow}^\dagger \\ \vdots \\ c_{N\uparrow} \\ c_{N\downarrow}^\dagger \end{pmatrix} \quad (9.52)$$

The terms of the Hamiltonian in (9.51) are visualized on the lattice chain in figure 9.2: We have an on-site chemical potential μ , a tight-binding hopping term with strength t , an on-site superconducting s-wave pairing Δ_s and finally a nearest-neighbour superconducting p-wave pairing Δ_p . We can now solve for the eigenvalues of the big Hamiltonian in (9.52) and look at its energy spectrum. Before doing that we will however have a look at its bulk.

9.3 Topological aspects and numerical simulations

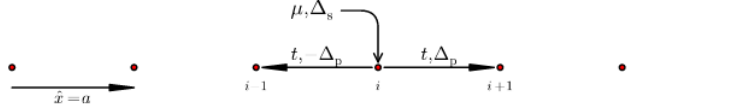


Figure 9.2: 1D-chain of lattice sites having on-site potential μ , tight-binding hopping strength t , s-wave on-site pairing Δ_s and p-wave next-neighbour pairing Δ_p .

TOPOLOGICAL PROPERTIES OF THE BULK

In order to find the topological invariants we assume translational invariance of the quantum chain and Fourier transform the Hamiltonian. As we are then in \vec{k} -space we consider only the bulk and are not looking at any boundaries. Here we only look at a constant p-wave pairing, i.e. we set $\Delta_{ii} = 0$ and $\Delta_{ij} = \pm |\Delta|$ in (9.51). The calculation for s-wave is completely analogous but does not exhibit any interesting topological features. Using translational invariance ,we Fourier-transform by setting:

$$c_i = \frac{1}{\sqrt{N}} \sum_k e^{ix_i k} c_k \quad (9.53)$$

$$c_i^\dagger = \frac{1}{\sqrt{N}} \sum_k e^{-ix_i k} c_k^\dagger, \quad (9.54)$$

and using that we have $\frac{1}{N} \sum_i e^{ix_i(k-k')} = \delta_{kk'}$. Then we obtain:

- on-site term:

$$\begin{aligned} -\mu \sum_i c_i^\dagger c_i &= \frac{-\mu}{N} \sum_{ijkk'} c_k^\dagger c_{k'} e^{-i(kx_i - k'x_j)} \delta_{ij} \\ &= -\mu \sum_k c_k^\dagger c_k \\ &= \sum_k \begin{pmatrix} c_k^\dagger & c_{-k} \end{pmatrix} \begin{pmatrix} -\frac{\mu}{2} & 0 \\ 0 & \frac{\mu}{2} \end{pmatrix} \begin{pmatrix} c_k \\ c_{-k}^\dagger \end{pmatrix} \end{aligned}$$

- hopping-term:

$$\begin{aligned}
 -t \sum_{ij} c_i^\dagger c_j \delta_{i\pm 1j} &= -\frac{t}{N} \sum_{ijkk'} c_k^\dagger c_{k'} e^{-i(x_i k - x_j k')} \\
 &= -t \sum_{kk'} c_k^\dagger c_{k'} \frac{1}{N} \sum_i e^{-ix_i(k-k')} (e^{-iak} + e^{iak}) \\
 &= -2t \sum_k \cos(ka) c_k^\dagger c_k \\
 &= \sum_k \begin{pmatrix} c_k^\dagger & c_{-k} \end{pmatrix} \begin{pmatrix} -t \cos(ka) & 0 \\ 0 & t \cos(-ka) \end{pmatrix} \begin{pmatrix} c_k \\ c_{-k} \end{pmatrix}
 \end{aligned}$$

- BCS p-wave term:

$$\begin{aligned}
 \sum_{ij} (c_i^\dagger c_j^\dagger |\Delta| + c_i c_j |\Delta|) (\pm \delta_{i\pm 1j}) &= \sum_{ijkk'} (c_k^\dagger c_{k'}^\dagger |\Delta| + c_k c_{k'} |\Delta|) \\
 &\quad e^{\pm i(x_i k + x_j k')} (\pm \delta_{i\pm 1j}) \\
 &= 2i \sum_k (\sin(ka) c_k^\dagger c_{-k}^\dagger |\Delta| \\
 &\quad - \sin(ka) c_k c_{-k} |\Delta|) \\
 &= \sum_k \begin{pmatrix} c_k^\dagger & c_{-k} \end{pmatrix} \begin{pmatrix} 0 & 2i \sin(ka) |\Delta| \\ -2i \sin(ka) |\Delta| & 0 \end{pmatrix} \begin{pmatrix} c_k \\ c_{-k}^\dagger \end{pmatrix}
 \end{aligned}$$

We can now shift our basis by an overall phase - without changing the physics since we have $\mathcal{U}(1)$ -gauge invariance - in order to make the gap real. Then we obtain:

$$\boxed{\mathcal{H}_{1D}^{\text{BdG}} = \frac{1}{2} \sum_k \begin{pmatrix} c_k^\dagger & c_{-k} \end{pmatrix} \begin{pmatrix} -\mu - 2t \cos(ka) & -2|\Delta| \sin(ka) \\ -2|\Delta| \sin(ka) & \mu + 2t \cos(ka) \end{pmatrix} \begin{pmatrix} c_k \\ c_{-k}^\dagger \end{pmatrix}.} \quad (9.55)$$

From this expression we can calculate the bulk topological number. For this we use the simplified formula for the topological invariant in 1D derived in [5] (there labeled by w_{1d}):

$$\boxed{N_1 = -\frac{1}{2} \sum_{k, \epsilon(k)=0} \text{sgn}[\Delta(k)] \text{sgn}[\partial_k \epsilon(k)],} \quad (9.56)$$

9.3 Topological aspects and numerical simulations

where $\Delta(k)$ and $\epsilon(k)$ are the entries of the Hamiltonian, i.e. in our case:

$$\mathcal{H}(k) \equiv \begin{pmatrix} \epsilon(k) & \Delta(k) \\ \Delta^*(k) & -\epsilon(k) \end{pmatrix} \quad (9.57)$$

$$= \begin{pmatrix} -\mu - 2t \cos(ka) & -2|\Delta| \sin(ka) \\ -2|\Delta| \sin(ka) & \mu + 2t \cos(ka) \end{pmatrix}. \quad (9.58)$$

Thus calculating the topological invariant requires summing over the zeros of $\epsilon(k)$. Therefore we need:

$$\epsilon(k) = -2t \cos(ka) - \mu = 0. \quad (9.59)$$

This equations has no solutions for $|\mu| > 2t$ as $\cos(ka)$ ranges from -1 to 1 . Therefore we have $N_1 = 0$ in this case.

However for $|\mu| < 2t$ equation (9.59) has two solutions:

$$k_{\pm} = \pm \frac{1}{a} \arccos\left(-\frac{\mu}{2t}\right). \quad (9.60)$$

Here we find the signs of $\partial_k \epsilon(k_{\pm})$ and $\Delta(k_{\pm})$:

- for \mathbf{k}_+ we obtain:

$$\partial_k \epsilon(k_+) = 2ta \sin\left(\arccos\left(\frac{-\mu}{2t}\right)\right) = 2ta \sqrt{1 - \frac{\mu^2}{4t^2}} > 0 \quad (9.61)$$

$$\Delta(k_+) = -2|\Delta| \sin\left(\arccos\left(\frac{-\mu}{2t}\right)\right) = -2|\Delta| \sqrt{1 - \frac{\mu^2}{4t^2}} < 0 \quad (9.62)$$

- for \mathbf{k}_- we obtain:

$$\partial_k \epsilon(k_-) = -2ta \sin\left(\arccos\left(\frac{-\mu}{2t}\right)\right) = -2ta \sqrt{1 - \frac{\mu^2}{4t^2}} < 0 \quad (9.63)$$

$$\Delta(k_-) = 2|\Delta| \sin\left(\arccos\left(\frac{-\mu}{2t}\right)\right) = 2|\Delta| \sqrt{1 - \frac{\mu^2}{4t^2}} > 0. \quad (9.64)$$

Thus the topological number is now given by

$$N_1 = -\frac{1}{2}((-1) \cdot (1) + (1) \cdot (-1)) = 1 \quad (9.65)$$

Summarizing we have two different topological regimes - trivial and non-trivial:

- $|\mu| > 2t \Rightarrow N_1 = 0$ (i.e. we are in the trivial phase)
- $|\mu| < 2t \Rightarrow N_1 = 1$ (i.e. topological phase).

TOPOLOGICAL SUPERCONDUCTORS [LENNART SCHMIDT]

From the index theorem (see for example [4] or [5] or section 9.3.1) we therefore expect to have no zero-energy modes for $|\mu| > 2t$ and one zero-energy mode at every topological defects (e.g. boundaries) for $|\mu| < 2t$.

It can be easily seen that this calculation for s-wave pairing will always lead to $N_1 = 0$: As s-wave pairing is on-site we will have no k -dependence after Fourier-transforming. Thus $\Delta(k)$ will always have the same sign for k_{\pm} and the sum cancels with the alternating sign of $\partial_k \epsilon(k_{\pm})$.

We can now check these mathematical results by implementing this model numerically.

NUMERICAL RESULTS

Taking the Hamiltonian given in equation (9.52) and numerically calculating its eigenvalues yields the energy spectrum of our quantum chain of length N . As we are back in real space and are not using periodic boundaries we therefore have two topological defects, as we have two boundaries separating the quantum chain from the vacuum. Thus - again from the index theorem (section 9.3.1) - we expect two zero-energy modes at the edges in the topological phase $|\mu| < 2t$. This can be seen in figure (9.3): On the left we are in the topological regime - i.e. $N_1 = 1$ - and we observe two zero-energy eigenvalues (marked in red), whereas on the right we are in the trivial phase - i.e. $N_1 = 0$ - and thus we do not find any zero-energy modes.

For the zero-energy modes in the topological phase of p-wave pairing one can also see that they are located - as expected - on the edges of our system, i.e. they are edge states. A visualization of this, i.e. of the absolute value squared of the corresponding eigenstates on the lattice, can be seen in figure (9.5).

In contrast to this in the case of an s-wave we can find no zero-energy modes for the energy spectrum of a Hamiltonian with s-wave pairing only - even in the filling range. This can be seen in figure (9.4).

DIFFERENT POINT OF VIEW: MAJORANA FERMIONS

The existence of zero-energy edge modes can be also interpreted from a different point of view, i.e. by splitting the operators into their real and imaginary Majorana parts. This is for example shown in [4]. One splits the creation and annihilation operators $c^{(\dagger)}$ and defines new Majorana operators:

$$\left. \begin{aligned} c_i &= \frac{1}{2} (a_{2i-1} + ia_{2i}) \\ c_i^{\dagger} &= \frac{1}{2} (a_{2i-1} - ia_{2i}) \end{aligned} \right\} \Leftrightarrow \left\{ \begin{aligned} a_{2i} &= \frac{1}{i} (c_i - c_i^{\dagger}) \\ a_{2i-1} &= c_i + c_i^{\dagger} \end{aligned} \right. \quad (9.66)$$

9.3 Topological aspects and numerical simulations

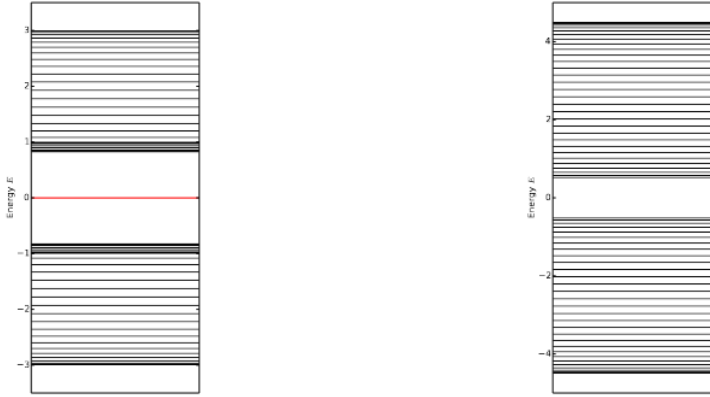


Figure 9.3: Energy spectrum for 1D Hamiltonian given in (9.52) with $\Delta_s = 0$, $\Delta_p = 0.5, t = 1$. Thus this spectrum is for purely p-wave like pairing. Left: $\mu = 1$, i.e. topological phase; Right: $\mu = 2.5$, i.e. trivial phase.

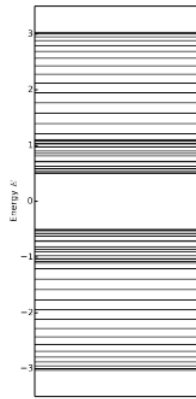


Figure 9.4: Energy spectrum for 1D Hamiltonian given in (9.52) with $\Delta_s = 0.5$, $\Delta_p = 0, t = 1, \mu = 1$.



Figure 9.5: Sum of the absolute value squared of the eigenstates corresponding to the two zero-energy modes in figure (9.3). The solid blue dots represent lattice sites, while the larger blue bubbles correspond to the magnitude of the absolute value.

TOPOLOGICAL SUPERCONDUCTORS [LENNART SCHMIDT]

Note that the operators a_{2i} and a_{2i-1} both solely act on the lattice site i , i.e. we have two types of Majorana fermions per site. From the definitions we can immediately deduce properties of the a -operators:

- a_i creates a Majorana-type fermion, as it is self-adjoint (i.e. the fermion's antiparticle is the particle itself):

$$a_{2i}^\dagger = \frac{c_i^\dagger - c_i}{-i} = a_{2i}; \quad a_{2i-1}^\dagger = c_i^\dagger + c_i = a_{2i-1} \quad \checkmark \quad (9.67)$$

- from the old anticommutation relations $\{c_i^\dagger, c_i\} = \delta_{ij}$, $\{c_i, c_j\} = \{c_i^\dagger, c_j^\dagger\} = 0$, we then can find the anticommutation relations for the new operators a_i :

$$\begin{aligned} \{a_{2i}, a_{2j}\} &= -\{c_i - c_i^\dagger, c_j - c_j^\dagger\} \\ &= \{c_i, c_j^\dagger\} + \{c_i^\dagger, c_j\} \\ &= 2\delta_{ij} \end{aligned} \quad (9.68)$$

$$\begin{aligned} \{a_{2i-1}, a_{2j-1}\} &= \{c_i + c_i^\dagger, c_j + c_j^\dagger\} \\ &= \{c_i, c_j^\dagger\} + \{c_i^\dagger, c_j\} \\ &= 2\delta_{ij} \end{aligned} \quad (9.69)$$

$$\begin{aligned} \{a_{2i}, a_{2j-1}\} &= \frac{1}{i} \{c_i - c_i^\dagger, c_j + c_j^\dagger\} \\ &= \frac{1}{i} (\{c_i, c_j^\dagger\} - \{c_i^\dagger, c_j\}) \\ &= 0 \end{aligned} \quad (9.70)$$

$$\Rightarrow \boxed{\{a_i, a_j\} = 2\delta_{ij}}. \quad (9.71)$$

Using the anticommutation relation given in (9.71) one can now rewrite the Hamiltonian in (9.51) and obtains the Hamiltonian in terms of the Majorana operators:

$$\boxed{\mathcal{H} = \frac{i}{2} \sum_i (-\mu a_{2i-1} a_{2i} + [-t + 2|\Delta|] a_{2i-1} a_{2i+2} + [t + 2|\Delta|] a_{2i} a_{2i+1})}. \quad (9.72)$$

Looking at two special cases of this Hamiltonian yields a pictorial view of the results obtained before:

9.3 Topological aspects and numerical simulations

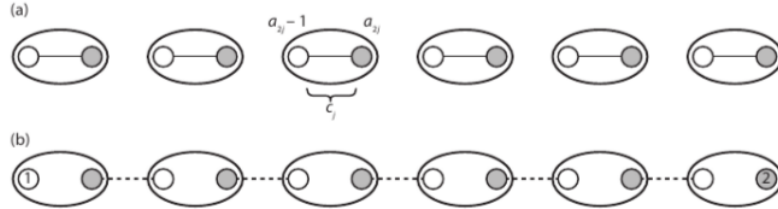


Figure 9.6: Case (a): In the trivial phase the Majoranas on each site are coupled; there are no special edge cases. Case (b): In the topological phase the Majoranas *between* lattice sites are coupled, thus there are uncoupled edge states - manifesting themselves as the zero-energy modes. Picture taken from *B. Andrei Bernevig, Top. Ins. & Top. SC*, [4]

- Case (a): $\mu < 0, t = 2|\Delta| = 0$, i.e. we are in the trivial phase as $|\mu| > 2t$. The Hamiltonian (9.72) becomes:

$$\boxed{\mathcal{H}_{1D}^{\text{BdG}} = -\frac{i\mu}{2} \sum_i a_{2i-1} a_{2i}} \quad (9.73)$$

Here we have only terms of the form $a_{2i-1} a_{2i}$, i.e. pairings of Majoranas on the **same** site i . Thus we do not get any isolated Majoranas on the edges. A pictorial view of this is shown in figure 9.6.

- Case (b): $\mu = 0, t = 2|\Delta| > 0$, i.e. we are in the topological phase as $|\mu| < 2t$. The Hamiltonian (9.72) now becomes:

$$\boxed{\mathcal{H}_{1D}^{\text{BdG}} = \frac{3it}{2} \sum_i a_{2i} a_{2i+1}} \quad (9.74)$$

Here we have terms of the form $a_{2i} a_{2i+1}$, i.e. we pair Majoranas of **different** sites i and $i+1$. Thus we get isolated Majoranas on the edges corresponding to the zero-energy modes found before. For a pictorial view again see figure 9.6.

9.3.3 2D: $p + ip$ -WAVE SUPERCONDUCTOR

We now consider the 2D case with a square lattice: we give the full Hamiltonian, then discuss its bulk topological properties and then solve the finite problem numerically.

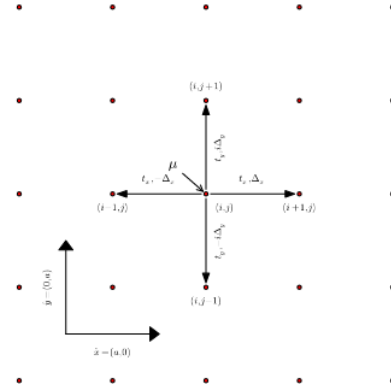


Figure 9.7: 2D square lattice with lattice constant a . We have on-site chemical potential μ , tight-binding hopping t_x, t_y and p-wave-like pairing terms Δ_x, Δ_y . Again for p-wave we have antisymmetry, i.e. we acquire a minus sign for Δ_x and Δ_y when pairing in the opposite direction.

THE HAMILTONIAN

We again take a tight-binding like Hamiltonian with BCS-pairing terms:

$$\mathcal{H}_{2D}^{\text{BdG}} = \sum_{ij} \begin{pmatrix} c_i^\dagger & c_i \end{pmatrix} \begin{pmatrix} \epsilon_{ij} & \Delta_{ij} \\ \Delta_{ji}^* & -\epsilon_{ij} \end{pmatrix} \begin{pmatrix} c_j \\ c_j^\dagger \end{pmatrix}. \quad (9.75)$$

Here we have as before on-site chemical potential and hopping terms in both x - and y -direction with $\epsilon_{ij} = -\mu\delta_{ij} - t_x\delta_{i\pm j} - t_y\delta_{i\pm j}$. Additionally we have p-wavelike superconducting terms again in x - and y -direction contained in $\Delta_{ij} = \Delta_x\delta_{i+xj} - \Delta_x\delta_{i-xj} + i\Delta_y\delta_{i+yj} - i\Delta_y\delta_{i-yj}$. Note that this form is exactly the chiral p-wave state whose symmetry class was discussed in section 9.2.4. A visualization of the terms in the lattice can be viewed in figure 9.7

TOPOLOGICAL PROPERTIES OF THE BULK

Again assuming translational invariance in both x - and y -direction - i.e. looking only at the bulk with no boundaries - we Fourier-transform the Hamiltonian in

9.3 Topological aspects and numerical simulations

(9.75). With

$$c_{\mathbf{i}} = \frac{1}{\sqrt{N_x N_y}} \sum_{k_x k_y} e^{i(x_i k_x + y_i k_y)} c_{\mathbf{k}} \quad (9.76)$$

$$c_{\mathbf{i}}^\dagger = \frac{1}{\sqrt{N_x N_y}} \sum_{k_x k_y} e^{-i(x_i k_x + y_i k_y)} c_{\mathbf{k}}^\dagger \quad (9.77)$$

the Hamiltonian then becomes:

$$\mathcal{H}(k) = \begin{pmatrix} -\mu - 2t(\cos(k_x) + \cos(k_y)) & 2i\Delta_0 (\sin(k_x) + i \sin(k_y)) \\ -2i\Delta_0 (\sin(k_x) - i \sin(k_y)) & \mu + 2t(\cos(k_x) + \cos(k_y)) \end{pmatrix} \quad (9.78)$$

$$\equiv \begin{pmatrix} \epsilon(\mathbf{k}) & \Delta(\mathbf{k}) \\ \Delta^*(\mathbf{k}) & -\epsilon(\mathbf{k}) \end{pmatrix}. \quad (9.79)$$

From this the topological invariant of the bulk can be calculated. The formula for the topological number in two dimensions can be found e.g. in [5] (therein labeled by w_{2D}):

$$N_3 = -\frac{1}{2} \sum_{\Delta(\mathbf{k})=0} \text{sgn}[\epsilon(\mathbf{k})] \text{sgn}[\det \partial_{k_i} \Delta_j] \quad (9.80)$$

where Δ_1 and Δ_2 label the real and imaginary parts of the gap Δ respectively. Then the matrix $\partial_{k_i} \Delta_j$ is given by

$$\begin{pmatrix} 0 & 2\Delta a \cos(k_x a) \\ -2\Delta a \cos(k_y a) & 0 \end{pmatrix} \Rightarrow \det \partial_{k_i} \Delta_j = 4\Delta^2 a^2 \cos(k_y a) \cos(k_x a). \quad (9.81)$$

In calculating the topological invariant we have to sum over the zeros of the gap $\Delta(\mathbf{k})$. From $\Delta(\mathbf{k}) = 2i\Delta (\sin(k_x a) + k \sin(k_y a)) \stackrel{!}{=} 0$ we get four points of interest:

- $\mathbf{k}_1 = (0, 0)$
- $\mathbf{k}_2 = (0, \frac{\pi}{a})$
- $\mathbf{k}_3 = (\frac{\pi}{a}, 0)$
- $\mathbf{k}_4 = (\frac{\pi}{a}, \frac{\pi}{a})$

For these points the signs of $\epsilon(\mathbf{k})$ and $\det \partial_{k_i} \Delta_j$ and thus the topological invariant N_3 are given by:

	$\mu < -4t$ [$\det \partial_{k_i} \Delta_j$] $\epsilon(\mathbf{k})]$	$-4t < \mu < 0$ [$\det \partial_{k_i} \Delta_j$] $\epsilon(\mathbf{k})]$	$0 < \mu < 4t$ [$\det \partial_{k_i} \Delta_j$] $\epsilon(\mathbf{k})]$	$4t < \mu$ [$\det \partial_{k_i} \Delta_j$] $\epsilon(\mathbf{k})]$
\mathbf{k}_1	\oplus	\oplus	\oplus	\ominus
\mathbf{k}_2	\ominus	\oplus	\ominus	\oplus
\mathbf{k}_3	\ominus	\oplus	\oplus	\ominus
\mathbf{k}_4	\oplus	\oplus	\oplus	\ominus
N_3	0	1	-1	0

Thus one obtains 4 different regimes: trivial phases for large absolute value of μ and two different topological phases for $-4t < \mu < 0$ ($N_3 = 1$) and $0 < \mu < 4t$ ($N_3 = -1$). As before - from the index theorem (see [4] or [5]) we therefore expect one gap crossing edge-state per topological defect - e.g. boundaries - in those topological phases and none for the trivial phases. Additionally the slopes of these gap crossings should be opposite for the two different topological regimes with numbers $N_3 = 1$ and $N_3 = -1$.

NUMERICAL RESULTS

In order to check the above results we assume translational invariance only in y -direction and we therefore have two boundaries in x -direction. Fourier-transforming only in y -direction with

$$c_{\mathbf{i}} = \frac{1}{\sqrt{N_y}} \sum_{k_y} e^{iy_i k_y} c_{i_x k_y} \quad (9.82)$$

$$c_{\mathbf{i}}^\dagger = \frac{1}{\sqrt{N_y}} \sum_{k_y} e^{-iy_i k_y} c_{i_x k_y}^\dagger \quad (9.83)$$

yields a Hamiltonian for every value of k_y :

$$\mathcal{H}_{2D}^{\text{BdG}}(k_y) = \sum_{i_x j_x} \begin{pmatrix} c_{i_x k_y}^\dagger & c_{i_x -k_y} \end{pmatrix} h_{i_x j_x}(k_y) \begin{pmatrix} c_{j_x k_y} \\ c_{j_x -k_y}^\dagger \end{pmatrix}, \quad (9.84)$$

where $h(k_y)$ is given by:

$$h_{i_x j_x}(k_y) = \begin{pmatrix} -\frac{\mu}{2} \delta_{i_x j_x} - \frac{t_x}{2} \delta_{i_x \pm 1 j_x} & \Delta_x (\delta_{i_x + 1 j_x} - \delta_{i_x - 1 j_x}) \\ -t_y \cos(k_y a) \delta_{i_x j_x} & + 2\Delta_y \sin(k_y a) \delta_{i_x j_x} \\ \Delta_x^* (\delta_{i_x + 1 j_x} - \delta_{i_x - 1 j_x}) & \frac{\mu}{2} \delta_{i_x j_x} + \frac{t_x}{2} \delta_{i_x \pm 1 j_x} \\ + 2\Delta_y^* \sin(k_y a) \delta_{i_x j_x} & + t_y \cos(k_y a) \delta_{i_x j_x} \end{pmatrix}. \quad (9.85)$$

Thus for every value of k_y we have a Hamiltonian of the type of the 1D-Hamiltonian in equation (9.52) for which the eigenvalues - i.e. the energy spectrum - can be

9.3 Topological aspects and numerical simulations

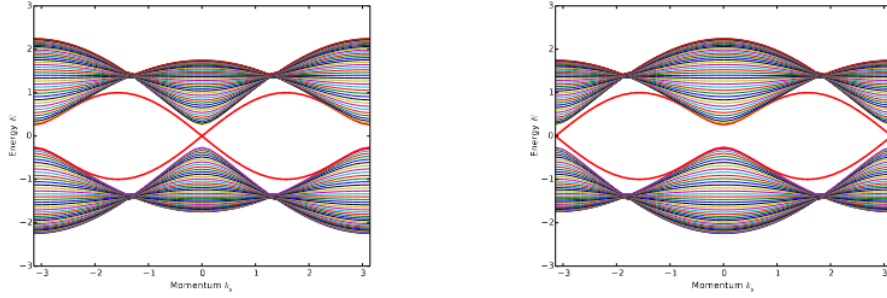


Figure 9.8: Energy spectrum of the 2D-Hamiltonian in (9.84) plotted over momentum k_y , with $\Delta_x = \Delta_y = 0.5$ and $t_x = t_y = 1$. Left: $\mu = -0.5$ and therefore $N_3 = 1$; Right: $\mu = 0.5$ and therefore $N_3 = -1$.

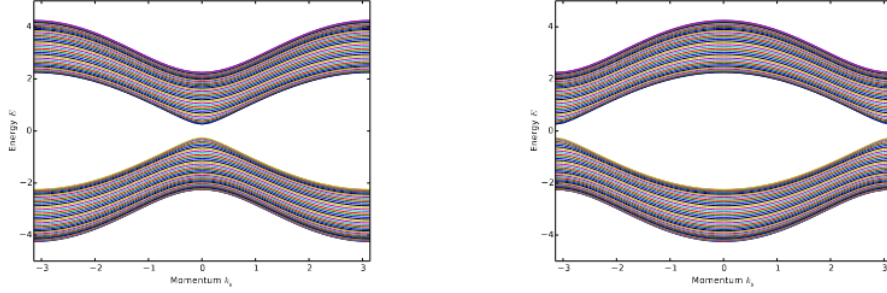


Figure 9.9: Energy spectrum of the 2D-Hamiltonian in (9.84) plotted over momentum k_y , with $\Delta_x = \Delta_y = 0.5$ and $t_x = t_y = 1$. Left: $\mu = -4.5$; Right: $\mu = 4.5$, therefore $N_3 = 0$ in both cases.

calculated.

For the topological phases we obtain 2 edge states, that cross the gap, as can be seen in figure 9.8. For the $N_3 = 1$ -phase the crossing occurs at $k_y = 0$ and the left edge state has positive slope while the right edge has negative slope. In contrast to that the $N_3 = -1$ -phase crosses the zero energy at $k_y = \frac{\pi}{a}$, and the roles of right and left edge are reversed. Note that the slice $k_y = 0$ or $k_y = \pi$ for the left and right pictures respectively corresponds to the spectrum of the 1D-chain we had before. Thus the 1D model is contained in the 2D lattice.

For the trivial phase we do not find any gap-crossing states (see figure 9.9)- as expected.

More examples - all showing the same basic features - can be seen in figure 9.10.

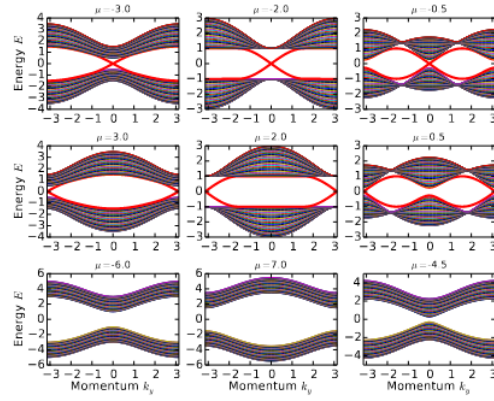


Figure 9.10: Energy spectrum of the 2D-Hamiltonian in (9.84) plotted over momentum k_y , with $\Delta_x = \Delta_y = 0.5$ and $t_x = t_y = 1$. Top row: $N_3 = 1$; Middle row: $N_3 = -1$; Bottom row: $N_3 = 0$.

9.4 Summary and Conclusions

9.4 SUMMARY AND CONCLUSIONS

The first part of this report used representation theory to classify the possible gap functions under the symmetry of a square lattice - namely under D_{4h} . To be able to study spin- $\frac{1}{2}$ -particles the double group of D_{4h} was introduced. The behaviour in spin space was described by the tensor product of two copies of the representation Γ_6^+ , which describes spin $\frac{1}{2}$. Then the decomposition of electron orbitals with angular momentum l was calculated. Assuming strong spin-orbit-coupling those two parts were combined by taking the tensor product and then finding suitable linear combinations of the previous basis functions, thus finding general forms for the gap function of general BCS-theory. Thus symmetry aspects and representation theory yield a very general and easy way to restrict the space of functions for the gap function. However symmetry aspects only yields qualitative statements, for quantitative information a physical model has to be included, e.g. BCS-theory.

In the second part this report took a closer look at the topology of superconductors - in addition symmetry. For this purpose the Hamiltonian of a 1D-Kitaev-chain with superconducting terms was discussed and its topological properties were calculated. Subsequent numerical simulations for this Hamiltonian then confirmed the previous theoretical calculations regarding topological statements. A different interpretation, first proposed by Kitaev [6] for the occurring edge states - in the form of Majorana fermions at the ends of the chain - was discussed. Then an equivalent treatment for a 2D-square lattice with a similar Hamiltonian was discussed. Again numerical simulations confirmed the theoretical calculations for the topological properties. Thus rather easy calculations for the topological numbers of the bulk of a given Hamiltonian can already give knowledge about the general form of the energy spectrum.

9.5 APPENDIX A - THE PROJECTION FORMULA

In representation theory of finite groups the *projection formula* is used to determine the decomposition of any representation into a direct sum of irreducible representations. It is given by

$$m_V^{(W)} = \frac{1}{|G|} \sum_{\mathcal{C}} |\mathcal{C}| \cdot \overline{\chi_V(\mathcal{C})} \cdot \chi_W(\mathcal{C}).$$

The following proof is taken from [9].

DERIVATION: We define the invariant of rep V under action of group G :

$$V^G \equiv \{v \in V : av = v \forall a \in G\}.$$

Then the dimension of V^G is the multiplicity of the trivial representation in V as V^G 'counts' the directions where the group acts trivially. Look at the endomorphism ϕ on V defined via

$$\phi \equiv \frac{1}{|G|} \sum_{a \in G} a \in \text{End}(V).$$

We can immediately recognize that ϕ is a G -module homomorphism - i.e. $b \circ \phi = \phi \circ b, \forall b \in G$:

$$\sum_{a \in G} a = \sum_{a' \in G} b^{-1}a'b \rightarrow b \circ \phi = \phi \circ b.$$

Then $\forall v \in \phi(V)$ we have:

$$v = \phi(w) \Rightarrow b\phi(w) = \frac{1}{|G|} \sum_a baw = \frac{1}{|G|} \sum_{a'} a'w = \phi(w) \Rightarrow \phi(V) \subset V^G$$

In the same vain, we have $\forall v \in V^G$:

$$v \in V^G \Rightarrow \phi(v) = \frac{1}{|G|} \sum_a av = \frac{1}{|G|} v = v \Rightarrow V^G \subset \phi(V).$$

Therefore we have $V^G = \phi(V)$. Note that we also have eigenvalue one for all $v \in V^G$ and thus we directly get the multiplicity of the trivial representation in V :

$$m_{\text{trivial}}^{(V)} = \dim V^G = \text{Tr}_V \phi = \frac{1}{|G|} \sum_{a \in G} \chi_V(a).$$

We then generalize this principle and look at $\text{hom}(V, W)^G$. For this realize that we have $\text{hom}(V, W) \cong V^* \otimes W$ and thus the action of $a \in G$ on $\text{hom}(V, W)$ is given by $a\phi(a^{-1}v)$. Thus $\forall \phi \in \text{hom}(V, W)^G$:

$$a\phi(a^{-1}v) = \phi(v) \Rightarrow \phi \circ a' = a' \circ \phi(a' \equiv a^{-1}),$$

i.e. ϕ is a G -module homomorphism. Thus we have:

$$\text{hom}(V, W)^G = \{\text{G-module hom. from } V \text{ to } W\}.$$

9.6 Appendix B - # cc = # irreps

Then if V is an irrep of G we have via the Lemma of Schur $\ker \phi = 0$ or $\ker \phi = V$. Then we get in similarity with before: $\dim \text{hom}(V, W)^G = m_V^{(W)}!$ We can then define a ϕ in the same way as we did before for the trivial case and obtain:

$$m_V^{(W)} = \dim [(V^* \otimes W)^G] = \text{Tr}(\phi)|_{V^* \otimes W} = \frac{1}{|G|} \sum_{a \in G} \overline{\chi_V(a)} \chi_W(a).$$

Here the complex conjugation stems from the fact that all eigenvalues of any action of a finite group must be roots of unity (follows from finiteness and the fact that representations respect group operations), and thus $\lambda_i^{-1} = \bar{\lambda}_i$ \square .

9.6 APPENDIX B - # CC = # IRREPS

For finite groups we will always have that the number of irreducible representations equals the number of conjugacy classes. This appendix will give a motivation for the reasons behind this taken from [9].

DERIVATION: Let $\alpha : G \rightarrow \mathbb{C}$ be any function, let V be a representation of G and look at the endomorphism ϕ on V given by:

$$\phi_{\alpha,V} \equiv \sum_{a \in G} \alpha(a) a \in \text{End}(V).$$

Then $\phi_{\alpha,V}$ is a G -module homomorphism, i.e. $b \circ \phi_{\alpha,V} = \phi_{\alpha,V} \circ b, \forall b \in G$, if and only if α is a class function, i.e. $\alpha(b^{-1}ab) = \alpha(a)$. This can be seen via:

$$(\phi_{\alpha,V} \circ b)(v) = \sum_a \alpha(a) a(bv) = \sum_{a'} \alpha(ba'b^{-1}) ba'b^{-1}(bv) = \sum_a \alpha(ba'b^{-1}) b(av).$$

Then if α is a class function we obtain $(\phi_{\alpha,V} \circ b)(v) = b \circ (\sum_a \alpha(a) av) = (b \circ \phi_{\alpha,V})(v)$.

If α is not a class function, i.e. form some a_0, b_0 we have $\alpha(b_0 a_0 b_0^{-1}) \neq \alpha(a_0)$. Then by the same calculation $\phi_{\alpha,V}$ is also not a G -module homomorphism.

Assume now α is a class function satisfies $\sum_{a \in G} \alpha(a) \chi_V(a) = 0$ for all (ir)reps of V , i.e. α is a class function and orthogonal to all characters of irreps - which themselves are class functions - with respect to the inner product given by the projection formula (9.18). Let V be one of those irreps, then from Schur's Lemma we know:

$$\phi_{\alpha,V} = \lambda \cdot \mathbb{1} \rightarrow \lambda = \frac{1}{\dim V} \text{Tr}(\phi_{\alpha,V}) = \frac{1}{\dim V} \sum_a \alpha(a) \chi_V(a) = 0$$

TOPOLOGICAL SUPERCONDUCTORS [LENNART SCHMIDT]

Therefore we then have $\phi_{\alpha,V} = 0$ for all irreps V and therefore for all representations - as these are just direct sums of irreps. Looking at the regular representation we then get:

$$\phi_{\alpha,V}(e_b) = \sum_a \alpha(a)e_{ab} = 0 \Rightarrow \alpha \equiv 0.$$

Therefore the characters of all irreps form a complete basis for the space of class functions, i.e. the number of irreps is equal to the number of conjugacy classes \square .

9.6 Appendix B - # cc = # irreps

BIBLIOGRAPHY

- [1] M. Dresselhaus, G. Dresselhaus, and A. Jorio, *Application of Group Theory to the Physics of Solids* (Springer, 2008).
- [2] M. Sigrist, *Introduction to unconventional superconductivity* (M.I.T. Press, 1963).
- [3] M. Sigrist and Rice, *Symmetry Classification of States in High Temperature Superconductors*, Z. Phys. B. - Condensed Matter **68**, 9 (1987).
- [4] B. Bernevig, *Topological insulators and topological superconductors* (Princeton University Press, Princeton and Oxford, 2013).
- [5] Y. Tanaka, M. Sato, and N. Nagaosa, *Symmetry and Topology in Superconductors - Odd-frequency pairing and edge states*, J. Phys. Soc. Jpn. **81**, 011013 (2012).
- [6] A. Y. Kitaev, *Unpaired Majorana fermions in quantum wires*, Phys.-Usp. **44**, 131 (2001).
- [7] A. Leggett, *A theoretical description of the new phases of liquid Helium*, Rev. of mod. Physics **47**, 2 (1975).
- [8] G. Koster, *Properties of the thirty-two point groups* (M.I.T. Press, 1963).
- [9] M. Gaberdiel, *Symmetries in Physics (Lecture Notes)* (ETH Zuerich, 2013).

BIBLIOGRAPHY

CHAPTER 10

POLARIZATION AND TOPOLOGICAL INSULATORS

THOMAS GUMBSCH

SUPERVISOR: ALEXEY SOLUYANOV

There is an unique way of distinguishing between a material which has a trivial topology and one which is topological.

10.1 INTRODUCTION

The discovery of new materials plays an important role in physics. Topological insulators, which is a new class of materials, are distinguished from ordinary insulators not by symmetry but via topology. This means that the characteristic properties of a topological insulator do not depend on the exact shape of the object. The study of topological insulators is a new branch of theoretical solid state physics with applications such as topological superconductivity or spintronics.

It was first predicted by Pankratov et al (1986) that bulk spin-orbit coupling may lead to charge transport along the edge [1]. However, the topological protection of these currents was understood in the last decade. In particular Kane and Mele [2] contributed the fact that these edge-states are protected by time-reversal symmetry. Moreover, Qi, Wu and Zhang [3] gave the proof that edge states are a property of the bulk.

In order to understand this phenomena, we will describe charge transport in an insulator from the viewpoint of electronic polarization. Then, we will impose time-reversal symmetry in order to explain the existence of a topological invariant, namely the Z_2 -invariant Δ . The main point of this essay is to check the $U(2N)$ gauge invariance of Δ explicitly. A non-trivial Z_2 -index corresponds to a

10.2 Polarization on a lattice

band inversion in the spectrum, *i.e.* edge-states.

10.2 POLARIZATION ON A LATTICE

This paragraph aims to explain how polarization can be used to explain that charge can be pumped in an insulator.

When looking at a system, polarization can be described in two different ways: Firstly, it is the dipole moment over its length. But this turns out to be very difficult to generalize to crystalline systems, since we encounter problems with having no "end charges". For the purposes discussed in this article, a formulation such as follows is used

$$P = \frac{e}{2\pi} \int_{-\pi/2}^{\pi/2} \mathcal{A}(k) dk. \quad (10.1)$$

When looking at the Wannier orbitals

$$|R, n\rangle = \frac{1}{2\pi} \int dk e^{-ik(R-r)} |u_{k,n}\rangle \quad (10.2)$$

which are defined as the Fourier transform of the Bloch states of our crystal, we can see that

$$\langle r \rangle = \langle 0, n | \hat{r} | 0, n \rangle = -i \langle u_{k,n} | \partial_k | u_{k,n} \rangle \quad (10.3)$$

the electromagnetic vector potential arising in equation 10.1 and the berry connection are closely related *i.e.* they share the same ambiguity.

Assuming we have a 1D crystal, we can now introduce a 2D periodic system where the second dimension is described via a pumping parameter τ of an adiabatic cycle. Because of the analogy between vector potential and berry connection, we can view this as a 2D lattice, where one axis lives in real space, the other one in reciprocal space. On this system (which is a torus now) we can define a chern number

$$P(T) - P(0) = \frac{1}{2\pi} \left[\int \mathcal{A}(k, T) dk - \int \mathcal{A}(k, 0) dk \right] = \quad (10.4)$$

$$= \frac{1}{2\pi} \int \mathcal{F}(k, t) dt dk = \quad (10.5)$$

$$= \Delta(T, 0) \quad (10.6)$$

where \mathcal{F} is the berry curvature encountered in previous talks and we set $e = 1$ for simplicity. $\Delta(T, 0)$ is closely related to the Z_2 -index Δ which will be discussed in

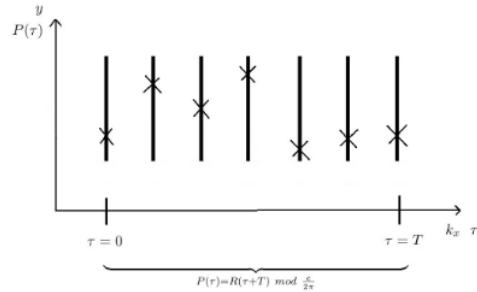


Figure 10.1: Evolution of polarization on a finite mesh. The y-axis one unit cell of the direct lattice is displayed. On the x-axis we perform an adiabatic cycle, which can be seen as the second dimension in a reciprocal lattice. The net polarization must stay the same, modulus a lattice vector.

thorough detail later.

We perform this cycle on a finite mesh consisting of many dipoles (figure 10.1) and track the corresponding polarization. The net polarization must stay the same. But during that cycle, we could have shifted our charges by one unit cell or more. We need to follow the polarization continuously (see figure 10.2) in order to make a statement about whether charge has been pumped or not.

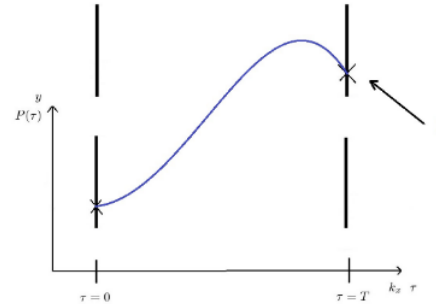


Figure 10.2: We follow the polarization continuously and end up in another unit cell. Here, $\Delta(T, 0) = 1$.

10.3 TIME REVERSAL SYMMETRY

We are not yet ready to distinguish between a material which has a non-trivial topology and one which does not. Since one can imagine a gauge which changes

10.4 $U(2N)$ gauge invariance of the chern number

the path of the polarization *s.th.* $\Delta(T, 0)$ changes, we fix time reversal symmetry. If we force the Hamiltonian H to be invariant with respect to the time-reversal operator θ , *i.e.*

$$\theta H \theta^\dagger = H \quad (10.7)$$

One can deduce that

$$\theta = R \cdot \mathcal{K} \quad (10.8)$$

the time-reversal operator consist of a anti-symmetric matrix R times a complex conjugation.

Kramers theorem states that for points which obey time-reversal symmetry, energy eigenstates are double degenerate. The time reversal invariant k-points are

$$k^* = 0, \pi. \quad (10.9)$$

Quantum mechanics gives us for spin- $\frac{1}{2}$ particles

$$\theta^2 = -1 \quad (10.10)$$

which, in turn, gives constraints for the two Kramer states. Most importantly, $|u_{k,n}^I\rangle$ and $|u_{k,n}^{II}\rangle$ are linearly independent and we can obtain transformation rules:

$$|\theta u_{k,n}^I\rangle = |u_{-k,n}^{II}\rangle \quad (10.11)$$

$$|\theta u_{k,n}^{II}\rangle = -|u_{-k,n}^I\rangle. \quad (10.12)$$

where n is the band index.

With the definition of the time-reversal polarization

$$P_\theta = P(|u_{k,n}^I\rangle) - P(|u_{k,n}^{II}\rangle) \quad (10.13)$$

we can define

$$\Delta = P_\theta(T/2) - P_\theta(0) \quad (10.14)$$

what turns out to be a Z_2 index. In the section below this fact is shown and there is also a detailed proof that Δ is gauge invariant given.

10.4 $U(2N)$ GAUGE INVARIANCE OF THE CHERN NUMBER

We fix a $U(1)$ gauge for each of the Kramer states

$$|u_{-k,n}^I\rangle = -e^{i\chi_{k,n}} |\theta u_{k,n}^{II}\rangle \quad (10.15)$$

$$|u_{-k,n}^{II}\rangle = e^{i\chi_{-k,n}} |\theta u_{k,n}^I\rangle \quad (10.16)$$

in order to quantify the description for the partial polarization

$$P^S = \frac{1}{2\pi} \int_{-\pi}^{\pi} dk i \sum_{\alpha} \langle u_{k,\alpha}^S | \nabla_k | u_{k,\alpha}^S \rangle . \quad (10.17)$$

where $S = I, II$ and the Kramer states are degenerate at $k^* = 0, \pi$. In the expression above we integrate over the berry connection, where the sum over α is the sum over the number of Kramer pairs. We drop this index for a while in order to make the calculations more accessible.

We would like to compare absolute values, that is why we try to relate the two P^S , *i.e.* we rewrite

$$\mathcal{A}^I(k) = i \langle u_k^I | \partial_k | u_k^I \rangle = \quad (10.18)$$

$$= i \langle \theta u_{-k}^{II} | e^{-i\chi_k} \partial_k e^{i\chi_k} | \theta u_{-k}^{II} \rangle = \quad (10.19)$$

$$= i \langle \theta u_{-k}^{II} | \partial_k | \theta u_{-k}^{II} \rangle - \partial_k \chi_k = \quad (10.20)$$

$$= i \langle u_{-k}^{II*} | R^\dagger \partial_k R | \theta u_{-k}^{II*} \rangle - \partial_k \chi_k = \quad (10.21)$$

$$= i \langle u_{-k}^{II*} | \partial_k | \theta u_{-k}^{II*} \rangle - \partial_k \chi_k = \quad (10.22)$$

$$= -i (\langle u_{-k}^{II} | \partial_k | \theta u_{-k}^{II} \rangle)^* - \partial_k \chi_k = \quad (10.23)$$

$$= \mathcal{A}^{II}(-k) - \partial_k \chi_k \quad (10.24)$$

In the first step, we inserted our gauge. Then, we executed the derivative where we obtained $-1 = \theta^\dagger \theta$. Afterwards, we applied the definition of $\theta = R\mathcal{K}$ with $R^\dagger R = 1$. When taking the complex conjugate over the whole transition, we obtain a minus sign because ∂_k is odd. In the last step, we used the fact that \mathcal{A} is totally imaginary.

We are now ready to obtain an expression which does not depend on the index S :

$$P^I = \frac{1}{2\pi} \int_0^{\pi} dk [\mathcal{A}^I(k) + \mathcal{A}^I(-k)] \quad (10.25)$$

$$= \frac{1}{2\pi} \left[\int_0^{\pi} dk \mathcal{A}(k) + \sum_{\alpha} (\chi_{\pi,\alpha} - \chi_{0,\alpha}) \right] = \quad (10.26)$$

$$= \frac{1}{2\pi} \left[\int_0^{\pi} dk \mathcal{A}(k) + i \log \left(\frac{\text{Pf}(\omega(\pi))}{\text{Pf}(\omega(0))} \right) \right] \quad (10.27)$$

A few remarks on the $U(1)$ gauge: Firstly, we need a continuous evolution of χ in order to guarantee the difference in the second line to be well defined. Secondly,

10.4 $U(2N)$ gauge invariance of the chern number

we note that a $U(1)$ gauge is the simplest way in order to introduce a jump in the partial polarization discussed in the previous sections.

From the second to the third line in equation 10.27 we introduce the sewing matrix

$$\omega_{mn}(k) = \langle u_{-k,m} | \theta u_{k,n} \rangle. \quad (10.28)$$

ω is unitary because our gauge is unitary and therefore we can use the Pfaffian Pf which is defined via

$$\text{Pf}(\omega(k^\star))^2 = \det(\omega(k^\star)). \quad (10.29)$$

Since all variables are complex valued we have an ambiguity in the above expressions. This reflects the ambiguity in the definition of the partial polarization (modulus a lattice vector).

A similar expression for P^{II} opens up the possibility to calculate the time reversal polarization

$$P_\theta = P^I - P^{II} = \quad (10.30)$$

$$= \frac{1}{2\pi} \left[\int_0^\pi dk \mathcal{A}(k) - \int_0^\pi dk \mathcal{A}(-k) + 2i \log \left(\frac{\text{Pf}(\omega(\pi))}{\text{Pf}(\omega(0))} \right) \right] = \quad (10.31)$$

$$\stackrel{(*)}{=} \frac{1}{2\pi} \left[\int_0^\pi dk \text{Tr}(\omega^\dagger \nabla_k \omega) - 2 \log \left(\frac{\text{Pf}(\omega(\pi))}{\text{Pf}(\omega(0))} \right) \right] = \quad (10.32)$$

$$= \frac{1}{2\pi} \left[\int_0^\pi dk \nabla_k \log(\det(\omega(k))) - 2 \log \left(\frac{\text{Pf}(\omega(\pi))}{\text{Pf}(\omega(0))} \right) \right] \quad (10.33)$$

The second step is explained in rigorous detail in the appendix 10.6. In the last step we recognize that the integral over the trace gives the winding of the $U(1)$ transformation. Or, looking at the 2x2 minimal example, one can deduce

$$\text{Tr} \left[\begin{pmatrix} 0 & -e^{-i\chi} \\ e^{-i\chi} & 0 \end{pmatrix} \begin{pmatrix} 0 & -\nabla e^{-i\chi} \\ \nabla e^{-i\chi} & 0 \end{pmatrix} \right] = i \nabla \chi. \quad (10.34)$$

P_θ is an integer mod 2, because the time reversal polarization can only change by a unit cell and it depends on which branch of the logarithm we chose. This value is still not gauge invariant. Nonetheless, the two values of P_θ are distinct in a sense that it cannot be altered by a change that protects time reversal symmetry. Therefore, an adiabatic cycle is a well defined change in P_θ . Therefore, we can write

$$(-1)^{P_\theta} = \frac{1}{\pi i} \log \left(\frac{\sqrt{\det(\omega(0))}}{\text{Pf}(\omega(0))} \frac{\sqrt{\det(\omega(\pi))}}{\text{Pf}(\omega(\pi))} \right) \quad (10.35)$$

With the definition of the Z_2 -index

$$\Delta = P_\theta(T/2) - P_\theta(0) \bmod 2 \quad (10.36)$$

one can show for all four time reversal invariant points Γ_i in the t - k -plane the relation

$$(-1)^\Delta = \prod_{i=1}^4 \frac{\sqrt{\det(\omega(\Gamma_i))}}{\text{Pf}(\omega(\Gamma_i))} \quad (10.37)$$

This is the major result of this calculation.

We assume a ground state degeneracy at $k = 0$ and $k = \pi$ and let P_θ evolve adiabatically from $t = 0$ to $t = T/2$. A band inversion is obtained when ending up on different branches of the square-root, that is when the two ground states switch partners during the cycle. (See 10.3). So, as long as there is no winding of the $U(2)$ transformation, our result is fine.

Producing a band inversion corresponds directly to the existence of edge-modes

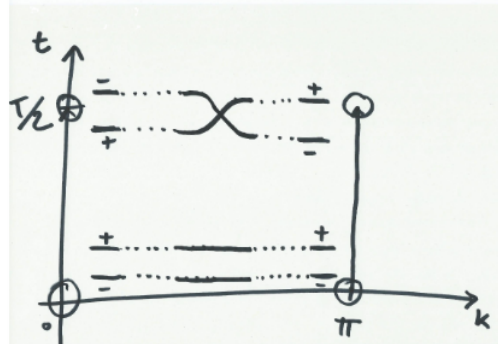


Figure 10.3: The two ground states (labeled as + and -) at $K^* = 0, \pi$ switch partners during the adiabatic evolution. This behaviour corresponds to ending up at different branches of the logarithm in 10.35.

and the material being topologically non-trivial.

10.5 CONCLUDING REMARKS

A topologically non-trivial material has a Z_2 -index $\Delta = 1$. This can be visualized by tracking the two partial polarizations, each of them corresponding to one of the Kramer pairs. On the time-reversal invariant k -points they have to concide, which yields two possibilities (see figure 10.4).

We have shown in great detail that Δ can only take two different values and it is $U(2N)$ gauge invariant.

10.6 Appendix: General behaviour under $U(2N)$ transformation

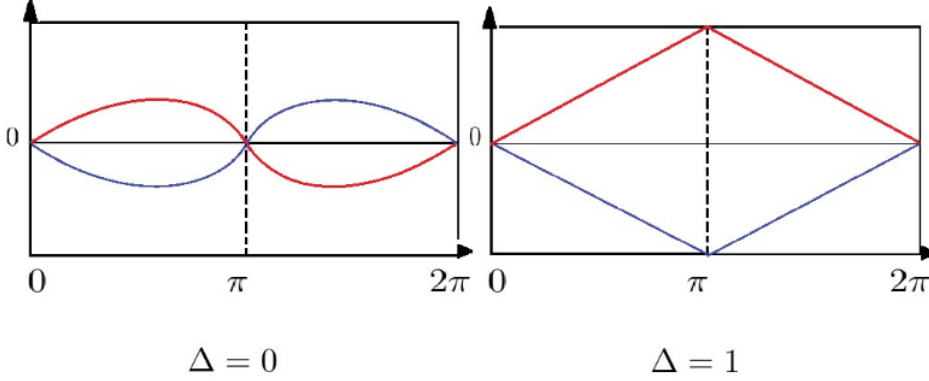


Figure 10.4: Kramers theorem states that $|u_{k^*,n}^I\rangle \geq |u_{k^*,n}^{II}\rangle$ must hold. This gives two possibilities: On the left, $\Delta = 0$ corresponds to no charge being pumped. On the right, we take advantage of the crystalline structure *i.e.* that the top end of our unit cell is effectively glued to the bottom and the two states (red and blue lines) indeed end up at the same point. $\Delta = 1$ now yields charge being pumped from one unit cell to the next. (The top left red line continues as the bottom right blue and vice versa)

10.6 APPENDIX: GENERAL BEHAVIOUR UNDER $U(2N)$ TRANSFORMATION

We look at a general $U(2N)$ transformation on Bloch states

$$|u_{jk}\rangle = \sum_m U_{mj}|u_{mk}\rangle . \quad (10.38)$$

Here, j and m are band indices.

Our goal is to deduce how P_θ behaves under this transformation. In order to do this, we look at the trace of the berry connection of all occupied states

$$\mathcal{A}_{ii}(k) = \delta_{ij} i \langle u_{ik} | \partial_k | u_{jk} \rangle = \quad (10.39)$$

$$= i \sum_{n,m} \langle u_{nk} | U_{in}^\star \partial_k U_{mi} | u_{mk} \rangle = \quad (10.40)$$

$$= i \sum_{n,m} \langle u_{nk} | \partial_k | u_{mk} \rangle + i \sum_{n,m} U_{in}^\star \partial_k U_{mi} \quad (10.41)$$

Therefore, when transforming $\mathcal{A} \rightarrow \tilde{\mathcal{A}}$

$$\text{Tr}[\tilde{\mathcal{A}}] = \text{Tr}[\mathcal{A}] + i \text{Tr}[U^\dagger \nabla_k U] \quad (10.42)$$

POLARIZATION AND TOPOLOGICAL INSULATORS [THOMAS GUMBSCH]

We put $U = \omega$ to obtain

$$\text{Tr}[\mathcal{A}(k)] = \text{Tr}[\mathcal{A}(-k)] + i\text{Tr}[\omega^\dagger \nabla_k \omega] \quad (10.43)$$

which is the proof for (\star) in equation 10.30.

10.6 Appendix: General behaviour under $U(2N)$ transformation

BIBLIOGRAPHY

- [1] O. A. Pankrativr, S. V. Pakhomovi, and B. A. Volkov, *Supersymmetry in heterojunctions: Band-inverting contact on the basis of Pb₁Sn Te and Hg₁CdTe*, Solid State communications **61**, 93 (1987).
- [2] C. L. Kane and L. J. Mele, *Z2 Topological Order and the Quantum Spin Hall Effect* , Physical review letter **95**, 146802 (2005).
- [3] S. C. Zhang, Y. S. Wu, and X. L. QI, *General theorem relating the bulk topological number to edge states in two-dimensional insulators* , Physical review B **74**, 045125 (2006).

BIBLIOGRAPHY

CHAPTER 11

CLASSIFICATION OF TOPOLOGICAL INSULATORS AND SUPERCONDUCTORS

STEFAN HUBER
SUPERVISOR: ANDREY LEBEDEV

11.1 Introduction

We study a general scheme to classify topological phases of insulators and superconductors. We consider discrete symmetries of quantum systems such as time reversal symmetry, particle-hole symmetry, and chiral symmetry, and study the restrictions to a quantum system arising from such symmetries. There are 10 symmetry classes when considering these discrete symmetries. We find the space of time evolution operators in each symmetry class and derive the Altland-Zirnbauer classification table. We show a table of corresponding homotopy groups to each symmetry class in different dimensionalities and show how it can be used to predict the existence of a \mathbb{Z} or a \mathbb{Z}_2 topological invariant which protect the topological phase. We show how different well-known examples for topological insulators and superconductors fit into this table and how the classification type of their topological sectors can be predicted by the table of homotopy groups. We discuss nonlinear σ models and their description of Anderson localization physics at the boundary of a system which is connected to the nontrivial topology of the band structure. We also construct an example for a \mathbb{Z} topological insulator in 3D using Dirac Hamiltonians, a procedure which can be used to construct examples for any of the 5 topological insulators that exist in 3D and in other dimensionalities.

11.1 INTRODUCTION

We review the classification scheme of topological insulators which was established by Schnyder, Ryu, Furusaki, and Ludwig in [1] and which was developed further in [2]. A topological insulator respectively superconductor is a gapped state of matter which has gapless modes along its boundary to a state of matter with different topology. These gapless modes are stable under perturbations which do not close the bulk gap and which preserve the symmetry properties of the Hamiltonian, because they are protected by a topological invariant which is either a \mathbb{Z} quantity, such as a winding number or a Chern number, or a \mathbb{Z}_2 quantity.

The Integer Quantum Hall Effect (IQHE) is probably the most popular example for a topological insulating phase. In the IQHE, the transverse Hall conductance is equal to a Chern number up to a constant factor. Two states ("plateaux") of the IQHE with different Chern numbers cannot be adiabatically transformed to each other without closing the bulk gap. Thus, each of the plateaux stands for a

CLASSIFICATION OF TOPOLOGICAL INSULATORS AND SUPERCONDUCTORS
[STEFAN HUBER]

different topological phase, and the phases are labeled by a \mathbb{Z} quantity [3].

In the past, more examples for topological insulators have been found, such as the \mathbb{Z}_2 topological insulator in 2D (also called the Quantum Spin Hall state, QSH) and in 3D [4, 5].

Now we can ask the question of which non-interacting fermion systems in a given dimension can have such nontrivial topological phases. Our approach to dealing with this is to first take a look at discrete symmetries, such as time reversal symmetry or particle-hole symmetry as well as chiral symmetry. The presence of such symmetries gives restrictions to the space of generic Hamiltonians and, as a consequence, to the time evolution operators of systems in a symmetry class. These restrictions change the topology of the symmetry class, or more specifically, of its target space (see below). Such a classification has been proposed by Altland and Zirnbauer when studying random matrices in the mid-1990s [6, 7]. Then, in order to study the possibility of adiabatically connecting two quantum states, we need to introduce the mathematical concept of fundamental groups and homotopy groups. They treat the question of continuous deformations of loops and more general periodic functions in an elegant way. At the end, we will have a general description of different symmetry classes in different spatial dimensions, and will be able to predict the existence of a \mathbb{Z} or \mathbb{Z}_2 quantity which labels the topological sectors of a system in a given symmetry class.

11.1.1 OUTLINE

We start by considering very generally the concept of time reversal symmetry (TRS). We will see that there are three possible cases of such a symmetry: no TRS, and two distinct cases of TRS being present which correspond to integer spin and half-integer spin statistics. This gives rise to 3 different symmetry classes, which are known as the Wigner-Dyson classes [8]. Then we go further on by considering particle-hole symmetry, a symmetry which is inherent to Bogolyubov-deGennes (BdG) Hamiltonians, which describe superconductivity. There, we also have three possible cases. Altogether, also considering a third, so-called chiral symmetry, we obtain 10 symmetry classes, which make up the Altland-Zirnbauer classification table. For each of these classes, we will show how there arise restrictions to the space of possible time evolution operators. A nearly complete treatment of these symmetry classes at an introductory level was written down in [9], and we stay close to the presentation given there. Next, we give a short introduction to fundamental groups and homotopy groups. For a given symmetry class, the homotopy group of a certain target space decides whether the system has a trivial topology or not, and if there is a nontrivial

11.2 Symmetry Classification of non-interacting Hamiltonians

topology, if we have a \mathbb{Z} or a \mathbb{Z}_2 classification. The way this connects to physics is that the appearance of an aforementioned gapless boundary mode can be modeled by a so-called nonlinear σ model (NL σ M) [10]. Such a NL σ M is a microscopic description of Anderson localization transitions, and if the homotopy group of the corresponding target space of the model is nontrivial, it is possible to introduce a topological term into its action [2]. We state the different nontrivial topological terms which can be introduced to the NL σ M action and show how they make the definition of topological invariants possible.

We find that in each dimension there are 5 nontrivial topological insulators (superconductors), 2 of which have a \mathbb{Z}_2 classification and 3 of which have a \mathbb{Z} classification.

At the end, we take a look at some popular examples for topological insulators and superconductors and show how they fit into our description and how their classification in terms of topological invariants can be predicted. Furthermore, we construct an example for a \mathbb{Z} topological insulator in 3D via Dirac Hamiltonians which was introduced in [1]. This procedure can be used for any of the 5 symmetry classes which allow a nontrivial topology in 3D, as was shown in [1], and can even be generalized to any spatial dimension, as can be found in [2].

This report is part of a proseminar in theoretical physics about topological insulators and superconductors which took place at ETH Zürich in the spring semester of 2014. It is based on a talk held by myself on May 26, 2014.

11.2 SYMMETRY CLASSIFICATION OF NON-INTERACTING HAMILTONIANS

We consider discrete symmetries such as time reversal symmetry, particle-hole symmetry or chiral symmetry and take a look at the restrictions to the space of possible Hamiltonians (or the space of time evolution operators, respectively) arising from the presence or absence of these symmetries. In general, any Hamiltonian is self-adjoint and the time evolution operator $\exp(-\frac{i}{\hbar}Ht)$ is unitary. Therefore, the time evolution operator lives in the Lie group $U(N)$ for a finite-dimensional Hilbert space of dimension N and the possible Hamiltonians can be associated with the generators iH of the corresponding Lie algebra $\mathfrak{u}(N)$. The presence of a discrete symmetry gives additional constraints to these objects, as we describe below. The presentation of the symmetry classes mainly follows the one given in [9], with some details and calculations added in order to make it easier to follow.

11.2.1 TIME-REVERSAL SYMMETRY (TRS)

The first discrete symmetry of interest is the time reversal symmetry, which we abbreviate by TRS. It describes the symmetry of a system under the reversal of time, meaning $t \mapsto -t$. We first take a look at the notion of TRS for classical systems and then introduce TRS at a quantum level. Then we investigate the implications of its presence to the space of time evolution operators respectively Hamiltonians of a system.

TRS AT A CLASSICAL LEVEL

DEFINITION. A classical Hamiltonian system is called time reversal invariant if from any given solution $\{x(t), p(t)\}$ of the equations of motion, we can construct an independent solution $\{x'(t'), p'(t')\}$ using some mapping between the coordinates $x \mapsto x'$, $p \mapsto p'$ and where $t' = -t$.

CONVENTIONAL TRS. A simple example for a TRS is the so-called *conventional* TRS. It is characterized by the mapping

$$x \mapsto x, p \mapsto -p. \quad (11.1)$$

A conventional TRS is present if the Hamiltonian fulfills $H(x, p) = H(x, -p)$, which is always the case if we have a simple kinetic term of the form $\frac{p^2}{2m}$ and a potential which is independent of p . We should remark that a transformation as given in (11.1) is not a canonical transformation of the coordinates. This is because it does not preserve the Poisson bracket: $\{x', p'\} = \{x, -p\} = -\{x, p\}$. Because of the additional sign in the Poisson bracket we might call this transformation *anticanonical*.

Next, we use the above notion of TRS as an inspiration to define what TRS means at a quantum level. In order to achieve that, we have to take a look at the Schrödinger equation.

TRS AT A QUANTUM LEVEL

We adapt the idea of TRS for quantum systems by using mappings between wavefunctions instead of mappings between phase space coordinates.

DEFINITION. The Schrödinger equation

$$i\hbar\partial_t\psi(x, t) = H\psi(x, t) \quad (11.2)$$

11.2 Symmetry Classification of non-interacting Hamiltonians

is called time reversal invariant if for any given solution $\psi(x, t)$, there is another solution $\psi'(x, t')$ with $t' = -t$ and $\psi' = \mathcal{T}\psi$ uniquely related to ψ .

Before looking at some simple examples, we take a very general look at the structure of the \mathcal{T} operator in this definition.

STRUCTURE OF THE \mathcal{T} OPERATOR. Due to Wigner's Theorem [11], which tells us that any symmetry which keeps the modulus of the overlap of two wavefunctions invariant is either unitary or antiunitary, we know that \mathcal{T} has to be unitary or antiunitary as well. Because of the factor of i in the left handside of the Schrödinger equation, the \mathcal{T} operator should be antiunitary, which means that

$$\langle \mathcal{T}\psi | \mathcal{T}\phi \rangle = \langle \phi | \psi \rangle. \quad (11.3)$$

Any antiunitary operator can be written as a product of a unitary operator U and complex conjugation K , giving us the decomposition

$$\mathcal{T} = UK. \quad (11.4)$$

This consequence of antiunitarity is an important property of any TRS operator. In order to specify the structure of \mathcal{T} some more, we require that if \mathcal{T} acts on a state twice, it does not change the state. This allows the state only to pick up a phase when being acted upon twice with \mathcal{T} . Hence, $\mathcal{T}^2 = \alpha$ for some α with $|\alpha| = 1$. Plugging in the decomposition (11.4), we obtain that

$$\mathcal{T}^2 = \pm \mathbb{1}. \quad (11.5)$$

Now we know that if we only consider TRS, there are three cases which can occur: The system has no TRS, the system has TRS with $\mathcal{T}^2 = \mathbb{1}$, and the system has TRS with $\mathcal{T}^2 = -\mathbb{1}$. Before classifying quantum systems according to their TRS, we give a simple example for each of the cases where TRS is present.

SPINLESS PARTICLE WITH REAL HAMILTONIAN. In case of a Hamiltonian of the form $H(x, p) = \frac{p^2}{2m} + V(x)$ where $V(x) = V^*(x)$, we have a TRS with $\mathcal{T} = K$, where K denotes complex conjugation. The spinless particle thus has a TRS with $\mathcal{T}^2 = \mathbb{1}$.

SPIN-1/2 PARTICLE. In order to find the \mathcal{T} operator for a spin-1/2 particle, we require that the spin angular momentum $\vec{S} = \frac{\hbar}{2}\vec{\sigma}$ is odd under time reversal, where $\vec{\sigma}$ is the standard vector of Pauli matrices:

$$\sigma_x = \begin{pmatrix} 0 & 1 \\ 1 & 0 \end{pmatrix}, \sigma_y = \begin{pmatrix} 0 & -i \\ i & 0 \end{pmatrix}, \sigma_z = \begin{pmatrix} 1 & 0 \\ 0 & -1 \end{pmatrix}. \quad (11.6)$$

CLASSIFICATION OF TOPOLOGICAL INSULATORS AND SUPERCONDUCTORS
[STEFAN HUBER]

Plugging in the decomposition (11.4), we get the following equations:

$$-\sigma_x \stackrel{!}{=} \mathcal{T} \sigma_x \mathcal{T}^{-1} = UK \sigma_x K U^{-1} = U \sigma_x U^{-1}, \quad (11.7)$$

$$-\sigma_y \stackrel{!}{=} UK \sigma_y K U^{-1} = -U \sigma_y U^{-1}, \quad (11.8)$$

$$-\sigma_z \stackrel{!}{=} UK \sigma_z K U^{-1} = U \sigma_z U^{-1}. \quad (11.9)$$

We can write the 2x2 matrix U as a linear combination of the 3 Pauli matrices and the identity:

$$U = \alpha \sigma_x + \beta \sigma_y + \gamma \sigma_z + \delta. \quad (11.10)$$

Using the commutation relation of the Pauli matrices, $[\sigma_i, \sigma_j] = 2i\epsilon_{ijk}\sigma_k$, we obtain from equation (11.7) that $\alpha = \delta = 0$. Equation (11.8) then gives $\gamma = 0$. Unitarity of U further restricts β to fulfill $|\beta| = 1$, and we choose $\beta = i$. Then, the \mathcal{T} operator reads $\mathcal{T} = i\sigma_y K$. This means the spin-1/2 particle has a TRS with $\mathcal{T}^2 = -\mathbb{1}$.

In spirit with the TRS properties of spinless and spin- $\frac{1}{2}$ particles, we call a TRS with $\mathcal{T}^2 = \mathbb{1}$ an integer spin TRS and a TRS with $\mathcal{T}^2 = -\mathbb{1}$ a half-integer spin TRS.

CLASSIFICATION OF SYSTEMS ACCORDING TO THEIR TRS

We now want to classify systems according to their TRS. As already discussed, there are three cases we need to consider. We start by imposing the presence or absence of a TRS and investigate the following constraints on the Hamiltonians. These three cases make up the so-called *Wigner-Dyson* classes.

CLASS A. SYSTEMS WITHOUT ANY SYMMETRY. In the most general case where no symmetry is present, we have no restrictions to the space of time evolution operators besides them being unitary: As we have already mentioned, in an N -dimensional Hilbert space, the time evolution operator of a time independent Hamiltonian is given by

$$U = \exp\left(-\frac{i}{\hbar} H t\right) \in U(N). \quad (11.11)$$

The time evolution operator lives in the unitary Lie group, and the corresponding Lie algebra is $\mathfrak{u}(N)$. The Hamiltonians, which are the self-adjoint operators in the N -dimensional Hilbert space, are then associated via $iH = X$ with the generators of the Lie algebra, which we will call X . These generators are precisely the anti-self-adjoint operators in the Hilbert space. Because of these properties, this symmetry class is called the *unitary symmetry class*. It has the so-called *Cartan*

11.2 Symmetry Classification of non-interacting Hamiltonians

label A. This goes back to lie Cartan who classified so-called *symmetric spaces* in 1926 [12]. In his list, he gave $U(N)$ the label A. All symmetry classes we are considering will have a Cartan label.

As a remark, we note that it is often easier to work with X 's instead of H 's because the X 's form a closed algebra under commutation.

CLASS AI. SYSTEMS WITH $\mathcal{T}^2 = \mathbb{1}$. In the case of a TRS with $\mathcal{T}^2 = \mathbb{1}$, we have $[H, \mathcal{T}] = 0$ which means $H = \mathcal{T}H\mathcal{T}$. We show that under these conditions H is *generically real*, meaning that it can be made real without being diagonalized: Take any state $|\phi_1\rangle \in \mathbb{C}^N, a_1 \in \mathbb{C}$. Then the vector

$$|\psi_1\rangle := a_1 |\phi_1\rangle + \mathcal{T}a_1 |\phi_1\rangle \quad (11.12)$$

is \mathcal{T} -invariant because $\mathcal{T}^2 = \mathbb{1}$. Now take any other state $|\phi_2\rangle \in \text{span}\{\|\phi_1\rangle\}^\perp, a_2 \in \mathbb{C}$. $|\psi_2\rangle$ constructed analogously is then again \mathcal{T} -invariant and orthogonal to ψ_1 . We continue this procedure (plus normalization) to obtain an orthonormal basis $\{|\psi_1\rangle, \dots, |\psi_N\rangle\}$ of \mathcal{T} -invariant states satisfying $\langle\psi_\mu|\psi_\nu\rangle = \delta_{\mu\nu}$. In this basis, the Hamiltonian is real, as we can easily check:

$$\begin{aligned} H_{\mu\nu} &= \langle\psi_\mu|H|\psi_\nu\rangle = \langle\mathcal{T}\psi_\mu|\mathcal{T}H\psi_\nu\rangle^* \\ &= \langle\psi_\mu|H\mathcal{T}\psi_\nu\rangle^* = \langle\psi_\mu|H\psi_\nu\rangle^* = H_{\mu\nu}^*. \end{aligned} \quad (11.13)$$

In the second equality we have used the antiunitarity of \mathcal{T} and in the third equality we have used that ψ_μ is \mathcal{T} -invariant as well as $\mathcal{T}H = H\mathcal{T}$. The fourth equality is again \mathcal{T} -invariance of the basis states. Therefore, in this basis H is indeed real and symmetric.

This real symmetry of the Hamiltonian gives an additional structure to the time evolution operator. Because H commutes with itself and $H = H^T$, we can write

$$\begin{aligned} \exp\left(-\frac{i}{\hbar}Ht\right) &= \exp\left(-\frac{i}{2\hbar}Ht\right)\exp\left(-\frac{i}{2\hbar}Ht\right) \\ &= \exp\left(-\frac{i}{2\hbar}Ht\right)\exp\left(-\frac{i}{2\hbar}Ht\right)^T. \end{aligned} \quad (11.14)$$

This means that we can write the time evolution operator as a product UU^T with $U \in U(N)$. However, this product remains unchanged if U is replaced by UO for any orthogonal matrix $O \in O(N)$. This means that the time evolution operators are only characterized up to multiplications with $O(N)$ and the space of time evolution operators is the coset $U(N)/O(N)$. The Hamiltonians are then associated with the generators of the corresponding Lie algebra, which is the tangent space of $U(N)/O(N)$ at the identity.

For all these reasons, the $\mathcal{T}^2 = \mathbb{1}$ symmetry class is called the *orthogonal symmetry class*. It has Cartan label AI.

CLASSIFICATION OF TOPOLOGICAL INSULATORS AND SUPERCONDUCTORS
[STEFAN HUBER]

CLASS AII. SYSTEMS WITH $\mathcal{T}^2 = -\mathbb{1}$. When there is a TRS present with a \mathcal{T} operator that squares to the negative identity, we have a Kramers's degeneracy, meaning that all eigenvalues of H are doubly degenerate and the dimension of the Hilbert space is even. This can be seen as follows:

Let $|\psi\rangle$ be an eigenstate of H with eigenvalue E . Then so is $\mathcal{T}|\psi\rangle$ because \mathcal{T} commutes with H . Furthermore, we have

$$\begin{aligned}\langle \psi | \mathcal{T} \psi \rangle &= \langle \mathcal{T} \psi | \mathcal{T}^2 \psi \rangle^* = -\langle \mathcal{T} \psi | \psi \rangle^* \\ &= -\langle \psi | \mathcal{T} \psi \rangle = 0.\end{aligned}\tag{11.15}$$

In the first equality we have used the antiunitarity of \mathcal{T} , in the second equality we have used that $\mathcal{T}^2 = -\mathbb{1}$, and the third equality holds because the scalar product is hermitian. So we have $|\psi\rangle \perp \mathcal{T}|\psi\rangle$, meaning that there is a degeneracy in the eigenvalue E because both these vectors live in the same eigenspace.

Before we can find the space of time evolution operators for this symmetry class, we need to take a closer look at the \mathcal{T} operator.

Kramers's degeneracy allows us to choose a basis of the form $\{|1\rangle, \mathcal{T}|1\rangle, \dots, |N\rangle, \mathcal{T}|N\rangle\}$.

In this basis, the unitary part of the \mathcal{T} operator $\mathcal{T} = UK$ is particularly simple.

Take any state and write it in the coordinates of the above basis:

$$|\psi\rangle = \sum_m (\psi_{m+} |m\rangle + \psi_{m-} \mathcal{T}|m\rangle).\tag{11.16}$$

Then, we have

$$\mathcal{T}|\psi\rangle = \sum_m (\psi_{m+}^* \mathcal{T}|m\rangle - \psi_{m-}^* |m\rangle).\tag{11.17}$$

Therefore, the unitary part of \mathcal{T} is block diagonal (it only mixes $|m\rangle$ and $\mathcal{T}|m\rangle$ coordinates) and in each of the 2D subspaces spanned by $\{|m\rangle, \mathcal{T}|m\rangle\}$, it has the form

$$\tau_2 := \begin{pmatrix} 0 & -1 \\ 1 & 0 \end{pmatrix}.\tag{11.18}$$

Now that we know how the \mathcal{T} operator looks, we can carry out a similar procedure as for class AI to find the structure of the time evolution operator. Below, we call the unitary part of \mathcal{T} Z . Commutativity of H with \mathcal{T} amounts to $H^R := ZH^TZ^{-1} = H$. We call an H that satisfies $H^R = H$ *self-dual*. Then, the time

11.2 Symmetry Classification of non-interacting Hamiltonians

evolution operator is also self-dual:

$$\begin{aligned}
\exp\left(-\frac{i}{\hbar}Ht\right)^R &= Z \exp\left(-\frac{i}{\hbar}Ht\right)^T Z^{-1} \\
&= Z \exp\left(-\frac{i}{\hbar}H^T t\right) Z^{-1} \\
&= \exp\left(-\frac{i}{\hbar}ZH^TZ^{-1}\right) \\
&= \exp\left(-\frac{i}{\hbar}H^R t\right) = \exp\left(-\frac{i}{\hbar}Ht\right).
\end{aligned} \tag{11.19}$$

Similarly to (11.14) we can write the time evolution operator as a product of the form UU^R with $U \in U(2N)$. This product is left invariant when U is replaced by US when S leaves Z invariant:

$$SZS^T = Z. \tag{11.20}$$

This is the defining equation of the so-called *symplectic group* $Sp(2N)$. Altogether, the time evolution operator is an element of the coset $U(2N)/Sp(2N)$. Therefore, the symmetry class with $\mathcal{T}^2 = -\mathbb{1}$ is called the *symplectic symmetry class* with Cartan label AII.

Now that we have classified systems solely according to their TRS we go on and classify them solely based on the next symmetry of interest which is the particle-hole symmetry.

11.2.2 PARTICLE-HOLE SYMMETRY

We take a look at the BCS Hamiltonian of a superconducting system

$$H = \frac{1}{2} \begin{pmatrix} c^\dagger & c \end{pmatrix} \begin{pmatrix} h & \Delta \\ -\Delta^* & -h^T \end{pmatrix} \begin{pmatrix} c \\ c^\dagger \end{pmatrix} + \frac{1}{2} \text{Tr}h, \tag{11.21}$$

with the restrictions

$$h_{\alpha\beta} = h_{\alpha\beta}^*, \quad \Delta_{\alpha\beta} = -\Delta_{\beta\alpha}, \tag{11.22}$$

due to self-adjointness of the Hamiltonian and Fermi statistics. We can associate the interesting part of this Hamiltonian with the $4N \times 4N$ matrix

$$\mathcal{H} = \begin{pmatrix} h & \Delta \\ -\Delta^* & -h^T \end{pmatrix}, \tag{11.23}$$

which we refer to as the Bogolyubov-deGennes Hamiltonian (BdG Hamiltonian). The fact that \mathcal{H} is a $4N \times 4N$ matrix means that our space of orbital and spin

degrees of freedom which is $2N$ -dimensional is enlarged by a 2D *particle-hole space*. Translating the restrictions of the BCS Hamiltonian to a property of the BdG Hamiltonian gives the restrictions

$$\mathcal{H} = -\Sigma_x \mathcal{H}^* \Sigma_x, \quad \Sigma_x = \begin{pmatrix} 0 & 1 \\ 1 & 0 \end{pmatrix}. \quad (11.24)$$

(We denote by $\Sigma_{x,y,z}$ a set of Pauli operators which act in particle-hole space and not in spin space.)

This symmetry describes an invariance of \mathcal{H} under the exchange of creation with annihilation operators, $c \leftrightarrow c^\dagger$, together with complex conjugation. This is why we call it a *particle-hole symmetry* PHS. We view the PHS as an antiunitary charge conjugation operator with the following properties:

$$\mathcal{C} = \Sigma_x K, \quad \mathcal{C}^2 = \mathbb{1}, \quad \{\mathcal{C}, \mathcal{H}\} = 0. \quad (11.25)$$

We should watch out because here, \mathcal{C} and \mathcal{H} do not commute, but anticommute - therefore, \mathcal{C} and \mathcal{H} do not share common eigenstates. Rather we have that if $|\psi\rangle$ is an eigenvector of \mathcal{H} with eigenvalue ω , then $\Sigma_x |\psi\rangle^*$ is also an eigenvector of \mathcal{H} with eigenvalue $-\omega$. This makes the spectrum symmetric about $E = 0$.

Despite the fact that \mathcal{H} and \mathcal{C} do not share common eigenvectors, this symmetry gives us interesting restrictions to the space of time evolution operators, as we will show soon. As with TRS, there are three cases to consider when classifying systems according to their PHS: no PHS, $\mathcal{C}^2 = \mathbb{1}$, and $\mathcal{C}^2 = -\mathbb{1}$. So far, we have seen that the case $\mathcal{C}^2 = \mathbb{1}$ is possible. We are going to see later how the case $\mathcal{C}^2 = -\mathbb{1}$ arises from requiring spin-rotation invariance.

Only considering PHS, the case of no PHS present is of course the same as the case of no symmetry at all present. This is the symmetry class A.

CLASS D. SYSTEMS WITH $\mathcal{C}^2 = \mathbb{1}$. We have already seen that systems with a PHS as described in (11.25) have a spectrum symmetric about zero. Imaginary hermitian matrices also have the property that their spectra are symmetric about zero. It turns out that we can always make a change of basis described by the unitary $4N \times 4N$ matrix

$$U = \frac{1}{\sqrt{2}} \begin{pmatrix} 1 & 1 \\ i & -i \end{pmatrix}, \quad (11.26)$$

which makes the BdG Hamiltonian imaginary. Now if the Hamiltonian is imaginary and hermitian, the generators of time translations $X = i\mathcal{H}$ are real and antisymmetric. This means that they make up the Lie algebra $\mathfrak{so}(4N)$. As a consequence, the space of time evolution operators is the Lie group $SO(4N)$. This symmetry class is called the *BdG symmetry class D* with Cartan label D.

11.2 Symmetry Classification of non-interacting Hamiltonians

CLASS C. SYSTEMS WITH $\mathcal{C}^2 = -\mathbb{1}$. We take a look at BdG Hamiltonians with spin-rotation symmetry. Then, the generators of spin rotations, which are the spin parts of the angular momentum, commute with \mathcal{H} . We denote these generators by J_k ($k = x, y, z$). After splitting the matrix index into an orbital and a spin part, $\alpha = qs$ with $q = 1, \dots, N$ and $s = \uparrow, \downarrow$, we have

$$J_k = \frac{\hbar}{2} \sum_{q,s,s'} c_{q,s}^\dagger \sigma_{k,s,s'} c_{q,s} = \frac{\hbar}{4} \begin{pmatrix} \sigma_k & 0 \\ 0 & -\sigma_k^T \end{pmatrix} \otimes \mathbb{1}_N. \quad (11.27)$$

Here, σ_k are the Pauli matrices. Now the requirement that the Hamiltonian respectively the anti-self-adjoint representative $X = i\mathcal{H}$ commutes with J_k , $[X, J_k] = 0$, gives restrictions for each of the four $2N \times 2N$ blocks of X in the particle-hole space:

$$\begin{aligned} X_{pp} &= ih = \mathbb{1}_2 \otimes a, \\ X_{ph} &= i\Delta = i\sigma_y \otimes b, \\ X_{hp} &= -i\Delta^* = -i\sigma_y \otimes c, \\ X_{hh} &= -ih^T = -\mathbb{1}_2 \otimes a^T. \end{aligned} \quad (11.28)$$

Written down in terms of orbital $N \times N$ blocks, this gives

$$X = \begin{pmatrix} a & 0 & 0 & b \\ 0 & a & -b & 0 \\ 0 & -c & -a^T & 0 \\ c & 0 & 0 & -a^T \end{pmatrix}. \quad (11.29)$$

This X is made up by two commuting subblocks, which we call X_\uparrow (the outer 2×2 block) and X_\downarrow (the inner 2×2 block). The two blocks are related by $b \rightarrow -b$, $c \rightarrow -c$. Therefore it is enough to consider only X_\uparrow . Now the restrictions from (11.22) translate into restrictions for X_\uparrow : $b = b^T$, $c = c^T$, and $a = -a^\dagger$ as well as $c = -b^\dagger$. Putting this together, we get the restrictions

$$-X_\uparrow^\dagger = X_\uparrow = -\Sigma_y X_\uparrow^T \Sigma_y, \quad \Sigma_y = \sigma_y \otimes \mathbb{1}_N. \quad (11.30)$$

These restrictions define the Lie algebra $\mathfrak{sp}(2N)$. The time evolution operators are then elements of the symplectic group $Sp(2N)$.

In analogy to (11.25), we can characterize PHS for this symmetry class via $\{\mathcal{H}_\uparrow, \mathcal{C}_\uparrow\} = 0$, with $\mathcal{C}_\uparrow = \Sigma_y K$ and $\mathcal{C}_\uparrow^2 = -\mathbb{1}$, and similarly for \mathcal{C}_\downarrow so that the total PHS operator squares to the negative identity. This symmetry class is the BdG symmetry class C.

Now that we have seen what impact the presence of a TRS or a PHS has on the space of time evolution operators of a system, we proceed by considering combinations of TRS and PHS.

CLASSIFICATION OF TOPOLOGICAL INSULATORS AND SUPERCONDUCTORS
[STEFAN HUBER]

Table 11.1: The Altland-Zirnbauer classification table. The first column lists the 10 symmetry classes by their Cartan label. The T and C columns state whether there is a TRS or PHS symmetry present and if the symmetry operator squares to plus (+1) or minus (-1) the identity. The S column states if there is a chiral symmetry present (1) or not (0). The third column gives the space of time evolution operators, and the last column lists the target spaces of the fermionic nonlinear sigma models which describe Anderson localization in the symmetry class [2].

Label	T	C	S	Space of time evolution operators	G/H (ferm. NL σ M)
A (unitary)	0	0	0	$U(N)$	$U(2n)/(U(n) \times U(n))$
AI (orthogonal)	+1	0	0	$U(N)/O(N)$	$Sp(2n)/(Sp(n) \times Sp(n))$
AII (symplectic)	-1	0	0	$U(2N)/Sp(2N)$	$O(2n)/(O(n) \times O(n))$
AIII (chiral unitary)	0	0	1	$U(N+M)/(U(N) \times U(M))$	$U(n)$
BDI (chiral orthogonal)	+1	+1	1	$O(N+M)/(O(N) \times O(M))$	$U(2n)/Sp(2n)$
CII (chiral symplectic)	-1	-1	1	$Sp(N+M)/(Sp(N) \times Sp(M))$	$U(2n)/O(2n)$
D (BdG)	0	+1	0	$SO(2N)$	$O(2n)/U(n)$
C (BdG)	0	-1	0	$Sp(2N)$	$Sp(2n)/U(n)$
DIII (BdG)	-1	+1	1	$SO(2N)/U(N)$	$O(2n)$
CI (BdG)	+1	-1	1	$Sp(2N)/U(N)$	$Sp(2n)$

11.2.3 COMBINATIONS OF THE SYMMETRY CLASSES

CLASS DIII. $\mathcal{C}^2 = \mathbb{1}$ AND $\mathcal{T}^2 = -\mathbb{1}$. We consider BdG Hamiltonians without spin-rotation symmetry (meaning that $\mathcal{C}^2 = \mathbb{1}$), but with half-integer spin TRS. The \mathcal{T} operator has the form

$$\mathcal{T} = i\sigma_y K = \mathbb{1}_2 \otimes i\sigma_y \otimes \mathbb{1}_N K := \tau K, \quad (11.31)$$

where the σ_y operator acts on the spin space. We already know from our discussion of class D that the anti-self-adjoint generators of time translations X form a $\mathfrak{so}(4N)$ algebra. In addition to that, we have the restriction coming from TRS,

$$X = \tau X^T \tau^{-1}. \quad (11.32)$$

Therefore, we want to find the set of solutions within $\mathfrak{so}(4N)$ that satisfy (11.32); let us call it \mathcal{P} . It is easy to see that \mathcal{P} is not closed under commutation: If $X_1, X_2 \in \mathcal{P}$, then

$$[X_1, X_2] = \tau [X_1^T, X_2^T] \tau^{-1} = -\tau [X_1, X_2]^T \tau^{-1}. \quad (11.33)$$

However, we see that the set of solutions of $Y = -\tau Y^T \tau^{-1}$ is closed under commutation. If we call this latter set \mathcal{K} , we can split the $\mathfrak{so}(4N)$ algebra up into $\mathfrak{so}(4N) = \mathcal{P} + \mathcal{K}$, and then the set $\mathcal{P} = \mathfrak{so}(4N) - \mathcal{K}$ is obtained by subtracting the \mathcal{K} algebra from $\mathfrak{so}(4N)$. It remains to identify \mathcal{K} .

11.2 Symmetry Classification of non-interacting Hamiltonians

We conduct a change of basis, obtaining $Y_U = U^{-1}YU$ where

$$U = \frac{1}{\sqrt{2}} \begin{pmatrix} 1 & i\sigma_y \\ \sigma_y & -i \end{pmatrix} \otimes \mathbb{1}_N. \quad (11.34)$$

Now the restrictions for \mathcal{K} become simply

$$-Y_U^\dagger = Y_U = -\Sigma_x Y_U^T \Sigma_x = \Sigma_z Y_U \Sigma_z^{-1}, \quad (11.35)$$

where $\Sigma_z = \sigma_z \otimes \mathbb{1} \otimes \mathbb{1}_N$ acts in particle-hole space. Because Y_U now has to commute with Σ_z it needs to be diagonal in particle-hole space. Furthermore, we have $Y_{U, hh} = -Y_{U, pp}^T$ from the second equality in (11.35). From anti-self-adjointness of Y , we obtain that we can write $Y_U = \begin{pmatrix} Z & 0 \\ 0 & -Z^T \end{pmatrix}$. Therefore, \mathcal{K} is isomorphic to the Lie algebra $\mathfrak{u}(2N)$ of antihermitian $2N \times 2N$ matrices, $\mathcal{K} \simeq \mathfrak{u}(2N)$. Thus \mathcal{P} is the complement of $\mathfrak{u}(2N)$ in $\mathfrak{so}(4N)$. It is the tangent space of the coset $SO(4N)/U(2N)$ which is the space of time evolution operators. This symmetry class is the BdG symmetry class DIII.

CLASS CI. $\mathcal{C}^2 = -\mathbb{1}$ AND $\mathcal{T}^2 = \mathbb{1}$. The class CI can be treated similarly to class DIII. However, due to $\mathcal{C}^2 = -\mathbb{1}$, we start with a \mathfrak{sp} algebra instead of an \mathfrak{so} algebra. At the end, the space of time evolution operators is $Sp(2N)/U(N)$ which has Cartan label CI.

11.2.4 CHIRAL SYMMETRY

Assume we have a Hamiltonian in the following block off-diagonal representation:

$$H = \begin{pmatrix} 0 & Z \\ Z^\dagger & 0 \end{pmatrix}. \quad (11.36)$$

This representation comes from a symmetry of the form

$$H = -S H S^{-1} \quad \mathcal{S} \mathcal{S}^\dagger = \mathbb{1}, \quad \mathcal{S}^2 = \mathbb{1}. \quad (11.37)$$

This symmetry is in practice often realized as a sublattice symmetry on a bipartite lattice: It is the operation that changes the sign of wave functions on all sites of one sublattice [1]. The \mathcal{S} operator is described by the product of the TRS and the PHS operators, $S = \mathcal{T} \cdot \mathcal{C}$. Therefore, in nearly every case, when we know what the system's TRS and PHS is, we know how it behaves under their product \mathcal{S} . However, it is possible for a system to have neither TRS nor PHS, but a chiral symmetry. This is the chiral class AIII which we discuss now.

CLASSIFICATION OF TOPOLOGICAL INSULATORS AND SUPERCONDUCTORS
[STEFAN HUBER]

CLASS AIII. SYSTEMS WITH CHIRAL SYMMETRY ONLY. We assume only that we have a Hamiltonian in the block off-diagonal representation as in (11.36), with $Z \in \text{Mat}(N \times M, \mathbb{C})$. Such block off-diagonal matrices make up the tangent space of the coset $U(N + M)/ (U(N) \times U(M))$ [6]. Thus the time evolution operators are in $U(N + M)/ (U(N) \times U(M))$, and for $M = N$, they live in $U(2N)/ (U(N) \times U(N))$. This is the *chiral unitary class* with Cartan label AIII. We have seen that for both TRS and PHS, we have 3 cases to consider. Combining these symmetries, we get 9 symmetry classes. For 8 of these 9 symmetry classes the behavior of the system under chiral symmetry is fixed by TRS and PHS. However, as mentioned above, if there is neither TRS nor PHS, we can be either in class A or in class AIII. This means that altogether, we have 10 symmetry classes. 8 of these classes we have already discussed. It remains to mention the last 2 classes, both of which have a chiral symmetry.

CHIRAL CLASS CII. $\mathcal{C}^2 = -\mathbb{1}$ AND $\mathcal{T}^2 = -\mathbb{1}$. If we have a system with a PHS with $\mathcal{C}^2 = -\mathbb{1}$ and a chiral symmetry present, then it automatically fulfills a half-integer spin TRS. The properties of the chiral symmetry and the PHS are enough to characterize the system. We already know from our discussion of class C that the time evolution operators in a $\mathcal{C}^2 = -\mathbb{1}$ system are elements of the symplectic group. Furthermore, the chiral symmetry gives the coset structure as in class AIII to the space of time evolution operators. The difference is just that here we have the Sp group as a starting point. Hence the space of time evolution operators is $Sp(N + M)/ (Sp(N) \times Sp(M))$. This is the *chiral symplectic class* with Cartan label CII.

CHIRAL CLASS BDI. $\mathcal{C}^2 = \mathbb{1}$ AND $\mathcal{T}^2 = \mathbb{1}$. In analogy to the chiral classes we have already discussed, in this class, the $\mathcal{C}^2 = \mathbb{1}$ gives us the orthogonal group as a starting point to form the space of time evolution operators. It is $O(N + M)/ (O(N) \times O(M))$. This class is the *chiral orthogonal class* with Cartan label BDI.

Now we have characterized all 10 symmetry classes via their symmetries and the space of time evolution operators. We compile all this information together now. Table 11.1 lists all symmetry classes together with their space of time evolution operators. It is the Altland-Zirnbauer classification table, named after Alexander Altland and Martin R. Zirnbauer who extended the Wigner-Dyson classes to these 10 symmetry classes in 1997 [7]. It originally comes from the field of random matrix theory because to each of the symmetry classes we can assign an ensemble of random matrices which describes the random potential in a solid state system. We have not yet explained the last column of the table. Its role will

11.3 Gapped bulk Hamiltonians

become clearer later, when we briefly discuss nonlinear sigma models and their connection to Anderson localization. In short, the last column tells us the target space of the nonlinear sigma model which should be used as a microscopic model when we ask the question if we have charge-carrying states on the boundary of our sample [2, 1, 13].

Next, we want to extract topological information out of the Altland-Zirnbaumer table. In order to achieve that, we need to introduce the *spectral projection operator* and the mathematical concepts of the *fundamental group* and *homotopy groups*.

11.3 GAPPED BULK HAMILTONIANS

11.3.1 PROJECTION OPERATOR

We consider Bloch Hamiltonians with a bulk band gap. In general, the band structure can be seen as a mapping from the Brillouin zone to the space of Hamiltonians. The spectral projection operator is a similar mapping from the Brillouin zone into the *space of projection operators* or *target space*. It reflects the topology of the band structure by carrying the topological information about a Hamiltonian, but having a simple spectrum which only consists of $\{\pm 1\}$. The construction follows [1] and [13].

Consider an eigenvalue problem with translational invariance. In momentum space, we can describe such a system by a matrix equation at each momentum k in the Brillouin zone:

$$\mathcal{H}(k) |u_{\hat{a}}(k)\rangle = E_{\hat{a}}(k) |u_{\hat{a}}(k)\rangle, \quad (11.38)$$

with a band index \hat{a} . We can define a projector onto the filled states in the following way:

$$P(k) := \sum_{\hat{a}}^{\text{filled}} |u_{\hat{a}}(k)\rangle \langle u_{\hat{a}}(k)|. \quad (11.39)$$

Now we can introduce the so-called *Q matrix*

$$Q(k) := 2P(k) - \mathbb{1}, \quad (11.40)$$

which has some useful properties. We see that for each k , $Q(k)$ is Hermitian, it squares to the identity and if we have m filled states and n empty states, it has trace $\text{Tr } Q(k) = m - n$. Moreover, for the basis Bloch states, we have $Q(k) |u_{\hat{a}}(k)\rangle = \pm |u_{\hat{a}}(k)\rangle$, with a + sign for a filled state and a - sign for an empty state.

Therefore the $Q(k)$ can be seen as a *simplified Hamiltonian* which carries all the topological information of the original Hamiltonian but has a simple spectrum $\{\pm 1\}$. It can be obtained from $\mathcal{H}(k)$ by "flattening the bands", namely assigning the energy $+1$ to the filled bands and -1 to the empty bands. This can be done by a continuous transformation and without closing the energy gap.

Now that we have constructed the Q matrix, we ask the question to what matrix space Q maps when we are in a given symmetry class.

11.3.2 THE TARGET SPACE

If we are in the simplest symmetry class A where no symmetries are present, the Hamiltonian is a general hermitian matrix. Then, the set of $n + m$ eigenvectors make up a unitary matrix in $U(n+m)$. However, when we consider as above projectors onto filled states, we can relabel empty and filled states among themselves without changing the physics. This gives us an additional "gauge symmetry" and makes the Q matrix $Q(k)$ be an element of $U(n+m)/(U(n) \times U(m))$. So our Q is a mapping from the reciprocal unit cell to $U(n+m)/(U(n) \times U(m))$, and for each k we have such a matrix $Q(k)$ as a "value" of Q at k .

Other symmetry classes have additional constraints to the space of projectors. For more details, see [1, 6].

This $Q(k)$ can, for instance, wind around in the target space as k runs over the Brillouin zone. Such a winding number is a topological invariant which cannot be changed by continuous deformations of the mapping. Now the question of the existence of different topological phases amounts to the question how many different mappings Q can be possible which cannot be deformed into each other continuously, without closing the band gap. This question is answered by the mathematical concept of the *homotopy group*, which we introduce below.

11.4 MATHEMATICAL CONCEPTS FROM TOPOLOGY

We give a short introduction to the concepts of the *fundamental group* and *homotopy groups*. They treat the question of the existence of a continuous deformation between periodic functions mapping into some space in an elegant way. A rough understanding of the geometrical ideas behind these concepts is useful for the rest of our discussion. A standard introduction to topology is [15], and an introduction of the homotopy group for physical purposes can be found in [16].

11.4 Mathematical concepts from topology

Table 11.2: The table of homotopy groups $\pi_{\bar{d}}(G/H)$ of symmetric spaces G/H for sufficiently large N,M. The table is 8-fold periodic in \bar{d} . The existence of a $(\bar{d} + 1)$ -dimensional topological insulator is marked with an underline. The symmetry classes with a chiral symmetry are marked bold in the first column. It is remarked that there are 5 nontrivial topological insulators/superconductors in each spatial dimension. Furthermore, for the special case $d = 3$ ($\bar{d} = 2$), every nontrivial topological insulator/superconductor has some TRS [2]. Moreover, there is a regularity pattern in this table [2, 14].

AZ	G/H	$\bar{d} = 0$	$\bar{d} = 1$	$\bar{d} = 2$	$\bar{d} = 3$	$\bar{d} = 4$	$\bar{d} = 5$	$\bar{d} = 6$	$\bar{d} = 7$
<i>Complex case:</i>									
A	$U(N+M)/(U(N) \times U(M))$	$\leftarrow \mathbb{Z}$	$\underline{\mathbf{0}}$						
AIII	$U(N)$	$\underline{\mathbf{0}}$	$\leftarrow \mathbb{Z}$						
<i>Real case:</i>									
AI	$Sp(N+M)/(Sp(N) \times Sp(M))$	$\leftarrow \mathbb{Z}$	0	0	$\underline{\mathbf{0}}$	$\leftarrow \mathbb{Z}$	\mathbb{Z}_2	\mathbb{Z}_2	$\underline{\mathbf{0}}$
BDI	$U(2N)/Sp(2N)$	$\underline{\mathbf{0}}$	$\leftarrow \mathbb{Z}$	0	0	$\underline{\mathbf{0}}$	$\leftarrow \mathbb{Z}$	\mathbb{Z}_2	\mathbb{Z}_2
D	$O(2N)/U(N)$	\mathbb{Z}_2	$\underline{\mathbf{0}}$	$\leftarrow \mathbb{Z}$	0	0	$\underline{\mathbf{0}}$	$\leftarrow \mathbb{Z}$	\mathbb{Z}_2
DIII	$O(N)$	\mathbb{Z}_2	\mathbb{Z}_2	$\underline{\mathbf{0}}$	$\leftarrow \mathbb{Z}$	0	0	$\underline{\mathbf{0}}$	$\leftarrow \mathbb{Z}$
AII	$O(N+M)/(O(N) \times O(M))$	$\leftarrow \mathbb{Z}$	\mathbb{Z}_2	\mathbb{Z}_2	$\underline{\mathbf{0}}$	$\leftarrow \mathbb{Z}$	0	0	$\underline{\mathbf{0}}$
CII	$U(N)/O(N)$	$\underline{\mathbf{0}}$	$\leftarrow \mathbb{Z}$	\mathbb{Z}_2	\mathbb{Z}_2	$\underline{\mathbf{0}}$	$\leftarrow \mathbb{Z}$	0	0
C	$Sp(2N)/U(N)$	0	$\underline{\mathbf{0}}$	$\leftarrow \mathbb{Z}$	\mathbb{Z}_2	\mathbb{Z}_2	$\underline{\mathbf{0}}$	$\leftarrow \mathbb{Z}$	0
CI	$Sp(2N)$	0	0	$\underline{\mathbf{0}}$	$\leftarrow \mathbb{Z}$	\mathbb{Z}_2	\mathbb{Z}_2	$\underline{\mathbf{0}}$	$\leftarrow \mathbb{Z}$

11.4.1 THE FUNDAMENTAL GROUP

Let X be a topological space and $p \in X$ be any base point.

LOOPS AT P

Consider continuous closed curves in X which pass through p , i.e.:

$$f : [0, 1] \rightarrow X, \quad f(0) = f(1) = p. \quad (11.41)$$

Such an f can be naturally viewed as a continuous map from the unit circle to X : $f : \mathcal{S}^1 \rightarrow X$.

HOMOTOPIES

Two loops f, g are called homotopic at p if there exists a based homotopy between them, meaning a continuous family of loops

$$\begin{aligned} h_t : [0, 1] \times \mathcal{S}^1 &\rightarrow X \\ \text{so that} \\ h_0 = f, \quad h_1 = g, \quad h_t(0) = h_t(1) = p \quad \forall t \in [0, 1]. \end{aligned} \quad (11.42)$$

This means that we can find a continuous deformation to bring f to g via loops only.

CLASSIFICATION OF TOPOLOGICAL INSULATORS AND SUPERCONDUCTORS
[STEFAN HUBER]

PRODUCT OF LOOPS

The product of two loops f, g is defined via

$$(f \circ g)(z) = \begin{cases} f(2z) & 0 \leq z \leq \frac{1}{2} \\ g(2z - 1) & \frac{1}{2} \leq z \leq 1 \end{cases} \quad (11.43)$$

This product connects two loops by "running" through the first one in double speed and then through the second one in double speed. Note that this product is not associative: $(f \circ (g \circ h))$ runs through f between 0 and 1/2, through g between 1/2 and 3/4 and through h between 3/4 and 1, while the product $((f \circ g) \circ h)$ runs through f between 0 and 1/4, through g between 1/4 and 1/2, and through h between 1/2 and 1.

However, we see that being homotopic defines an equivalence relation. We call the equivalence classes under this equivalence relation *homotopy classes*. Then the parametrization of a loop as well as continuous deformations do not matter, and we can give a group structure to the set of homotopy classes via

$$[f] \circ [g] = [f \circ g], \quad (11.44)$$

where $[f]$ means the homotopy class to which f belongs.

The set of all homotopy classes with this product is the so-defined *fundamental group* $\pi_1(X, p)$ of X at p . We remark that $\pi_1(X, p)$ only depends on the path-connected component of p , and for path-connected spaces, $\pi_1(X, p) \simeq \pi_1(X)$ is independent of p . Therefore we drop the p from now on.

11.4.2 EXAMPLES

Before proceeding to generalizations, we give some geometrically simple examples:

- The plane without a point has a winding number that indexes the homotopy classes: $\pi_1(\mathbb{C} \setminus \{z_0\}) \simeq \mathbb{Z}$.
- The circle also has a winding number that indexes the homotopy classes: Due to continuity, for any loop $f : S^1 \rightarrow S^1$, we need $f(x+2\pi) = f(x)+2\pi k$ for some $k \in \mathbb{Z}$. This k is the winding number of f , also called its degree. $\pi_1(S^1) \simeq \mathbb{Z}$.
- The sphere is simply connected. Therefore, every loop is contractible to the constant map, and the fundamental group is trivial. This generalizes to higher dimensions; hence we have:

$$\pi_1(S^n) \simeq \{0\} \forall n \geq 2.$$

11.4 Mathematical concepts from topology

- The torus has two independent winding numbers because it is the Cartesian product of two circles, $\pi_1(T^2) \simeq \mathbb{Z}^2$. Therefore, tuples of integers index the homotopy classes.

11.4.3 HOMOTOPY GROUPS

So far, we have taken a look at continuous maps $f : \mathcal{S}^1 \rightarrow X$ from the unit circle to the topological space X . From homotopy classes of such maps, we have built up the fundamental group $\pi_1(X)$. The fundamental group is also called the *first homotopy group*. In order to generalize this to homotopy groups, we take a look of images of d -spheres for $d \geq 1$. The d -th homotopy group is then the set of homotopy classes of maps $f : \mathcal{S}^d \rightarrow X$. These are no longer loops, but areas, volumes and generalized volumes (nonetheless with periodicities) in the topological space X .

Before giving some examples, we explain that we have a need for this generalization to higher homotopy groups because the Brillouin zone can be higher-dimensional as well. The fundamental group only covers periodic maps from a 1D space to the target space. It is remarked that although our Brillouin zone might not be topologically equivalent to a sphere but to, say, a torus, all the so-called *strong* topological features are covered by our approach of using the homotopy group which describes maps from spheres to the target space. Such strong topological features are independent of the presence of translational symmetry. Additional features may occur from a Brillouin zone which has different boundary conditions, but these are the so-called *weak* topological features which are essentially layers of strong topological insulators of lower dimensionality. They are not specifically covered by our approach. For more details, see [2] and [4, 5].

11.4.4 SIMPLE EXAMPLES FOR HIGHER HOMOTOPY GROUPS

We give some simple examples for homotopy groups of spheres to get some intuition of what is going on in a homotopy group.

- The second homotopy group of the 2-sphere describes the wrapping of a sphere around a sphere. Such a wrapping can also have a winding number, just like the wrapping of a circle around a circle, and $\pi_2(\mathcal{S}^2) \simeq \mathbb{Z}$.
- We have seen that the fundamental group of the circle is isomorphic to \mathbb{Z} , and the same holds for the second homotopy group of the 2-sphere. This generalizes to $\pi_n(\mathcal{S}^n) \simeq \mathbb{Z} \forall n \in \mathbb{N}$.

- We have seen that the fundamental group of the 2-sphere is trivial because of simply connectedness. This also generalizes to higher dimensions: $\pi_i(S^n) \simeq \{0\}$ if $i < n$.
- The only interesting examples when looking at spheres are the homotopy groups $\pi_i(S^n)$ for $n > i$. However, the simplest such example is trivial: $\pi_2(S^1) \simeq \{0\}$. A rather well-known example for a non-trivial homotopy group of this category is $\pi_3(S^2) \simeq \mathbb{Z}$ which is generated by the *Hopf fibration*.

In general, it is very hard to calculate homotopy groups even for spheres. Fortunately, there is a theorem in mathematics that gives us relations of the homotopy groups of the classical Lie groups U , O , and Sp . This is the Bott periodicity theorem, first stated by Raoul Bott in the late 1950s [17, 18].

11.4.5 BOTT PERIODICITY THEOREM

The Bott periodicity theorem states that the homotopy groups of the infinite classical Lie groups are periodic:

$$\begin{aligned}\pi_k(U) &= \pi_{k+2}(U), \\ \pi_k(O) &= \pi_{k+4}(Sp), \\ \pi_k(Sp) &= \pi_{k+4}(O).\end{aligned}\tag{11.45}$$

Here, U is understood as the direct limit of the sequence of inclusions

$$U(1) \subset U(2) \subset \cdots \subset U = \cup_{k=1}^{\infty} U(k),\tag{11.46}$$

and analogously for O and Sp .

Due to the Bott periodicity theorem, we expect an 8-fold periodicity in the homotopy groups of our target spaces. Our N is the number of bands respectively the number of sites, which we take to be very large. Then, the homotopy group of our target space is independent of N and only dependent on the dimensionality. Table 11.2 gives the homotopy groups of the target spaces of the different symmetry classes for different boundary dimensionalities \bar{d} . Before we see what the results for each dimension and class mean, we give an introduction to nonlinear sigma models (NL σ M) which describe Anderson localization transitions in the different symmetry classes.

11.5 Nonlinear sigma models

11.5 NONLINEAR SIGMA MODELS

A nonlinear σ model (NL σ M) is a scalar field theory whose field takes values in some target manifold which is equipped with a Riemannian metric. It is a generalization of the Heisenberg ferromagnet, which implements $O(3)$ symmetry breaking. However, in a general NL σ M, the spins can sweep out a general symmetric space (the target space) and not only the unit sphere. Anderson localization is the phenomenon of the appearance of completely localized eigenstates of an electron moving in a random potential. Anderson transitions break a more abstract $O(N)$ symmetry, which is why the generalization of the Heisenberg ferromagnet can be used to describe such transitions. A more detailed discussion of the connections of Anderson localization to $O(N)$ symmetry breaking and NL σ Ms can be found in [10].

Now if we terminate the bulk of a topological insulator sample with a boundary, there appear gapless surface states at the boundary which should be extended. The microscopic model of such an insulator can be described by a NL σ M. The symmetry class in which we are tells us which target space to use for the NL σ M, see the last column of table 11.1. Depending on the homotopy group of the target space, there are different nontrivial topological terms which can be added to the action of the NL σ M and which then introduce topological invariants. These topological invariants then protect the topological phase - two insulating states with different topological invariants cannot be deformed into each other by a perturbation that does not close the bulk gap.

We use the field $Q \in G/H$ for the NL σ M. The simplest action for such a field is given by

$$S = \sigma_{xx} \int d^d r \text{Tr} [\partial_\mu Q \partial_\mu Q], \quad (11.47)$$

where σ_{xx} is a constant. The partition function is then calculated by the path integral

$$Z = \int \mathcal{D}Q \exp(-S). \quad (11.48)$$

There are two nontrivial topological terms in our interest: The so-called WZW term and a term of \mathbb{Z}_2 type.

THE WESS-ZUMINO-WITTEN TERM

When the d -th homotopy group of the target space, where d is the spatial dimensionality (the dimensionality of the bulk), is isomorphic to \mathbb{Z} , $\pi_d(G/H) \simeq \mathbb{Z}$, the so-called *Wess-Zumino-Witten term* (WZW term) can be introduced to the

CLASSIFICATION OF TOPOLOGICAL INSULATORS AND SUPERCONDUCTORS
[STEFAN HUBER]

action.

$$Z = \int \mathcal{D}q \exp(2\pi i\nu \Gamma_{WZW}) \exp(-S[q]),$$

where

$$\Gamma_{WZW} = \frac{1}{24\pi^2} \int_{B^3} \text{Tr} \left[(q^{-1} \partial q)^3 \right], \quad (11.49)$$

in 3 dimensions, for instance. The constant ν is a coupling constant which is typically an integer. The WZW term describes a winding of the q mapping in the target space. We will see the meaning of using q instead of Q later when we take a look at the formulation of topological invariants.

Since a WZW term can be nontrivial when $\pi_d(G/H) \simeq \mathbb{Z}$ and $d = \bar{d} + 1$ and table 11.2 gives the homotopy groups for given \bar{d} , we put an arrow to the left when the homotopy group is isomorphic to \mathbb{Z} . Then, the existence of a $(\bar{d} + 1)$ dimensional \mathbb{Z} topological insulator is marked by an underlined 0 in the table, when in the next higher dimension the homotopy group is \mathbb{Z} .

THE \mathbb{Z}_2 TERM

When the \bar{d} -th homotopy group of the target space, where $\bar{d} = d - 1$ is the dimensionality of the boundary, is isomorphic to \mathbb{Z}_2 , $\pi_{\bar{d}}(G/H) \simeq \mathbb{Z}_2$, a nontrivial \mathbb{Z}_2 term can be introduced to the action.

$$Z = \int \mathcal{D}Q (-1)^{n[Q]} \exp(-S[Q]), \quad n[Q] \in \{0, 1\}. \quad (11.50)$$

The $n[Q]$ invariant can be, for instance, the usual bulk \mathbb{Z}_2 invariant which uses the Pfaffian of the sewing matrix, or the sign of a Chern number, which we have seen in the dimensional reduction procedure in the topological field theory section of the proseminalar.

As this \mathbb{Z}_2 term can be nontrivial when $\pi_{\bar{d}}(G/H) \simeq \mathbb{Z}_2$, the existence of a $(\bar{d} + 1)$ dimensional \mathbb{Z}_2 topological insulator is marked by an underlined \mathbb{Z}_2 in table 11.2. This is the case for all \mathbb{Z}_2 's in the table.

In the rest of our discussion, we do not specifically use NL σ Ms. Rather, we take a look at the different topological invariants which protect the topological phase and give some well-known examples of topological insulators and show how they fit into the machinery developed so far, especially table 11.2.

11.6 TOPOLOGICAL INVARIANTS

We state some different topological invariants which can be used to characterize the topological phase of an insulator. A detailed discussion for different symmetry

11.6 Topological Invariants

classes and dimensionalities can be found in [2].

11.6.1 WINDING NUMBERS FOR CHIRAL SYMMETRY CLASSES

We already know that for systems with chiral symmetry, the Hamiltonians can be brought into a block off-diagonal form as in equation (11.36). This also holds for the Q matrices, and we have for instance, in class AIII:

$$Q(k) = \begin{pmatrix} 0 & q(k) \\ q^\dagger(k) & 0 \end{pmatrix}, \quad q \in U(N). \quad (11.51)$$

The off-diagonal part $q(k)$ defines a map from the Brillouin zone onto $U(N)$, and the homotopy group $\pi_d(U(N)) \simeq \mathbb{Z}$ is isomorphic to \mathbb{Z} for d odd and trivial for d even, see table 11.2. Therefore, in odd spatial dimensions, we can have a winding number characterization of the topological phases. Such a winding number in a general odd spatial dimension has the form

$$\nu_{2n+1}[q] = \frac{(-1)^n n!}{(2n+1)!} \left(\frac{i}{2\pi} \right)^{n+1} \int_{BZ} \epsilon^{\alpha_1 \alpha_2 \dots} \text{Tr} [q^{-1} \partial_{\alpha_1} q \cdot q^{-1} \partial_{\alpha_2} q \dots] d^{2n+1} k. \quad (11.52)$$

Now, Q matrices with different winding numbers cannot be adiabatically deformed into each other without closing the bulk gap. In this special case of the symmetry class AIII, we have a \mathbb{Z} characterization in all odd spatial dimensions and a trivial topology in even spatial dimensions.

In the case where there is no chiral symmetry present, we can use the Chern numbers to characterize the Q matrix.

11.6.2 CHERN NUMBERS

In general, a Chern character respectively Chern number has the form

$$\text{Ch}_{n+1}[\mathcal{F}] = \frac{1}{(n+1)!} \int_{BZ} \text{Tr} \left(\frac{i\mathcal{F}}{2\pi} \right)^{n+1}, \quad (11.53)$$

where \mathcal{F} is the Chern-Simons form. It is defined without assuming chiral symmetry and the corresponding block off-diagonal representation of the Q matrix and can also be used for symmetry classes without chiral symmetry.

We conclude our discussion by showing how some well-known examples for different \mathbb{Z} and \mathbb{Z}_2 topological insulators/superconductors fit into our machinery and giving an explicit example for a 3D Dirac Hamiltonian in symmetry class AIII.

11.7 EXAMPLES

Throughout this proseminar, we have seen a few examples of topological insulators and superconductors. Now we take a look at some of them and see how they fit into table 11.2, and how we could have anticipated the classification type of them.

11.7.1 \mathbb{Z} CLASSIFICATION

Probably the best-known example for a \mathbb{Z} classification is the IQHE, which is in symmetry class A in 2D. It has no discrete symmetries. Looking up the entry in table 11.2 for class A and $\bar{d} = 1$, we see an underlined zero: The second homotopy group of $U(2N)/ (U(N) \times U(N))$ is isomorphic to \mathbb{Z} , $\pi_2(U(2N)/ (U(N) \times U(N))) \simeq \mathbb{Z}$. This means that the topological sectors of a class A system in 2 spatial dimensions ($d = 2$ and $\bar{d} = 1$) are characterized by a winding number quantity. This winding number tells us in which quantum hall plateau we are. All these plateaux make up a series of insulators which are topologically inequivalent. Another example for a \mathbb{Z} classification are the $p + ip$ - and $d + id$ -wave superconductors: The $p + ip$ -wave superconductor is an example for class D in 2D and the $d + id$ -wave superconductor lives in class C in 2D. Both these classes allow an integer labeling of their topological sectors.

11.7.2 \mathbb{Z}_2 CLASSIFICATION

A well-known example of a topological insulator with a \mathbb{Z}_2 classification is the \mathbb{Z}_2 topological insulator, which has a half-integer spin TRS. It lives in class AII in 2D or 3D. In both cases, the relevant homotopy group is isomorphic to \mathbb{Z}_2 : $\pi_1(O(2N)/ (O(N) \times O(N))) \simeq \pi_2(O(2N)/ (O(N) \times O(N))) \simeq \mathbb{Z}_2$. The relevant topological invariants are the \mathbb{Z}_2 topological invariants, which, for instance, can be the ones which use the Pfaffian of the sewing matrix. The 2D case has already been shown in the proseminalar.

The Kitaev Majorana Chain lives in symmetry class D in 1D. It has a PHS with $\mathcal{C}^2 = \mathbb{1}$ and also allows for a \mathbb{Z}_2 invariant.

The results of the dimensional reduction procedures which can be done in the topological field theory description are also examples for a \mathbb{Z}_2 classification: When going from TQFT in $(2+1)$ D to TQFT in $(1+1)$ D in Class D (maintaining PHS), we were able to define a \mathbb{Z}_2 invariant by taking the sign of the Chern number in 2D, where we came from. The relevant homotopy group in 1D is $\pi_0(O(2N)/U(N)) \simeq \mathbb{Z}_2$, which makes us anticipate that this topological invariant

11.7 Examples

will be a good topological invariant. The same applies for the reduction procedure from TQFT in (4+1)D to TQFT in (3+1)D in class AII, maintaining half-integer TRS. There we go from a \mathbb{Z} classification to a \mathbb{Z}_2 classification and can also take the sign of the Chern number as the new topological invariant. Details of this procedure can be found in Florian Johne's report about Topological Field Theory. At the end of our discussion, we give an example for a Dirac Hamiltonian in class AIII in 3D and show how we can apply the worked out machinery to it.

11.7.3 3D FOUR-COMPONENT DIRAC HAMILTONIAN

We take a look at a four-component (3+1)D Dirac Hamiltonian. The connection between topological insulators and Dirac Hamiltonians is that topological insulators typically have a strong spin-orbit coupling. The Dirac equation takes care of a strong spin-orbit coupling and therefore the chances are good that a Dirac-type Hamiltonian gives us a simple description of a topological insulator which already has nontrivial topological properties. A detailed treatment of the connections of topological insulators with the Dirac equation is given in [19]. A treatment of the given example for other symmetry classes, and some more examples (one for each nontrivial topological insulator in 3D), can be found in [1].

Consider a four-component (3+1)D Dirac Hamiltonian,

$$\mathcal{H} = -i\partial_\mu\alpha_\mu + m\beta, \quad \mu = x, y, z, \quad m \in \mathbb{R}, \quad (11.54)$$

where we use the Dirac representation of the gamma matrices:

$$\alpha_\mu = \tau_x \otimes \sigma_\mu = \begin{pmatrix} 0 & \sigma_\mu \\ \sigma_\mu & 0 \end{pmatrix}, \quad \beta = \tau_z = \begin{pmatrix} 1 & 0 \\ 0 & -1 \end{pmatrix}. \quad (11.55)$$

Going to momentum space, the Hamiltonian becomes

$$\mathcal{H}(k) = \alpha_\mu k_\mu + m\beta = \begin{pmatrix} m & k \cdot \sigma \\ k \cdot \sigma & -m \end{pmatrix}, \quad (11.56)$$

with a spectrum $E(k) = \pm\sqrt{k^2 + m^2} =: \pm\lambda(k)$ which is twofold degenerate for each k . We want to view this Hamiltonian (11.54) as an insulator in class AIII with the chiral symmetry $\tau_y \mathcal{H} \tau_y = -\mathcal{H}$. There are different ways to interpret it as a member of different symmetry classes which is due to a freedom in interpretation of the two gradings represented by σ_μ and τ_μ , but we want to focus on class AIII here. For more details, see [1]. We can bring our Hamiltonian into its block off-diagonal form by a rotation $\tau_y \mapsto \tau_z$, which makes the mass term imaginary, to obtain

$$\mathcal{H}(k) = \begin{pmatrix} 0 & k \cdot \sigma - im \\ k \cdot \sigma + im & 0 \end{pmatrix}. \quad (11.57)$$

CLASSIFICATION OF TOPOLOGICAL INSULATORS AND SUPERCONDUCTORS
[STEFAN HUBER]

The chiral symmetry is now reflected by the fact that $\beta\mathcal{H}(k)\beta = -\mathcal{H}(k)$. Now we want to find the Q matrix of this Hamiltonian. In order to do that, we first find its eigenfunctions. We define $k_{\pm} = k_x \pm ik_y$ and have the negative energy eigenfunctions

$$\begin{aligned} |u_1(k)\rangle &= \frac{1}{\sqrt{2\lambda(\lambda+m)}} \begin{pmatrix} -k_- \\ k_z \\ 0 \\ \lambda+m \end{pmatrix}, \\ |u_2(k)\rangle &= \frac{1}{\sqrt{2\lambda(\lambda+m)}} \begin{pmatrix} -k_z \\ -k_+ \\ \lambda+m \\ 0 \end{pmatrix}. \end{aligned} \quad (11.58)$$

The positive energy eigenfunctions are

$$\begin{aligned} |u_3(k)\rangle &= \frac{1}{\sqrt{2\lambda(\lambda-m)}} \begin{pmatrix} k_- \\ -k_z \\ 0 \\ \lambda-m \end{pmatrix}, \\ |u_4(k)\rangle &= \frac{1}{\sqrt{2\lambda(\lambda-m)}} \begin{pmatrix} k_z \\ k_+ \\ \lambda-m \\ 0 \end{pmatrix}. \end{aligned} \quad (11.59)$$

Next we calculate the projector onto the two negative energy states:

$$\begin{aligned} P(k) &= |u_1(k)\rangle \langle u_1(k)| + |u_2(k)\rangle \langle u_2(k)| \\ &= \frac{1}{2\lambda(\lambda+m)} \left(\begin{pmatrix} -k_- \\ k_z \\ 0 \\ \lambda+m \end{pmatrix} \begin{pmatrix} -k_- \\ k_z \\ 0 \\ \lambda+m \end{pmatrix}^\dagger + \begin{pmatrix} -k_z \\ -k_+ \\ \lambda+m \\ 0 \end{pmatrix} \begin{pmatrix} -k_z \\ -k_+ \\ \lambda+m \\ 0 \end{pmatrix}^\dagger \right) \end{aligned} \quad (11.60)$$

After simplifying, it is equal to

$$P(k) = \frac{1}{2\lambda} \begin{pmatrix} \lambda-m & 0 & -k_z & -k_- \\ 0 & \lambda-m & -k_+ & k_z \\ -k_z & -k_- & \lambda+m & 0 \\ -k_+ & k_z & 0 & \lambda+m \end{pmatrix}. \quad (11.61)$$

Then the Q matrix is given by

$$Q(k) = 2P(k) - \mathbb{1} = -\frac{1}{\lambda} (k_\mu \alpha_\mu + m\beta). \quad (11.62)$$

11.7 Examples

Similarly to the Hamiltonian, in the block off-diagonal representation, the mass term becomes imaginary, and so the off-diagonal component of the Q matrix is

$$q(k) = -\frac{1}{\lambda} (k_\mu \sigma_\mu - im). \quad (11.63)$$

The winding number (11.52) for the mapping q which maps from the 3D Brillouin zone (which is topologically equivalent to a 3-sphere) into $U(2)$, $q : S^3 \rightarrow U(2)$, is then

$$\nu [q] = \frac{1}{2} \frac{m}{|m|}. \quad (11.64)$$

Firstly, this winding number should be read as $\frac{m}{|m|}$. The prefactor of 1/2 is common to continuum models and needs to be supplemented by information about the structure of wave functions at high energy, away from the Dirac point [1]. A discussion of this in relation to the IQHE was done by Haldane [20].

Secondly, this quantity looks like a \mathbb{Z}_2 quantity, because it can only be ± 1 , but a look into the table 11.2 reveals that it is really a \mathbb{Z} winding number. We have considered the simplest four-component model which only describes one flavor of fermions. When we consider more complex models with more flavors, the winding number can increase and take more integer values than just ± 1 .

Now we want to show that there is a gapless surface state present which reflects the nontrivial topology of the bulk. Let us terminate the 3D bulk by a 2D boundary at $z = 0$. Then take a z -dependent mass term

$$m(z) \rightarrow \begin{cases} +m, & z \rightarrow +\infty \\ -m, & z \rightarrow -\infty \end{cases}, \quad (11.65)$$

where $m > 0$. This produces a boundary between two different topological sectors. Next, we look for 2D fermion solutions localized at the boundary $z = 0$. There is a solution to the 3D Dirac equation

$$\psi(z) = \begin{pmatrix} 0 \\ a(k_\perp) \\ b(k_\perp) \\ 0 \end{pmatrix} \exp \left[- \int^z dz' m(z') \right], \quad (11.66)$$

where $k_\perp = (k_x, k_y)$ is the 2D momentum along the surface and $a(k_\perp)$ and $b(k_\perp)$ are obtained from the solution to the 2D Dirac equation. Writing $x_\perp = (x, y)$ for the coordinates along the surface, we have

$$\begin{pmatrix} a(k_\perp) \\ b(k_\perp) \end{pmatrix} = \frac{\exp(ik_\perp \cdot x_\perp)}{\sqrt{2}} \begin{pmatrix} \exp(i\arg k_+) \\ \pm 1 \end{pmatrix}, \quad (11.67)$$

with energy dispersion $E(k_\perp) = \pm\sqrt{k_x^2 + k_y^2}$. Therefore, we see that there is a surface state with a gapless spectrum which is only dependent on the surface momentum in the $z = 0$ plane. This gapless surface state is protected against perturbations by the nontrivial winding number (11.64). A possible perturbation of such a single flavor of 2D Dirac fermions in the chiral symmetry class AIII is a static, homogeneous vector potential, which does only shift the location of the node, but not open a gap. For more complex models with a higher number of flavors of gapless surface states, the winding number (which can then take on more values than just ± 1) protects these states as well.

11.8 CONCLUSION

We have presented a general way to classify the types of topological insulators and superconductors depending on their symmetry properties. The different symmetry classes we used originally occurred in the Altland-Zirnbauer classification scheme for random matrices, developed in the mid-1990s [6, 7]. These 10 symmetry classes generalize the Wigner-Dyson classes which had been introduced much earlier [8] to TRS and PHS, as well as chiral symmetry.

The connection of these symmetry classes to topology comes from the question of inter-deformability of quantum ground states within a symmetry class, while the symmetries keep being present. This question is answered by the homotopy group. Table 11.2 then gives us a powerful tool to predict the existence of topological insulators and superconductors in a given symmetry class and dimensionality. It is the central result of this report. The table tells us that in every dimension, there are 5 nontrivial topological insulators respectively superconductors. In 3D, all nontrivial cases have a TRS of some kind. We have shown how certain well-known examples for topological insulators and superconductors fit into this table and we have given a rudimentary example for constructing a topological insulator in 3D via Dirac Hamiltonians. Our example was a \mathbb{Z} topological insulator in class AIII. Similarly, it is possible to construct examples for all the 5 nontrivial topological insulators respectively superconductors that exist in 3D [1], and in any dimension [2]. The shortly mentioned regularity in this table is further examined in [2, 14].

We have also learned that there is a connection between the topology of the band structure in the bulk and the Anderson localization properties of the boundary of such a system, which is described by a NL σ M [2, 1, 10]. Depending on the symmetry class, we have to use a different target space for the NL σ M, and depending on the homotopy group of the target space, different nontrivial topological terms

11.8 Conclusion

can be introduced to the action. These terms can then lead to an evasion of Anderson localization at the boundary, as we have seen in the given example. As for the \mathbb{Z}_2 term - this has been discussed in detail in [21].

BIBLIOGRAPHY

- [1] A. P. Schnyder, S. Ryu, A. Furusaki, and A. W. W. Ludwig, *Classification of topological insulators and superconductors in three spatial dimensions*, Phys. Rev. B **78**, 195125 (2008).
- [2] S. Ryu, A. P. Schnyder, A. Furusaki, and A. W. W. Ludwig, *Topological insulators and superconductors: tenfold way and dimensional hierarchy*, New Journal of Physics **12**, 065010 (2010).
- [3] D. J. Thouless, M. Kohmoto, M. P. Nightingale, and M. den Nijs, *Quantized hall conductance in a two-dimensional periodic potential*, Phys. Rev. Lett. **49**, 405 (1982).
- [4] L. Fu, C. L. Kane, and E. J. Mele, *Topological insulators in three dimensions*, Phys. Rev. Lett. **98**, 106803 (2007).
- [5] L. Fu and C. L. Kane, *Topological insulators with inversion symmetry*, Phys. Rev. B **76**, 045302 (2007).
- [6] M. R. Zirnbauer, *Riemannian symmetric superspaces and their origin in randommatrix theory*, Journal of Mathematical Physics **37**, 4986 (1996).
- [7] A. Altland and M. R. Zirnbauer, *Nonstandard symmetry classes in mesoscopic normal-superconducting hybrid structures*, Phys. Rev. B **55**, 1142 (1997).
- [8] F. J. Dyson, *Statistical theory of the energy levels of complex systems. i*, Journal of Mathematical Physics **3**, 140 (1962).
- [9] F. Haake, *Quantum Signatures of Chaos* (Springer, 2010), chap. 2, 5th ed.
- [10] F. Wegner, *The anderson transition and the nonlinear -model*, in *Anderson Localization*, edited by Y. Nagaoka and H. Fukuyama (Springer Berlin Heidelberg, 1982), vol. 39 of *Springer Series in Solid-State Sciences*, pp. 8–14, ISBN 978-3-642-81843-1.

BIBLIOGRAPHY

- [11] E. Wigner, *Gruppentheorie* (Friedrich Vieweg und Sohn, Braunschweig, Germany, 1931), pp. 251–254, [Group Theory (Academic Press Inc., New York, 1959) pp. 233-236].
- [12] E. Cartan, *Sur une classe remarquable d'espaces de riemann, i*, Bulletin de la Socit Mathmatique de France **54**, 214 (1926).
- [13] A. P. Schnyder, S. Ryu, A. Furusaki, and A. W. W. Ludwig (2009), [cond-mat.mes-hall/0905.2029v1](#).
- [14] A. Kitaev, in *American Institute of Physics Conference Series*, edited by V. Lebedev and M. Feigel'Man (2009), vol. 1134 of *American Institute of Physics Conference Series*, pp. 22–30, [0901.2686](#).
- [15] J. R. Munkres, *Topology* (Pearson, 2000), 2nd ed.
- [16] N. D. Mermin, *The topological theory of defects in ordered media*, Rev. Mod. Phys. **51**, 591 (1979).
- [17] R. Bott, *The stable homotopy of the classical groups*, Proceedings of the National Academy of Sciences of the United States of America **43**, pp. 933 (1957).
- [18] R. Bott, *The stable homotopy of the classical groups*, Annals of Mathematics **70**, pp. 313 (1959).
- [19] W.-Y. S. Shun-Qing Shen and H.-Z. Lu, *Topological insulator and the dirac equation* (2012), [cond-mat.mes-hall/1009.5502v3](#).
- [20] F. D. M. Haldane, *Model for a quantum hall effect without landau levels: Condensed-matter realization of the "parity anomaly"*, Phys. Rev. Lett. **61**, 2015 (1988).
- [21] S. Ryu, C. Mudry, H. Obuse, and A. Furusaki, *Z2*, Phys. Rev. Lett. **99**, 116601 (2007).